OPTIMAL DESIGN OF A HIGH SPEED ROTARY BRAIDER

by

James Goodwin

This thesis is submitted as part of the requirements for the degree of Doctor of Philosophy to the Council for National Academic Awards.

Sponsored by:

The Department of Mechanical, Marine and Production Engineering,
Liverpool Polytechnic.

In collaboration with:

Babcock Wire Equipment Limited
Waterloo Street
Bolton BL1 8HW.

March 1990

Acknowledgements

The author wishes to thank his academic supervisor Professor John Rees Jones for his assistance, encouragement and guidance throughout the project.

Thanks are due, also, to Mr Maurice Williams, Mr Ken Windsor, and Mr Roger Baron of Babcock Wire Equipment for their constructive comments and their efforts in designing the prototype machine.

Thanks also to Mr Brian Davies (Braimak Ltd.) and Mr Michael J Hyde (Cobra Machinery Ltd.) for their views on the braiding machinery market both past and present.

Finally, thanks are due to Tania Hunt, Claire Jones and Samarind Ltd. for help in preparing this thesis.

ABSTRACT

Optimal Design of a High Speed Rotary Braider

By J Goodwin

The aim of the work is to improve the performance of rotary braiding machines. An appraisal of existing rotary braiders concludes that all are limited in performance by one or more of the concepts they employ. None have been designed to optimise more than one or two aspects of the rotary braiding concept. An increase in overall machine performance may be wrought by ensuring all the major areas of the rotary braiding concept are optimised in unison. The design optimisation is divided into two sections.

The first is the theoretical and experimental study of the wire (product) behaviour. This allows a "wand" mechanism, that guides the wire, to be designed which complements the criteria for wire control. The control of the outer wires being fundamental to the performance of a rotary braider.

The second is the inner bobbin carrier format which encompasses optimisation of bobbin orientation, design of the carrier support bearing system, and selection of the inner carrier intermittent drive.

Within these two broad sections are five study areas which are ordered to allow a logical progression, in which the conclusions from one study ideally form the boundary conditions or specification for the next, although a degree of iteration is necessary to achieve the overall optimal design.

Test rigs are built to correlate theory with experimental results in two of the study areas above. These are an experimental study of wire behaviour and wand motion, and an experimental study into inner carrier track roller bearing behaviour.

These study areas are those primarily governing performance and, based on the results, a proposal for the concept of a prototype machine design is made which increases performance by 75% over the current market leading machine.

The collaborating company's implementation of this machine concept is outlined together with a recommendation for further work.

Ph.D. Thesis **March 1990**

CONTENTS

APPENDICIES

ANALYTIC NOTATION

Symbol	Description
a	conical region base shape height
b	bobbin core diameter
c	bobbin outer radius
d	conical region base shape width
dj	air bearing jet dia.
f	bobbin flange thickness
g	gravitational acceleration
$\ddot{g}(z,t)$	forcing function in wire theory (ψ - z plane)
h	bobbin length
i	integer
$\ddot{j}(z,t)$	forcing function in wire theory (ϕ -z plane)
Kg	pressure factor
mu	dynamic viscosity of air
om	angular velocity of carrier around the machine
pa	atmospheric pressure
pd	discharge pressure under air jet
po	supply air pressure
q	air jet recess radius
r	radius of air jet pad
rc	radius of carrier C of G
ro	air density
rr	track roller radius from machine centre
rt	track radius
s	wave velocity in wire theory
t	time
t'	normalised time
u	air bearing clearance
u*	air bearing optimum clearance
v	inner carrier velocity
w	distance from wand cam follower to wand tip
x	cartesian coordinate
x(t)	wand tip coordinate relative to pivot
xs	air bearing load factor

symbol	description
y	cartesian coordinate
y(t)	wand tip coordinate relative to pivot
z	cartesian coordinate
z'	cartesian coordinate along wand pivot axis
A(x)	cross sectional area of wand at x
Ag	air gap in electromagnetic bearing
A1 - A2	constants in wire motion theory
B	wand amplitude (rads)
C(t)	circumferential distance travelled by wand pivot point
Cd	air bearing discharge coefficient
C1 - C4	integration constants
D	inner carrier track diameter
F	external preload on inner carrier
Fc	centrifugal force on inner carrier
Fn	repulsive force of electromagnetic bearing
G	slot factor of air bearing
I	second moment of area
Ia	inner carrier moment of inertia about the roller contact point
Io	inner carrier moment of inertia about the carrier C of G
I1 -I2	integrals in wire theory
L	outer wire span
Lg	track slot width
M	bending moment
M(w)	maximum bending moment at wand follower pivot
Ma	air mass flow rate through one air bearing
Mc	inner carrier mass
Mt	total air mass flow rate
N1 - N2	straight track slot profiles
P	pressure on plain bearing
R	wand length
Rg	gas constant for air
S2	slanted track slot profile
T	wire tension
Ta	torque about carrier roller contact point

symbol	description
Tg	air temperature
V	axial velocity of wire
Vc	cylindrical bobbin volume
Vcw	volume of wire on cylindrical bobbin
Vnw	volume of wire on conical bobbin
Vt	total volume of bobbin
Vw	volume of wire on bobbin
W	load capacity of air bearing
X(t)	wand tip coordinate relative to inner carriers
Xi	normal modal shape in wire behavioural theory
Y(t)	wand tip coordinate relative to inner carriers
$\alpha(t)$	angle between wire and ϕ' - z' plane
β	angle of tilt of bobbin axis in type two orientation
μ	mass per metre of wire
ρ	density of wand material
ϕ	coordinate plane moving with wire
ϕ'	stationary coordinate plane
ϕi	normalised coordinate in wire theory
ψ	coordinate plane moving with wire
ψ'	stationary coordinate plane
$\theta(t)$	angle between wire and ψ' - z' plane
$\theta_1(t)$	wand motion relative to pivot
ω	base angular velocity of wand

CHAPTER ONE

INTRODUCTION

1.0 The Braiding Process

Braiding is a reinforcing or covering technique usually applied to a product core, using wire, yarn or composite strands and is effectively continuous, circular weaving (fig 1.0.1).

Braid is used for an increasingly wide range of products which span over 30 different industries. Some of the familiar applications include cotton shoe laces, nylon cord, copper wire cable screening (co-axial cable), steel wire reinforced hydraulic hose, kevlar cable armouring and more recently using carbon fibre for propellor blades, drive shafts and aircraft components (flap control rods and ducts, etc.).

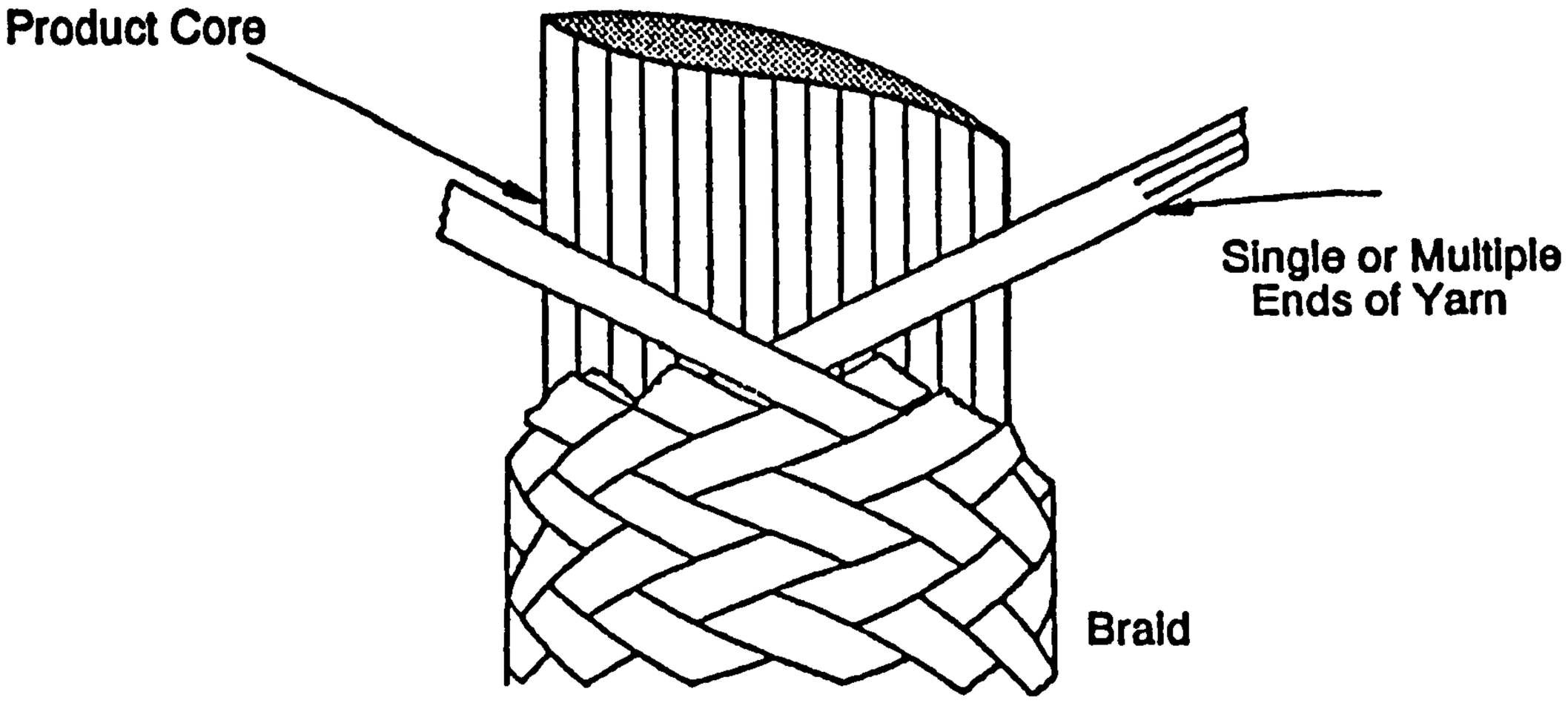

Figure 1.0.1 Braided product

To produce braid the material, in the form of single or multiple ended strands, is woven onto and around a core to form intertwining helical lays from opposite directions of rotation. As in weaving, many different braid patterns are possible but the type most common in industrial use is the "over two, under two" (2:2) pattern in which each strand passes first over two and then under two strands

from the opposite direction of lay. Other, less common, patterns in use are 1:1 (basket weave), 2:1 and 3:1, and all can be produced by automatic machines (i.e. braiding machines). Certain types of braider also produce a flat braid and many other variations are used for very specialist markets.

The weaving motion required to form braid can be achieved by either moving the entire strand carriers in and out of one another along contra-rotating, undulating paths, or, by guiding only the strands from one set of carriers around the other set of carriers to form the weaved braid pattern at the machine centre. The former concept is associated with so called "maypole" braiding machines, because of the similarity with the traditional folk rites dance, and the latter is associated with the "rotary" braiding machine since the strand carriers move with purely rotary motion.

Most braid may be broadly categorised into two basic types regarding their purpose or function:

a)The braid adds strength and is an integral part of the product to such a degree that it must be practically fault free to retain uniformity. Hydraulic hose is generally reinforced by this method of braiding.

b)The braid acts as a secondary protection or covering for the core product and minor faults (such as individual wire joins) may be tolerated. This type of braid is used as electrical cable screening and armoring.

The major differences between the two types of braid is the length of product which can be braided in one continuous run and, to a lesser degree, the strand tension.

The braid type described in a) normally requires large strand package sizes since, to avoid wire joining faults, all bobbins are replaced when one runs out. High tensions are often used for this type of braiding and it is therefore termed "heavy" braid and is generally produced on "maypole" braiders.

In contrast the braid described in b) requires lower tensions and, since strand joining faults are tolerated, smaller package sizes. The bobbins are replaced separately as they run out which enables infinitely long lengths of product to be braided if necessary. This type of braid is often referred to as "light" braid and is produced on rotary braiders where a high production rate is required.

Although braiding is a relatively slow process compared to other covering techniques, such as spiral wrapping and circular knitting, it has superior properties as a structural, reinforcing and electrical screening medium. In many structural and reinforcing applications, such as hose and drive shaft manufacture, spiralling has superior unidirectional strength yet is extremely difficult, hence costly, to produce correctly and does not have the overall robustness and versatility of braid.

Indeed many of braidings latest applications take advantage of its ease of manufacture and multidirectional strength properties. A good example of this is the carbon fibre propellor blade.

Composite material technology has opened a whole new area of applications for braid and particularly one-off maypole braiders.

1.1 Conceptual Differences between Maypole and Rotary Braiders

Braid is produced on two types of machine, termed the "maypole" braider and the "rotary" braider.

The maypole machine effects a braid by displacing the entire bobbins (and carriers) radially in and out of one another as they rotate. The two sets of bobbins are driven in opposite directions around the machine on two intertwining, continuous, tracks cut into a base plate, as shown in figure 1.1.1.

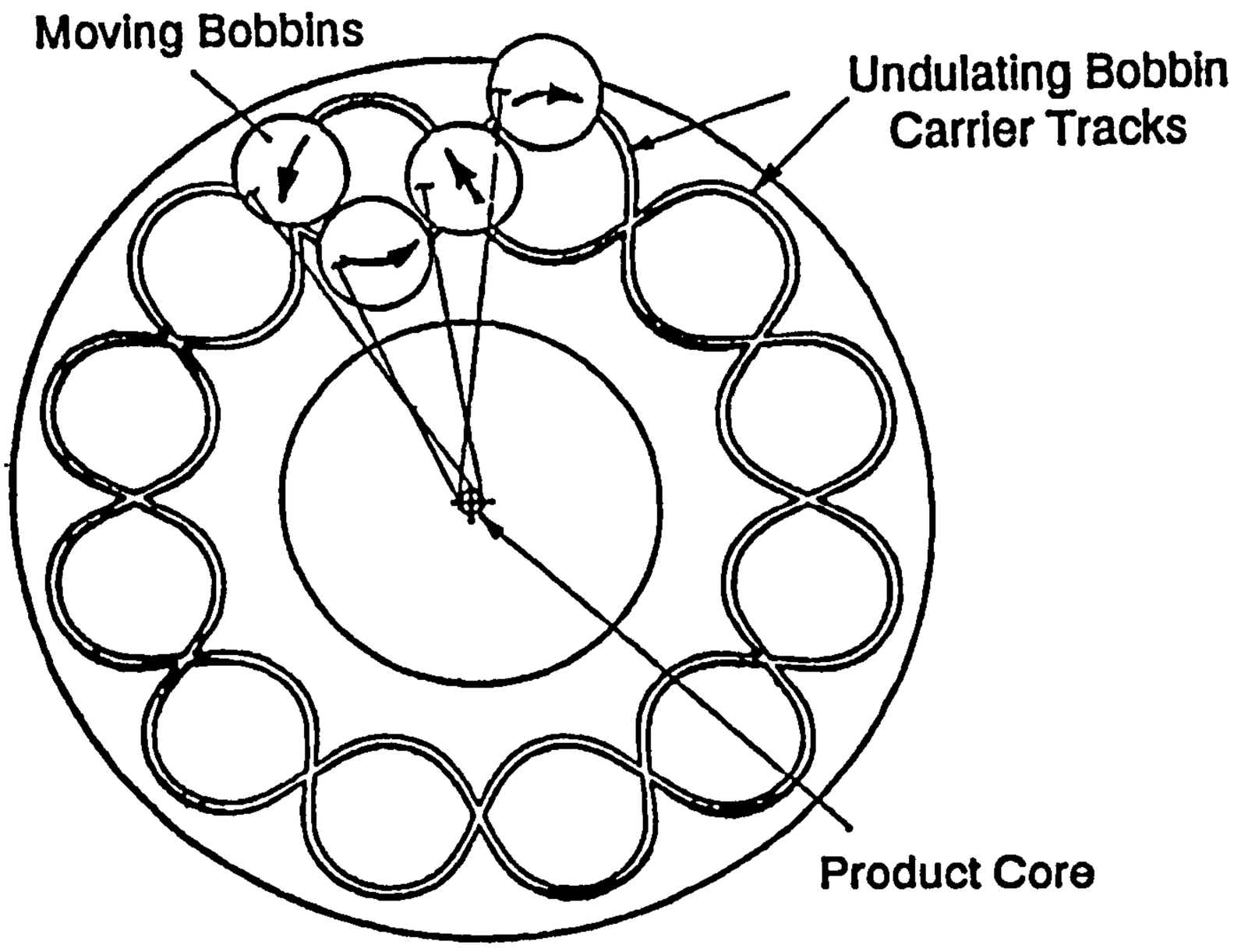

Figure 1.1.1 Schematic of a maypole braider

The drive to each carrier is performed by slotted discs called horngears which lie within the two tracks. Each disc engages with a peg on the base of the bobbin carrier and the carrier is guided over the track cross over point by a boat shaped follower which runs in the track. The carrier drive is thus transferred to the next slotted disc and is propelled around the machine in this manner. The major shortcomings of the maypole braiding concept are the large changes in acceleration induced on the carrier and bobbin mass as it passes over the track crossings. These changes are usually discontinuities in acceleration but even if eliminated the forces involved severely limit the speed of the maypole braider.

An added drawback is that without a large braiding ring, the length of wire from the bobbin to the product varies enormously leading to poor tension control which is generally undesirable, although this can be usefully exploited in hose braiding.

The rotary machine, in contrast, effects a braid by displacing only the wires, from the outer of two sets of contra-rotating bobbins, in and out of every other inner bobbin and carrier as shown in figure 1.1.2.

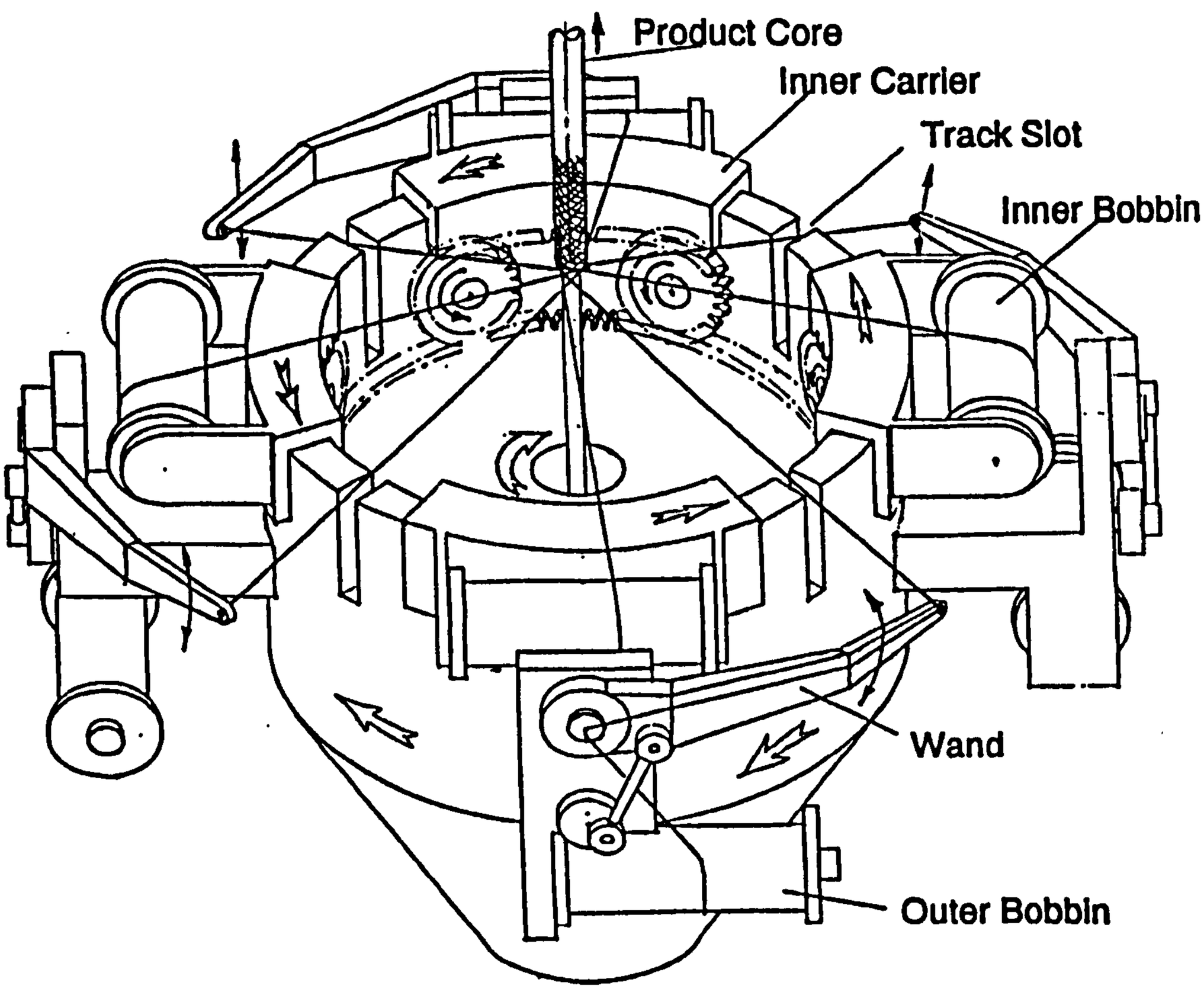

Figure 1.1.2 Schematic of a rotary braider

The outer wires are deflected by stationary guides or separate "wand" mechanisms. As its name suggests, both inner and outer bobbin sets move with purely rotary motion and are not subject to any changing accelerations. The inner bobbin carriers run on a track which may be stationary but usually rotates with the outer bobbin carriers and wand mechanisms. This track features deep slots which allow the outer wires to be guided between the inner carriers and also allow the inner carriers to pass over the outer wires whilst at the bottom of the slot.

The inner carriers are propelled across the slot in the track by an intermittent drive system (shown as bevel gears in fig 1.1.2). In this way the weaving action is produced at the product which passes through the machine centre.

This point, on all types of machines, is referred to as the braiding point. To achieve a desired braiding angle between outer wires and product centreline the braiding point is positioned using a die, or ring, which fits closely around the product as shown in figure 1.1.3.

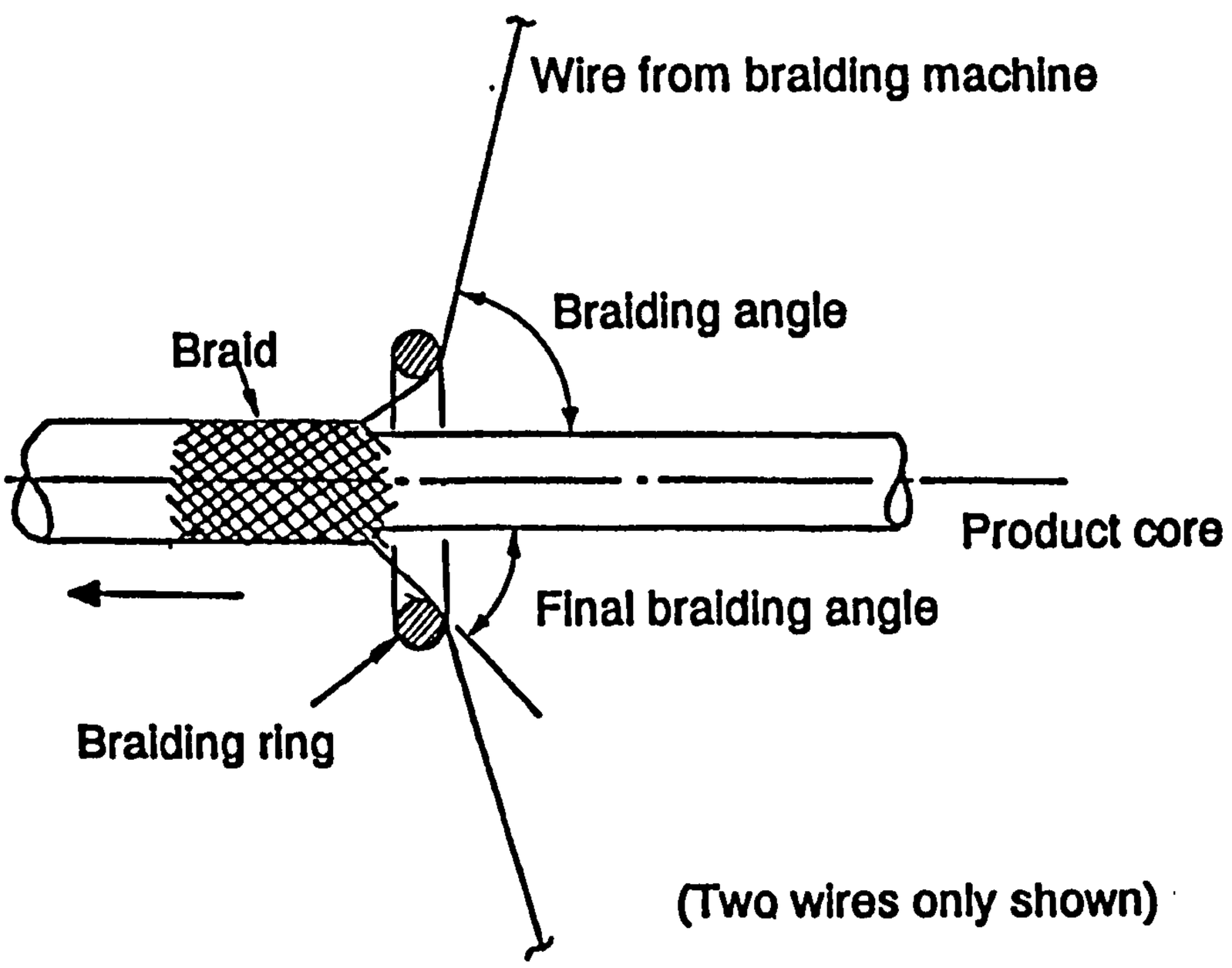

Figure 1.1.3 Braiding ring

The fundamental differences between the maypole and rotary braiding machine concepts accounts for the difference in running speed of between 1.5 and 3, in the rotary braiders favour. Indeed most rotary braiders are over twice as fast as their maypole counterparts.

This would suggest that maypole braiders are not appropriate where production rate is of any importance. However, the maypole is an essentially planar machine and a standard horngear and carrier may be used on many sizes of machine, only the track plate need be different. This vastly reduces the complexity and cost of

manufacture over the essentially spacial rotary braiding machine, which requires large castings or fabrications for the basic framework. For this reason the rotary braider is generally used only when high production rates warrant the extra cost.

1.2 History of Braiding Machines

The first braiding machine is thought to have been invented by Thomas Walford in Manchester in the 1740's. His patent from 1748 describes "an engine or machine for the laying or intermixing of threads, cord or thongs of different kinds, commonly called plaiting", which was later referred to as the maypole braider concept in that the bobbins moved to produce the weave.

Shortly after this, in 1767, Johan Heinrich Bockmuhl is thought to have invented a similar machine in Wuppertal, Germany, which was copied and developed mainly in Wuppertal and France. Many braiders were adapted to manufacture bobbin lace by controlling the separate bobbin paths using a Jacquard device.

Maypole braiders have been steadily developed and currently run at horngear speeds of up to 250 rpm, equivalent to 42 rpm of the carriers around a 24 carrier machine. The principle of moving each bobbin along undulating paths, however, still remains.

Rotary braiders, or rapid runners as they were first called, originated from twin deck maypole braiders and appear to have emerged as early as 1866 when Von Veerkamp and Leopold patented such a machine in Britain. Although this format has been used on many machines since, a layout patented in the USA by James Tragurtha in 1891 has become the norm for high speed machines. Wardwell (1907) in America and Tobler and Horn (1916) in Germany patented and successfully developed to manufacture various types of rotary braider.

Although slowly advancing, the design of rotary braiding machines has effectively stood still for 20 years with Spirka being the last moderately successful new machine which is itself based on the machine described by Tragurtha. A twenty four carrier state of the art rotary braider will run at approximately 90 rpm unless very light bobbin pay loads are employed.

1.3 The Braiding Machine Market

There are approximately 250,000 braiding machines in use worldwide, of which 90% are maypole braiders.

The majority (70%) of braiders are operated by small companies whose activities cover a wide range of industries. This is probably the reason why 60% of braiders are over 20 years old, since the smaller companies have a lower "turnover" of braiding machines.

There are, at present, over 40 different braiding machine manufacturers world wide and the market may initially be split into that for the maypole braider and that for the rotary braider.

Maypole Braiders

The maypole braider market may be broadly divided into three groups:

1)The very large "one-off" braiders such as the Babcock, 196 carrier, propellor braider which often receive widespread publicity yet represent only a small proportion of the market. This type of braider is often a larger version of a more common, smaller machine and uses standard horn gears and carriers, etc.. They are normally very slow since speed is rarely a prerequisite of a "one-off" braider. This market is growing, with the increasing use of composite materials to braid large diameter products, particularly in the aerospace industry.

2)The commonly termed "super maypoles", which range from 16 carriers upwards, represent the forefront of maypole braider technology and are capable of high output, have high tension capability, and a large carrier pay load capacity. Most are used in the hose industry where the high production rates achieved are of paramount importance and capital cost less so. The leading companies producing such machines are Mayer-Rothkopf (MR-11), Rockwell (225), De Angeli and in the very near future Babcock Wire Equipment. This type of machine represents a very lucrative market, although limited in numbers, and machines typically cost (for a basic 24 carrier braider) between £40,000 and £80,000 each.

3)The most common maypole braiding machines are the much more basic, and generally smaller machines ranging from 3 to 48 carriers. These are slower than "super maypoles" and have a lower carrier payload capacity, yet can cost as little as one quarter of that of a comparable "super maypole". Many of these machines are

specials, adapted from a standard machine for a specific product. There are over 30 small maypole braider manufacturers world wide today and this market is not dominated by any single company at present.

The inherent versatility and range of applications of the maypole braider results in a relatively stable market, especially for the smaller machine manufacturers, which is not greatly effected by changes in any one product demand.

Rotary Braiders

The rotary braider market may also be divided into several groups, largely dependent on the type of product.

1)Rotary hose braiders occupy the larger end of the scale (24 + carriers), with the best competing directly with the "super maypole" machines. Most rotary hose braiders do not match the maypoles carrier payload (eg. Spirka)and are therefore restrictive in the length of hose they can produce but do, however, have a significantly higher production rate than even "super maypoles". The rotary braiders in this market are usually technologically advanced and those that compete in all areas with "super maypoles" (ie. the Rockwell RB-2 and, one day maybe the Karg) are very expensive, and obviously prohibitively so, for they at present do not enjoy the success of the "super maypoles". This market sector is relatively stable and small since it moves with the demand for braided hose.

2)The second broad market sector is the cable screening and armouring industry. Machines in this area usually range from 8 to 36 carriers, with the most common being the 16 and 24 carrier braiders. High production rate, and hence speed, are important and it is in this area that the most technologically advanced machines exist. In terms of revenue, Spirka (West German) lead this market with their 24 and 36 carrier machines which are approximately £27,000 each. However, the smaller, 16 carrier braider market is led by Wardwell (USA) whose machine costs only £8,000 but has neither the capacity nor the speed of the Spirka. Yet Wardwell sell many more machines than Spika and, although their machines are smaller, they are close to Spika in revenue from this market sector. These machines flourish in this market because it is extremely lucrative with the cost of the materials, etc., far outweighing the capital cost of the braiding machine. This lucrativity is due in part to the boom in the telecommunication industry and is very much dependant upon it. It is not difficult to forecast the devastating effect a change to fibre optic communications would have on this market. Indeed

much the same situation occurred in the late 1940's and 1950's when extruded plastic wire insulation was introduced and braider demand virtually stopped for many years (though the second hand market then flourished).

3)The third rotary braider market is the "yarn" braiding industry. This is concerned with braiding small diameter products from any non-metallic "yarn" and covers many products, including all types of cord, washing line, and shoe laces, to name but a few. The braiding machine capital cost is of paramount importance here because the product is relatively cheap and yet a maypole braider may not achieve the production rate required. Wardwell are the market leaders here, but almost every other rotary braider produced will braid yarn, if required. Most braiders in this market are operated by small companies.

An overview of the Rotary Braider Market

Wardwell (USA) currently produce the highest numbers, and have the highest revenue from rotary braiders, in the world. They produce at a rate of about 150 machines per month. The best selling machine is the 16 carrier braider which is cheap (£8,000), reliable and compact. However, these machines are not "user friendly" (ie. they are difficult for the inexperienced to repair and maintain), they have a small carrier payload capacity, they will not allow the use of some materials (since the strands are deflected rather crudely by a stationary guide), and the spares are expensive. Indeed Wardwells "balance" between machine cost and subsequent spares cost has been criticised by many users.

Spirka are currently running in second place in the world market for rotary braiders. In terms of numbers of machines, Spirka are a long way behind Wardwell, but in revenue terms they are very close. The most popular is the 24 carrier machine which, has a relatively large payload capacity, a very high production rate (speed), can handle any material, and is extremely reliable. However, again these machines are not "user friendly", are very expensive both in capital cost (£27,000) and spares and use a large floor space since a sound proof enclosure is generally required. Spirka also has a 2 year waiting list for delivery, due, principally, from an American company ordering 500 machine:

Karg (USA) produce 24 and 36 carrier rotary braiders with large pay load capacity and a medium to high speed rating. The machines are still not running to

spec. and cannot accept full bobbin payload at maximum speed. Less than 100 machines in total have been sold to date.

Rockwell (formerly Textile Machinery Works, USA) produce 24 and 36 carrier heavy hose braiders which compete directly with the "super maypoles". These have a very high capacity and high speed and are very sophisticated, but cost approximately £120,000 each which is 50% more than the best "super maypole", and consequently they have sold very few (less than 10).

Other companies perporting to market rotary braiders are, KWO (East German), De-Angeli (Italy) and Sokol (USA), but none are of any relevance to the overall market. Coba (West German), the worlds leading manufacturer of winding machinery have recently announced that they intend to enter the rotary braider market and compete directly with Spirka.

Suitable Markets

There are several markets in which a new and substantially improved rotary braider could successfully compete. However, it is clearly being unrealistic in attempting to design a machine to cover all the different markets simultaneously. Not, primarily, because this is impossible, but because such a machine must be a compromise and would excel in no single market, and for a new braider to succeed it must have a clear advantage over that particular market's leader, in at least one area.

The possible target markets may be divided into three different sections. These being:

a) To complete directly with existing maypole braiders of whichever industry is chosen.

b)To compete directly with existing rotary braiders of a chosen industry.

c)To introduce a rotary braider which competes directly with neither maypole or rotary braiders and yet is applicable to a specific industry or product.

The market described in c) above is potentially both the most lucrative and risky since the opinions of braider manufacturers may not coincide with that of users. A good example of success here is Spirka who virtually created the market sector they now lead. Few, however, would recommend this course to a company based

in a country recovering from a recession and a decline in its manufacturing industry (ie. Babcock Wire Equipment, in Britain, in the mid 1980's). To compete directly with maypole braiders reveals two alternatives. Firstly, to compete with the "super maypole" hose braiders appears relatively straight forward, and the market is lucrative if a little small.

Secondly, to compete with the much smaller, slower, cheaper and simpler "bread and butter" maypole braiders is very attractive indeed as development in this area has stood still for decades. However, the collaborating company (BWE) already market the latter machines described above and were planning a new "super maypole" braider. There was no point in developing a new rotary machine to compete directly with its own established product range.

Competing directly with existing rotary machines, again, reveals two alternatives, both of which seem daunting.

To compete against Wardwell would require a machine with substantially increased performance and a lower capital cost. The Wardwell is, effectively, a mass produced machine and this specification seemed unrealistic without substantial investment.

It was decided, by BWE, to compete directly with Spirka since their machines are not mass produced, the target market was, and is, very lucrative and there is great demand for this type of braider (hence the two year Spirka delivery time). In addition, the high technological content required in such a design enabled collaboration with the SERC and, hence financial aid from government departments.

1.4 Review of Current Rotary Braiders

At the time of writing the only production rotary braider in the market targeted for the new Babcock machine is the 24 carrier Spirka. There are, however, machines from other markets which can, under certain guises, braid products within the Spirka's range.

Rockwell and Karg braiders are both larger bobbin capacity machines capable of moving down market, and Wardwell braiders are capable of moving up-market although the bobbin size remains small.

1.4.1 Spirka

The Spirka rotary braider has an initial braiding angle of 80° and bobbin capacity varies from 3 to 5 kg of copper wire, whilst the corresponding machine speed varies from 85 rpm to 55 rpm respectively.

The inner carriers run on a plain intermittent oil fed track which revolves with the outer bobbins. The track features slots (25mm wide), for the outer wire paths, and the carriers are propelled over these, and around the track, by idler bevel gears mounted on the track base and driven from a central gear. These idler gears engage with bevel gear sections mounted on each bobbin carrier and the carrier drive is passed from one idler to the next. The outer wires are deflected by simple rocker arm wand mechanisms which are driven by a stationary wall cam around the periphery of the machine and so the wands move around the machine with the outer bobbins. The pivot for each wand is positioned to allow constant outer wire length throughout the wand's motion.

In analysis, the machine speed is limited by the wand motion which, in turn, is restricted by the fatigue life of the alloy wand. The wand cam follower consists of a plastic shoe that wears rapidly and results in severe backlash in the wand drive, which exacerbates the problem of fatigue failure. The carrier track bearing is also near its speed/load limit since a fan is fitted to larger capacity (lower speed) machines to cool the track with a continuous blast of air.

The Spirka machine bears an uncanny similarity with a rotary braider developed by Babcock Wire Equipment (then B & F Carter) in the 1960's which did not get

past production prototype stage. This, however, is not surprising since both machines originated from a Geider Horn design dating from 1916.

1.4.2 Wardwell

The Wardwell 24 carrier braider is intended for small diameter products and has a bobbin capacity of less than 1 kg and a running speed of approximately 90 rpm. The inner carriers run on a plain bearing track and drive is achieved with oscillating fingers which allow the wire to pass between carrier and drive hub. The outer wires are deflected by stationary guides which do not allow a constant wire length and, therefore, achieve poor tension control. Most problems with this machine are with the outer wires snagging due to inconsistent wire tension.

The Wardwell is based on a design from 1907 but performs well in its present size. If an increase in bobbin capacity is required the shortcomings of using the Wardwell concepts would become acutely apparent.

1.4.3 Karg

The Karg 24 carrier braider is a large bobbin capacity (7 kg wire) machine which runs at 55 rpm. The inner carriers are driven by a system of spur gears and the carriers have roller bearings which run in contoured tracks. The braiding angle is 55° and because the inner bobbins adopt this angle the bearings suffer very high loads.

The outer wires are deflected by stationary guides and it is probably this in conjunction with the high carrier bearing loads which limit the speed.

1.4.4 Rockwell

The Rockwell RB2, 24 carrier rotary braider is primarily a hose braider and competes directly with the "super maypoles", which it comfortably out performs, and out prices by at least 50%! The RB2 may use 11.3 kg bobbins and runs at 60 rpm.

Each inner carrier is supported by six rollers which run on a contoured track and is driven over the slots in the track by a pair of oscillating latches mounted on a

rotating hub, similar to the Wardwell system. The drive to each carrier is continuously changed from one latch finger to the other to allow the passage of the outer wire between the hub and the carrier.

Each outer wire is deflected by a crank driven six bar wand arrangement which provides a degree of dwell at the extreme of wand travel but does not allow a perfectly constant wire length (from outer bobbin to braiding point) throughout the wand motion. The dwell in the wand motion is intended to allow larger bobbins to be utilised, but this effect is somewhat wasted since the motion of the wire is curtailed by a stop used to position the wire for correct operation of the carrier finger drive system.

The braiding angle is 37°, again chosen to allow increased inner bobbin size without increasing the machine diameter, and a double braiding ring is used in which one of the rings oscillates to relieve wire binding and avoid braid crossover faults. The inner bobbins axes are also at 37° to the machine axis and bobbin volume utilization of the available space is therefore extremely good when using yarn. When wire is used the bobbin size must be reduced to reduce the loading on the track bearings.

1.4.5 Summary of Present Rotary Braider Design

All the current rotary braiders on the market are limited in performance by the concepts used in their design, and inevitably cost. The performance of these machines cannot be significantly improved by minor modifications to the existing designs. Whilst all the machines have good or novel features, none have been designed to optimise more than one or two aspects of the rotary braiding concept. For this reason it is not inconceivable that a substantial increase in overall machine performance can be wrought by merely ensuring all the major areas of the rotary braider concept are optimised in unison.

1.5 Design Strategy

1.5.1 Design Aspects and Specifications

The major aspects of a new design of rotary braider considered most important are:

i) Cost
ii) Reliability
iii) Machine Speed
iv) Bobbin Capacity
v) Power Consumption
vi) Noise

The cost target of £27,000 for a 24 carrier machine is based on the price of a Spirka machine.

The reliability of the overall machine is somewhat intangible until the whole machine is constructed and run. However, each component part must have an (L_{10}) life of at least 25,000 hours. Although accelerated life tests are useful indicators, testing of this type is not convenient, and in many instances not feasible, in an academic environment, and were not undertaken.

The target for machine speed was initially 150 rpm, although this was later deemed unecessarily high, for the envisaged market.

The target bobbin capacity was initially as close to 10 kg of copper wire as possible, but was again changed throughout the project.

The power consumption target was set at 5 kw, but considering the target speed and bobbin size, this figure was not rigidly fixed.

The noise level of 85dB(A) was required for the machine running in it's sound proof enclosure. This is clearly outside the scope of the work covered here, the major difficulty being to translate individual component noise levels to total noise levels for the enclosed machine. However, noise reduction is considered where appropriate in the design of the various sections of the machine.

1.5.2 Proposed Design Procedure

The fundamental functions required of a rotary braider are all interrelated to a certain degree, but the two broad areas of analysis and design are:

a)Outer wire deflection. This involves the deflection mechanism and the method of controlling the wire behaviour and wire tension.

b)Inner carrier format. The carrier, and everything attached to it, must fit into the conical region formed by the superposition of all the outer wire paths. There are three main areas of study related to inner carrier design:

i) The size, configuration and orientation of the bobbin within the conical region.

ii) Inner carrier support. This is effectively the carrier track bearing design.

iii) Inner carrier intermittent drive system design.

These broad areas of study encompass almost every moving part on a rotary braiding machine and must, therefore, determine it's performance. The obvious starting point in the design procedure is to determine the limits imposed on the rotary braiding concept by the dynamic behaviour of the materials to be braided. This forms a natural "boundary condition" for the complex relationships which exist between the various functions of a rotary braider.

This starting point is, therefore, a study of the dynamic behaviour of the oscillating outer wire. The aim is to formulate a criteria relating wire end, or wand tip, motion to wire vibration between the wand tip and braiding point, where it is unsupported.

The next logical area of study is to find a wire deflecting mechanism which satisfies the criteria for outer wire motion. This involves the selection and subsequent development of a wand mechanism.

The motion of the outer wires is necessary to form a weave around the inner carriers, which follow a purely circular path around the machine. The wire motion, and hence wand motion, is optimised to allow the largest volume possible for the conical space (formed by outer wire path superposition) into which the inner carrier and bobbin must fit.

The bobbin configuration, shape, and orientation must be optimised to ensure the best use is made of the conical space formed by the outer wire paths.

The aim is to find the smallest diameter machine which allows the specified bobbin capacity to fit into the conical space formed by the paths of the outer wires which are within the specified limit of control (ie. within a specific amplitude of vibration).

Having determined the minimum theoretical machine size, the bobbin carrier and its support (track bearing) must be designed to also fit within the conical region. The performance of the bearing should allow the specified maximum machine speed whilst complying with general longevity requirements.

The final step is to choose an inner carrier drive system and arrange the inner carrier to accommodate this.

The order in which the various braiding machine functions are studied is intended to allow a logical progression in which the conclusions from each study (chapter) forms the boundary conditions or specification for the next.

However, the entire optimisation process is iterative in an attempt to maximise the overall machine performance.

To summarise, the study areas and the order in which they are presented is:

i) Analysis of an oscillating wire
ii) Wand Analysis
iii) Inner Bobbin Optimisation
iv) Inner Carrier Track Bearing
v) Inner Carrier Drive and General Arrangement

CHAPTER TWO

ANALYSIS OF THE MOVING OUTER WIRE

2.1 Introduction

The concept which is fundamental to rotary braiding is that of deflecting the wires from each of the bobbins in the outer set to pass in and out of every other inner bobbin and its carrier. The wire is deflected by a wand arrangement which guides the outer end of each wire with an oscillatory motion.

In ideal circumstances the wire between the wand tip and the braiding point should remain straight at all times, as any deflection from this detracts from the space available to the inner bobbin and carrier. The wire must also pass into a slot in the inner carrier supporting track and any substantial deflection of the wire in this direction necessitates the use of a wider slot or stationary guides, both of which are detrimental to machine performance.

The dynamic behaviour of the wire when oscillated must be determined to allow an acceptable wand motion to be found. This, in turn, enables the configurations of the inner bobbins and carriers to be optimised for maximum machine performance.

The study of the wires behaviour entails the correlation of two different investigative methods, which are:

a) Traditional dynamics which considers the individual influences on the wire behaviour at a fundamental level (ie. differential equations). This is solved in the major motion direction (ψ - z plane) by using normalised coordinates and treating the wand tip motion as a driving function. Duhamels' integral method yields an expression for the various modal shapes possible for the wire span. The drag on the wire due to air resistance and the stiffness of the wire have been neglected since both induce relatively small forces on the wire.

b) Experimental results from test rigs. These show modal shapes and maximum deflections for two types of wand motion, which are;

i) A wand motion which induces instability in the wire at relatively low speed.

ii) A wand motion which the theory indicates is the optimum, and which is chosen for the final machine design.

2.2 Theory of Wire Behaviour

There are three basic end conditions or movements applied to the wire span.

a) The wand tip end of the wire is subject to an essentially oscillatory motion which effects the weave around the inner bobbins and which may be expressed as a fourier series.

b) All the wands rotate at a constant speed about the machine/braid central axis.

c) The wire is continuously drawn from the bobbin onto the product and therefore has a constant axial velocity relative to the end points.

The end of the wire, at the braiding point, is assumed to have zero transverse velocity at all times, although it actually rotates with the outer wand pivot, but on a radius slightly greater than the product radius (ie. very small).

The influence of the wires from the inner bobbins is neglected as this too occurs at a very small radius from the fixed braiding point.

The wire between the wand tip and braiding point is subject to a number of forces which may be transposed into three axes as shown in fig 2.1.01.

1) Inertia effects due to the wires own mass in the direction of net transverse accelerations (ie. Along axes ψ and $\varnothing$).

2) Tension force acting axially along the wire, although not necessarily always in the z direction, unless the wire is straight. The tension is assumed constant which is reasonable if both of the following conditions are satisfied:

i) The transverse deflections are small.

ii) Either a) The tensioning mechanism is capable of sustaining a constant tension even if the wire length fluctuates, which is unlikely.

or b) The wire length, from wand tip to braid point, remains constant throughout the wands movement cycle.

3) A coriolis component is present, albeit small, due to the axial velocity of the wire, as it is consumed in the z direction and the net angular velocity of the entire wire about the braid point.

4) Aerodynamic drag on the wire which is proportional to the net wire velocity. This is shown to be negligible in Appendix 2.2.1.

5) The braiding stiffness of the wire (ie. its reluctance to bend from its natural shape, which may not be straight). This is proven to be negligible at the wire tensions envisaged in Appendix 2.2.2

6) The wands move at constant speed around the product. The wand speed therefore varies slightly, but this is negligible both in terms of a tension field along the wire and increasing the coriolis effect over that covered in (3) above.

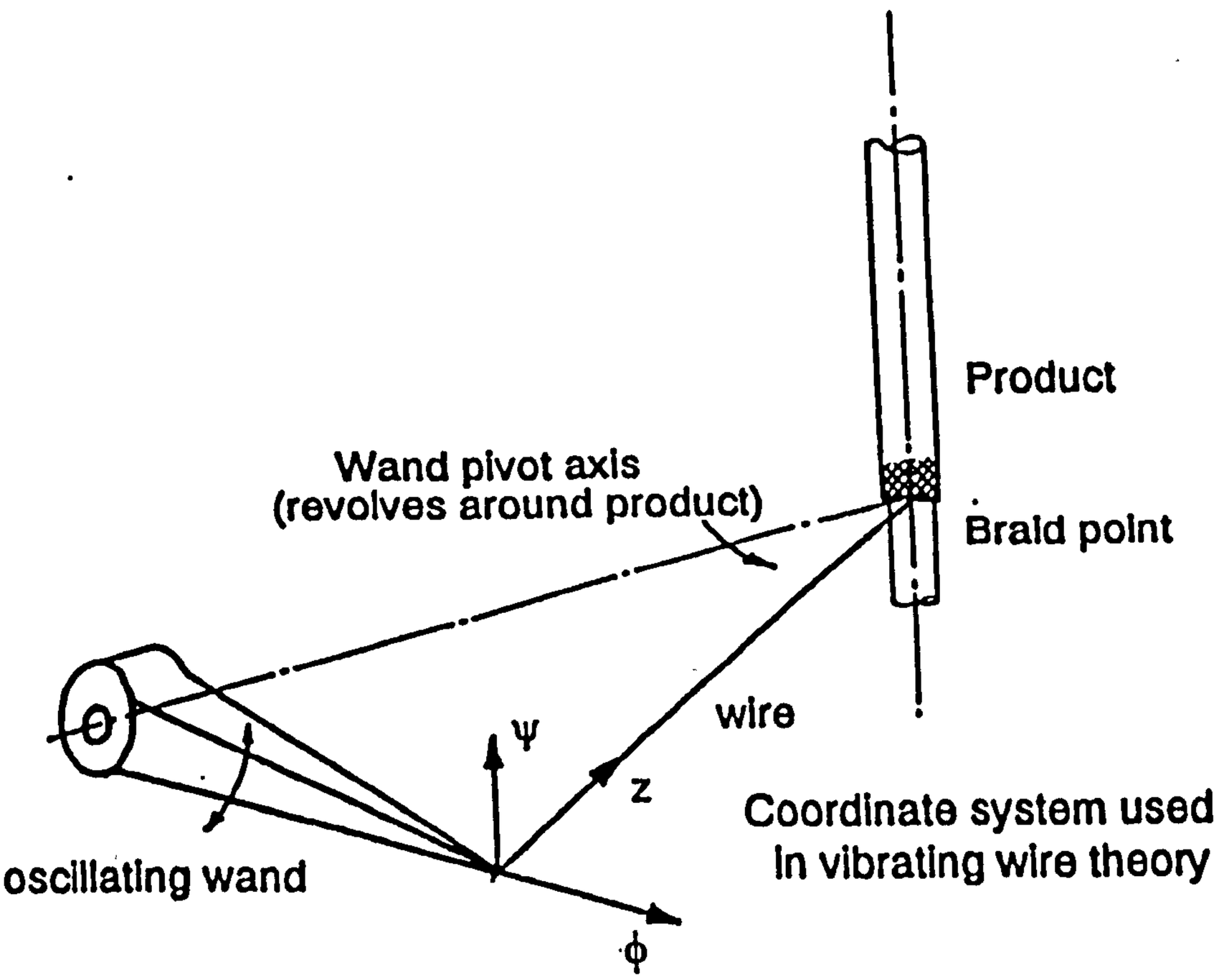

Figure 2.1.01 Outer wire and wand

Although the wand mechanism may be planar, it is assumed here that a simple rocker wand is employed. This being the simplest current method of achieving constant wire tension. The use of such a wand also leads to deflections of the wire in two planes. Figure 2.1.02 shows the orientation of these planes relative to the wand motion. These planes are split for convenience into the ψ' plane and the ϕ' plane. The net forces on the wire segments is likewise split into components in each of these two planes.

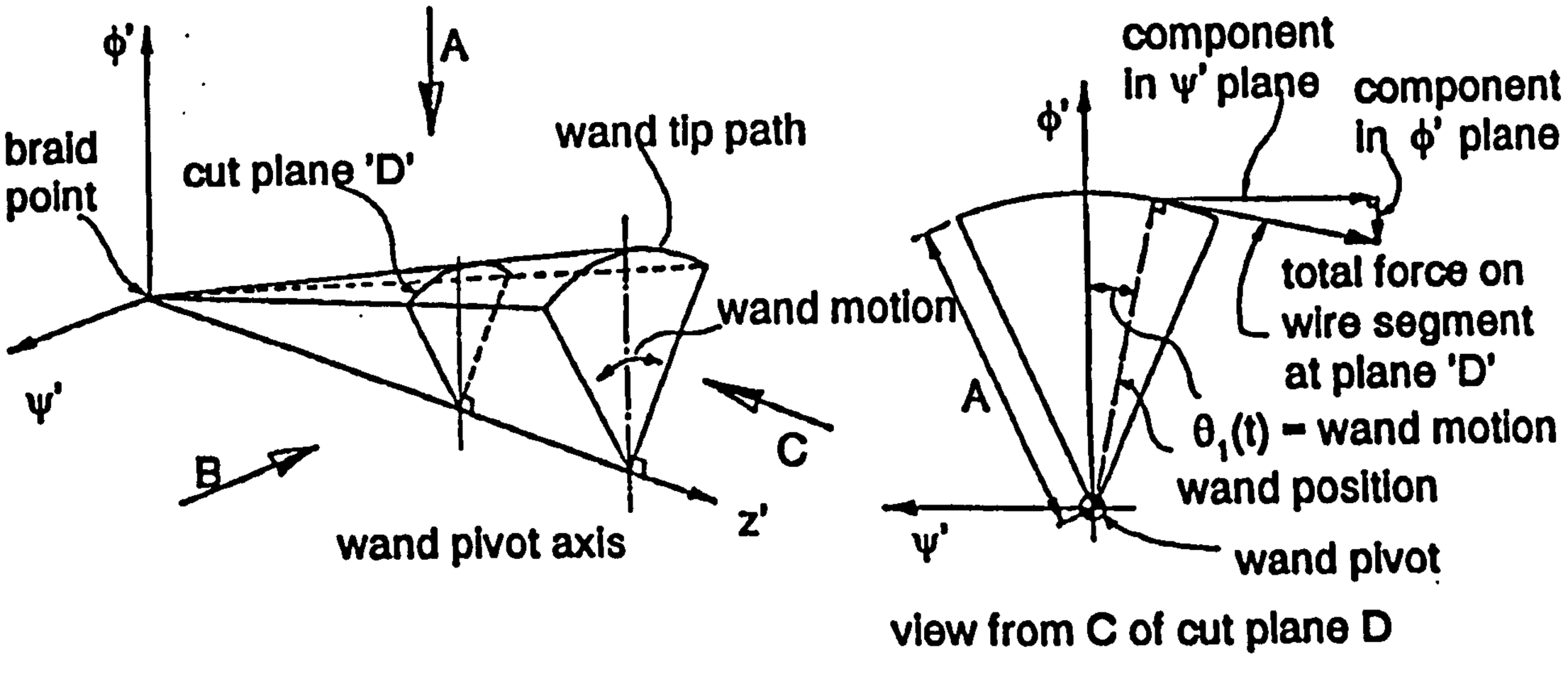

Figure 2.1.02 Base coordinate system used in the theoretical model

The major plane (ψ') is essentially the plane of major wand motion whilst the minor plane (ϕ') incorporates the terms due to the non planar nature of the wand tip locus (ie. crudely described as the centrifugal forces due to the wand rocking about a pivot). The coordinates ψ and ϕ represent the deflections of the wire perpendicular to, and relative to, the ideal straight path in the ψ' - z' and ϕ' - z' planes respectively.

The theory presented to combine the localised wire vibration (relative to its own axes ψ - ϕ - z) and the major driving force function at the wand tip (expressed in the ψ' - ϕ' - z' coordinate system) give rise to a tension field along the wire as long as the wire is moving. This change in tension is a maximum of approximately 0.03 N/m for a triple harmonic motion. This is assumed to be negligible since the minimum nominal tension is 5 N.

2.2.1 Theory for Wire Behaviour in the ψ - z Plane

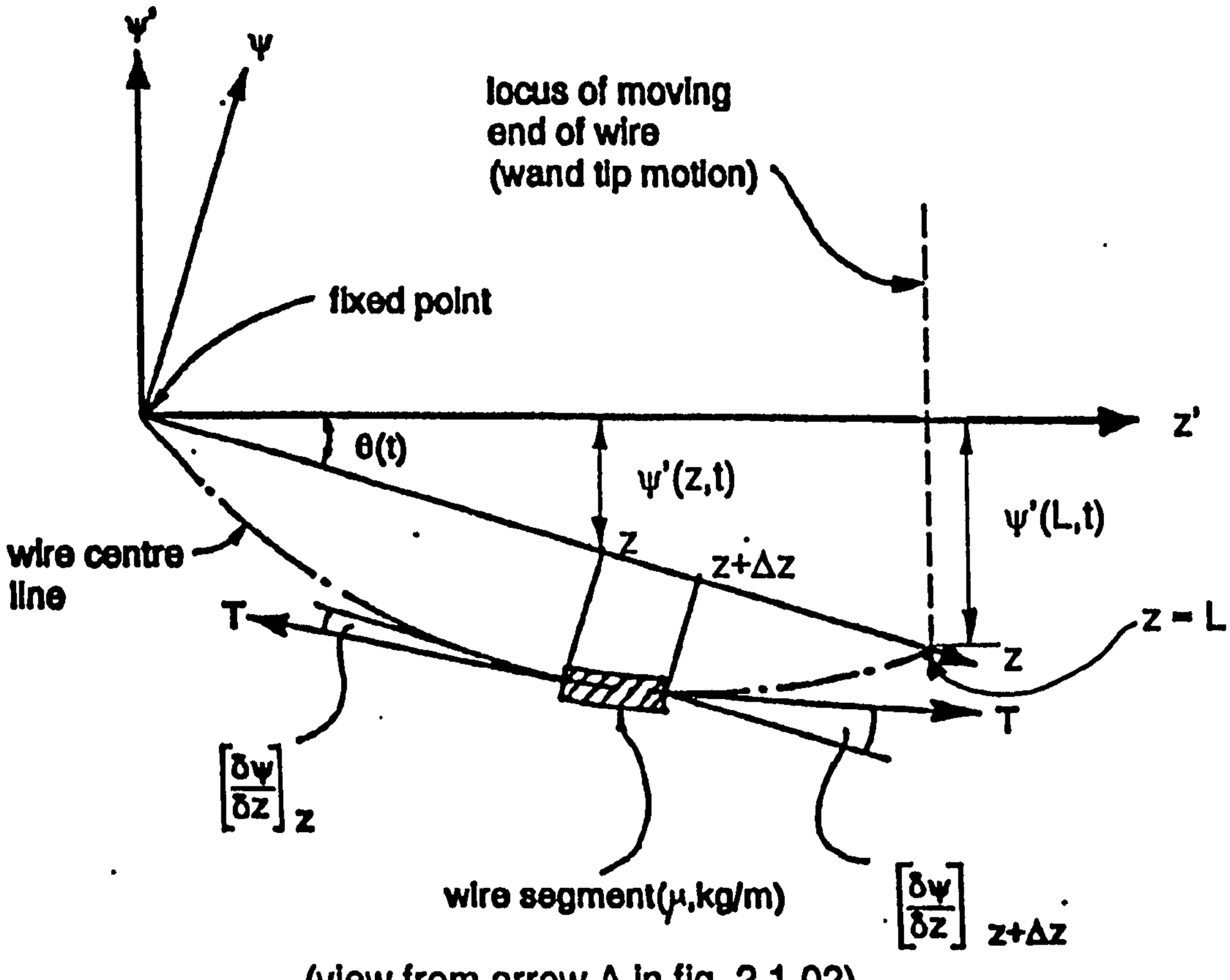

Figure 2.2.10 Segment of moving wire in the ψ - z plane

The wire is continuously moving towards the fixed point with velocity V.
Resolving tension forces and accelerations in the ψ direction.

$$-T\left(\frac{\delta\psi}{\delta z}\right)_z + T\left(\frac{\delta\psi}{\delta z}\right)_{z+\Delta z} = \mu.\Delta z\left[\frac{\delta^2\psi}{\delta t^2} + \cos\theta.\left(\frac{\delta^2\psi'}{\delta t^2} + \frac{2.V}{z}.\frac{\delta\psi'}{\delta t}\right)\right]$$

where $\theta = \arctan(\psi'(L,t)/L1)$ and $L1 = (L^2 - R^2)^{0.5}$

$$T\left(\frac{\delta^2\psi}{\delta z^2}\right)\Delta z = \mu\Delta z\left[\frac{\delta^2\psi}{\delta t^2} + \cos\theta\left(\frac{\delta^2\psi'}{\delta t^2} + \frac{2.V}{z}.\frac{\delta\psi'}{\delta t}\right)\right]$$

$$\frac{T}{\mu}\left(\frac{\delta^2\psi}{\delta z^2}\right) - \left(\frac{\delta^2\psi}{\delta t^2}\right) = \cos\theta.\left(\frac{\delta^2\psi'}{\delta t^2} + \frac{2.V}{z}.\frac{\delta\psi'}{\delta t}\right) \qquad (1)$$

This fundamental partial differential equation is solved in appendix 2.2.3 by a technique which first normalises the coodinates and then uses Duhamels integral method to give a general solution requiring integration. The integration of the forcing function, which is the right hand side of equation (1) and represents the motion imparted by the wand mechanism, is extremely complex and a numerical method is employed. This, unfortunately, prevents the formulation of an explicit analytic solution for the wire behaviour (ie. $\psi(z,t)$) which is the intention of this method for solving partial differential equations (ref. Timoshenko et al, reference (1)).

The wire form at each desired point in time now requires numerical integration of the forcing function which can be time consuming (for the computer). However, this is of little practical consequence and enables relatively complex wand motions to be analysed.

Typical wire behaviour (ψ) at various times in the wand cycle are shown in figure 2.2.11 for a single, triple, and quintic harmonic wand motion of amplitude 220 mm, wire tension of 5N (which is the minimum used on a rotary braider), and at 15Hz frequency of oscillation which is equivalent to 150 rpm machine speed. Figure 2.2.12 shows the typical conical base shapes, formed by the superposition of all the outer wire paths, for single, triple, and quintic harmonic wand motions. These clearly show the benefits gained in the increased volume available to the inner bobbins and carriers when higher harmonic wand motions are employed.

The collaborating company set a limit, based on past experience, of ± 10mm maximum wire deflection at any point.

The figures show that in theory the triple harmonic wand motion is just on this limit. The quintic harmonic is shown to be unsuitable at the speed (15Hz) envisaged, but the ideal motion is that of the single harmonic.

The peak deflections (with all motions) occur at or near the point of peak wand amplitude. The deflection in the ψ - z plane when in the mid-point of wand amplitude is greatly reduced from the maximum shown. Indeed the deflections in the ϕ - z plane are greater at this point, where the wire enters the inner carrier track slot. The plots of wire behaviour also reveal that the wire is always bowing outwards away from the wands central position. This, in theory, increases the conical region volume.

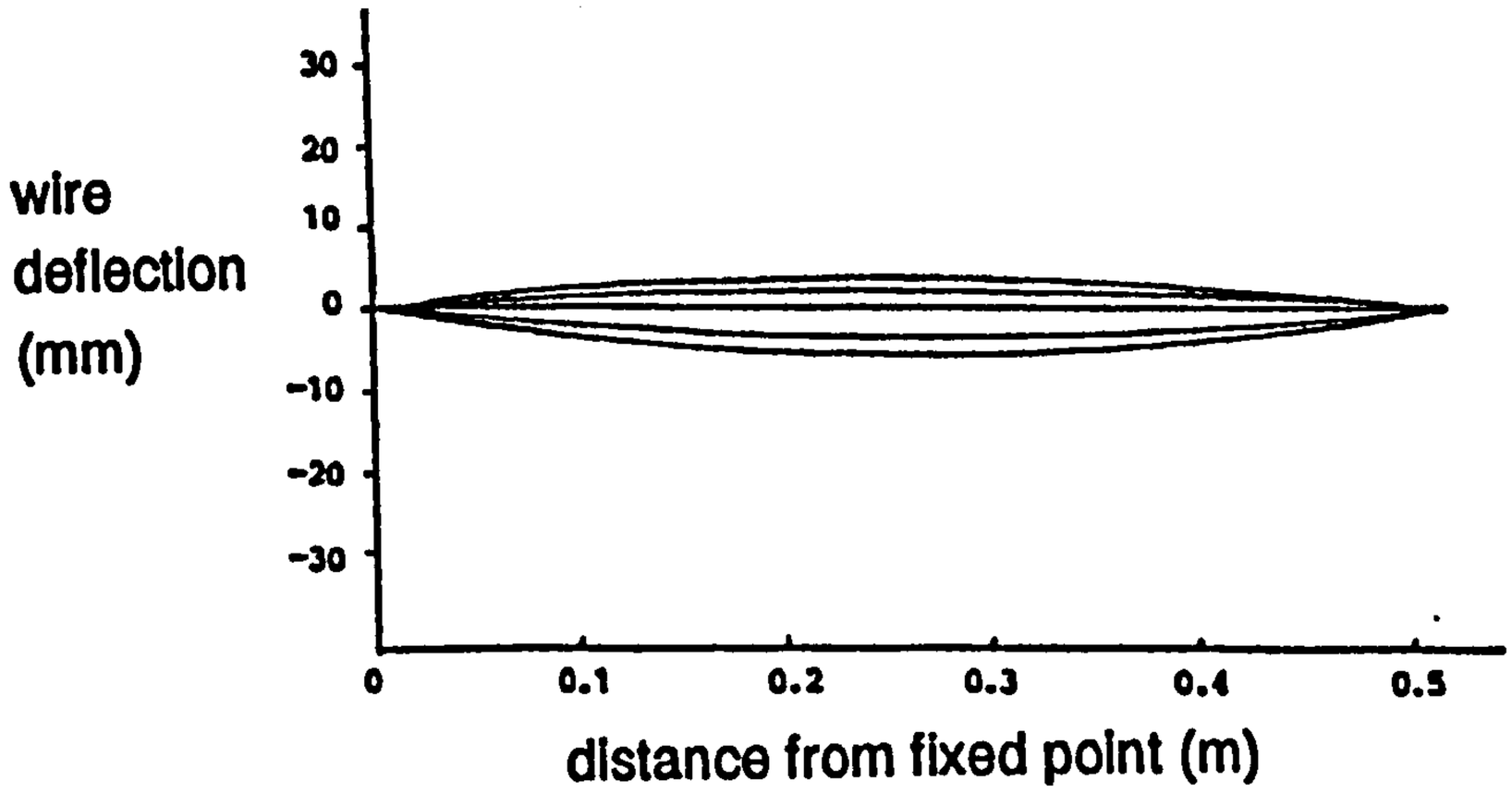

Single harmonic motion

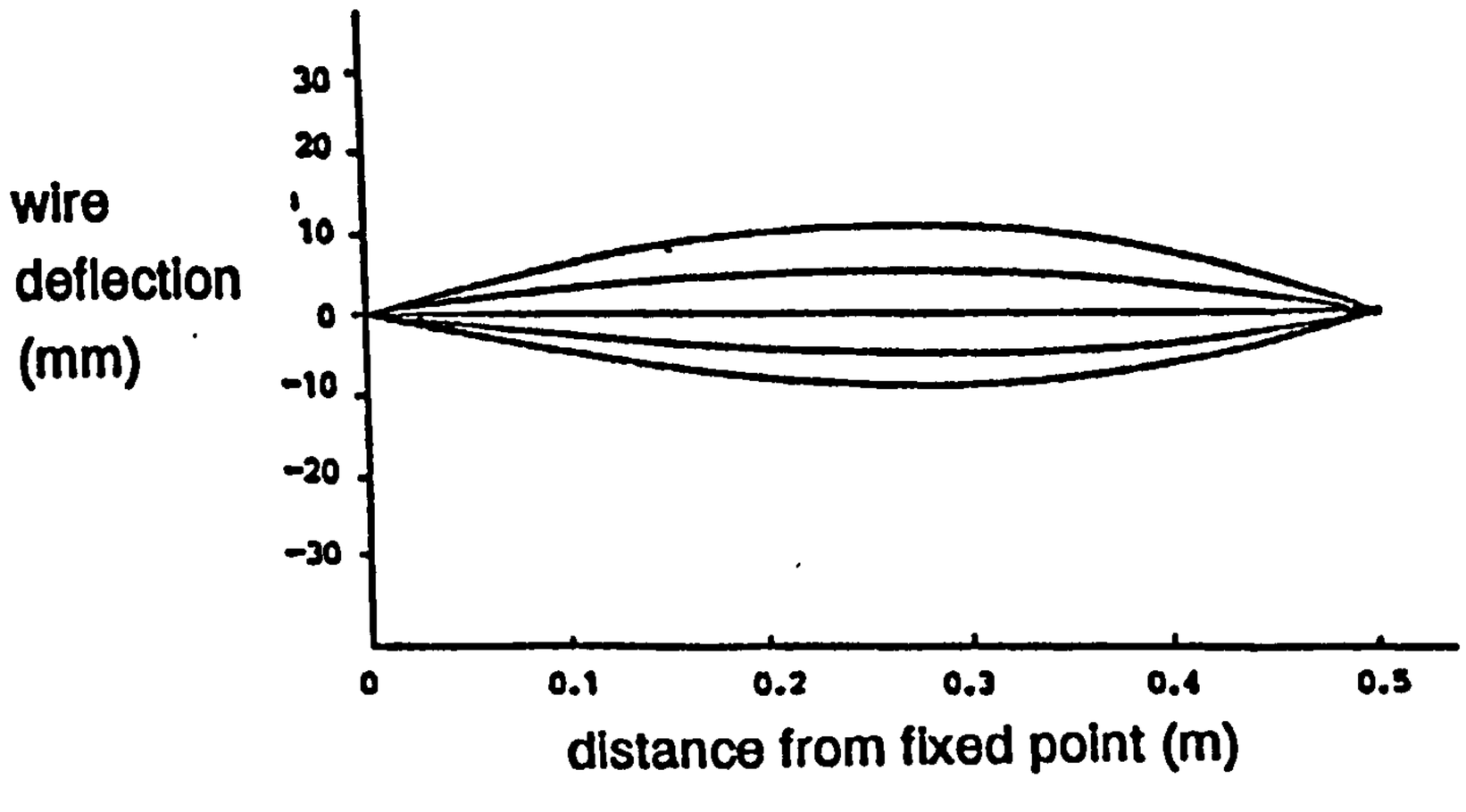

Triple harmonic motion

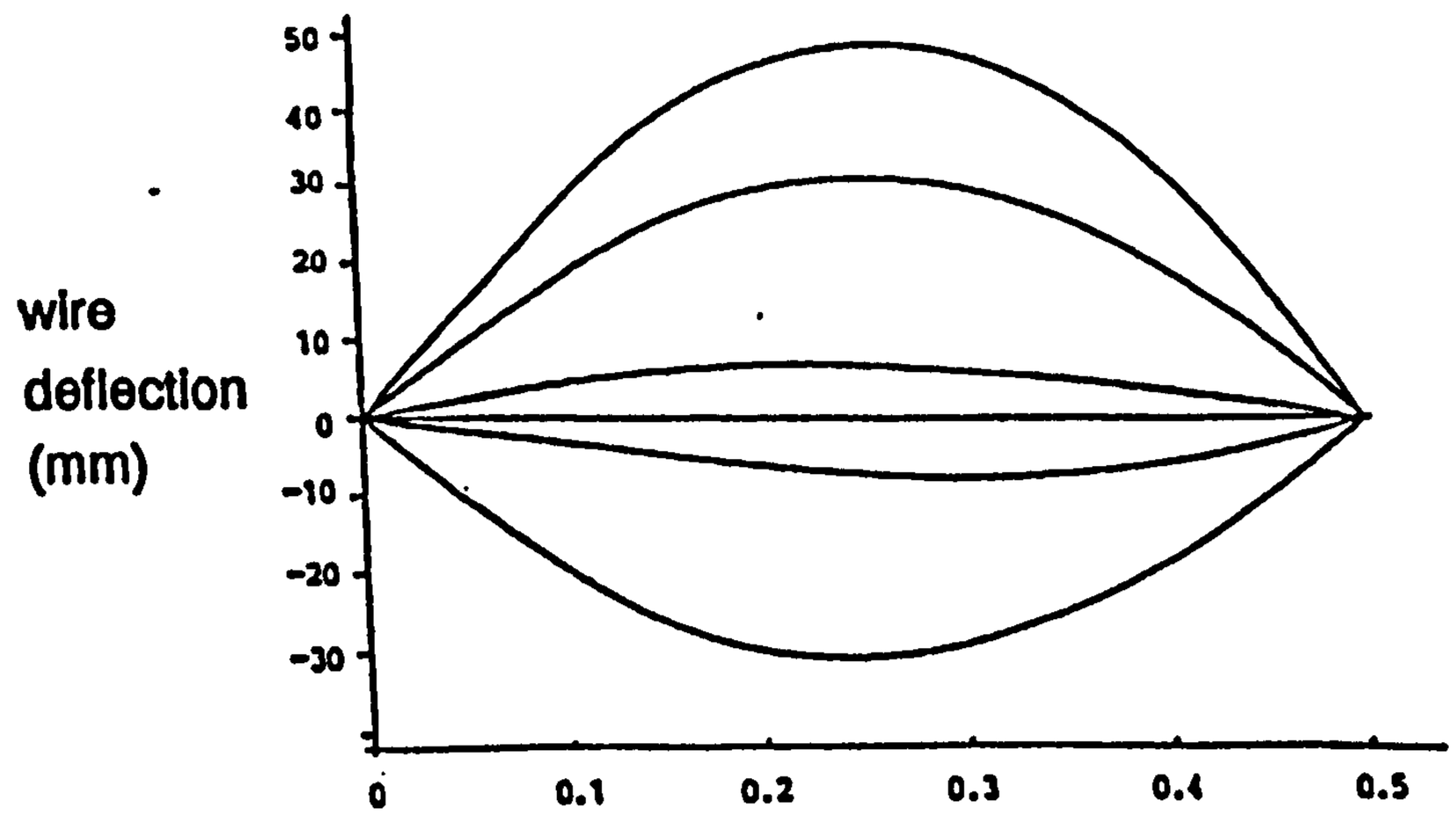

Quintic harmonic motion

Figure 2.2.11 Wire deflection in the ψ - z plane for different wand motions

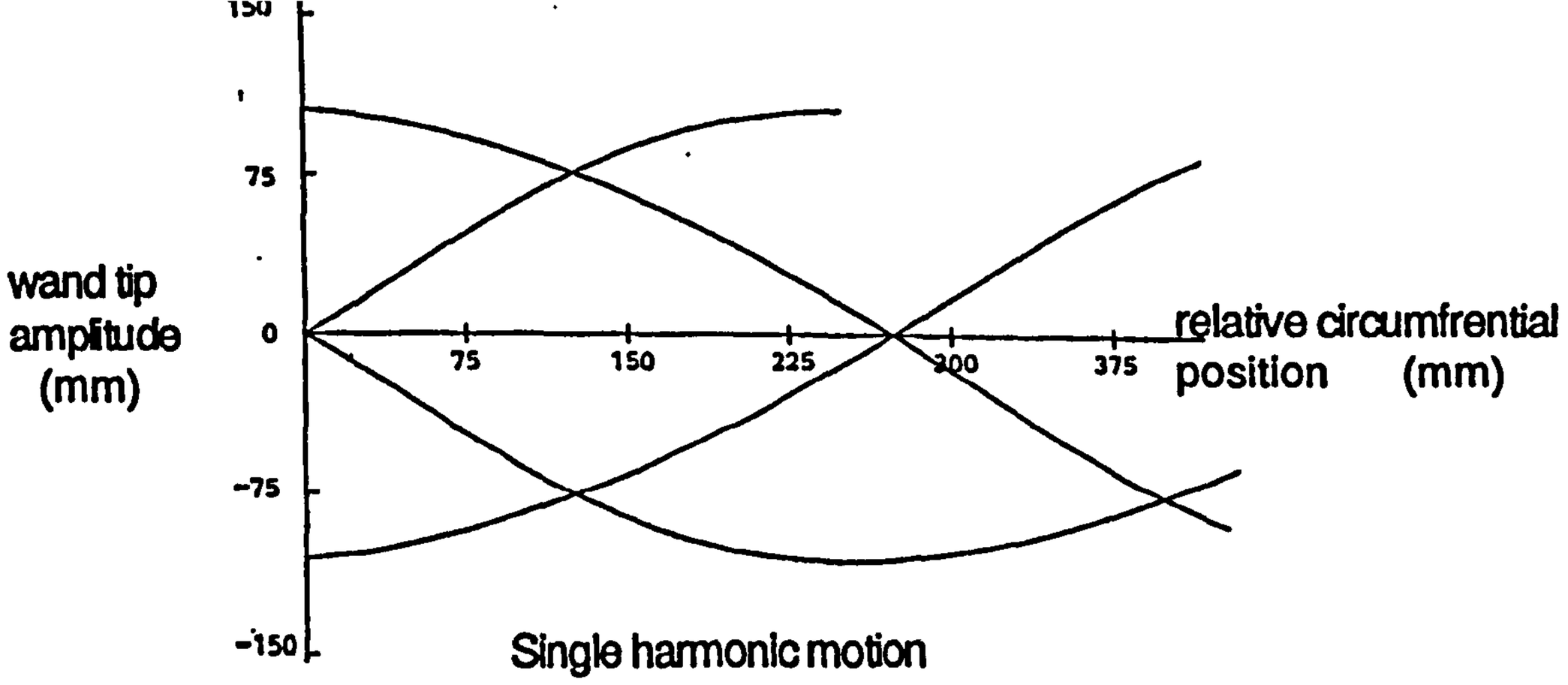

Single harmonic motion

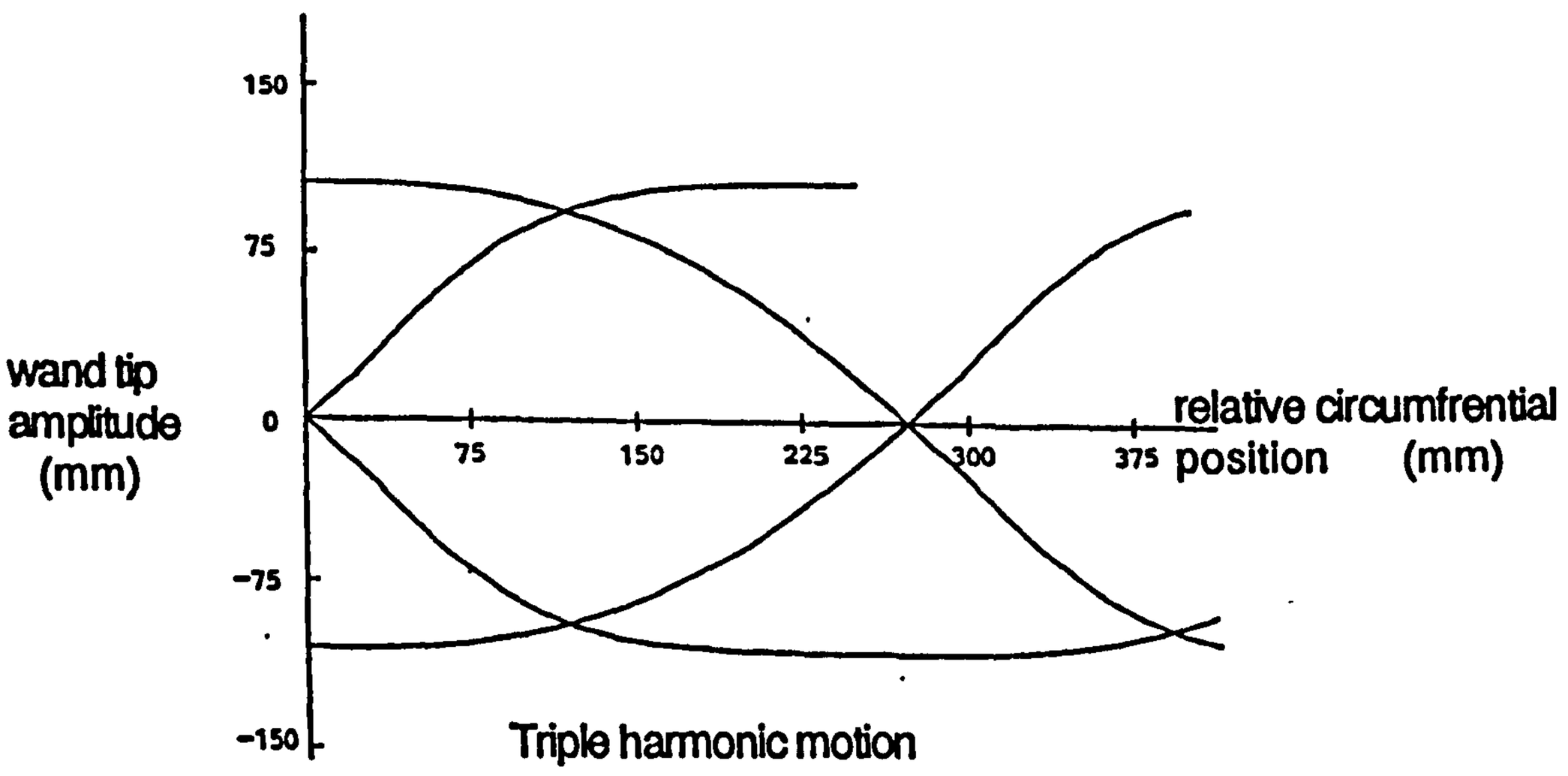

Triple harmonic motion

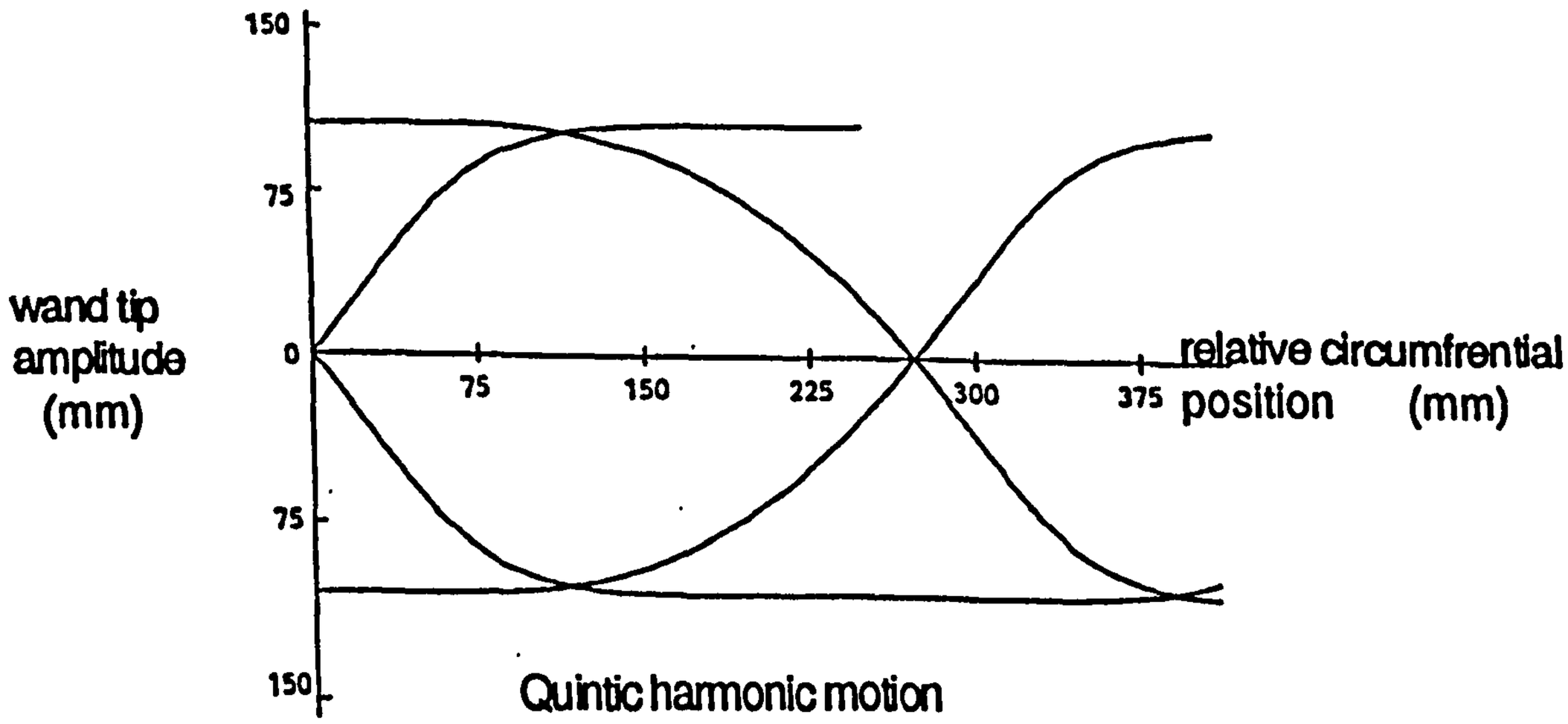

Quintic harmonic motion

Figure 2.2.12 Conical region base shapes for different wand motions

All these deflection plots are for motions with identical wand tip amplitudes, yet the single harmonic could be run using a higher amplitude before the deflection specified is exceeded. This may well be advantageous for inner bobbin/carrier orientation and position, even though a larger wand swing results.

2.2.2 Theory for Wire Behaviour in the ϕ - z Plane

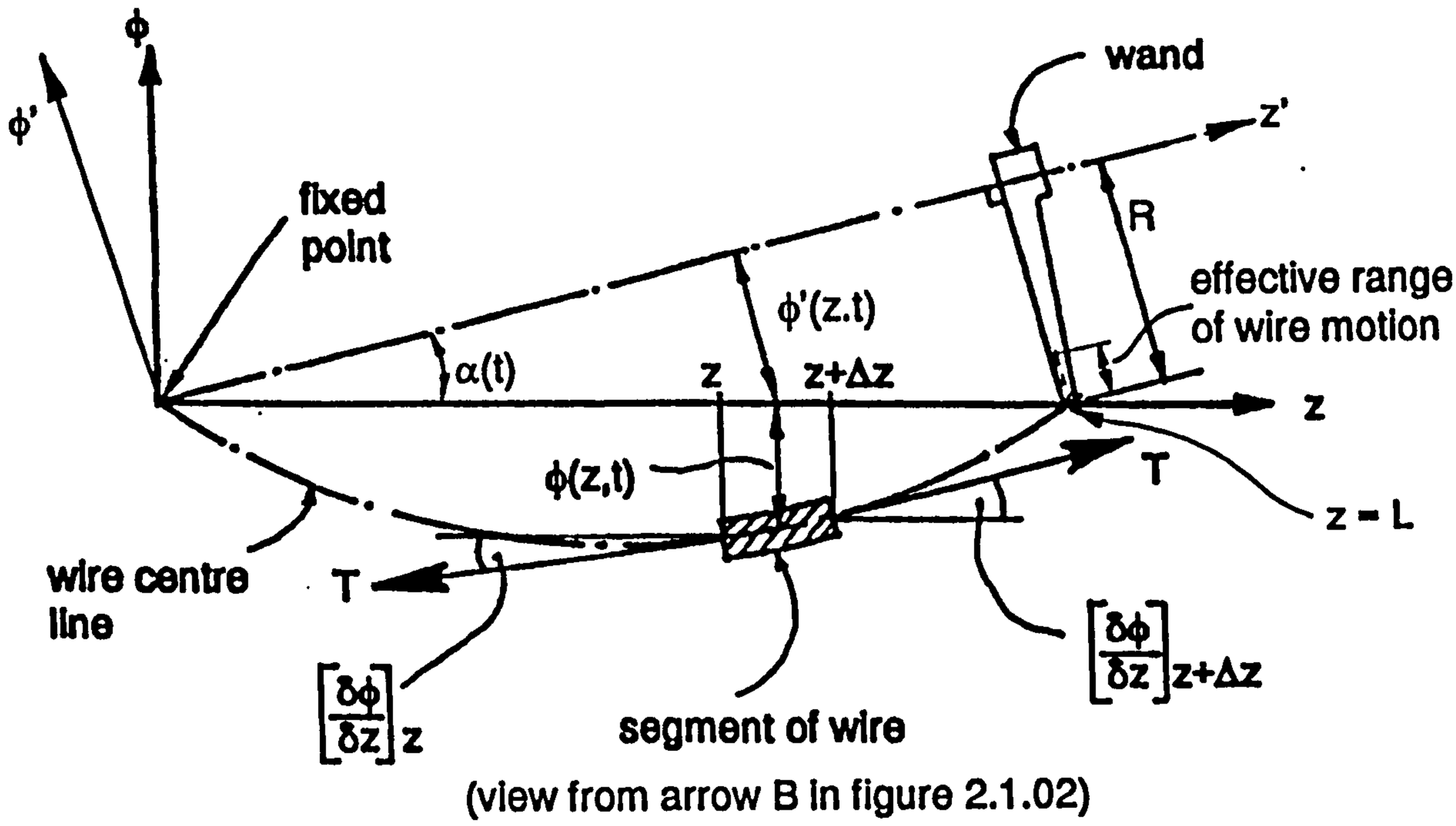

Figure 2.2.20 Segment of moving wire in the ϕ - z plane

The wire is continuously moving toward the fixed point with velocity V.
Resolving tension forces and accelerations in the ϕ direction.

$$-T\left(\frac{\delta\phi}{\delta z}\right)_z + T\left(\frac{\delta\phi}{\delta z}\right)_{z+\Delta z} = \mu.\Delta z\left(\frac{\delta^2\phi}{\delta t^2} + \cos\alpha.\frac{\delta^2\phi'}{\delta t^2}\right)$$

where $\alpha = \arctan(\phi'(L,t)/L1)$ and $L1 = (L^2 - R^2)^{0.5}$

The coriolis term present in the theory for the ψ - z plane is now negligible due to the limited range of motion and low angular velocity the wire experiences in this plane.

Thus;

$$T\left(\frac{\delta^2\phi}{\delta z^2}\right)\Delta z = \mu\Delta z\left(\frac{\delta^2\phi}{\delta t^2} + \cos\alpha\ \frac{\delta^2\phi'}{\delta t^2}\right)$$

Therefore:

$$\frac{T}{\mu}\left(\frac{\delta^2\phi}{\delta z^2}\right) - \left(\frac{\delta^2\phi}{\delta t^2}\right) = \cos\alpha.\left(\frac{\delta^2\phi'}{\delta t^2}\right) \qquad (13)$$

This fundamental equation for the behaviour of the wire in the ϕ - z plane is solved in an identical manner to equation (1) in section 2.2.1 (the wire behaviour in the ψ - z plane). The solution to equation (13) is outlined in appendix 2.2.4.

The wire form (ϕ) relative to the straight wire ideal, is almost identical to that found for the ψ - z plane but with reduced amplitude. A triple harmonic wand motion results in a maximum deflection in the ϕ - z plane of 4.5 mm at the positions of maximum wand amplitude. Of more importance is the amplitude of deflection at the mid-point of wand travel, where the wire enters the inner carrier track slot, of 2.5 mm as this influences the design of the track slot and so effects inner carrier bearing performance.

2.2.3 Conclusions

The wires behaviour is governed primarily by its own inertia when submitted to rapid oscillation. The effects of aerodynamic drag and wire stiffness are negligible at the speeds envisaged. The theory also reveals that the "bowing" deflection of the wire, in the ψ - z plane (plane of major wand amplitude), actually increases the volume available to the inner carriers, over a system with no deflection. This is only true, however, if the tension is maintained above the 5N minimum or if the modal shape does not depart from its fundamental.

The deflection in the ϕ - z plane, whilst generally smaller than those in the ψ - z plane, do influence the design of the track slot into which the wire must be guided and, for this reason, cannot be ignored.

The theory clearly suggests that the lower the harmonic content of the wand tip motion, the lower the deflections will be for the same wand tip amplitude.

However, increasing the harmonics of the motion in certain ways, by using triple and quintic harmonic motions, increases the space available to each inner bobbin carrier (refer to chapter 5 - Bobbin optimisation) and are included for this reason.

The alternative, which is a superior solution in theory (up to a point), is to increase the wand amplitude and use a single harmonic motion.

The theory also shows the critical effect the tension has on the wire behaviour. For this reason a constant tension throughout the wand motion is vital for acceptable wire deflection control.

The whole theory relates only to one wire strand, where as often multi-wire strands are used. However, the ratio of cross sectional area to individual wire tension does not vary greatly (ie. minimum tensile stress in the wires are approximately constant whether there is one 0.3mm diameter wire or seven 0.1mm diameter wires).

Often in practice one or more wires in a strand are wound loose on the bobbin and this results in zero tension wires which theoretically have a large deflection. However these "loose" wires are constrained by the length of the other tight wires and cannot realise their theoretical zero tension shapes. The magnitude of deflection of any loose wires is thus approximately the same as a "canteenary" test would show. In addition, these loose wires adopt an outer position on the product core and are therefore consumed at a greater rate until the canteenary is removed.

The aim of the theory was ideally to develop an analytic technique for simulating wire behaviour. The use of numerical integration routines, whilst moving away from the ideal sought, represents a relatively flexible and accurate method of analysis.

It also begs the question of numerically solving the fundamental second order partial differential equations associated with deflections in the two orthogonal planes. Subsequent testing of one of these techniques (the explicit finite difference method) shows good correlation with the results presented here, provided time intervals, etc, are judiciously selected to avoid instability.

These techniques also highlight the fact that because of the nature of the model and solution used here the response is always periodic, with a period equal to one wand cycle. This is clearly not the case in practice where an underlying periodic trend (with a period greater than one wand cycle) often manifests itself on the essentially wand speed related periodic wire behaviour. The numerical techniques often display similar tendencies which are almost certainly due to the inherent inaccuracy of these principals. However, this phenomena suggests a deficiency in

the original model which has possibly been over simplified to enable an analytically based solution. It is recommended that any further work in this area is based on a numerical solution of the fundamental differential equations.

2.3 Experimental Study of Wire Behaviour

Two different test rigs were built at different stages of the project. Both were attempts to show the actual wire behaviour on full sized wand mechanisms. Three basic behavioural characteristics of the vibrating wire were required:

a) The absolute maximum wire deflection in each plane (ie. both the φ-z and $\varnothing$-z planes).

b) The modal shapes of the vibrating wire were required. Ideally a sequential display of the shape was required (ie.video) but this was not vital.

c) The wire tension was required, immediately after the braid point (or its equivalent), or at the wand tip.

2.3.1 Test Rig One

Test rig number one was built early in the project and was an attempt to correlate the theory with a mechanism similar to that used on a current rotary braider (Rockwell RB2). The rig consists of a bobbin, from which wire is drawn, a wire tension control system, a crank driven wand mechanism and a slow turning "wind on" spindle which represents the product core, as shown in figure 2.3.10. The wire tension is measured immediately prior to the wind on spindle using a slipper and load cell arrangement. The tension control system consists of a spring loaded arm attached to a spindle. A band brake acting on the bobbin brake drum is wrapped around the spindle. The wire is passed around the roller on the tip of the arm so that an increase in tension deflects the arm which turns the spindle, releasing the brake and allowing wire to be drawn off the bobbin. The wand mechanism is a 4-bar crank-rocker with a relatively long coupler to provide approximately sinusoidal wand tip motion. The orientation of the mechanism is based loosely on that used on the Rockwell RB2 rotary braider. This results in the wire length from wand tip to braiding point (tension measuring pulley) changing by 38mm every half wand cycle. This rapid change in wire length cannot be catered for effectively by the tension control mechanism and results in a region of low tension as the wand moves towards its central position, and a region of high tension when moving away from the central position.

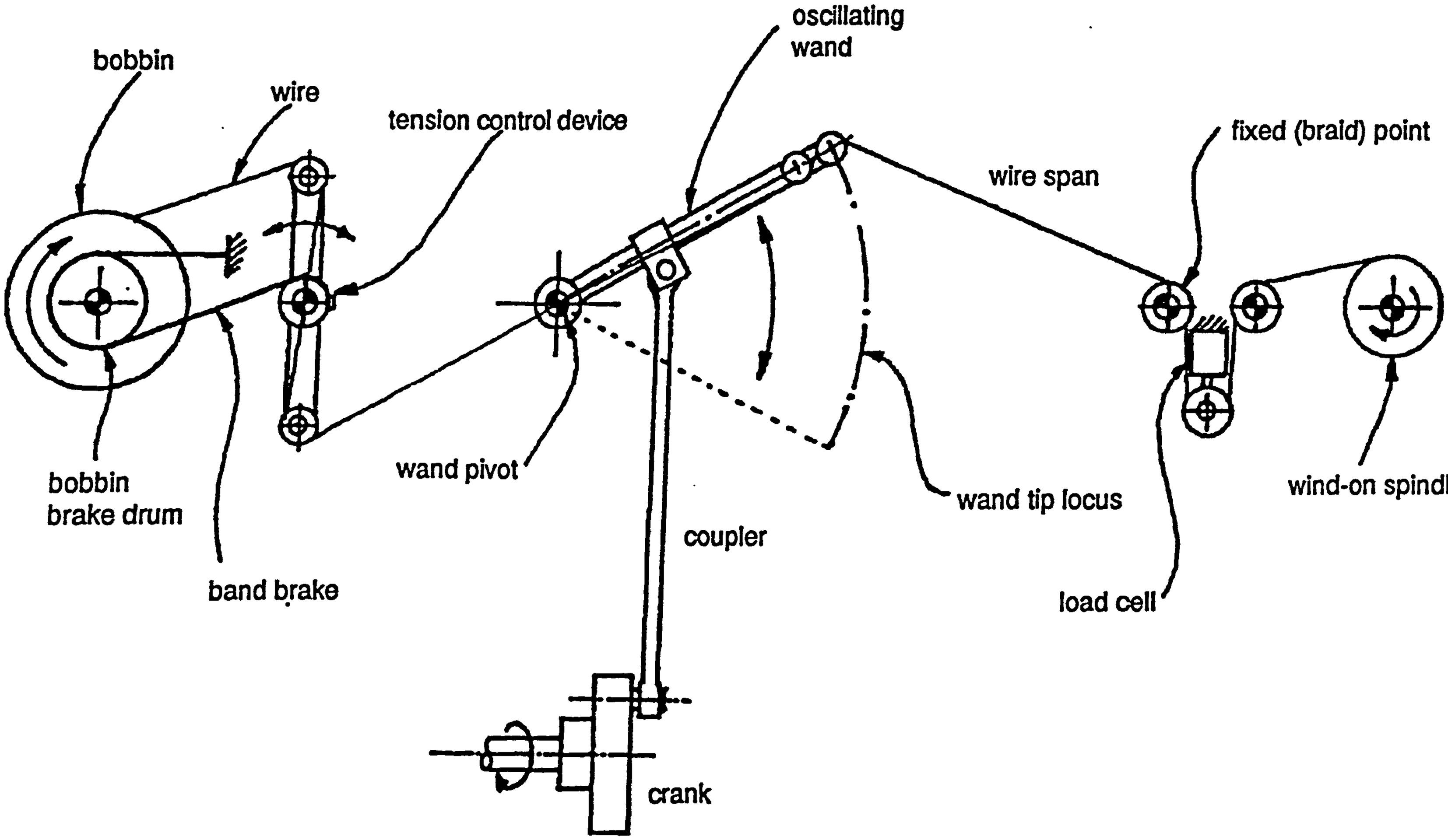

Figure 2.3.10 Schematic of test rig 1

Experimental Results - Test Rig One

The absolute wire deflection was measured using an adjustable "slot". The size of the slot was decreased until the moving wire touched it, which was determined using electrical contacts on the slot and wire. At the envisaged maximum speed of 15Hz, (900rpm) which represents 150rpm of the machine, the critical slot width was found to be 8 - 10mm and the maximum wire overshoot in the direction of motion was 10 -15mm.

The shapes of the wire at outswing and inswing were photographed using a high speed camera and were viewed "manually" using a strobe. The shape of the wire at wand outswing, and therefore high tension, is shown in figure 2.3.11.

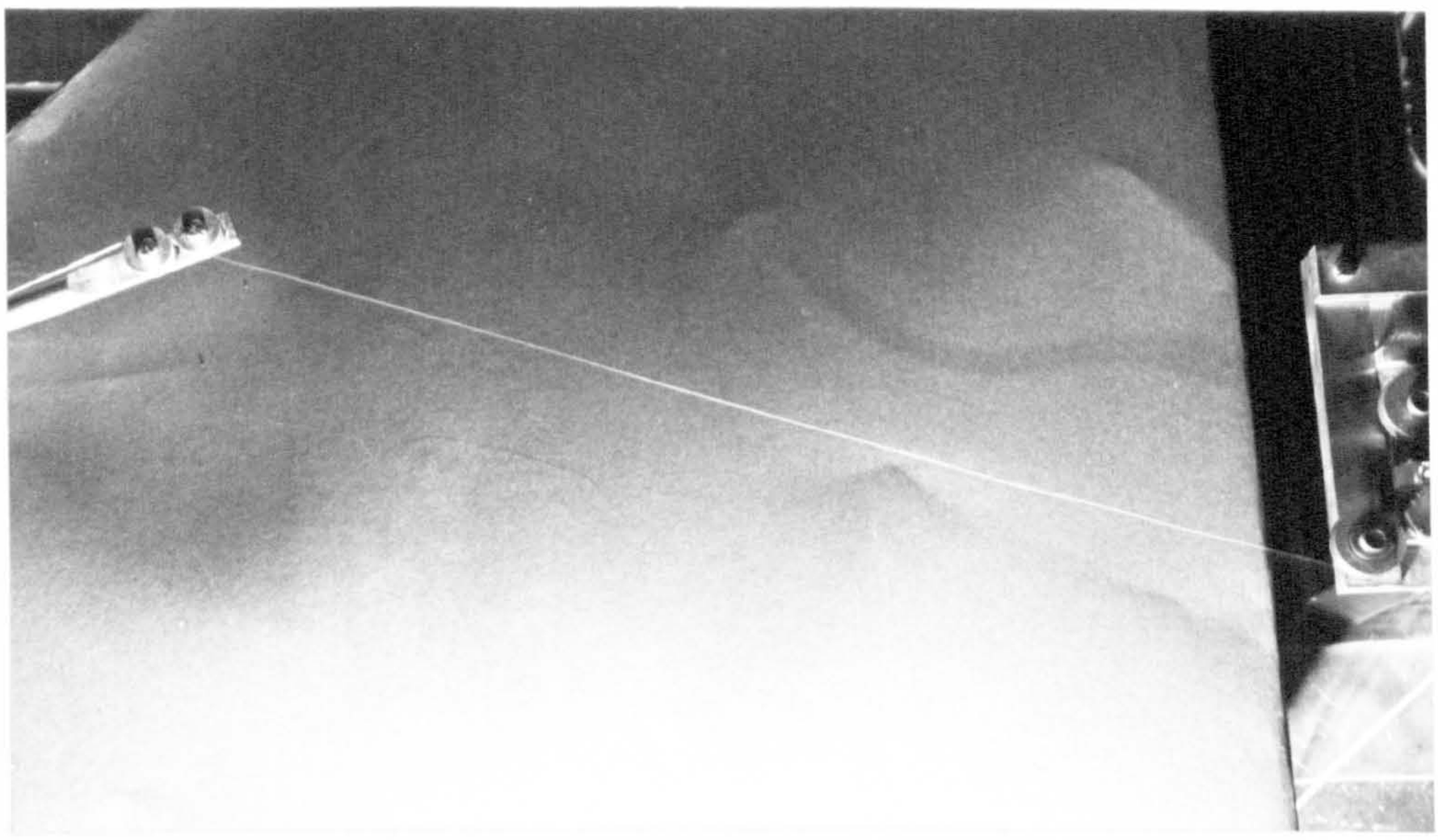

Figure 2.3.11 Wire behaviour at high tension

The shape at wand inswing (low or zero tension) is shown in fig 2.3.12. These clearly demonstrate the wave form which the wire adopts under very low tension and that there is practically no deflection at a higher wire tension.

The corresponding wire tension history plot is shown in figure 2.3.13 and clearly shows the two broad regions of different tension for wand outswing and inswing.

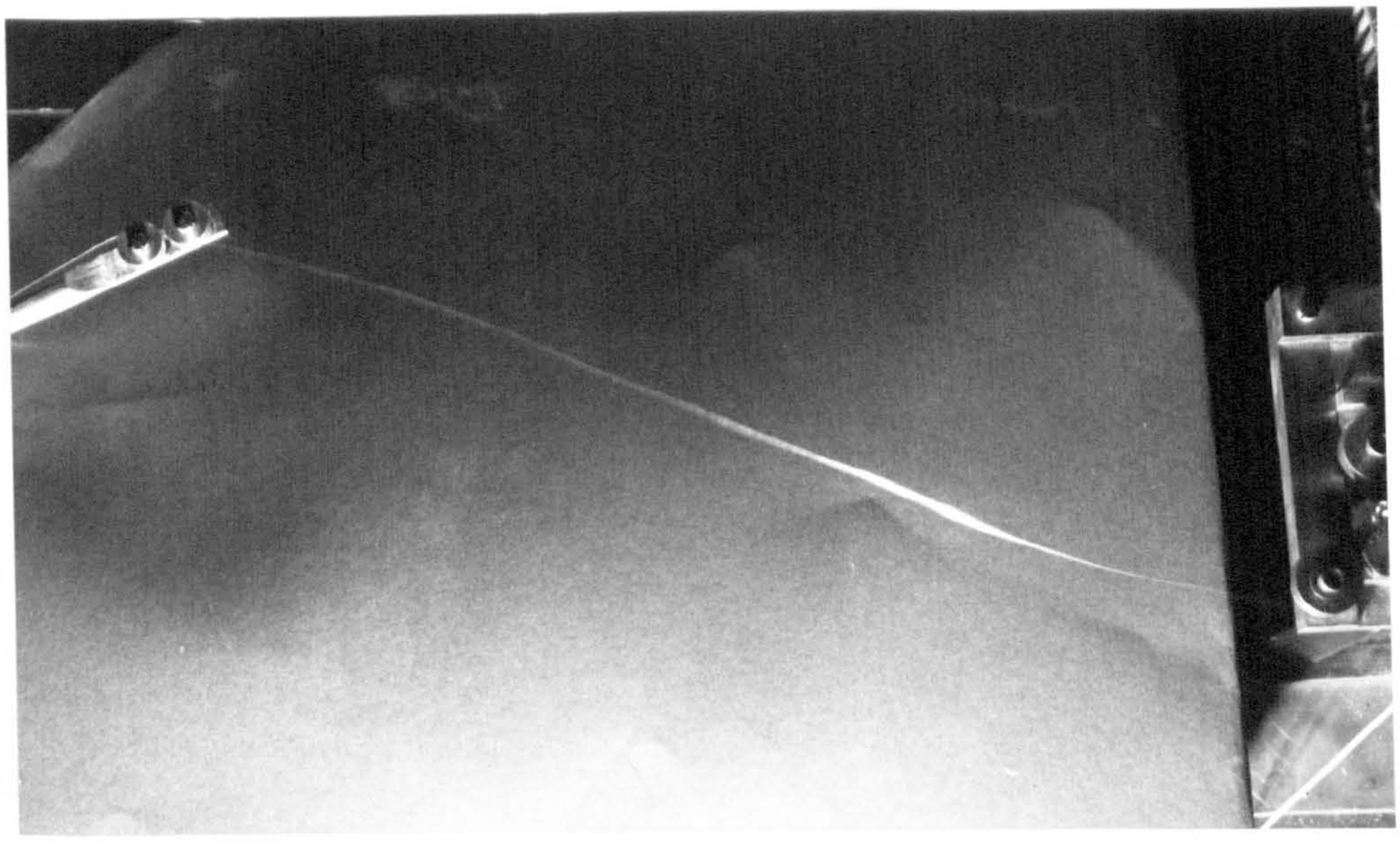

Figure 2.3.12 Wire behaviour at low tension

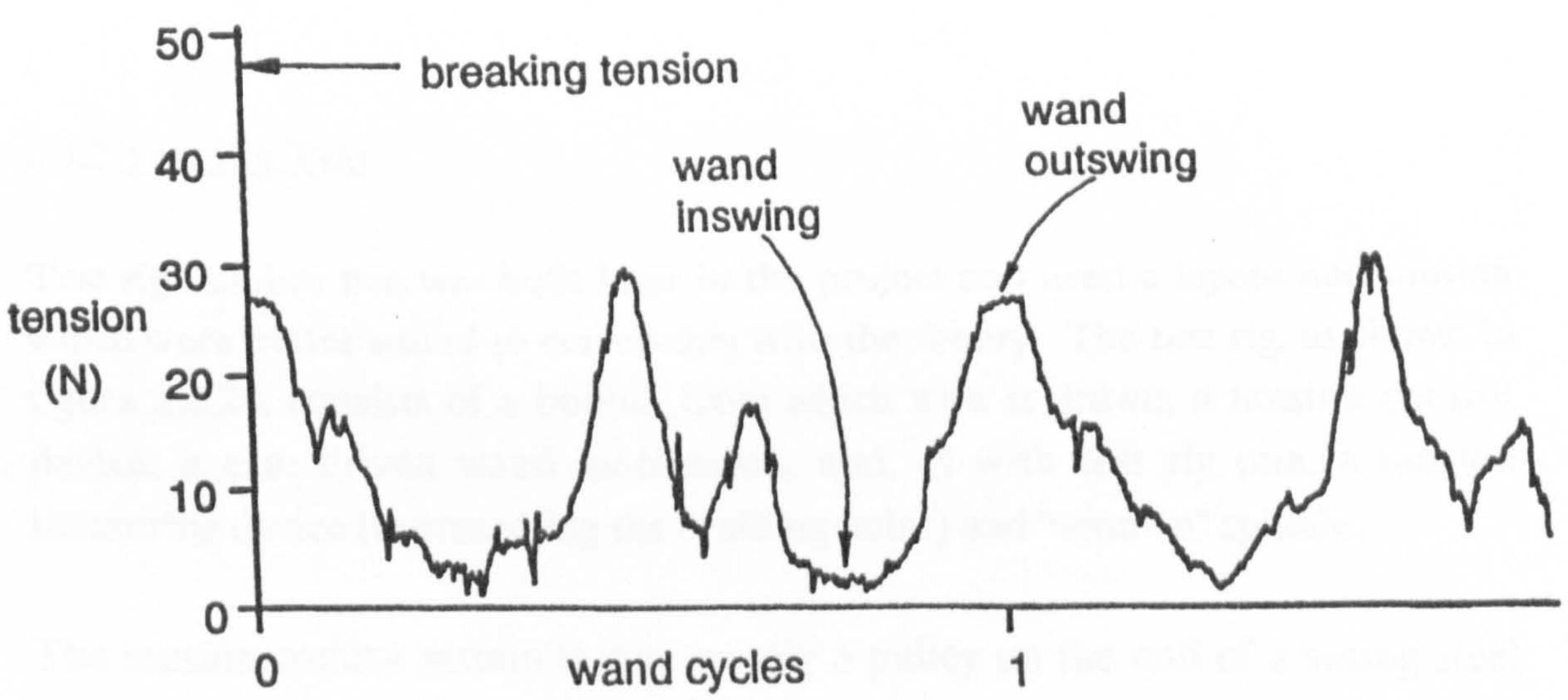

Figure 2.3.13 Wire tension history plot for test rig one, at 15 Hz.

Conclusions From Test Rig One

The major conclusions to be drawn from experiments on this rig is that to maintain a tension tolerance, the wire length from wand tip to braid point should not change throughout the wand cycle.

Expecting the tensioning mechanism to cope with a change in wire length of 38mm at a frequency of 30Hz is unreasonable (especially bearing in mind that 5N tension is the minimum, and the device must allow up to 50N tension).

The wire shapes photographed indicated that the theory may be in the right ball park but without a more constant tension, reasonable correlation is not possible.

In theory there should have been no deflection in the plane perpendicular to wand tip amplitude ("minor" plane) since the wand and wire move in one plane. This indicates that the measured minimum tension is incorrect and that the actual wire tension between wand tip and braid point is zero for a period, which initiates deflections in the "minor" plane.

The relatively large deflections measured in both planes probably occur at very low tension and are therefore not representative of those expected on a constant tension system.

2.3.2 Test Rig Two

Test rig number two was built later in the project and used a layout and motion which were better suited to correlation with the theory. The test rig, as shown in figure 2.3.20, consists of a bobbin from which wire is drawn, a tension control device, a cam driven wand mechanism, and, as with test rig one, a tension measuring device (representing the braiding point) and "wind on" spindle.

The tension control system is now merely a pulley on the end of a spring steel strip. The bobbin brake is a constant force band brake.

The wand is a rocker arm which pivots about an axis which passes through the braiding point. The wire length from wand tip to braiding point now remains constant throughout the wand movement. The wand features two track rollers which follow a trough cam cut into the face of a disc. The motion of the wand is a triple harmonic. The wand is constructed from carbon fibre to reduce its inertia and, therefore, increase the life of the follower rollers.

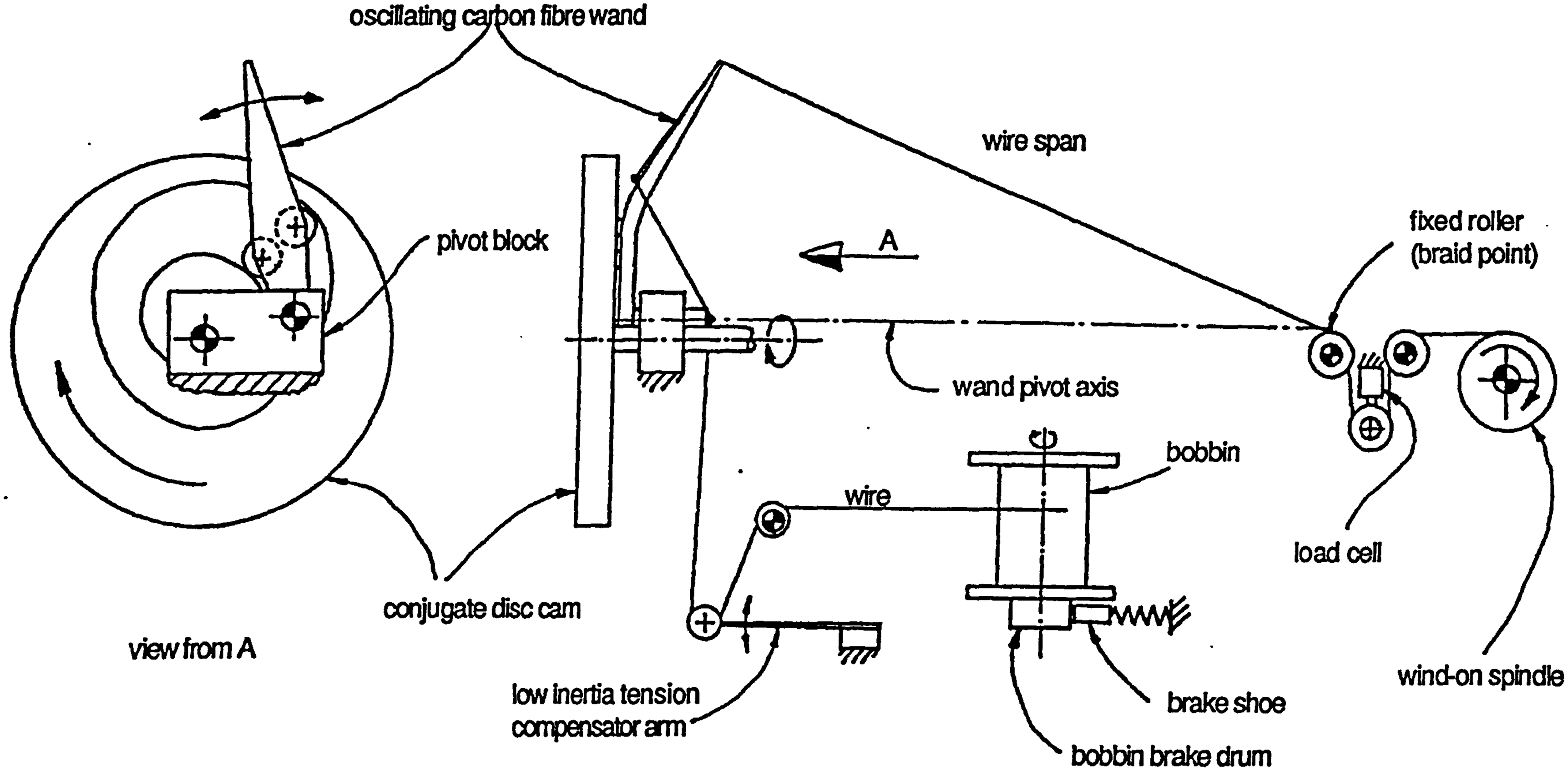

Figure 2.3.20 Schematic of test rig 2

Experimental Results - Test Rig Two

The absolute wire deflection was measured using an adjustable slot as on test rig one. At 15Hz wand frequency (150rpm of the machine) the critical width of the slot was 5mm and the maximum wire overshoot in the major amplitude axis was 10 - 12mm.

The shape of the wire was viewed with a strobe and a video camera used to obtain sequential frames. The high speed video could not detect all of the wire, so sections only were viewed to obtain maximum deflections.

The corresponding tension plot at 15Hz (fig 2.3.21) shows the greater uniformity compared to that for test rig one.

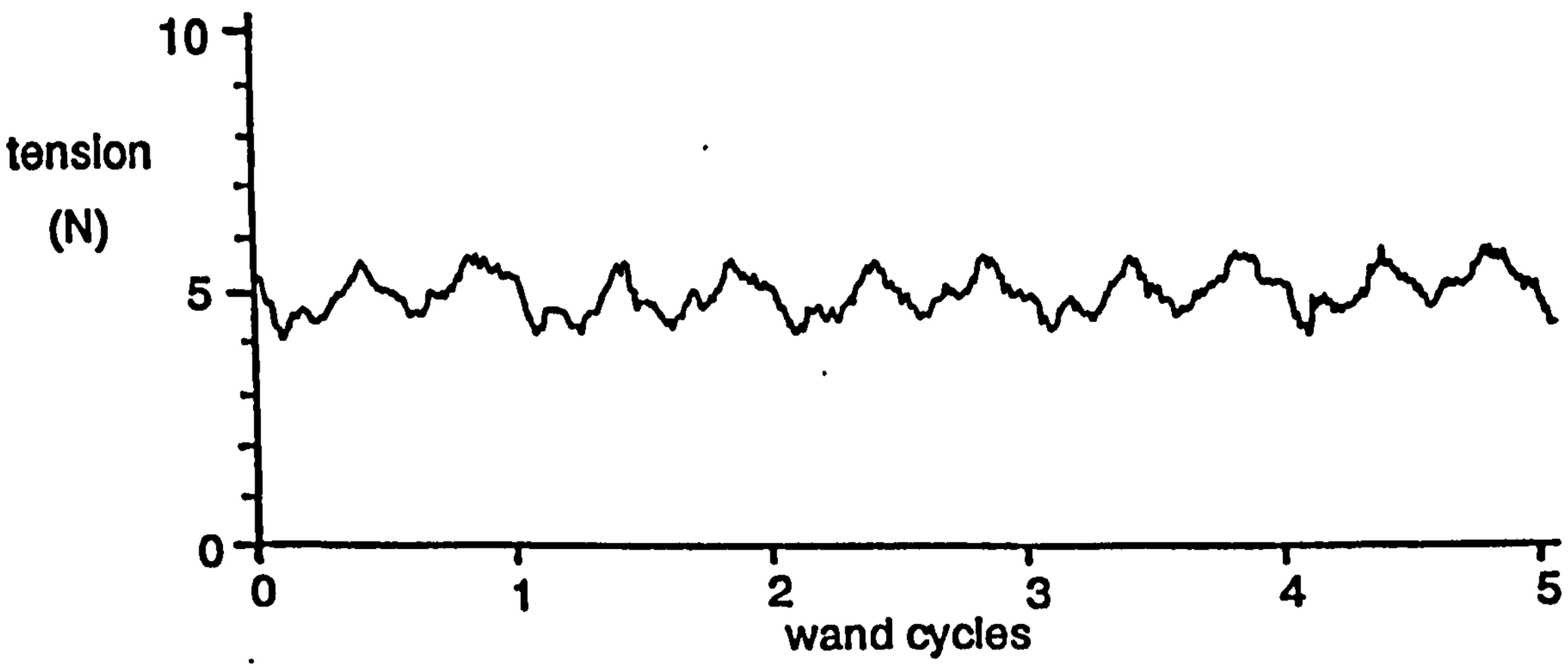

Figure 2.3.21 Wire tension history for test rig two, at 15 Hz.

The video recording revealed the wire motion to be different to the essentially sinusoidal wand motion used on test rig one. The triple harmonic motion employed on test rig two results in a period of low acceleration at full wand amplitude. At this point the wire vibrates, adopting its fundamental mode shape, but does not complete a full cycle of vibration before the wand accelerates away.

When using a multi wire strand the spread of the (seven) wires can be seen to be a maximum of 7mm.

Conclusions from Test Rig Two

The wire behaviour, when at a reasonably constant tension, correlates well with the theory and the deflection in the major amplitude plane measured on test rig two show this.

The deflections of 5mm recorded perpendicular to this were greater than the 2.5mm expected at the wand amplitude mid position, but are still within reasonable experimental error. The results using a multi wire strand show that any loose (catenary) wires are supported to a large degree by the remaining strands in tension. The 7mm maximum spread of wires verifies this as a typical catenary test over this span yields around 10mm.

2.4 Correlation of Theory and Experimental Results

The theory for the behaviour of an oscillating wire correlates exceptionally well with experimental results.

Both the shape of the wire and the corresponding maximum deflection in the plane of major wand tip amplitude support this.

The theoretical deflection of the wire perpendicular to this plane is not so accurate and this suggests a deficiency in the theory particularly regarding the separation of the wire behaviour into two planes, and the possible over simplification of the original model in search of an analytical solution.

However, with these accounted for the theory as a whole can be used to predict the behaviour of a wire for most wand motions envisaged.

2.5 Conclusions from Analysis of the Moving Outer Wire

The major conclusions which influence the choice of wand and wand motion are:

1) To retain low wire deflections the tension level in the wire must be maintained above a certain level.

2) To achieve constant tension the length of wire from wand tip to braid point and from bobbin to wand tip should remain constant throughout the wand motion cycle.

3) For a given wand tip amplitude the lower harmonic content in the wand motion the lower will be the wire deflection.

4) The triple harmonic wand motion recorded peak wire deflections within the specifications required by the collaborating company.

5) In terms of lower wire deflections the ideal is the single harmonic motion.

6) A useful reduction in deflections when using multi wire strands could be achieved by improving the bobbin winding quality which in most circumstances is very poor.

CHAPTER THREE

KINEMATIC STUDY OF WAND MECHANISMS

3.1 Introduction

The wire deflector, or wand mechanisms are required to deflect each wire from an outer bobbin in and out of every other inner bobbin and its carrier. The wire is passed inside an inner bobbin by being guided into a slot in the track which supports the inner bobbin carriers. The inner carriers can then be driven over the slot and the wire then guided out to form the weave at the machine centre. Under ideal circumstances the slot in the inner bobbin carrier track should be as narrow as possible to avoid large changes in loading on the inner carrier bearings as they cross the slot. For this reason it is important that the outer wire span from wand tip to braiding point remains as straight as possible. Any deflection from the ideal straight line path requires a wider slot and results in either less space available to each inner bobbin and carrier, or a risk of wire snagging.

The theoretical and experimental analysis of the oscillating wire span reveals the major criteria for optimum wire control and minimum deflection:

i) The major requirement is for a constant wire length, from outer bobbin to braid point, throughout the cycle of wand motion since even a small change in length produces a change in tension which has a drastic effect on wire deflection.

ii) A range of motions and the corresponding wire deflections indicate the type of motion possible for a prescribed maximum deflection.

3.2 Mechanisms Which Allow Constant Wire Length Between Bobbin and Braid Point

There are two broard types of mechanism for providing a constant wire length from bobbin to braid point:

a) Any wand mechanism is used and a constant wire length is achieved by using a compensatory device which is synchronous with, and probably driven by, the wand drive system as shown in figure 3.2.01.

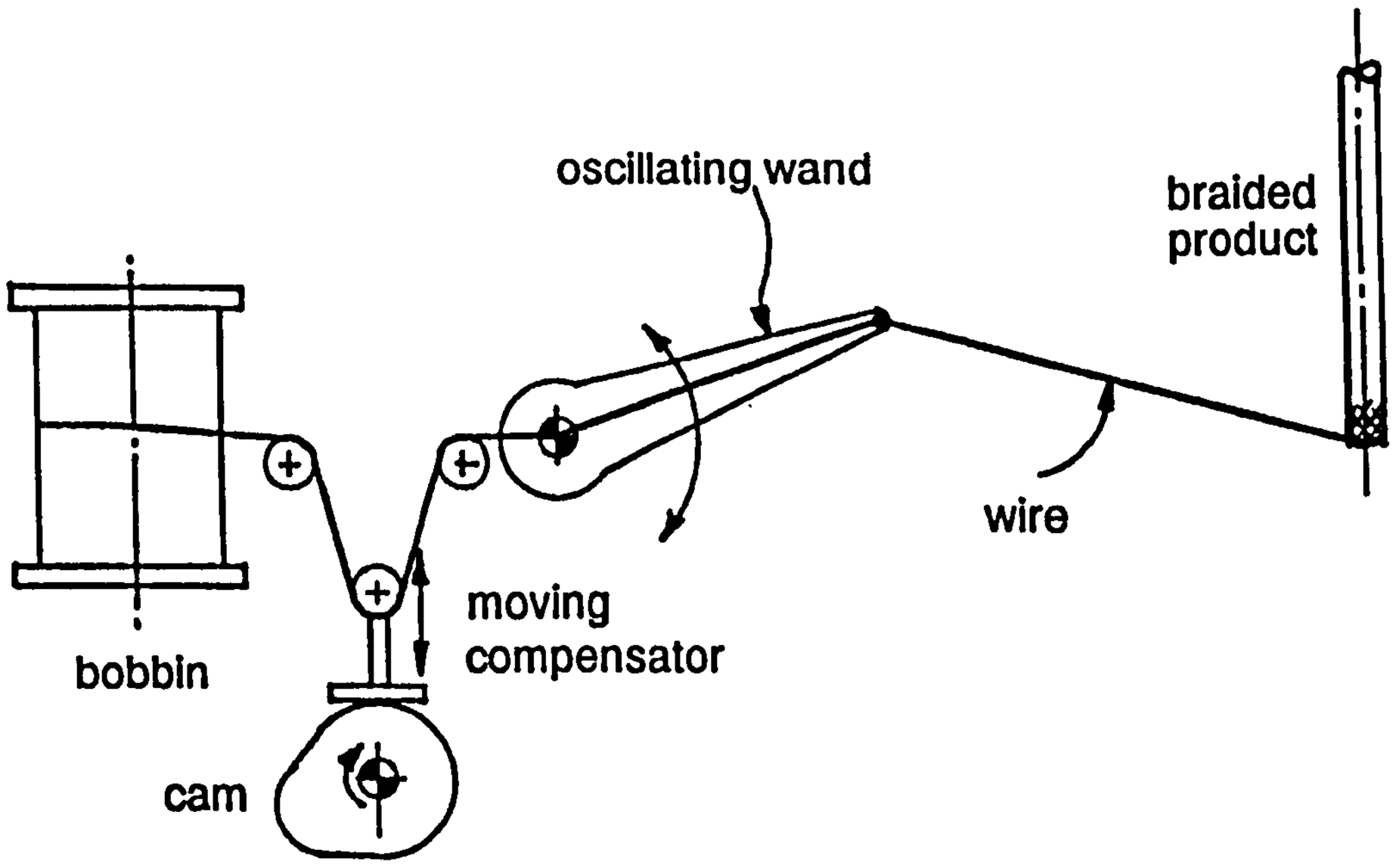

Figure 3.2.01 Wand with cam driven compensator

This type of device is not ideal, for although the overall wire length is constant, the length of wire span from wand tip to braid point is not (or the device would be unnecessary). Each pulley the wire passes around, however small the wrap may be, incurs a slight tension imbalance and this inevitably leads to a change in tension of the wire between wand tip and braid point.

b) A wand mechanism in which the wand tip locus is located at all times on a sphere whose centre is the braid point as shown in figure 3.2.02. The locus need not be merely arced or set in a plane, but the inner carrier track slot shape and the volume available to the inner bobbin will reflect any form the locus has.

This method of retaining a constant wire length assumes that there is a path from wand tip to ground of constant length through the linkages, and that it is feasible to accommodate the wire along such a route.

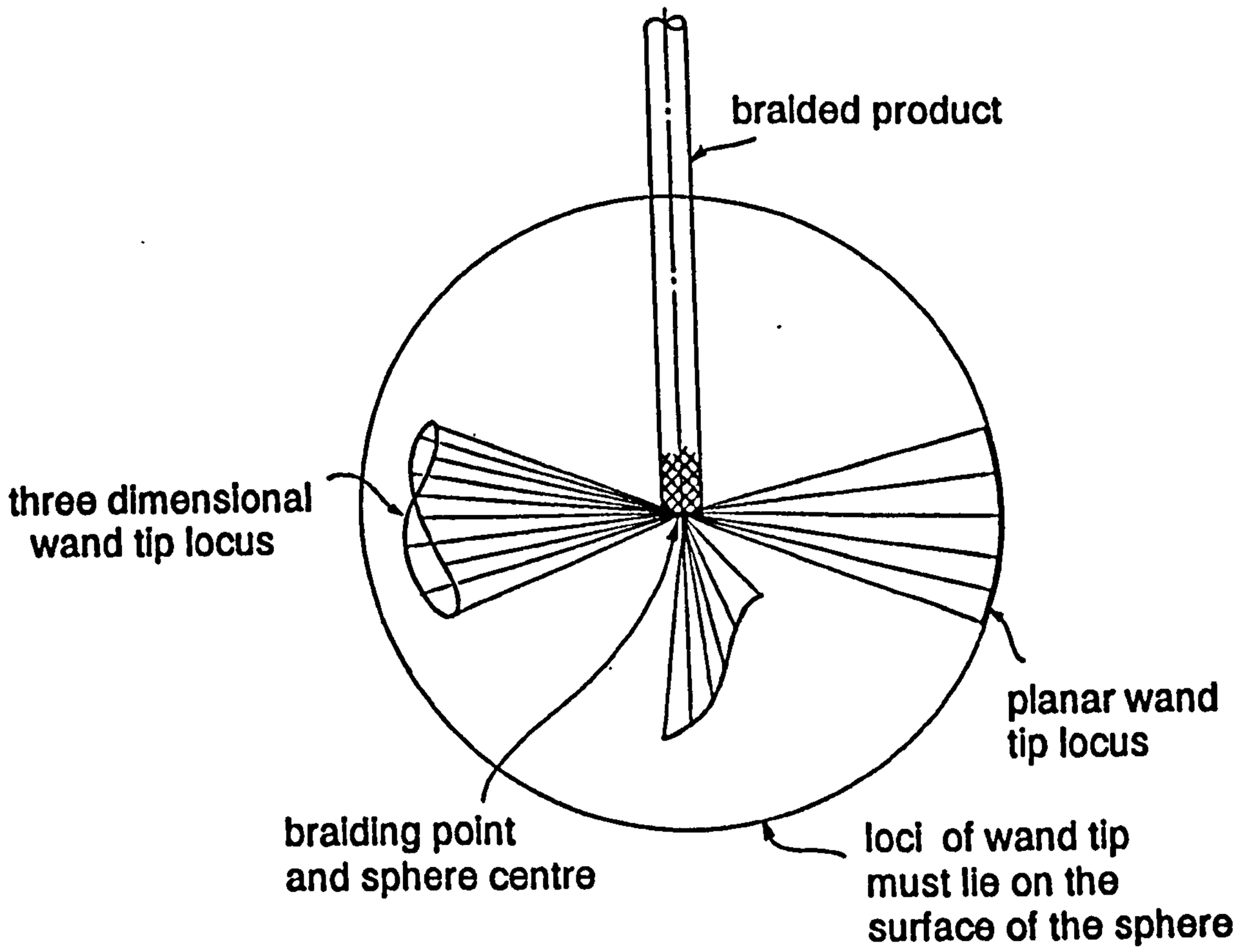

Figure 3.2.02 Possible wand tip loci for constant wire length

Of the two methods described in a) and b) above, method b) is the more attractive and potentially more elegant, less complicated and less costly. For these reasons this method is investigated first.

3.2.1 Wand Mechanisms which allow Constant Wire Length from Wand Tip to Braid Point

Of the many wand tip loci available, all of which lie on the surface of a sphere whose centre is the braid point, there are basically two which are readily produced by mechanisms featuring linkages. Both these are single line loci where the 'forward' and 'return' portions of the motion cycle are coincident, and both are simple arced lines.

a) <u>Wand Tip Locus Type (A)</u>

This locus is an arc with its centre at the braiding point and which lies in the plane containing the machine central axis (product axis) as shown in figure 3.2.10.

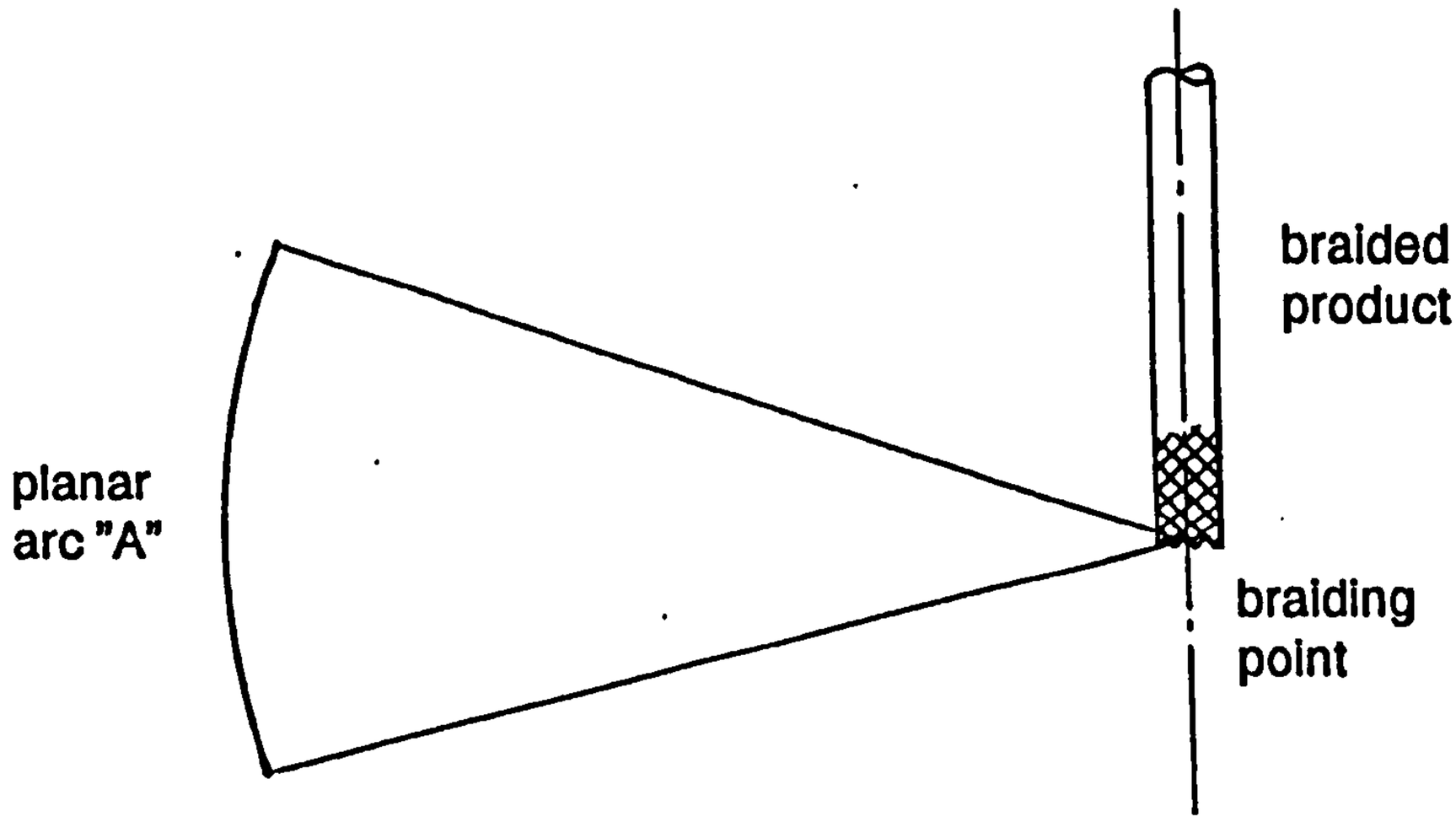

Figure 3.2.10 Wand tip locus arc 'A'

This locus type has the advantage that the wand tip motion is always perpendicular to the relative motions of inner bobbins and outer bobbins/wands. The wand tip motion now has the opportunity to create a symmetrical shape for the inner bobbin/carrier whilst using a "symmetrical" wand motion. This is advantageous to both wand and inner bobbin carrier design and to the overall machine optimisation.

This motion symmetry is very difficult, or impossible in many cases, if the wand tip locus does not lie in the same plane as the product/machine central axis. Additionally, the mechanism which produces such a motion is likely to also lie in the same plane as the locus and this is better able to support the loads imposed by a high wire tension.

b) Wand Tip Locus Type (B)

This is the arc of the circle obtained by slicing the appropriate sphere with a plane. The arc is therefore part of the perimeter of the base of a cone whose apex coincides with the braiding point as shown in figure 3.2.11.

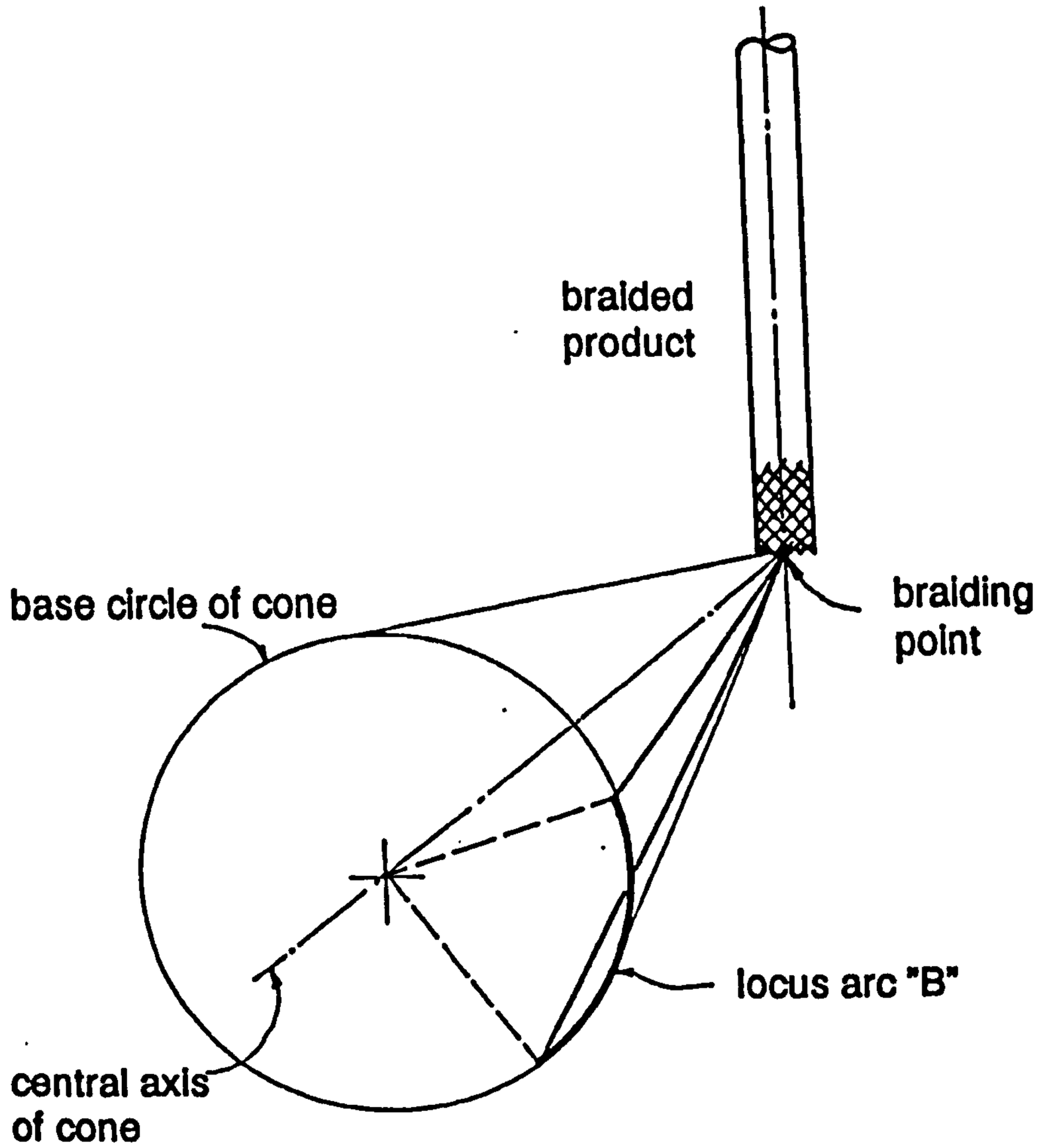

Figure 3.2.11 Wand tip locus arc 'B'

This type of wand tip path is potentially much easier to produce than arc (A) but the motion is not always perpendicular to the relative motions of inner and outer bobbins. The shape produced by the moving outer wires (into which the inner bobbins/carriers must fit) is, therefore, not symmetrical when the wand motion is, and vice-versa. The inner carrier track slot must now also be arced, or wider than necessary.

3.2.2 Considerations when Examining Wand Mechanisms

Two major considerations are reliability and cost, both of which are a result of the nature of braiding process and the current market climate. General reliability of wand systems has not in the past been good. Failures are usually related to fatigue of either the wand, or its drive, or the various bearings in the system. These failures can be attributed to various shortcomings. An "over engineered" wand, whilst structurally reliable, increases load on the drive system and bearings, leading to failure. An inappropriate or badly chosen wand motion also increases wand/drive/bearing loads, often by a large amount (as can wear or back lash). A wand material which does not have a fatigue limit stress will eventually fail, even though the bearing and linkage loads are may be reduced by use of a lighter material.

Most of the above factors affecting failure are exacerbated by increasing the number of links in the wand mechanism. This also increases the cost of each wand system. Other points which must be considered are the frame forces and moments transmitted by each system and whether balancing is appropriate, and the difficulty and cost of driving each wand mechanism. It must also be remembered that any wand system must lie radially outside the sphere on which the wand tip path lies. Thus, large linkage mechanisms will increase the overall size of the braider which is undesirable for aesthetic reasons.

Since arc (A) is theoretically more desirable, initially a mechanism to produce this arc is sought.

3.2.3 Mechanisms to Produce Arc (A)

4-Bar Wand Mechanisms

A range of Grashoff-1 4-bar wand mechanisms are examined in an attempt to obtain arc (A). An analogue computer is used to model a large range of possible 4-bars in order to find approximate configurations of suitable mechanisms. The analogue representation enables link lengths to be changed quickly and an immediate moving display of the mechanism and coupler curve can be seen.

The more suitable mechanisms are analysed in more detail on a digital computer

to optimise the coupler curve, thereby ensuring:

i) The coupler curve consists of a line (i.e. the coupler curve has no envelope).

ii) The coupler curve radius of curvature remains as constant as possible ($\pm 2\%$ is considered desirable) throughout the complete mechanism cycle.

The analysis of a large number of 4-bar configurations shows that, to retain a constant radius of curvature of the coupler curve (i.e. under $\pm 2\%$), the ratio of coupler curve arc length to radius of curvature is too large. The best mechanism found is shown in fig. 3.2.30.

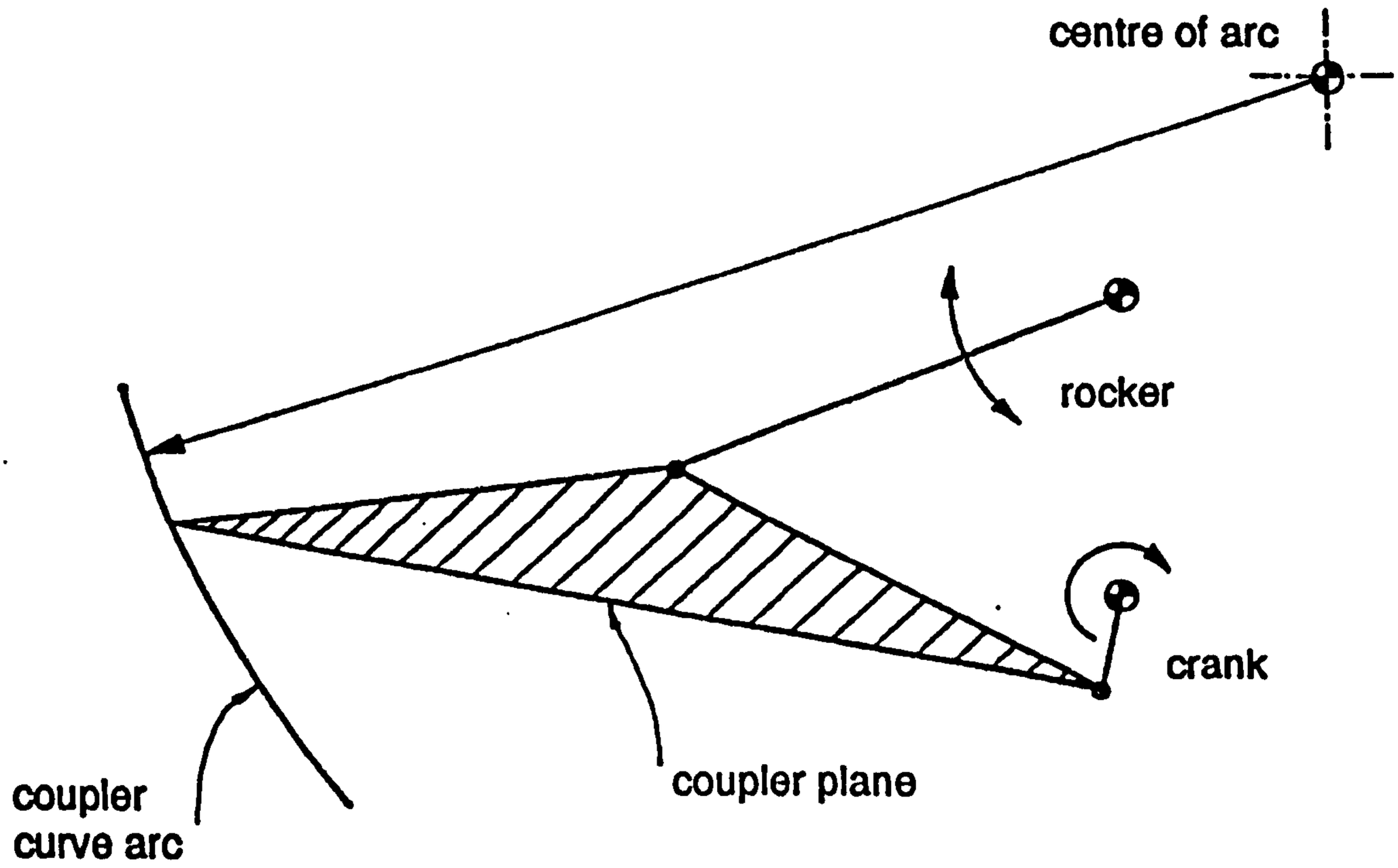

Figure 3.2.30 Grashoff-1 four bar wand mechanism

This mechanism has a large coupler plane and the centre of curvature is on the opposite "side" of the mechanism to that required (i.e. the mechanism is inside the wand tip path "sphere"). Indeed most suitable Grashoff-1 4-bars feature a large coupler plane which would lead to difficulties in balancing which, in turn, restricts maximum speed.

For these reasons a wand mechanism consisting of a Grashoff-1 four-bar (i.e. crank driven rocker) which produces a coupler curve of type "arc (A)" is unsuitable as a final wand design.

Crank-slider Wand Mechanisms to produce Arc (A)

A different type of "four-bar" mechanism capable of producing arc (A) is the crank and slider, or slipper, arrangement. The slipper represents the wand tip (i.e. the wire passes through an eye in the slipper) and runs in a curved track which traces an arc about the braiding point so replacing the rocker of the four-bar as shown in figure 3.2.31.

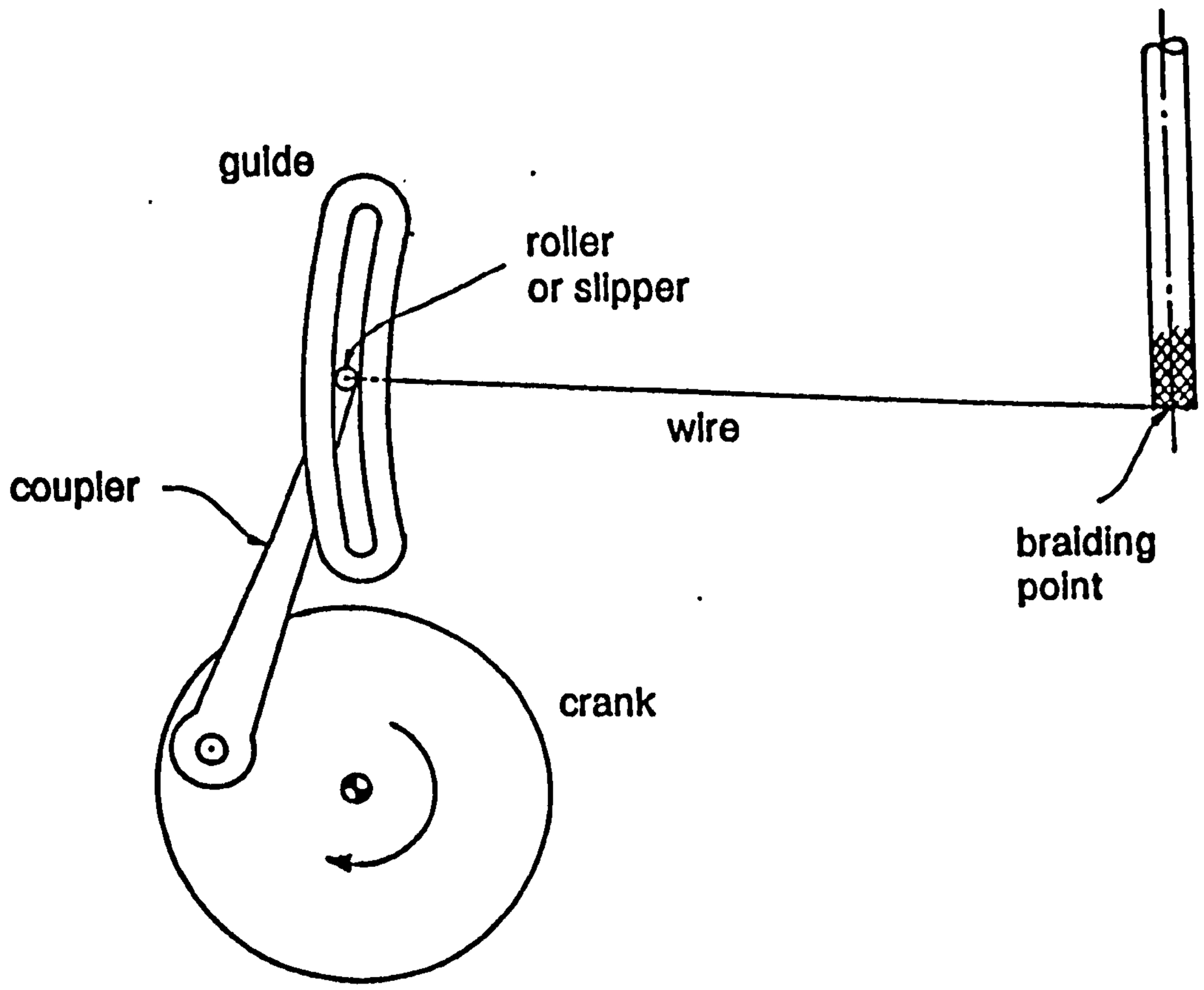

Figure 3.2.31 Slider crank wand mechanism

The major drawbacks with this system are that to achieve simplicity the crank must provide the full range of "wand tip" motion. An amplifying effect can be achieved by introducing an additional dyad, making the mechanism a six bar.

The high speeds necessary at the slipper/track introduce bearing longevity problems and a direct crank drive is not desirable as it demands a large crank at the periphery of the machine. But, although feasible, for these reasons the slider-crank system is not ideal as a wand mechanism.

Six-Bar Wand Mechanisms to Produce Arc (A)

All the six-bar mechanisms studied are Watt type six-bars (this is the type of six-bar used by Rockwell on the RB2).

Two approaches are used to obtain the desired arced path of the coupler curve, arc (A).

i) Using a portion of a Grashoff-2 four bar couple curve which gives the desired path, and subsequently driving this four bar in that region with a crank and coupler (diad), or a cam, so producing a six-bar mechanism. Thus the rocker output from the first Grashoff-1 four bar is used as the input of the second Grashoff-2 four bar. This is represented in figure 3.2.32.

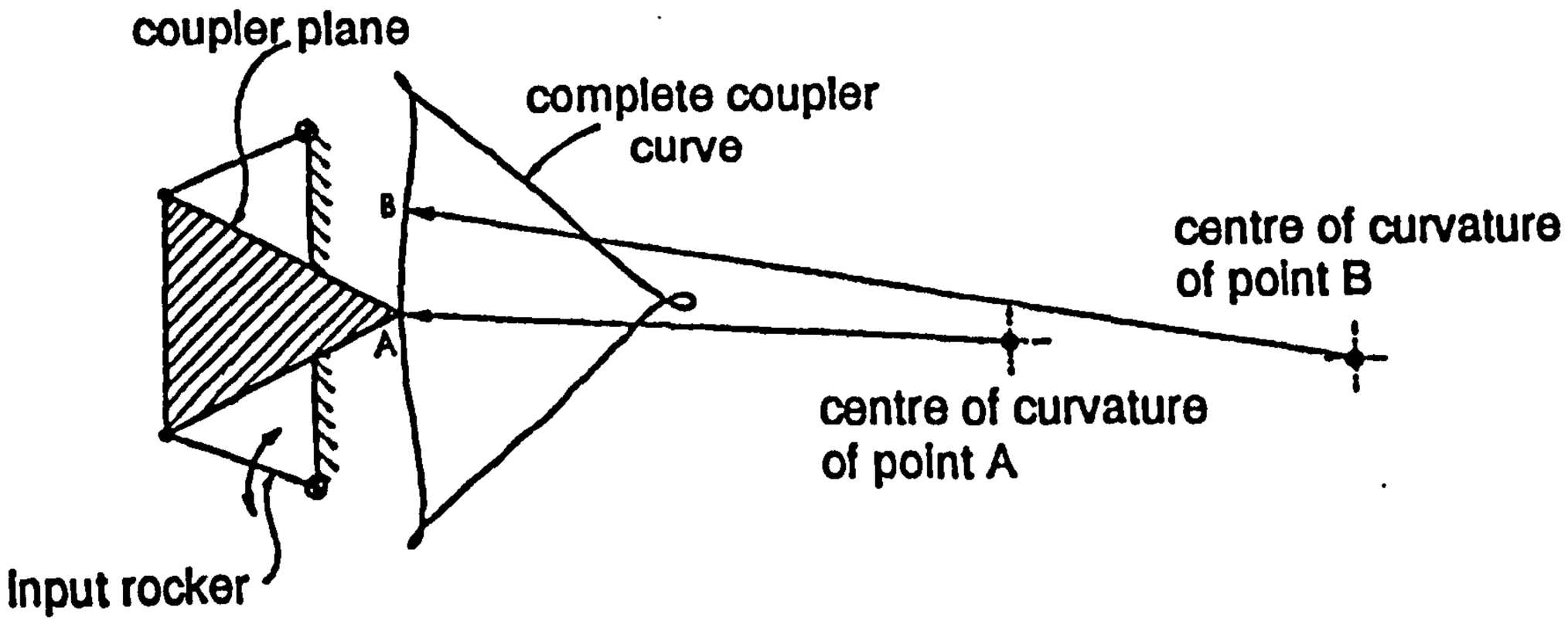

Figure 3.2.32 Grashoff-2 four bar wand mechanism

A range of Grashoff-2 four bar coupler curves which have a portion of approximately constant radius of curvature are, again, initially found using an analogue computer model of a four bar mechanism.

The appropriate four bars were examined in more detail on a digital computer program model for Grashoff-2 four bars. The radius, and centres, of curvature of the coupler curve points were found and minor adjustments to link lengths made to optimise the range over which the centre of curvature remains, to a degree, stationary.

The procedure shows that of the coupler curves examined, the centre of curvature will not remain in precisely the same position for the length of arc required, unless the four bar is of such a large proportion as to render it impractical.
The radius of curvature at points along the coupler curve tend to infinity as a crunode or cusp is approached. Since the basic criteria for an arc (A) of $\pm 2\%$ error in radius is not satisfied, unless a massive mechanism is used, this system is not suitable as a wand mechanism.

ii) The second type of six-bar mechanism examined in an attempt to produce an arced coupler curve (Arc (A)) is a modified focal mechanism. A focal mechanism is a four bar with four additional links that can be separately pivoted to each of the sides of the four bar and which join at a common pivot point, usually within the four bar mechanism, and allow the mechanisms to move freely. Thus if a Grashoff-1, crank-rocker, four bar is chosen in which the rocker represents the wire, from the braiding point to wand tip, then upon addition of a focal mechanism the rocker may be removed to leave a Watt type six-bar as represented in figure 3.2.33. The coupler point, or wand tip, is the end of the original four-bar coupler which was attached to the rocker. The mechanism may be driven by the original crank or by one of the focal links, and traces an exact arc about the original rocker pivot point. This mechanism appears to be an ideal solution, but at a certain position the links become folded and so joint pressure angles become 90°. Thus, without the addition of further links to define the mechanism in the folded position, or an additional driving crank/coupler or cam system to utilise part of the range of motion, the mechanism becomes unsuitable for practical reasons.

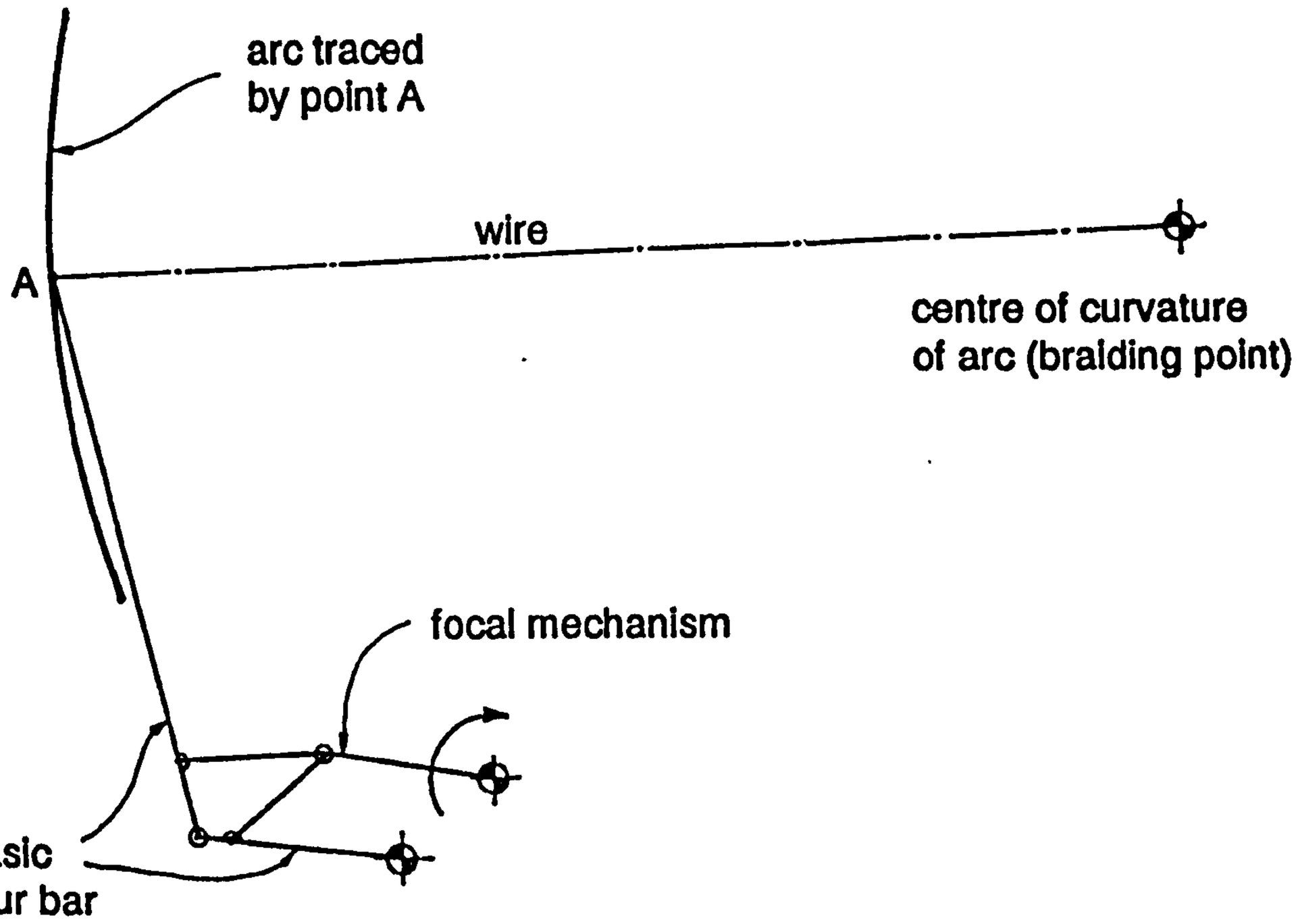

Figure 3.2.33 Focal wand mechanism

3.2.4 Mechanisms to Produce Arc (B)

A wand mechanism which provides a coupler curve as arc (B) is simply an oscillating rocker that pivots about an axis which passes through the braiding point as shown in figure 3.2.40.

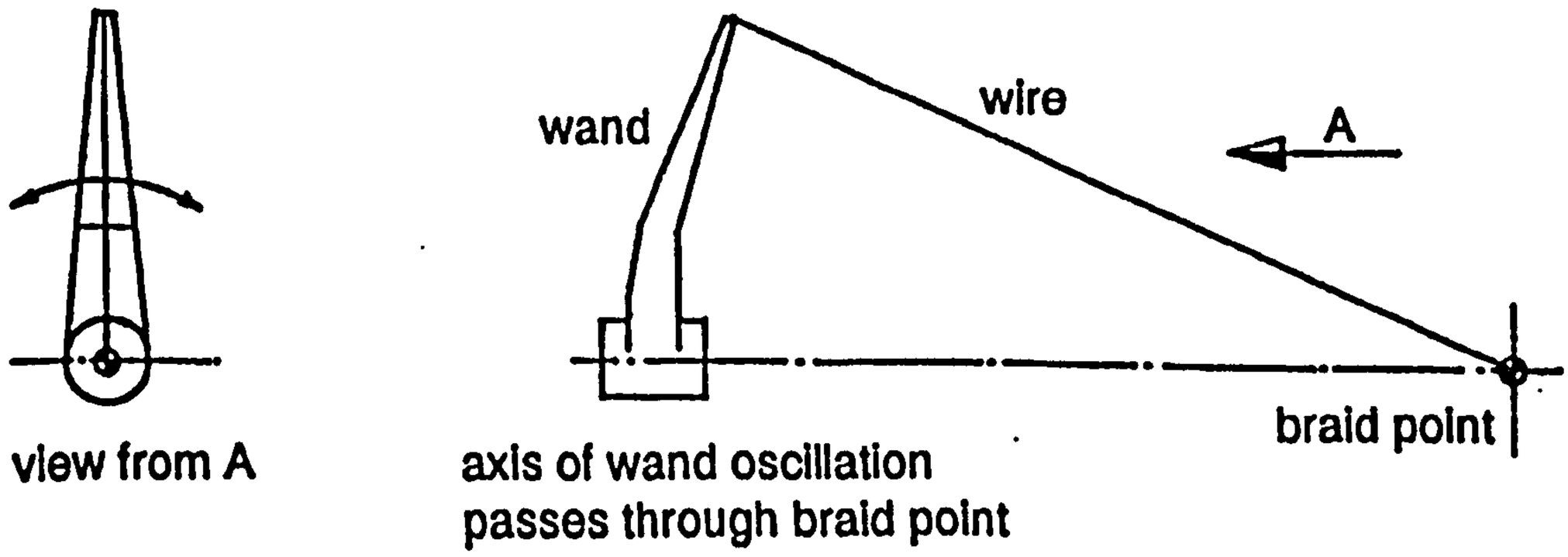

Figure 3.2.40 Rocker mechanism to produce arc B

The wand may represent the rocker of a Grashoff-1 four bar and provide a means of amplifying the displacement available from the crank. The wand drive may alternatively be a cam system of some description acting through a coupling link or directly onto the wand (i.e. the cam follower is part of the wand).

The position of the wand pivot point relative to the track may be varied to allow different portions of the arced wire path to be utilised in the inner carrier track slot. This allows a slanted slot to be used as shown in figure 3.2.41, which may increase inner carrier/track bearing performance.

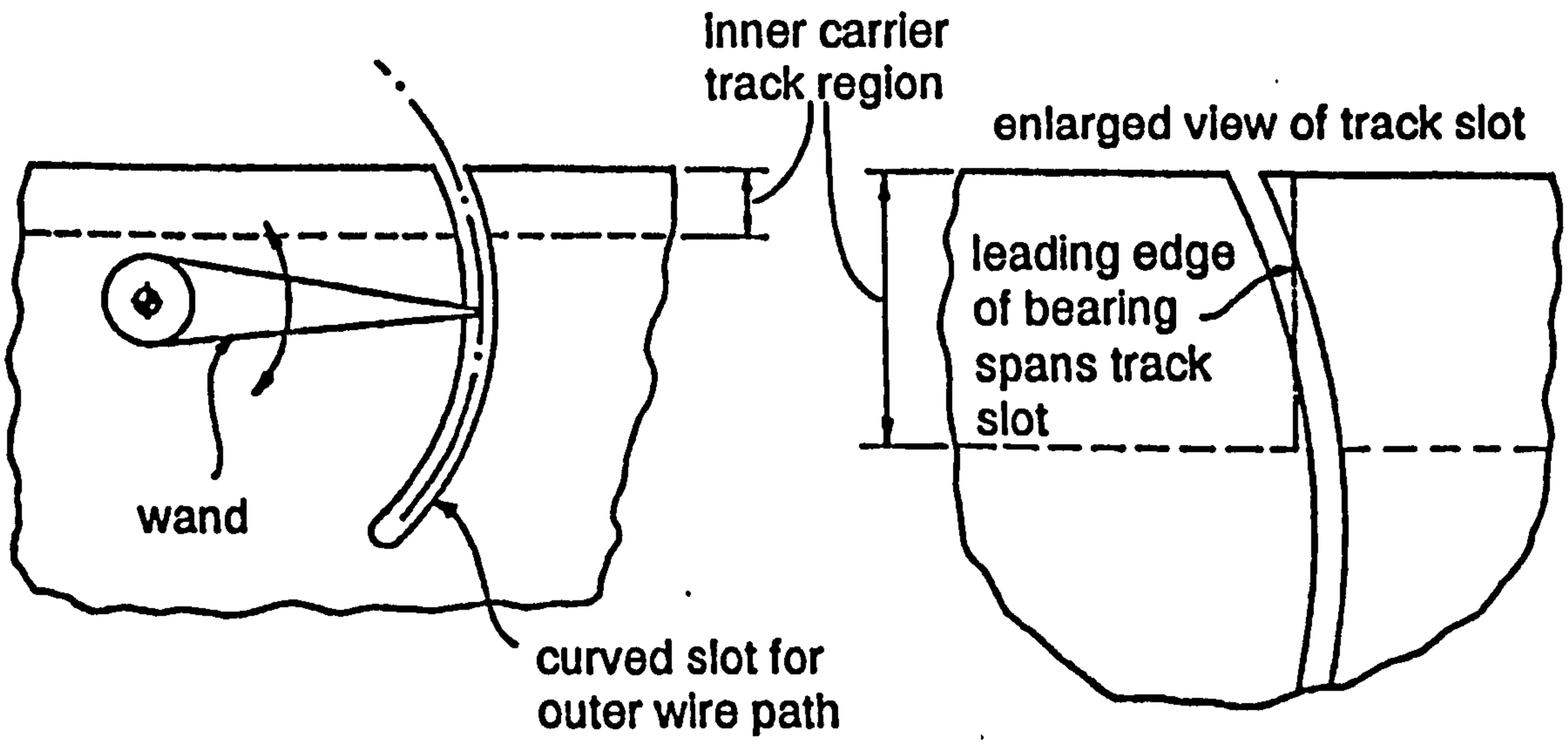

Figure 3.2.41 Wand arrangement allowing a slanted track slot

This wand mechanism for producing arc (B) is so elementary and simple that further devices to achieve this were not sought.

3.2.5 Wand Mechanism Selection

The most desirable wand tip path is arc (A). However, the search for a suitable mechanism to achieve this concludes that a slider-crank device with marginal performance prospects and relative complexity is the best choice.

In contrast, the simple rocker necessary to produce arc (B) shows great promise in both its crank/coupler and cam driven forms. The advantages of this system, (simple, inexpensive, compact, versatile and reliable) out weigh the disadvantages, inherent in a system using arc (B) as its wand tip locus.

For these reasons the rocker arm which produces arc (B) as its wand tip locus is chosen as the design for a wand.

The final form of the basic wand mechanism, the motion imparted to it, and the means by which this is achieved is formulated in conjunction with all the other major machine elements on the rotary braider.

3.3 Wand Motion Generation

The wand motion may be generated by any drive system (including servo motors, hydraulics, pneumatics etc.), but there are three realistic types of drive which are considered.

i) Crank driven wand mechanism.
ii) Cam driven wand.
iii) Hybrid crank/cam driven wand.

The wand mechanism chosen is the simple rocker arm which may readily be driven by any one of the above methods. It is important to remember that, on a 24 carrier braider, there are 12 outer bobbins and wand mechanisms revolving relative to ground and that the drive to each wand should not compromise the inner bobbins/carriers operation.

3.3.1 Crank Driven Wand Mechanisms

Each wand rocker is driven by a separate crank-coupler arrangement, and each crank drive is (probably) taken from a common gear at the machine centre, as represented in figure 3.3.10.

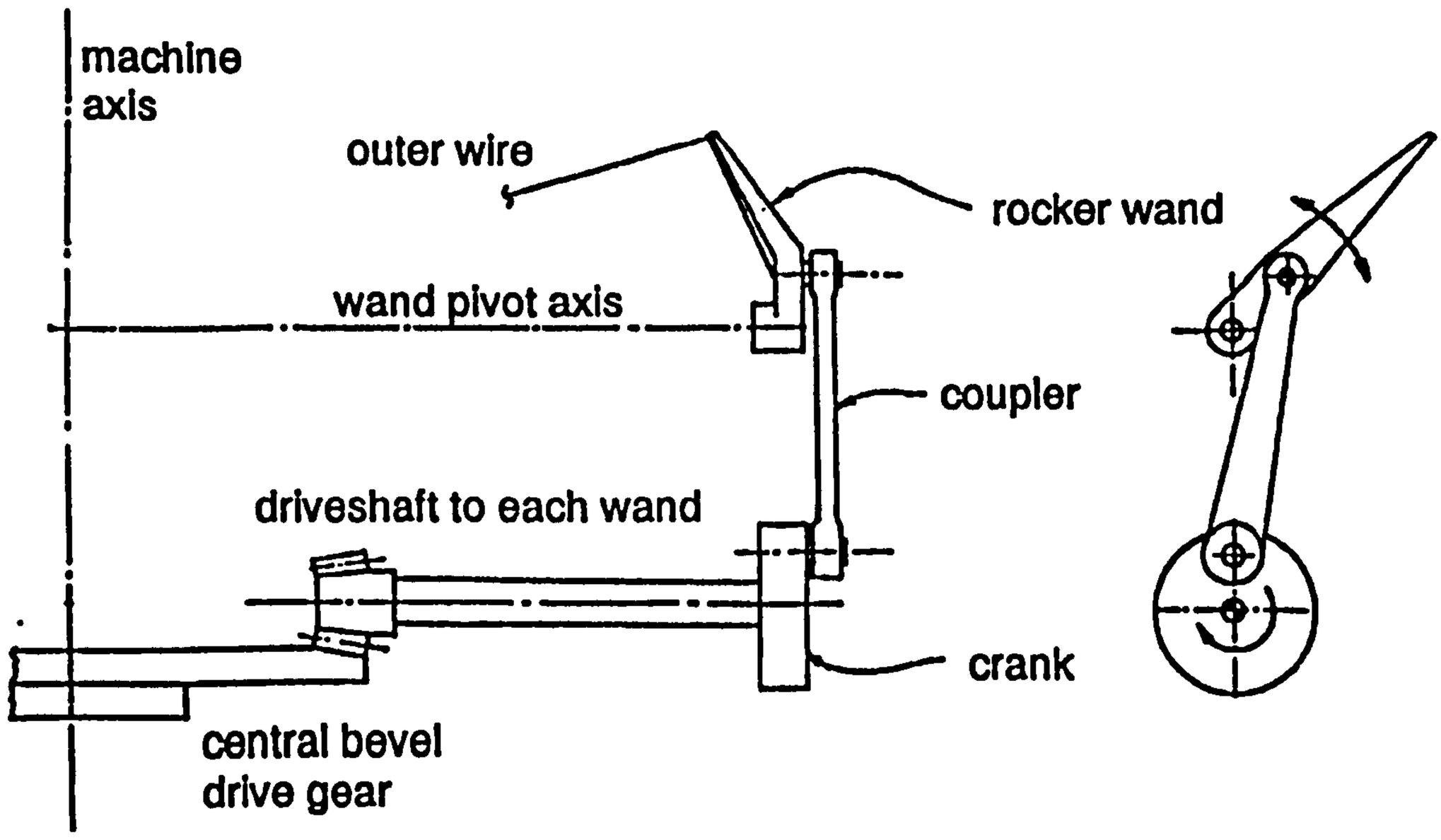

Figure 3.3.10 Crank driven wand

A drive of this type produces essentially single harmonic type motion (although it never produces true single harmonic motion). The motion may be modified slightly by changing the geometry of the linkages, but link angles are compromised as the motion becomes less "symmetrical" and higher harmonic content increases. A single harmonic motion is most desirable for minimum wire deflection. The shape/volume, produced by the outer wires, available to the inner bobbins is equal to that for a triple harmonic motion, if the wand amplitude is increased. Providing the inner carrier drive can accommodate such a seemingly unnecessary outer wire "overshoot" without restricting performance, this increased amplitude is not a problem (Ref. figure 2.2.12, chapter 2, base shapes for various motions). Although the system is relatively complex and costly compared to certain cam systems it is potentially the most reliable wand drive type. It has no major disadvantages, other than appearing anaesthetic, in comparison with other braider wand systems on the market.

3.3.2 Cam Driven Wand Mechanism

A cam driven wand offers an infinite range of motions and allows the wand to be controlled (kinematically) in a precise manner. It is also the most direct method of driving the wand since the cam follower may be part of, or attached directly to the wand itself. The major drawback when using a cam is the follower longevity, which requires copious amounts of oil (very undesirable) or must be a rolling bearing of some description.

There are basically two alternative types of cam arrangement possible.

a) Each wand has its own cam as shown in figure 3.3.20. This system is costly and almost as complex as a crank/rocker wand system. The major advantage with this system is that the cam, follower, and wand pivot axes can all be parallel which allows the use of a simple plate cam or a conjugate trough cam. However, in order to reduce the pressure angle, between follower and cam, the cam must be relatively large, which is not aesthetic and increases follower speed, unless the follower is positioned close to the wand pivot, which increases wand stress and follower load.

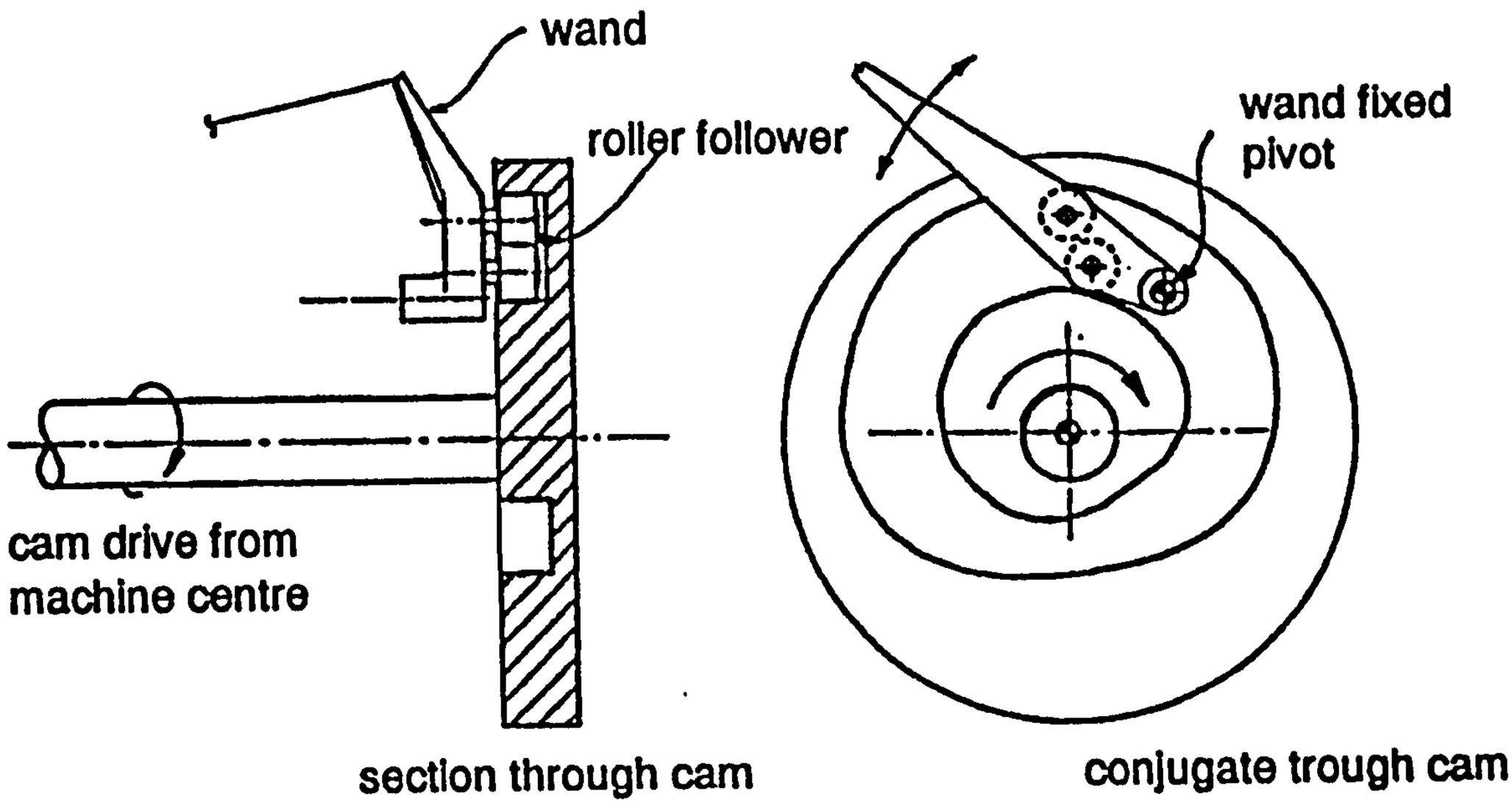

Figure 3.3.20 Wand drive using separate cams

b) All the wands are driven by a single stationary cam which forms a wall around the periphery of the machine as shown in figure 3.3.21. A stationary cam of this type would have (for a 24 carrier machine) six profiles machined into it. The major advantages of this system are the reduced cost over individual cam systems, and the reduced pressure angles due to the relatively long distance available to each cam profile although this also increases follower speed.

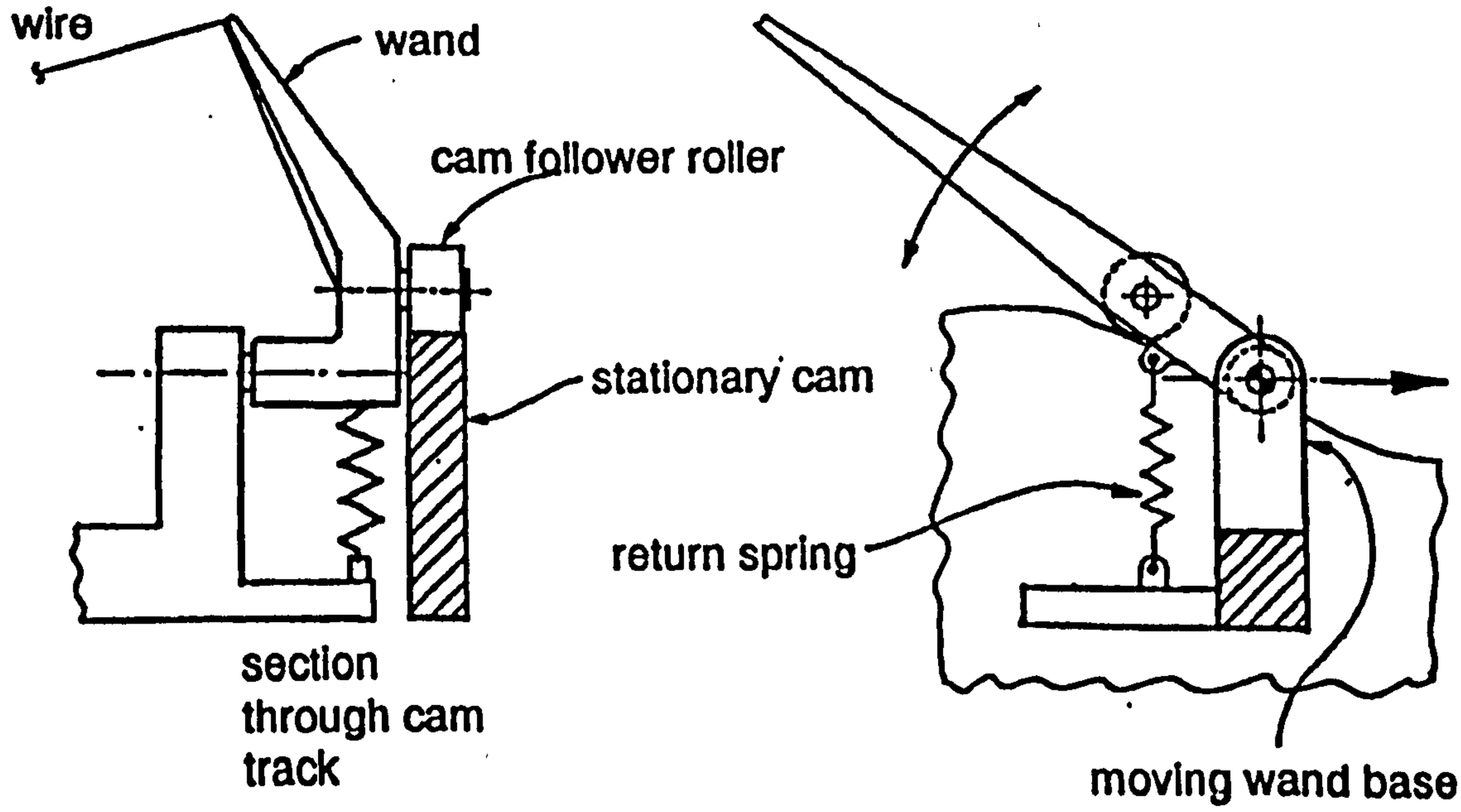

Figure 3.3.21 Wands driven by a single wall cam

Since a plain bearing follower is undesirable a roller follower must be employed which introduces several drawbacks. To avoid excessive skidding the follower axis should also pass through the machine centre line (although not necessarily the braiding point). This, in turn requires the cam track to be "banked" at each extreme of travel if normal, slightly barrelled, roller followers are used. Figure 3.3.22 shows the effect of not having the wand pivot and follower axes parallel.

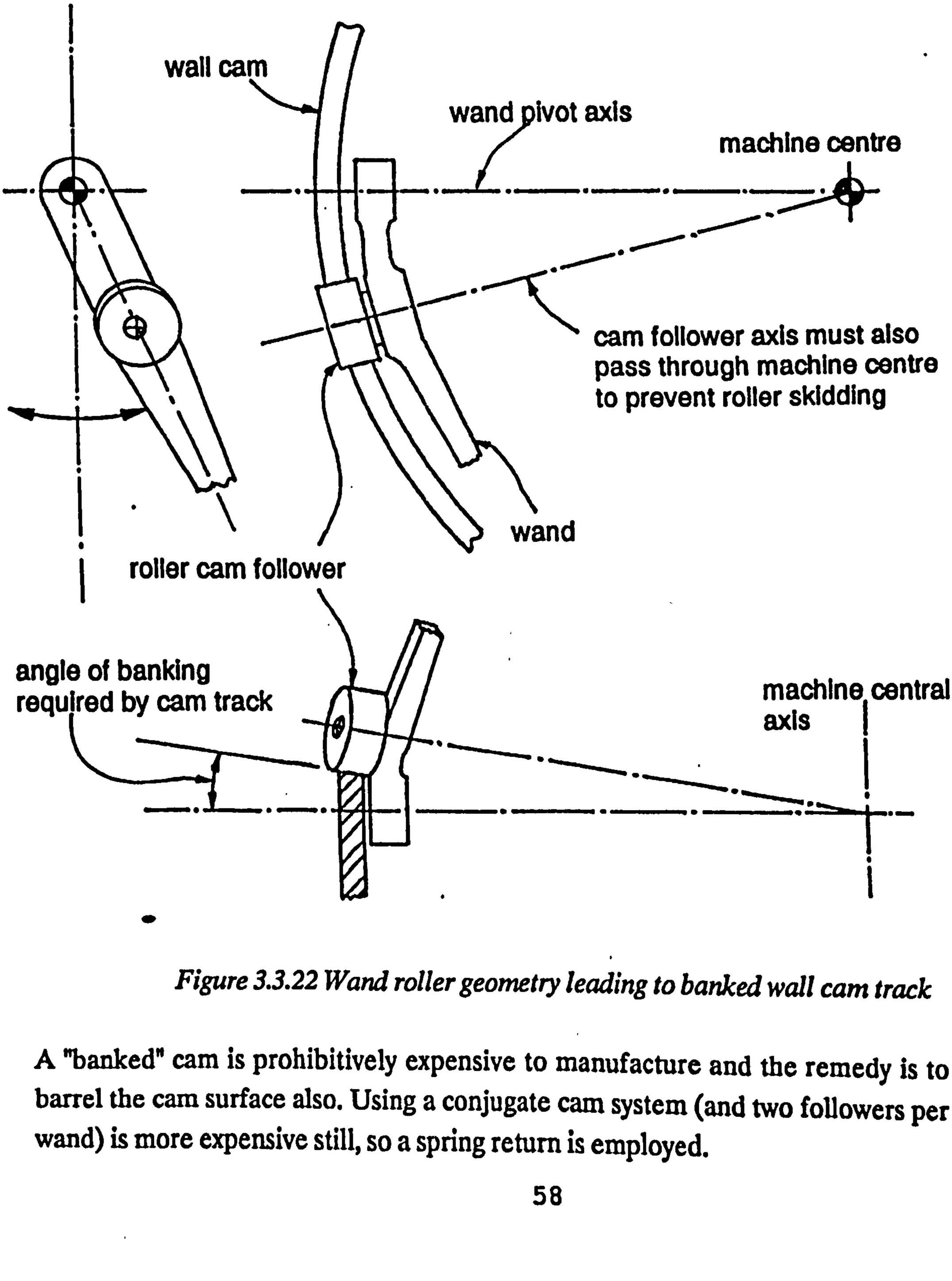

Figure 3.3.22 Wand roller geometry leading to banked wall cam track

A "banked" cam is prohibitively expensive to manufacture and the remedy is to barrel the cam surface also. Using a conjugate cam system (and two followers per wand) is more expensive still, so a spring return is employed.

The combination of barrelled cam and follower increases the effective load on the follower bearing which is further increased by the spring preload on the wand. However, this follower system still out performs a plain follower with the limited amount of lubrication available.
The various cam system parameters are shown in Figures 3.3.23 and 3.3.24 for a typical light alloy wand system using single and triple harmonic motion laws for the wand.

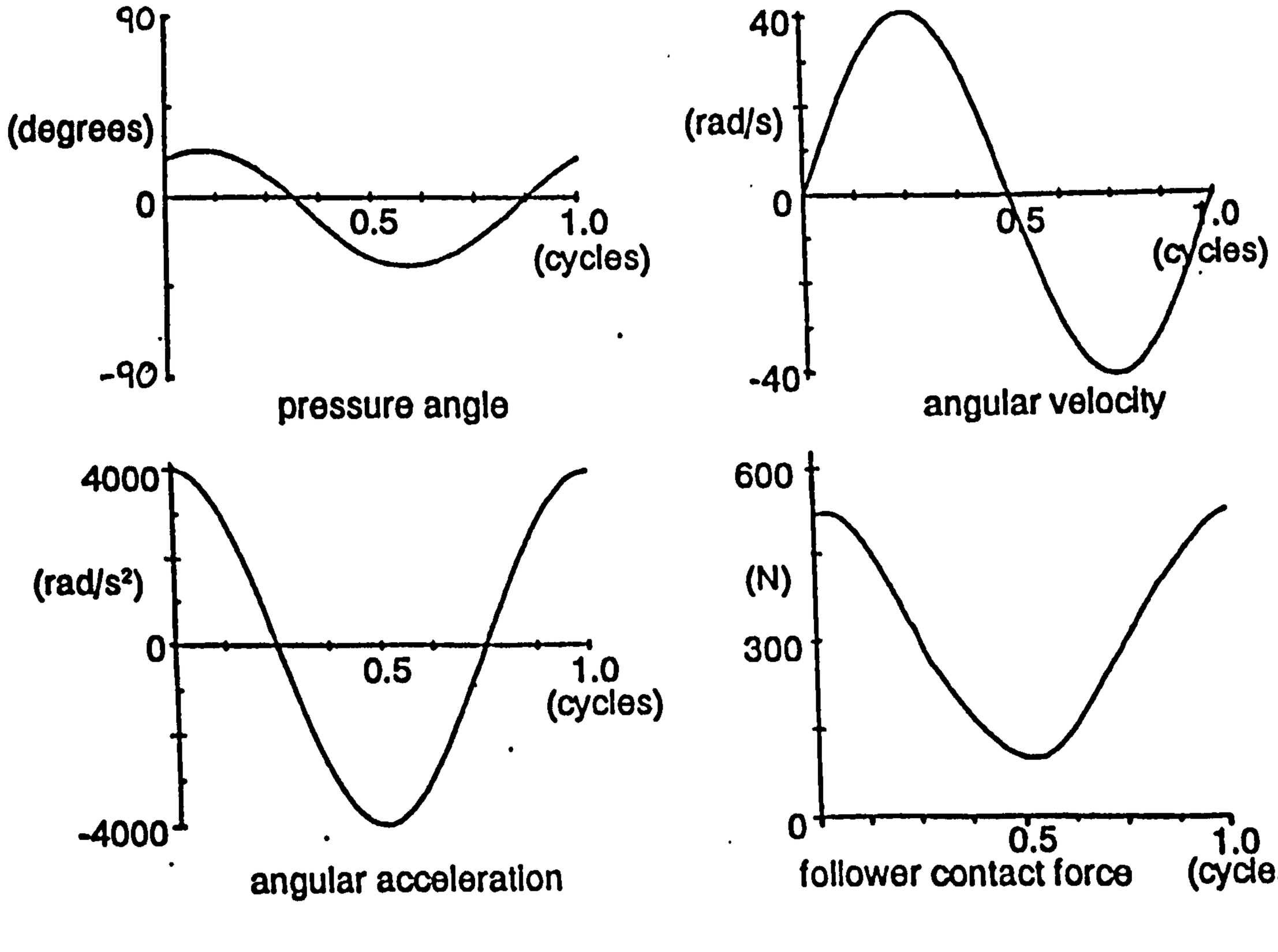

Figure 3.3.23 Single harmonic motion cam driven wand characteristics

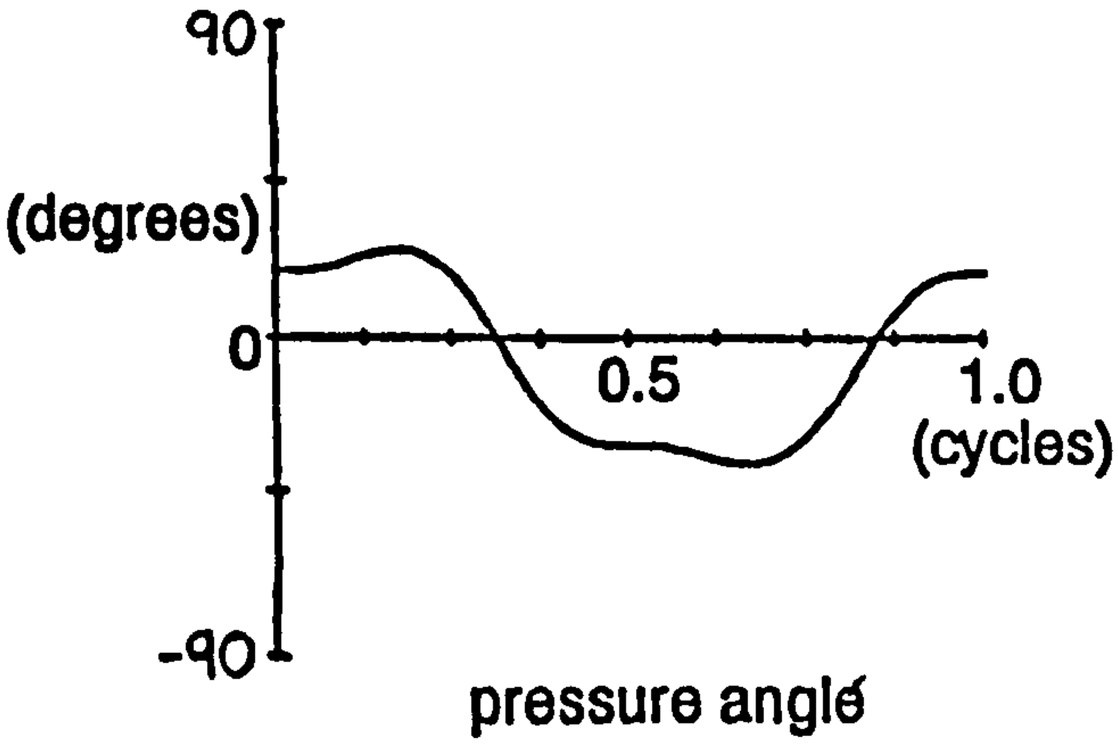

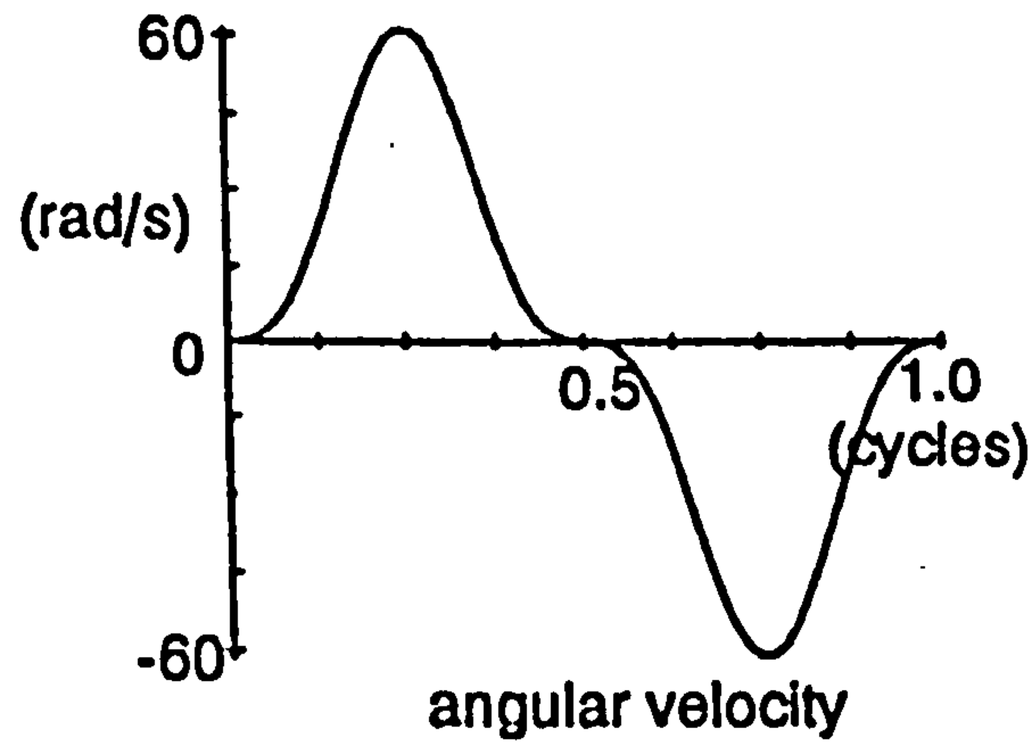

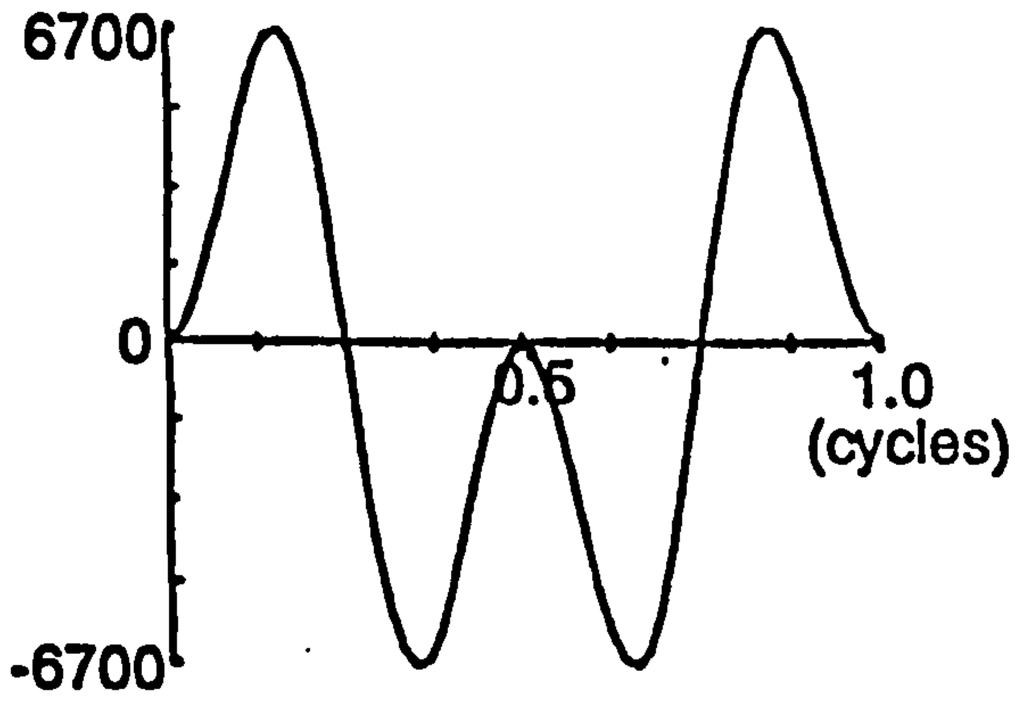

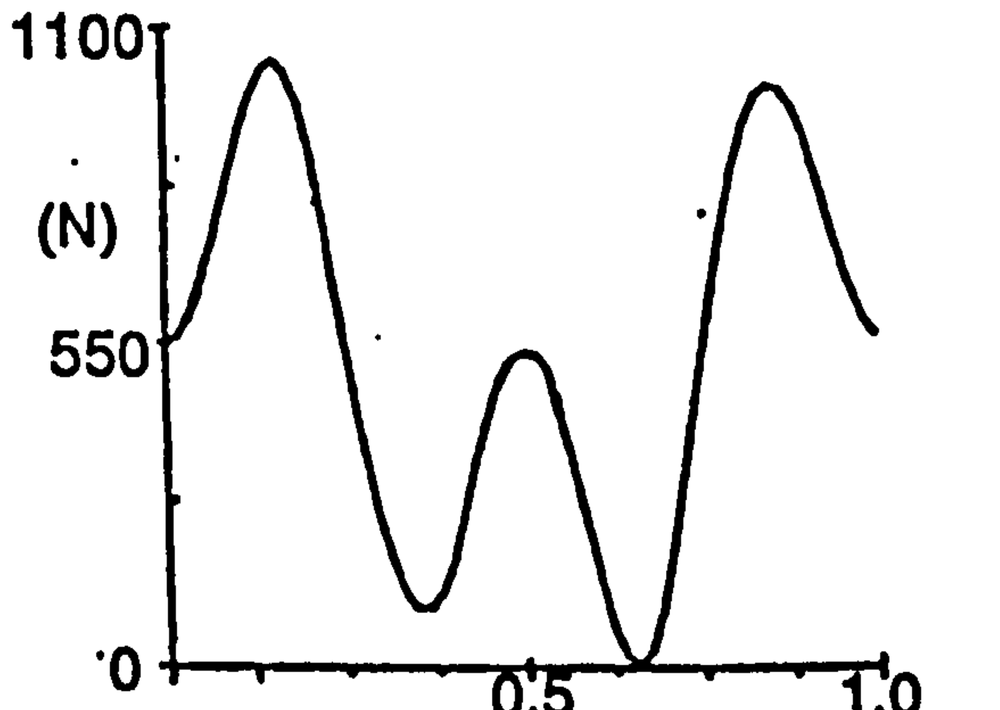

Figure 3.3.24 Triple harmonic motion cam driven wand characteristics

The effect of increasing the harmonic content of the motion on the pressure angle and roller contact force can be clearly seen.
It is obviously preferable to employ a wand motion which has the lowest contact force and pressure angles as it is this which determines the longevity of the system.

3.3.3 Hybrid Crank/Cam Driven Wand

This type of drive is intended to allow the longevity of the crank/coupler driven wand system and the versatility of the cam system to be combined. The system, shown in figure 3.3.30, consists of a crank driven wand but the input to the crank is modified by a drag link arrangement which introduces the higher harmonics into the basic single harmonic wand motion.

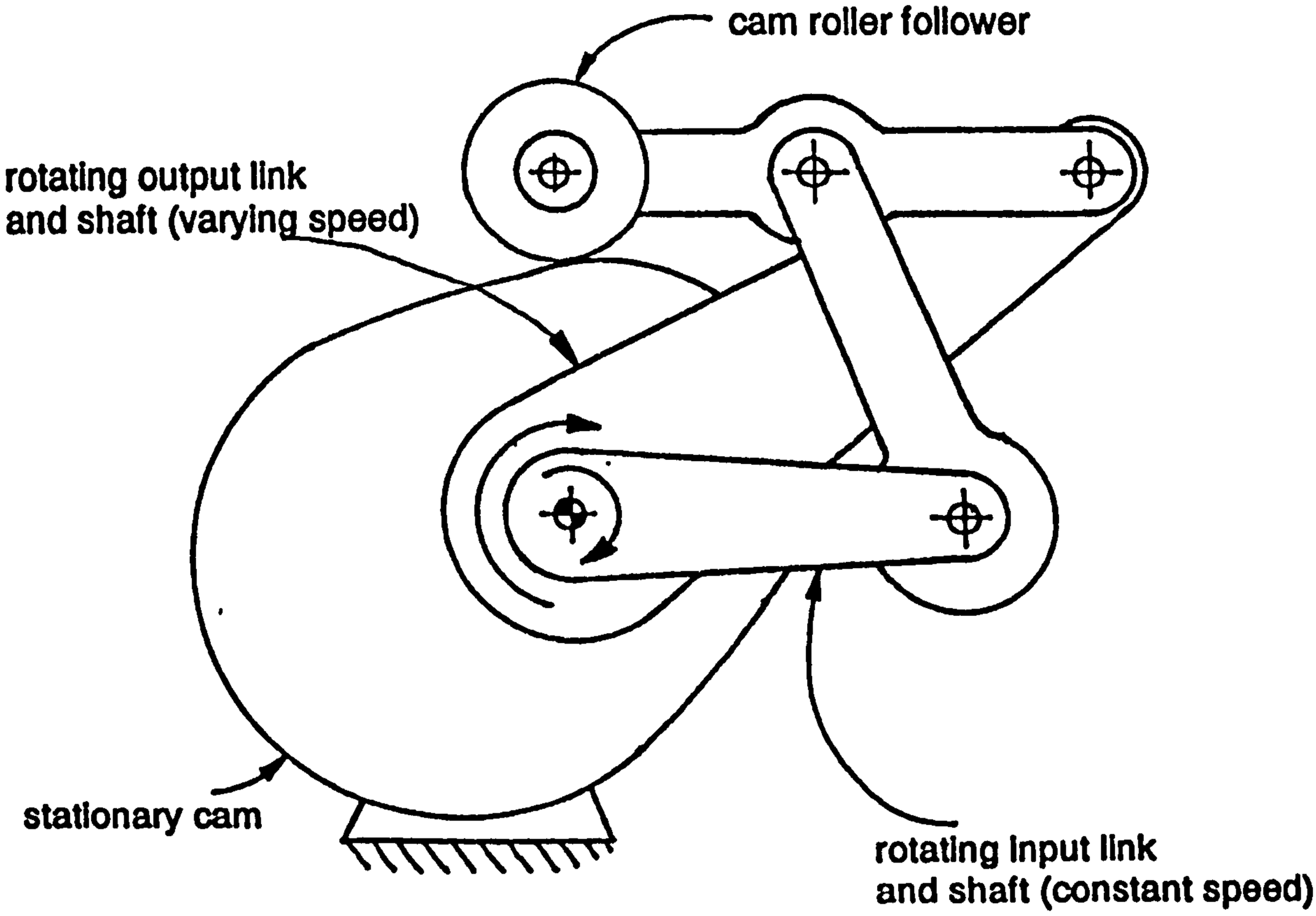

Figure 3.3.30 Drag link mechanism

This system is the most costly and complex but allows versatility (if required) by "locking out" the drag link which results in almost single harmonic motion. It is more appropriate to view this as a modified crank/rocker driven wand.

3.3.4 Selecting a Wand Motion Generation System

Initially, the ideal motion of the single harmonic was sought using an amplitude which results in a similar wire deflection to a triple harmonic motion of smaller amplitude (i.e. using ± 10mm deflection).

This motion is possible using both a cam or a four-bar, crank-rocker system.
The crank-rocker system is easier to implement and potentially more reliable and would be the first choice.

The cam system featuring a single "ridge" cam around the machine which serves all wands is dynamically superior although the use of sealed track rollers is not conducive to longevity.

However, a market requirement, perceived by the collaborating company, is the limiting of the wand tip amplitude to 220 mm peak to peak for aesthetic reasons.

The most appropriate wand motion within these guidelines is now the triple harmonic law. This cannot be obtained by using a crank rocker and must be achieved by a cam or a hybrid crank/cam device (drag link). Since the latter holds no advantage the cam drive is chosen for the wand motion generation system. The wand system should ideally allow the speeds dictated by the wire deflection predictions/tests (detailed in chapter 2) whilst allowing a longevity typically expected from machines in this market (i.e. 25,000 hrs for bearings).

The cam profile cannot be finalised until various other parameters relating to the wand design have been decided. It is important that the maximum pressure angle between the cam and follower is no more than 40° , and preferably below 35°. Thus, for a given wand length, determined again for aesthetic reasons, such that the wands do not "overlap" around the machine, there is a maximum distance at which the follower may be located from the wand pivot to comply with the pressure angle restraints. This is because, for a given wand amplitude and motion, the pressure angle increases as the distance from pivot to follower increases.
The life of the follower is dependent upon the roller bearing speed and the contact stress in the outer race. This stress is dictated firstly by the load which is dependent on wand inertia, position of the follower from the wand pivot, the pressure angle, and the wand acceleration, and secondly the form of the two

surfaces which is dependent on the degree of camber which the cam surface must have to prevent the roller follower running on its edge, which in turn increases with the distance between wand pivot and follower. The wand must have the lowest inertia possible and this requires a stress analysis to be performed. This will also reveal whether a wand may be designed to allow the follower to be positioned closer to the wand pivot than that previously mentioned (as this could possibly increase overall wand system performance). Using a wand length and amplitude dictated by the collaborating company/market, the follower should be positioned approximately one quarter of the wand length from the wand pivot. This dimension is used, initially, in all motion, follower life, and wand stress analyses.

3.4 Conclusions from the Kinematic Study of Wand Mechanisms

The criteria for the wand tip locus is to retain a constant wire span from wand tip to braiding point.

Of the many loci available, that described as "Arc A" is theoretically ideal (Fig. 3.2.10). However, a suitable mechanism to achieve this was not found.

The next best Locus is that described as "Arc B" (Fig. 3.2.11). This is easily obtained using a simple rocker whose pivot axis passes through the braiding point (Fig. 3.2.40).

The wand motion is determined primarily by the wire deflection criteria (Chapter 2). The ideal motion is a single harmonic motion. However, the perceived market requirement is for an aesthetically acceptable wand with a limit on its amplitude. The best motion within this frame work is the triple harmonic motion.

The cam system offers the easiest and dynamically superior wand drive. The simplest form being a stationary ridge cam around the periphery of the machine which serves all the wands. The cam follower speed favours the use of a roller bearing, which requires the cam to be crowned to avoid "corner" running. A spring return is employed on cost grounds and the location of the cam follower roller on the wand is chosen to allow a maximum pressure angle of 40° . The follower life is achieved by reducing the inertia of the wand, if possible.

CHAPTER FOUR

DYNAMIC ANALYSIS OF THE WAND MECHANISM

4.0 Introduction

A dynamic analysis of the wand is required to minimise wand inertia yet allow a reasonable wand fatigue life. A low inertia is imperative in attaining the specified longevity of the wand cam follower roller. To this end a stress analysis is used to aid wand design and determine the optimum form of the wand. The various materials suitable for a wand are appraised and the choice for the final wand design is justified. The aspects of balancing a wand are considered, and finally an evaluation of the wands natural frequencies is made to ensure both the wire vibration and stresses in the wand are not exacerbated.

4.1 Stress Analyses of the Wand

Three theoretical stress analysis techniques are considered. Two are a variation on a classical stress analysis theme, and the other is a finite element method (PAFEC). All stress analysis assumes a triple harmonic wand motion and a cam follower positioned a quarter of the wand length from the wand pivot, as this corresponds to the 40° maximum pressure angle.

4.1.1 Stress Analysis of a Wand with a Uniformly Changing Cross Section

The wand is represented as a simply supported beam whose cross sectional shape can be expressed as a single function from wand tip to follower pivot. The loads on the wand are due to angular acceleration of the wand and the wire tension, acting in a perpendicular plane to this, at the wand tip. These may also be expressed as a single function. From these the stresses in the wand may be determined at any point by integrating the function between the wand tip and follower pivot, (Fig. 4.1.10). It is assumed that the peak bending moment occurs at the follower pivot point.

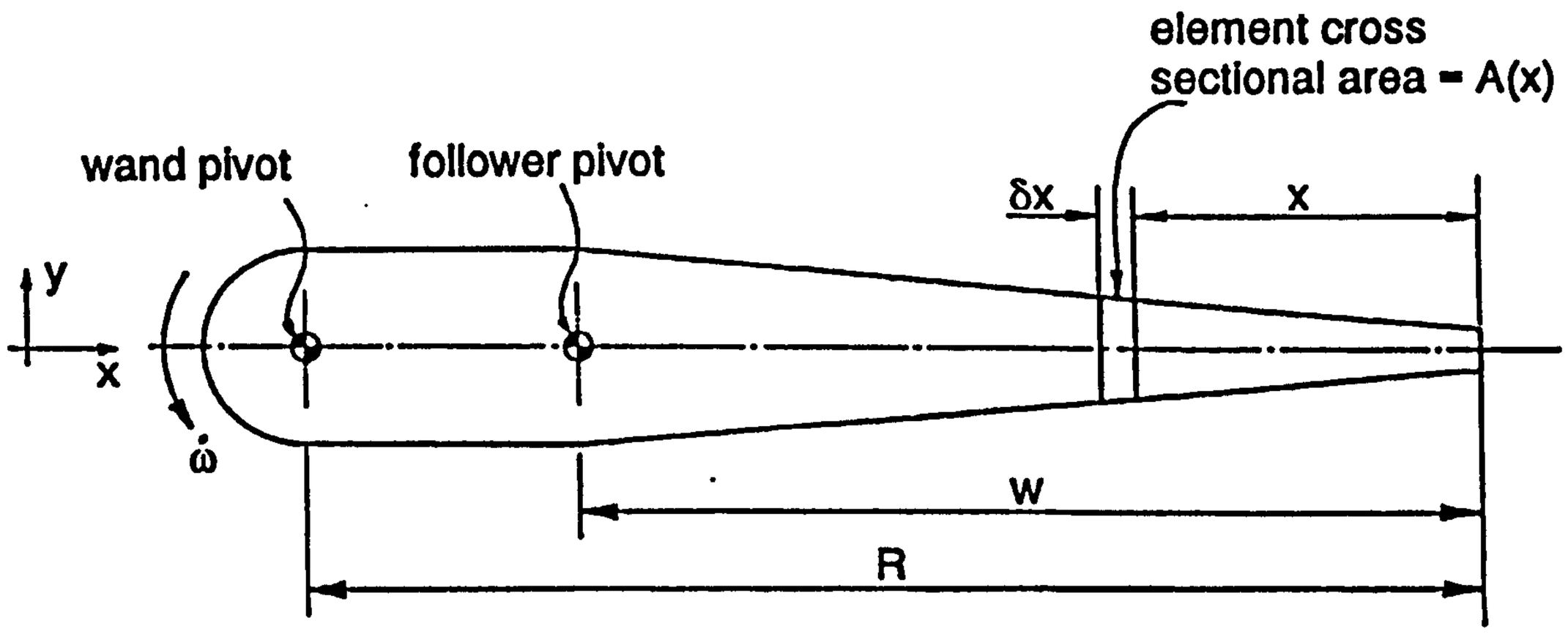

Figure 4.1.10 Stress analysis wand model

Inertia force of element

$$\delta F(x) = A(x).\rho.\dot{\omega}.(R-x)\,\delta x$$

Bending moment at the follower pivot (x = w) due to δF

$$\delta M = \delta F.(w-x)$$

$$\text{Total BM,}\quad M = \sum_{x=0}^{x=w} (w-x).\delta F = \int_0^w \rho.\dot{\omega}.A(x).(R-x)\,dx$$

The stress can now be found simply by substituting this bending moment into:

$$\sigma_{xy} = (M.y/I)_{x=w}$$

The stress due to wire tension is found in a similar manner for the x-z plane.

If the wand is cranked to position the wand tip nearer the machine centre, which minimises the wire span, the force along the wand due to its inertia also produces a torque which is a maximum at the start of the cranked section.
The torque together with the normal inertia derived bending, produces shear stresses across the wand section.

A complex stress system results from the superposition of all the "component" stresses. This is solved in the usual way and principal stresses are found.
The wand design is optimised to reduce these whilst also reducing the force at the follower pivot (i.e. follower load) by reducing the wand inertia.
This form of stress analysis can only be applied to sections which can easily be represented algebraically.

If the section changes, the algorithm defining the cross section must also change yet "carry" the bending moments/shear forces from the previous section. This can be achieved with a computer model of the wand. The section changes are accompanied by stress concentration factors.

4.1.2 Stress Analysis of a Wand of Any Cross Section

This technique for segmentation of the wand is taken a step further and forms the basis of the second theoretical stress analysis.

The wand form is defined as a series of finite elements (usually over 100) and the stress in each element is determined. Starting at the wand tip, the Bending moment at every point is found from the force centroid of the section between it and the wand tip. This method enables the stresses, slopes and deflections at all points on the wand to be found using relatively simple routines on a computer. This method proves very easy to implement and allows rapid changes in wand section etc. to be analysed relatively quickly since no integration (usually manual) is necessary. The only drawback is the need to introduce stress concentration factors at any abrupt changes in section along the wand.

4.1.3 Finite Element Stress Analysis

The PAFEC finite element stress analysis suite is used to analyse the wand design. The main drawback with this system is the inability, within the standard loading routines, to submit the wand to an angular acceleration (i.e. a linear variation in acceleration along the wand from the pivot point). This load condition can be included by developing software to achieve this, but this was thought at the time to be an unnecessary extravagance. The wand may be loaded in a similar manner using a relatively crude arrangement of multiple loads along the wand.

However, the primary purpose of the finite element method is to detect and, if possible, evaluate stress concentrations at the various section changes.
Stress concentrations occur, as expected, at the follower pivot point where the follower roller locates. These areas are modified after the major form of the wand is derived using the analytic methods of 4.1.1 or 4.1.2.

4.2 Optimisation of the Wand Structural Form

The wand is subject to forces in two major planes:
i) Forces due to the angular acceleration of the wand acting through the cam follower. These act in the plane of the wand motion.
ii) Forces due to the wire tension. These act in the plane containing the wand and the wire and are of a magnitude which allows the wire to break (i.e. without over stressing the wand).

The wand must also be cranked (bent), or curved towards the machine centre in order to clear the cam and reduce the length of the outer wire span. The inertial forces in the accelerated wand now cause torques due to the crank in the wand. The optimum form for the wand is one in which the maximum principal stress is equal at all sections along the wand from tip to pivot point. Due to the different loads applied in each plane ((i) and ii) above) the form of the wand will also differ in each plane. However, within this criteria there is a choice of wand section shape and various practicalities such as a method of mounting the cam follower and wand pivot, and the need for an eyelet at the wand tip. These considerations lead to the conclusion that attempting to find a theoretically optimum wand is impractical. The wand, therefore, tapers linearly towards the tip and any stress concentrations are found using the finite element stress analysis. The point of highest bending moment caused by the acceleration is at the roller follower and the wand form between this point and the tip accounts for the major part of the wand inertia about its pivot. The optimum cross sectional shape of the wand in this region is found using the method described in 4.1.2, to be a hollow rectangular section of a form which tapers, in both planes, toward the wand tip, as shown in figure 4.2.01. However, even using a constant wall thickness, this form of wand is prohibitively expensive to manufacture and a suitable solid section is sought.

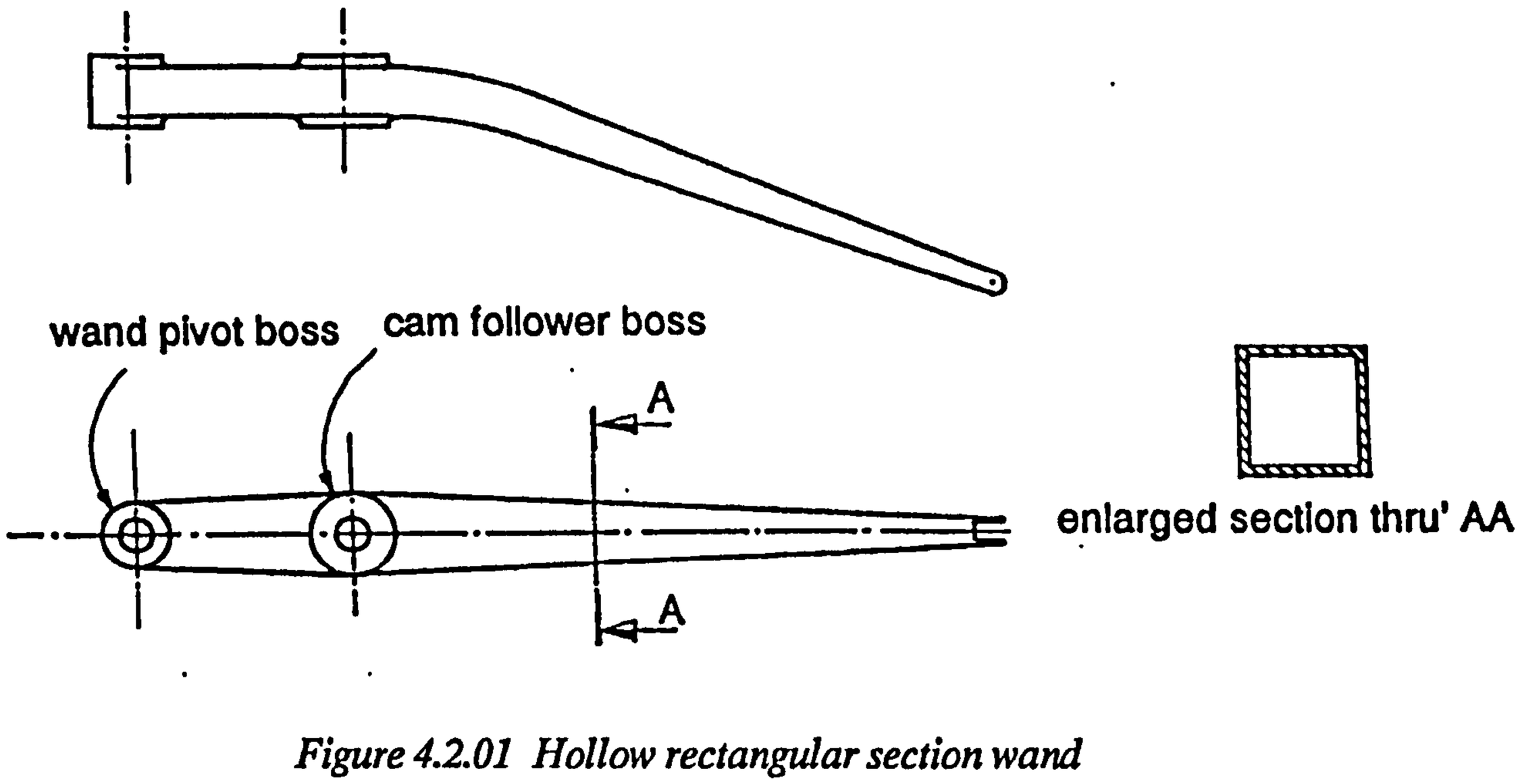

Figure 4.2.01 Hollow rectangular section wand

The optimum solid section in terms of pure bending stresses is the "I" section wand as shown in Fig. 4.2.02.

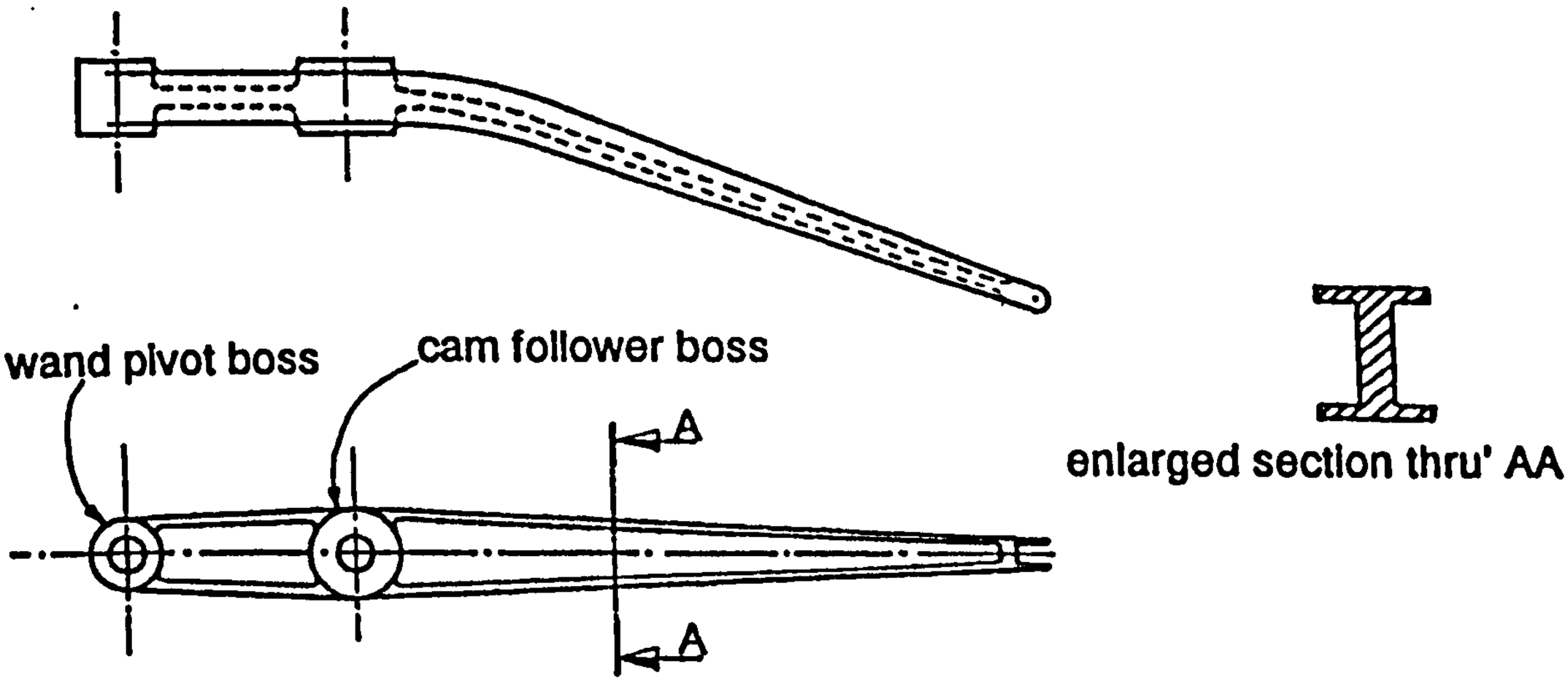

Figure 4.2.02 'I' section wand

But when the complete stress situation is considered the shear stress due to the torque, caused by the cranked (or curved) wand, may be counteracted to a degree by using an asymmetric "I" or a "C" section.

The shear centre of these sections, under normal bending is shifted and lies outside the section shape. Thus by judicious selection (and orientation) of the section, the torque produced by the cranked wand may be counteracted. This reduces the total shear stresses and twist likely to occur in the wand.

Figure 4.2.03 shows a "C" section wand and its shear centre.

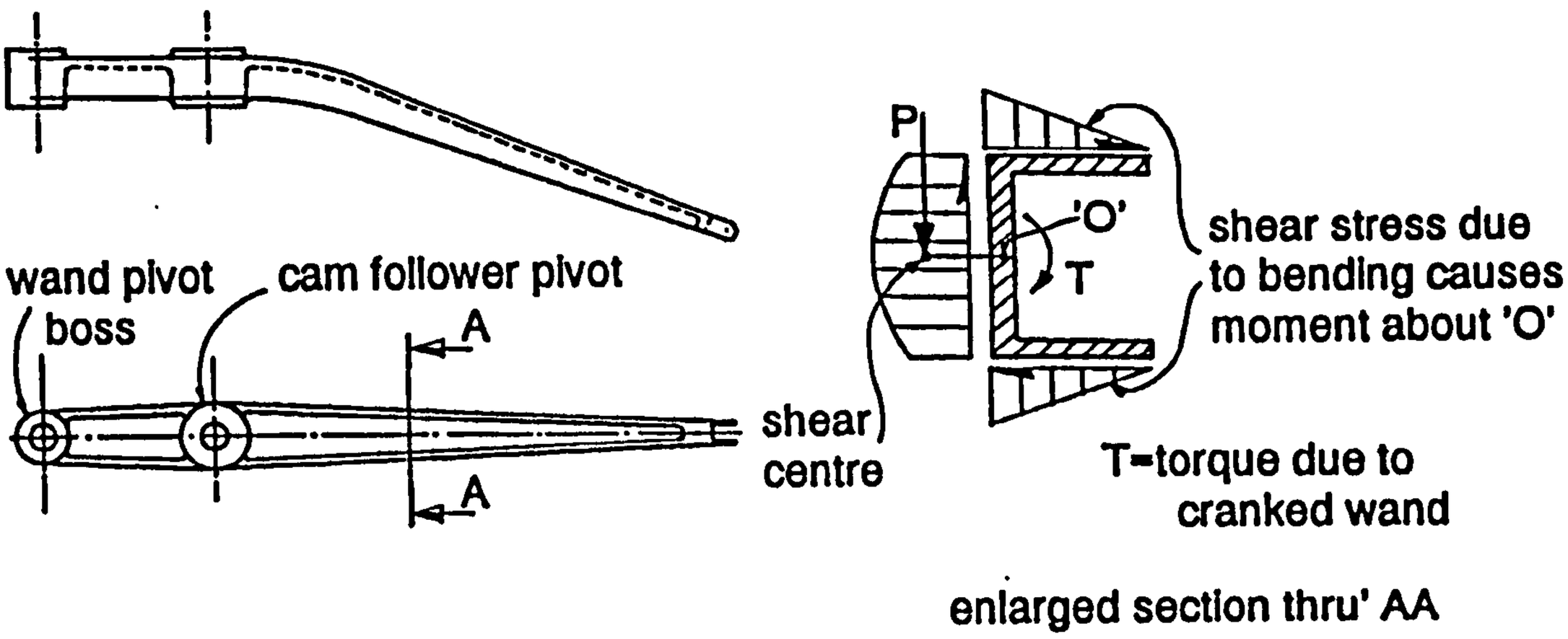

Figure 4.2.03 'C' section wand

The final form of the wand is shown in Fig. 4.2.04. This is a "C" section and becomes an "L" section near the wand tip. This is purely for convenience of manufacture and to aid routing the wire which must pass along the wand pivot line to retain constant length.

WAND FOR ROTARY BRAIDER

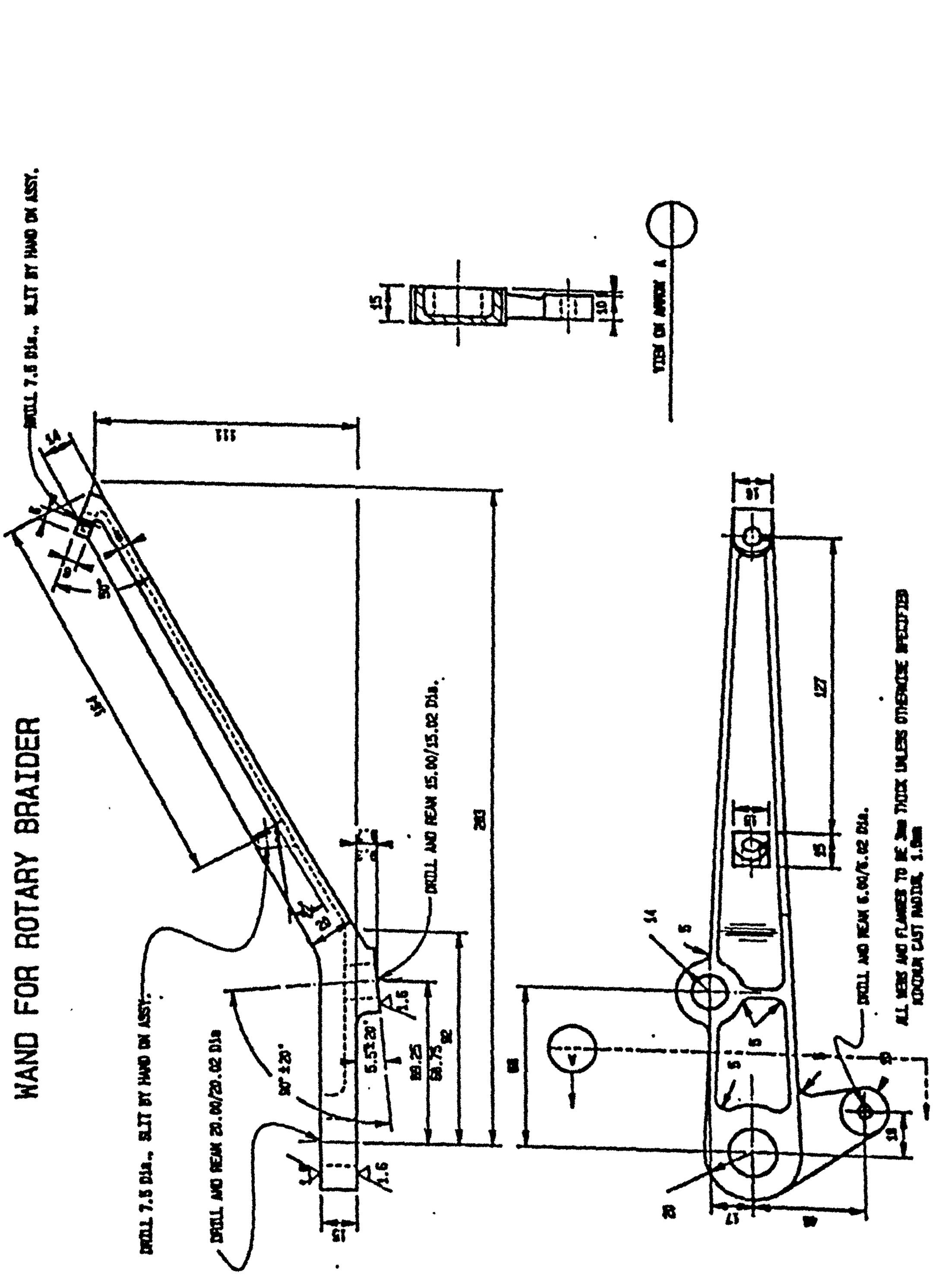

Figure 4.2.04 Final wand design

4.3 Wand Material Selection

The material chosen for the wand is, inevitably, dictated by expense of both material and manufacture. To reduce the wand inertia, and cam follower load, the wand material must have a high stress to density ratio. It must also have a working stress limit of an acceptable value for up to 10^7 cycles. Under ideal circumstances the material has an endurance stress limit below which fatigue failure is unlikely. Steel is attractive for this reason, but although having sufficient strength, has a lower stress to density ratio than other materials. Aluminium alloy has no endurance stress limit yet in certain conditions displays acceptable "endurance" stress levels for up to 10^8 cycles which is well within that expected from a wand.

Composite materials such as carbon, glass and Kevlar (etc.) reinforced plastics display very high stress/density ratios. However, relatively little data is available on endurance stress limits over 10^6 cycles. Composite materials, by their nature, are not homogeneous materials and theoretically cannot be analysed using the methods outlined in 4.1.1 to 4.1.3 (although some finite element stress analysis packages claim this can be achieved) and so accurate stress analysis becomes difficult.

Test wands were constructed from three types of material. The first utilises the optimum cross sectional shape of a hollow rectangle. This is fabricated from sheet steel and was intended to be driven by a crank and coupler arrangement (i.e. The wand motion is approximately single harmonic). Because a track roller is not used and wand accelerations are slightly lower, the wand inertia tolerable is relatively high ($0.031 kgm^2$). Figure 4.3.01 shows a photograph of thé fabricated steel wand. The second wand is made from carbon fibre and has a solid rectangular section as shown in figure 4.3.02. The section also tapers towards the wand tip and is cranked immediately after the cam followers. The wand is driven by a conjugate cam which imparts a triple harmonic motion on the wand. This wand was used primarily to study the vibrating wire behaviour, but also to investigate the feasibility of using carbon fibre. The wand is constructed by laying sheets of pre-impregnated carbon fibre matting upon one another in a mould. The material is cured by heating at 130° C in an oven. Cam follower stud bearings locate in steel inserts glued into holes bored in the carbon fibre after curing. The wand pivot shaft is located in a similar fashion. The section used is excessive yet offers the least expensive manufacturing method compared to other, lower inertia yet

more complicated, section shapes. Even so the carbon fibre wand cost £300 to manufacture and would still cost £130 for a quantity of one hundred.

Figure 4.3.01 Fabricated steel wand

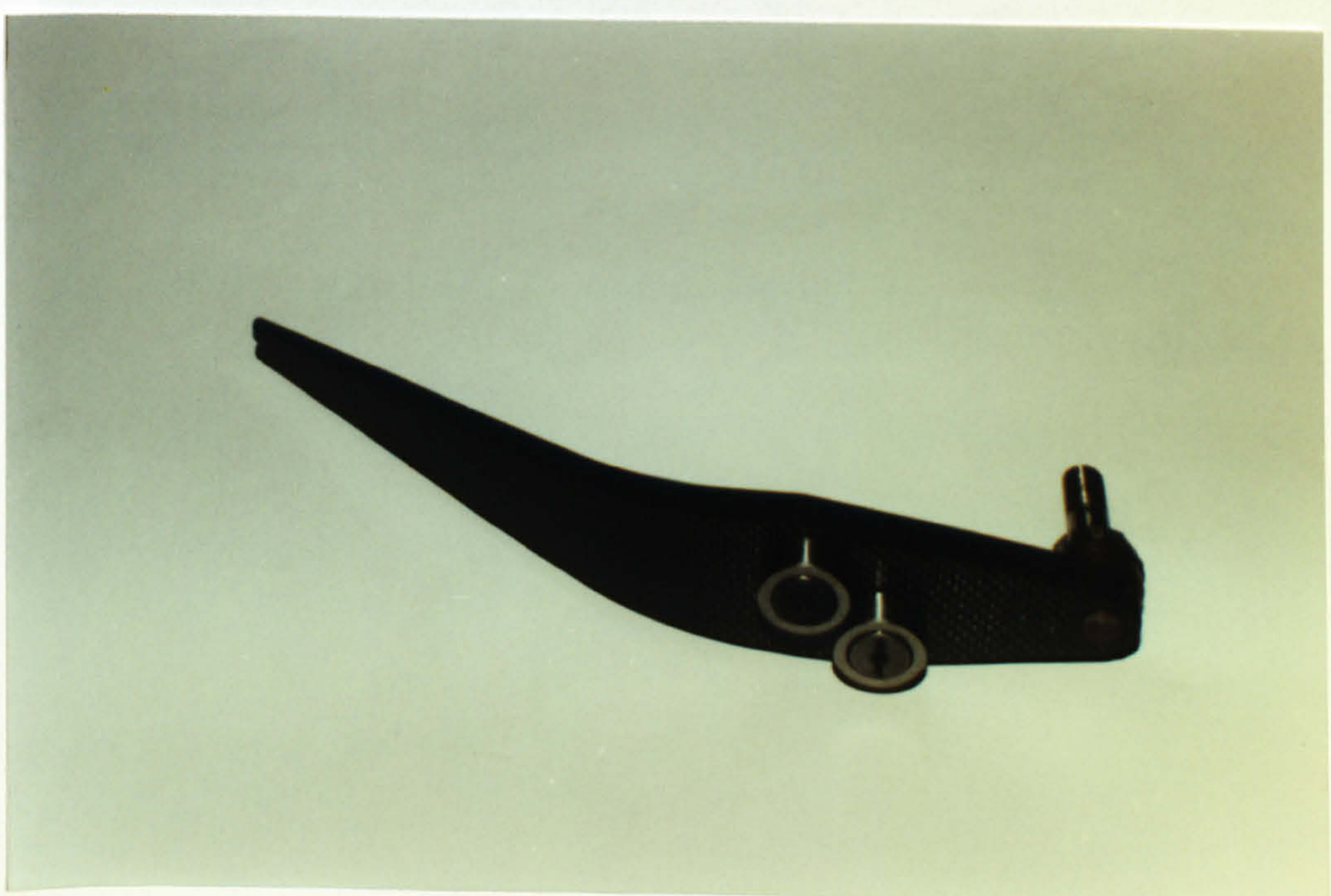

Figure 4.3.02 Carbon fibre wand

This compares unfavourably to a light alloy forged "I" section wand which costs £37 each for 100 off. The inertia of the carbon fibre wand is 0.0027kgm^2 . The third wand type is made from forged aluminium alloy and is chosen as the final design, as shown in figure 4.3.03. The ideal section is a "C" section from the follower pivot for half the wand length, and an "L" section for the remainder (see section 4.2). The inertia of this wand is approximately 0.0038kgm^2 . The cam follower roller bearing and pivot spindle bolt directly to the machined alloy and a ceramic eyelet is bonded to the tip to guide the wire.

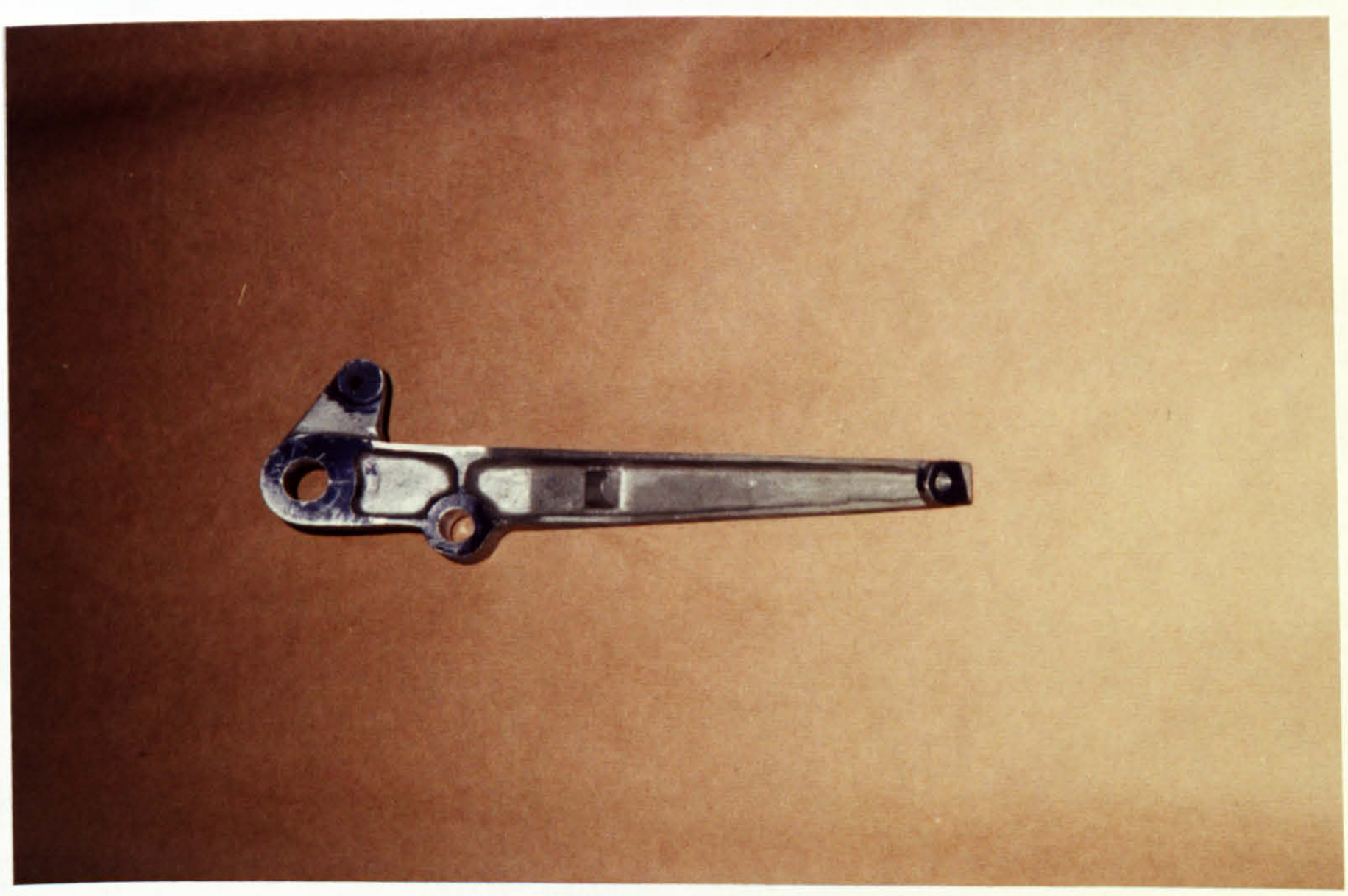

Figure 4.3.03 Aluminium alloy wand

4.4 Balancing

The aim of balancing a cam driven rocker wand is to reduce the forces and moments transmitted to the base through the wand pivot. To balance a mechanism usually entails increasing the inertia, and since this is detrimental to follower life, balancing is not considered an advantage. If the transmitted forces are such that they compromise the machine performance, a form of "detached" balancing may be used (e.g. using balancer shafts located near the wand pivot). However, the inertias expected from the stress analysis/wand structural design is such that balancing is unlikely to be required.

4.5 Natural Frequency Evaluation

The natural frequencies of the wand system must be determined for several reasons:

a) The first natural frequency must be over three times the operating frequency (i.e. It is not a "high speed machine") to avoid resonance.

b) The frequency of oscillation of the wire should not excite the wand.

c) Any natural frequency of the wand should not excite the wire and increase deflections unduly (assuming a) above is not satisfied).

The natural frequency of the wand can be calculated easily if the section is constant and the general design is much simplified from that actually used. This "vibrating rod" theory becomes difficult to justify, however, when the section is changing and the system is not "clamped" at one end. A finite element frequency analysis is used since these have proven acceptably accurate for determining natural frequencies and modal shapes of relatively complex forms. Figure 4.5.01 shows the first mode shape for a typical alloy wand. The calculated first natural frequency of the wand is approximately 800Hz. At 150 rpm machine speed, the wand driving frequency is 15Hz, which gives a "period ratio" (i.e. first natural frequency divided by forcing frequency), of 53. The rotary braider wand mechanism can, therefore, not be considered a "high speed machine" which implies a period ratio of less than 3.

Such is the difference between the first natural frequency and operating frequency that non of the potential problems (listed in a), b) or c) above) are likely to occur. Even using the triple harmonic motion law decreases the period

ratio to 18.
Backlash, whether inherent in the drive system or as a result of wear, will potentially increase the apparent operating frequency of the wand mechanism.
The wand system chosen utilises a spring return which, whilst increasing follower load, virtually eliminates backlash.

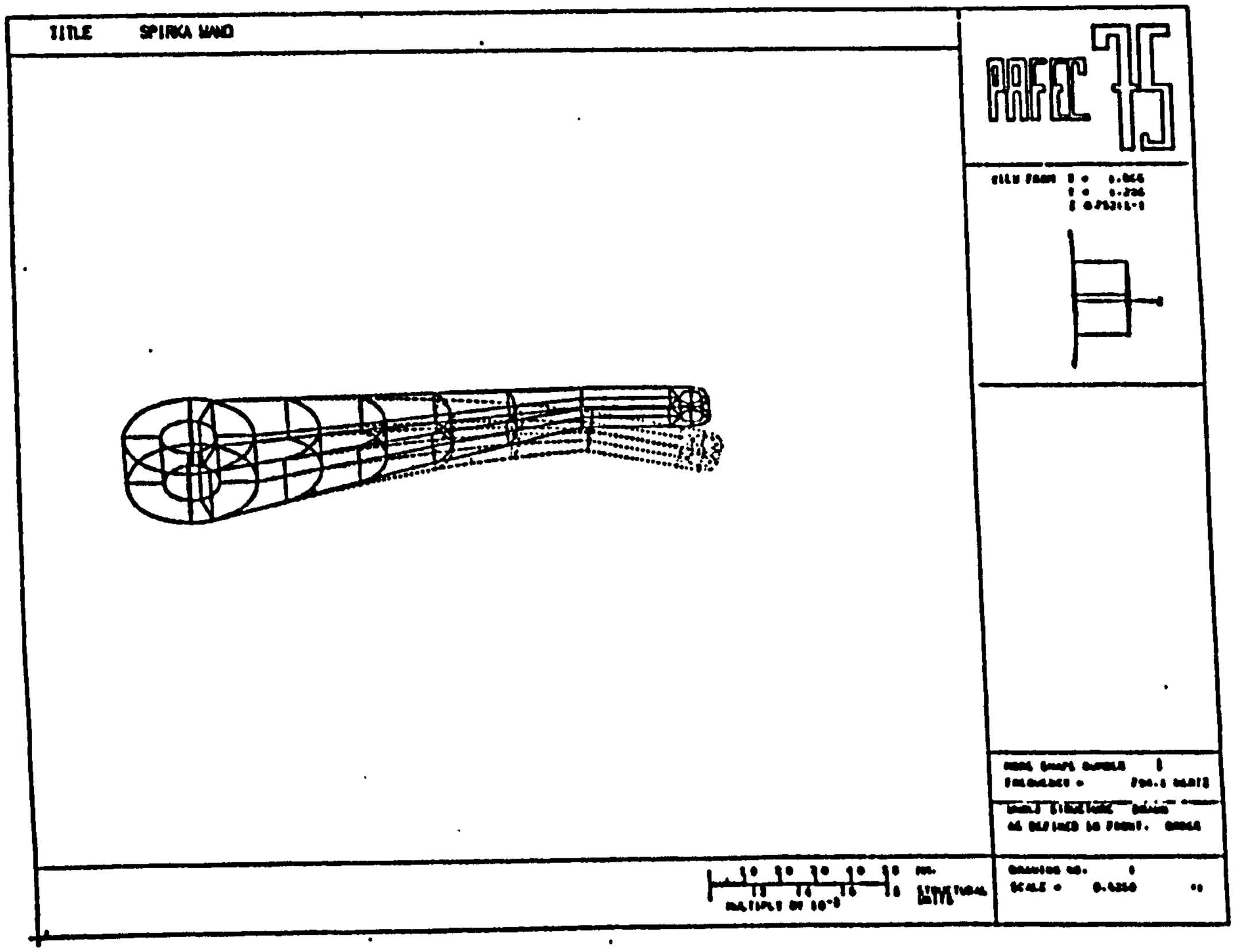

Figure 4.5.01 First natural frequency mode shape for an alloy wand

4.6 Conclusions from the Dynamic Analysis of the Wand Mechanism

A stress analysis based on both traditional stress theories and computer aided finite element routines allows the optimum wand form to be found. This is inevitably compromised by cost restrictions and the result is a forged aluminium alloy wand which is initially a "C" section but becomes an "L" section towards the wand tip, as shown in figure 4.2.04.

Since direct balancing increases the wand system inertia, this is not employed.

The natural frequency of the wand is approximately 800Hz which results in a period ratio of 18 using the triple harmonic motion law. Problems associated with resonance are not expected.

The inertia of the forged aluminium alloy wand ($0.0038 kgm^2$) allows the cam follower roller to achieve a longevity of over 25,000 hrs when positioned at a distance of 70mm from the pivot point of a 265mm long wand. This follower position results in a maximum pressure angle of 40° . A ceramic eyelet is bonded to the wand tip and another to the wire guide half way along the wand.

CHAPTER FIVE

INNER BOBBIN OPTIMISATION

5.0 Introduction

The inner bobbins on a rotary braider carry half the strands/wires which constitute the final product. There are 12 inner bobbins on a 24 carrier machine and each is supported by an inner carrier which runs on a track around the machine centre and product. The outer wires are guided between, and past, adjacent inner bobbins and carriers as they rotate. The relative motions of the outer wires form a conical shaped region into which the inner bobbin and its carrier must fit. The cross-sectional shape of the conical region is formed by the superposition of the wand tip motions as shown in figure 5.0.01. The volume of this conical region can be increased by:

a) Increasing the wand tip amplitude (conical base area increases).
b) Modifying the wand tip motion (base area increases).
c) Increasing the distance of the wand tip from the machine centre (increases base area and cone length).

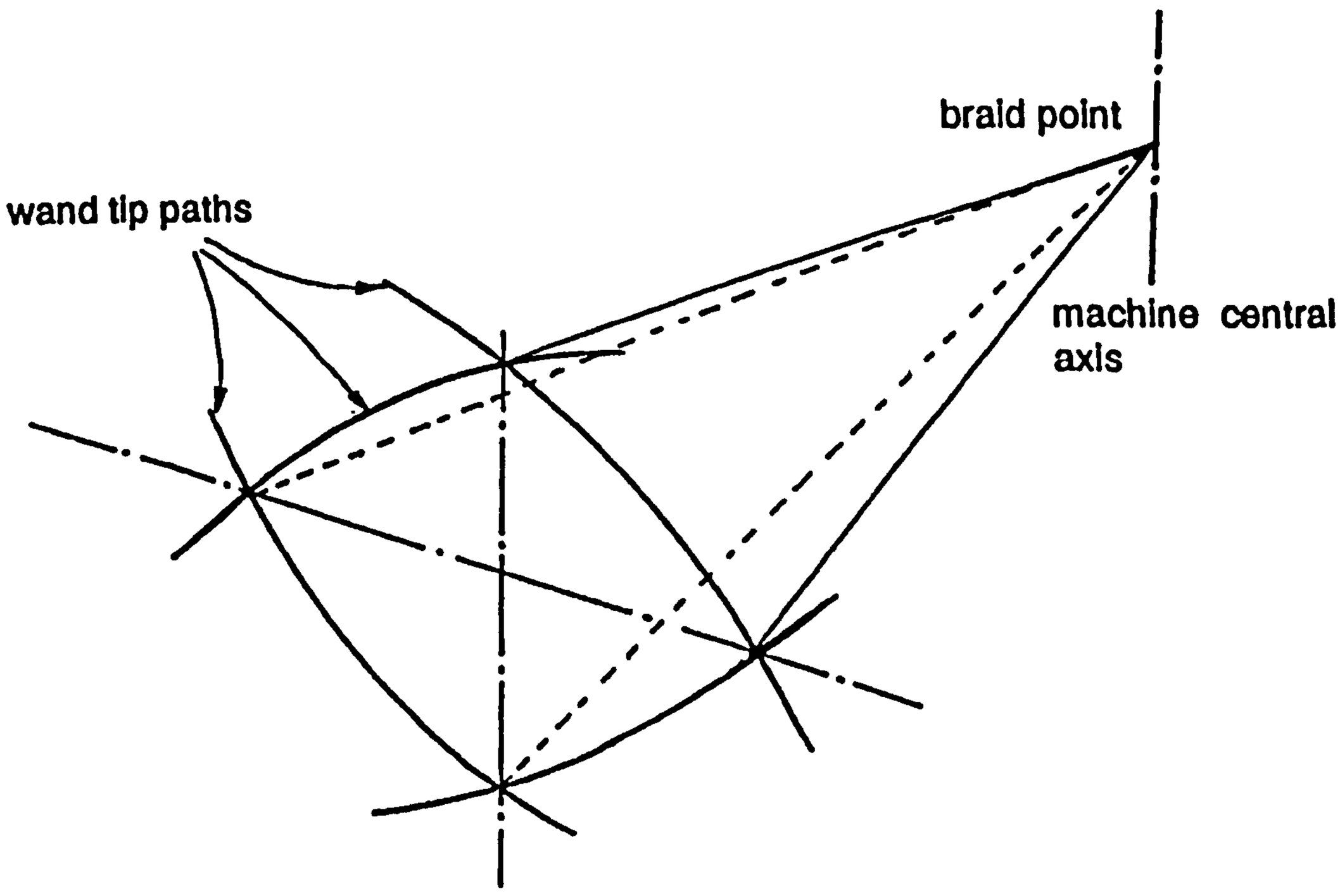

Figure 5.0.01 Conical region formed by outer wire paths

However, all these factors are influenced by the wand and wire behaviour. The wand tip amplitude is limited for aesthetic reasons dictated by the market. This, in turn, dictates, to a degree, the wand motion which provides the greatest base area for the conical region whilst complying with the peak wire deflection criteria (ref. chapter 2, figures 2.2.11 and 2.2.12). The same criteria applies to the span of wire from braid point (machine centre) to wand tip, since the larger the span the greater the wire deflection. The net effect of this is that increasing the volume of the conical region decreases the speed capacity of the outer wire/wand system. However, the inner bobbin and carrier must have its combined centre of mass as close to the machine centre as possible to reduce the loading on the carrier-track bearing.

The optimum machine performance is attained when the speed capacity of both the inner carrier bearings and outer wire/wand systems are identical. To this end it is important that the bobbin, which has greater mass and volume than the inner carrier, is arranged within the conical region to occupy as great a proportion of the volume as possible (and, therefore, a given volume bobbin requires the smallest volume conical shape). The ideal form or shape of bobbin and its orientation within the conical region are therefore required.

5.1 Bobbin Form

Bobbins used on current braiding machinery are cylindrical in shape and have an "aspect ratio", (bobbin diameter/bobbin length) of between 0.25 and 1.2. The bobbin must be a volume of revolution since a stationary bobbin and rotating take-off will continuously twist the wire. This is not acceptable with multi strand wires which must be braided as a flat ribbon. There are basically three types of bobbin possible. These are a plain cylinder, a barrel, or a (truncated) cone as shown in figure 5.1.01.

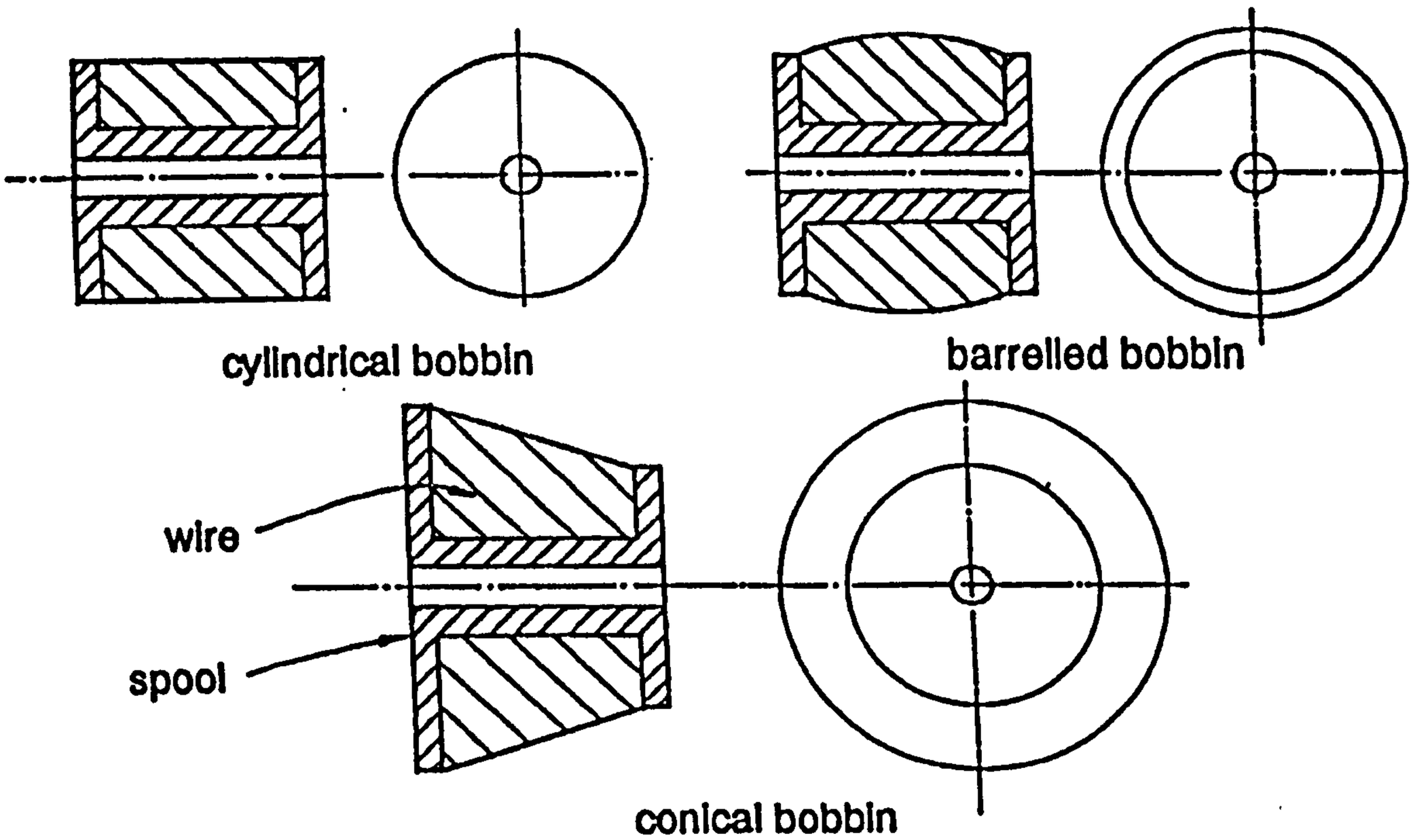

Figure 5.1.01 Bobbin types

A conically wound bobbin, with its axis orientated along the axis of the conical region (into which bobbin and carrier must fit), is ideal and allows up to a 70% increase over a plain cylindrical spool of similar length (refer Appendix 5.1.01). However, current winding machines do not wind conically and major modifications are required to prevent excessive catenary sag in multi strand wires when winding in this manner. The increase in volume attainable by using conically wound bobbins is such that a final choice of bobbin configuration will benefit from being one in which a conical bobbin can be correctly utilised, should the facility to conically wind become available in the future.

A barrel shaped bobbin suffers from the same winding difficulties as the conical bobbin. For these reasons a cylindrical bobbin is chosen. The aspect ratio is not restricted (although towards the end of the project Spirka bobbin dimensions were specified), and this is found in conjunction with the bobbin orientation optimisations. The volume of wire is specified (i.e. a minimum is specified) and the minimum bobbin core diameter is also defined (to allow a reasonably simple tension control device), as is the minimum flange thickness. Thus, as a bobbin with a set wire capacity changes aspect ratio, so the proportion of wire volume to total (wire + bobbin) bobbin volume changes. The graph in figure 5.1.02 shows the optimum bobbin aspect ratio under this criteria, (ref Appendix 5.1.02 for theory) and shows also that long, small diameter bobbins are undesirable (as are short, large diameter bobbins to a lesser degree).

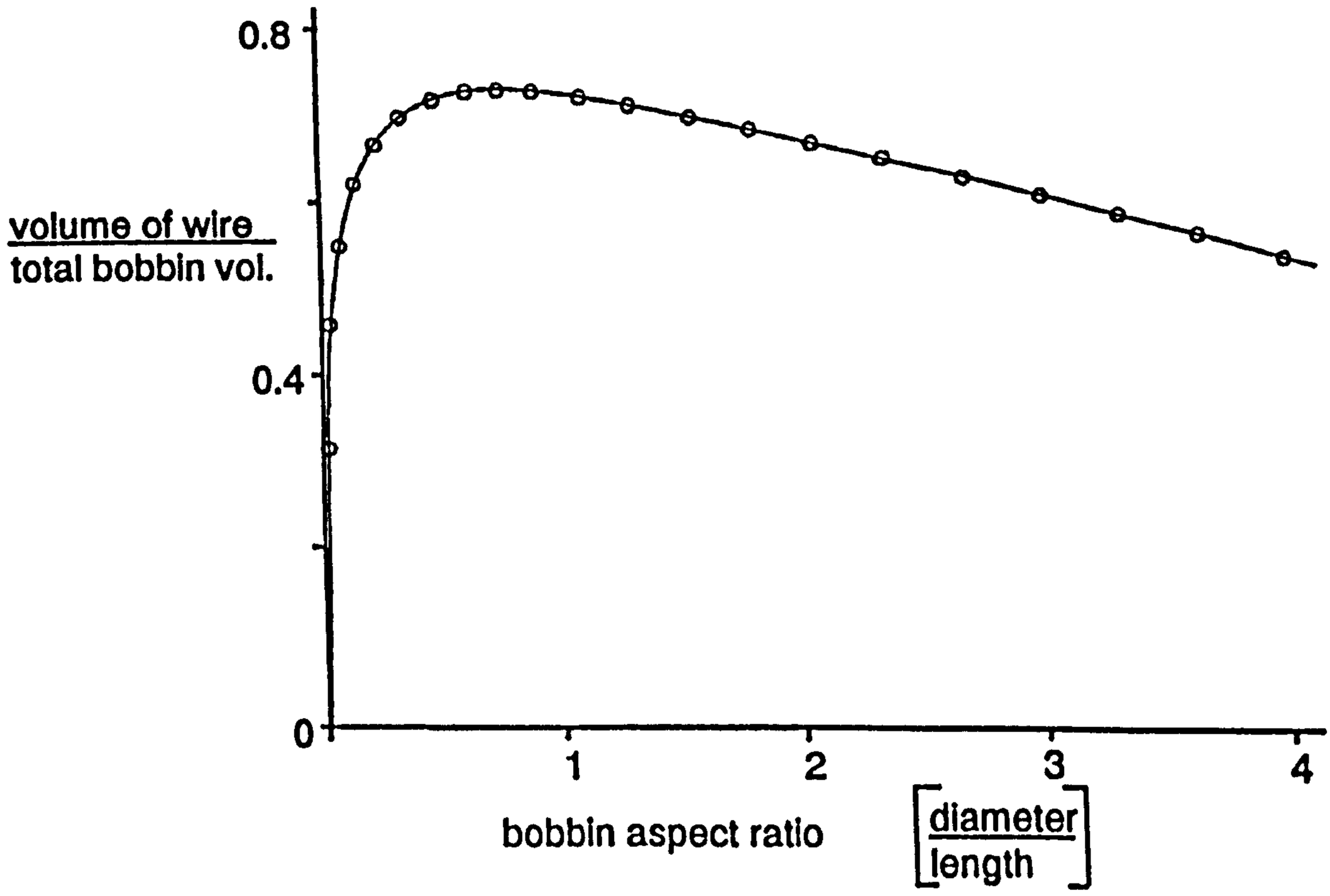

Figure 5.1.02 Bobbin volume ratio vs aspect ratio for a typical bobbin

The minimum volume of wire on each bobbin was specified, eventually, as 550cm^3. The minimum flange thickness and core diameter are specified as 9mm and 33mm respectively.

5.2 Bobbin Orientation

The cylindrical bobbin may adopt any orientation within the conical region available to each bobbin and carrier. There are various assumptions made before developing general purpose bobbin orientation theories. These are that:

a) The carrier and its track bearings will fit into the space left within the conical region by the bobbin.
b) Any braid angle is possible. This is closely related to carrier position and design. The higher the braid angle the shorter the conical regions length for a given machine diameter.
c) The conical regions base plane is that of the wand tip (i.e. spherical). However, this is approximated to a flat plane to simplify the theory.
d) The conical region is reduced by the maximum wire deflection along each wire path. This highlights the advantages of a single harmonic wand motion in which wire deflection increases the volume of the conical region, which is not the case when using a triple harmonic wand motion.

A general theory is developed and the various specified parameters and constraints (above) are then imposed on the system. There are, realistically, two general orientations which the bobbin may adopt within the conical region.

i) The bobbin axis is coincident with the central axis of the conical region. This is referred to as type 1 orientation and is shown in figure 5.2.01.

ii) The bobbin axis lies at 90° to the central axis of the conical region and is at any angle to the circumferential line (horizontal axis line). This is referred to as type 2 orientation and is shown in figure 5.2.02.

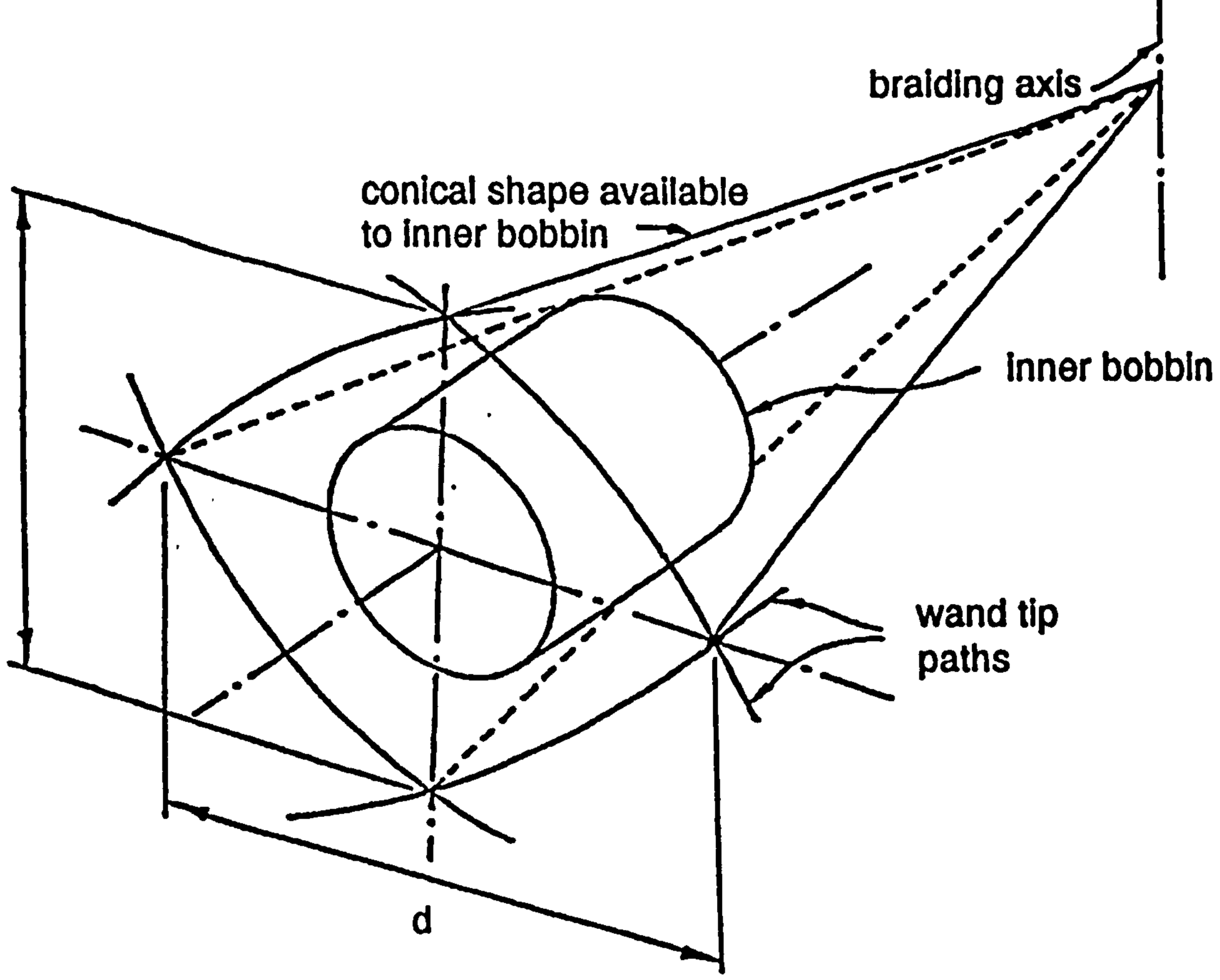

Figure 5.2.01 Type 1 bobbin orientation

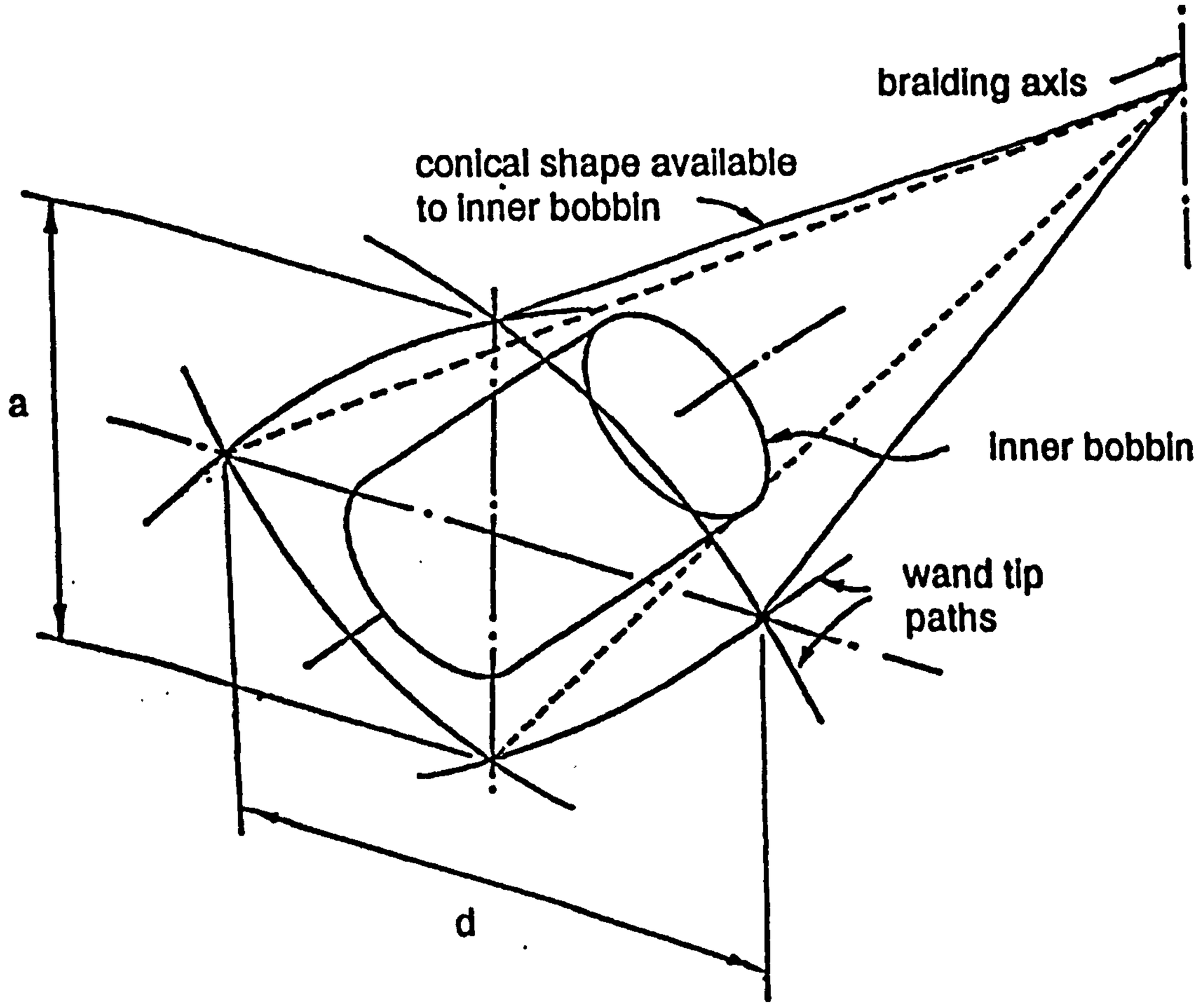

Figure 5.2.02 Type 2 bobbin orientation

5.2.1. Optimising Type 1 Bobbin Orientation

Since in this orientation the bobbin axis is coincident with the conical region's axis optimisation is simply determining the largest circular cone which will fit into the conical region and then determining the proportions of the largest cylinder which will fit into this cone. To find the largest possible cone base diameter the maximum circle which can be inscribed in the conical region's base shape must be found (Fig. 5.2.11). Each wand tip path is expressed algebraically (ref. Appendix 5.2.11) and, whilst an explicit solution for the maximum inscribed circle is possible, a numerical technique is used which is faster and more versatile should the wand tip motion, or any other parameters, be changed.

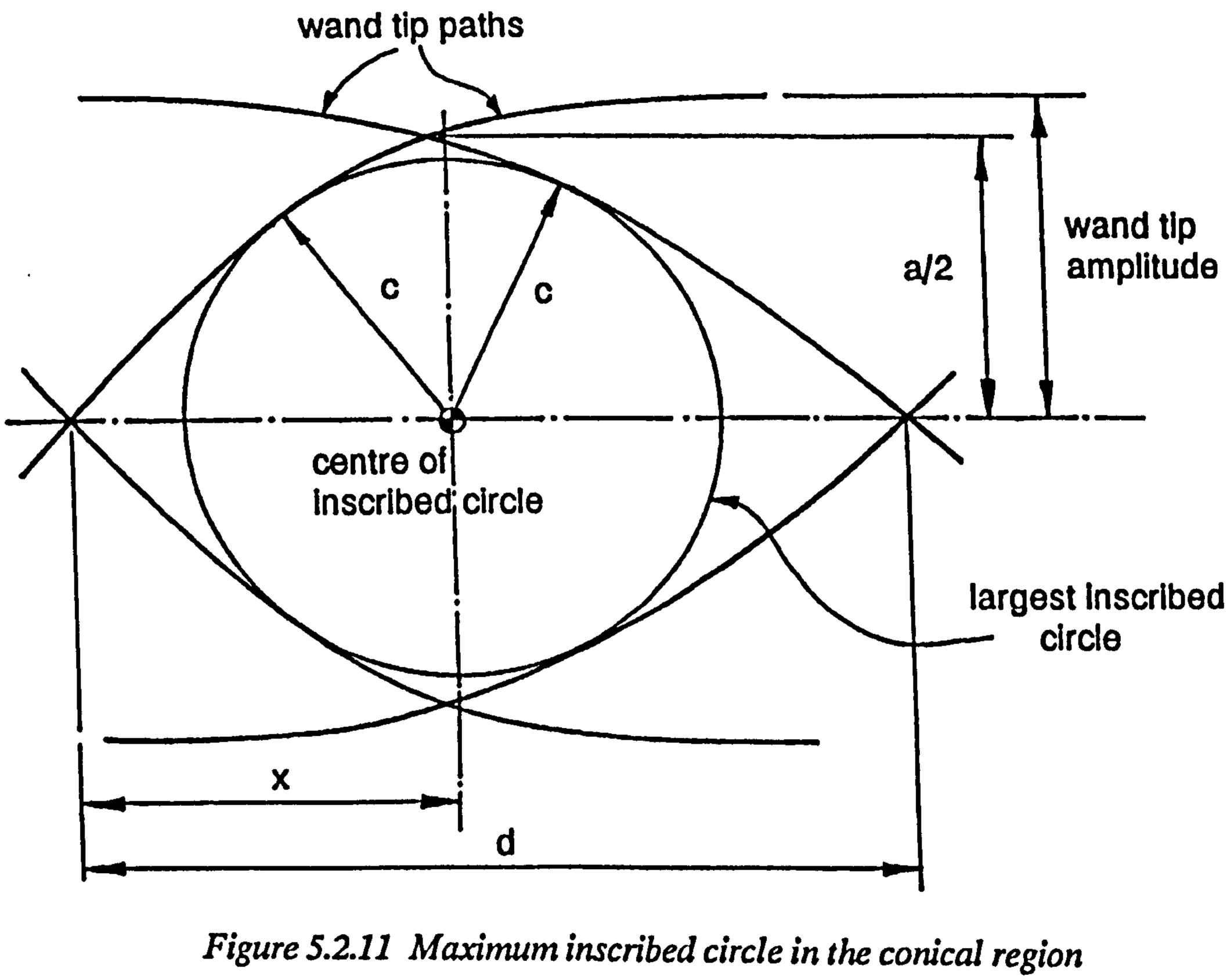

Figure 5.2.11 Maximum inscribed circle in the conical region cross section

This method provides the base diameter for the largest inscribed cone and also the central axis relative to the central axis of the conical region (which is where the lines joining opposite apexes cross).

The proportions of the maximum volume of cylinder which will fit into this cone are found algebraically (ref. Appendix 5.2.12). This reveals that the ideal cylinder is always one third of the length of the cone and two thirds the cone base diameter.

If the radius from machine centre to wand tip is changed the ratio a/d also changes (Fig. 5.2.11), since a is a function of the wand tip path only and d is a twelfth of the circumference at the wand tip diameter. The volume utilization ratio (volume of conical region over volume of bobbin) reaches a minimum of approximately 2.75. Figure 5.2.12 shows the effect on volume utilisation of the ratio a/d.

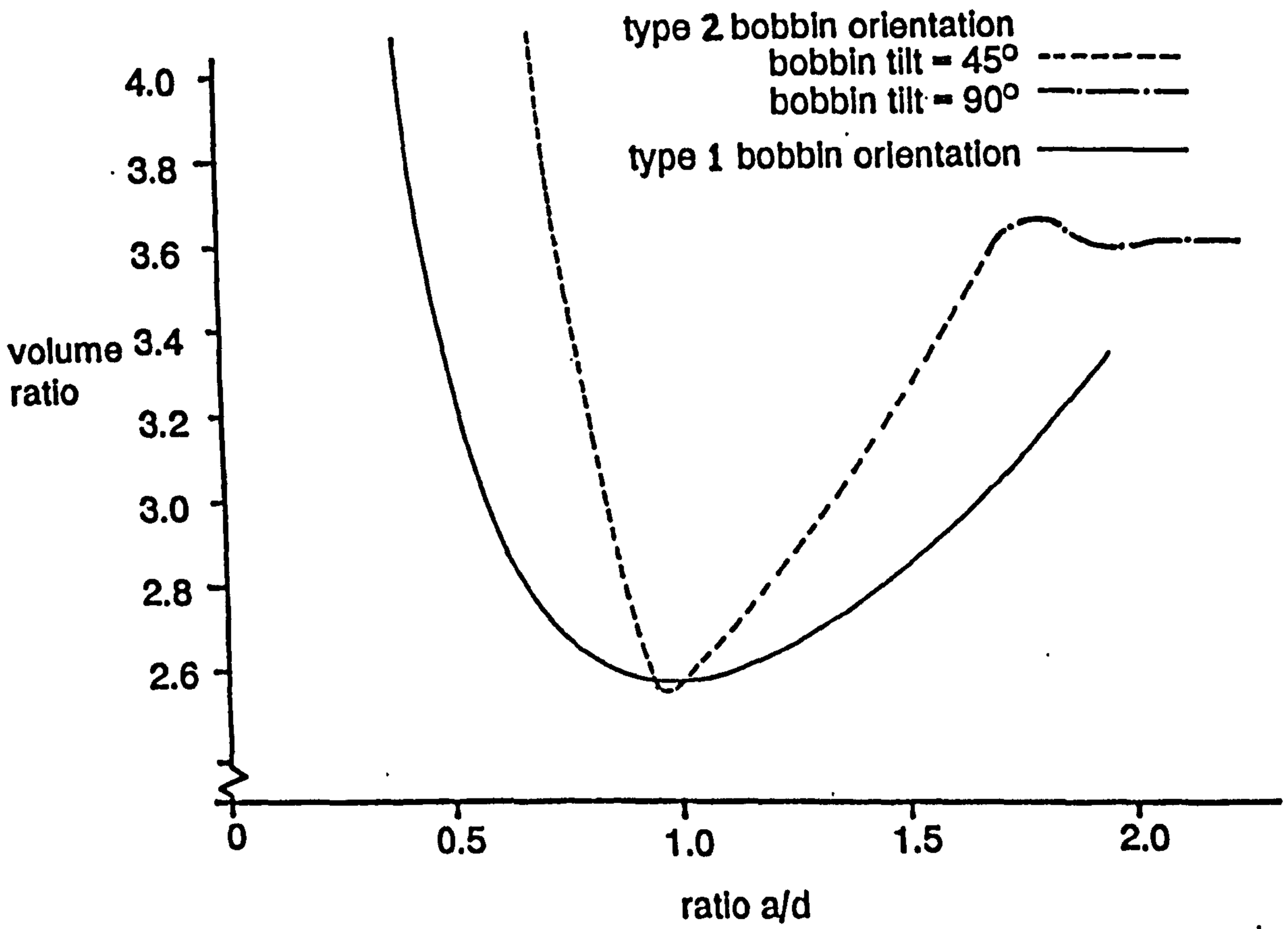

Figure 5.2.12 Graph of bobbin volume utilisation

The advantages with bobbin orientation type 1 are:
a) The range of values of a/d over which the volume utilization ratio is less than 3.5 is relatively large.

b) If a 90° braid angle is used the spindle becomes very small as there is little or no bending moment applied by the bobbin.

c) This orientation of bobbin allows full utilisation of a conically wound bobbin and the large wire volume gained which renders other systems, which cannot use a conical bobbin, uncompetetive.

The limitations with this orientation of bobbin (type 1) are:
a) If the braiding angle is not 90° the bobbin spindle must be strengthened to accommodate the bending moments, or the bobbin must be supported at both ends which increases inner carrier cost and complexity.

b) The aspect ratio of the ideal bobbin in this orientation tends to be lower than that for the optimum wire volume/bobbin volume ratio (Fig. 5.1.02).

To achieve 550cm^3 of wire the bobbin aspect ratio is approximately 0.51 and the ratio a/d is 0.72. The corresponding machine (wand tip to braid point) radius is 480mm.

5.2.2 Optimising Type 2 Bobbin Orientation

Bobbin orientation type 2 has the bobbin axis at 90° to the central axis of the conical region as shown in figure 5.2.02. The overall optimisation consists of a combination of several different smaller numerical optimisation routines "nested" within one another and implemented in a computer program. Figure 5.2.21 shows the geometric model used for optimisation.

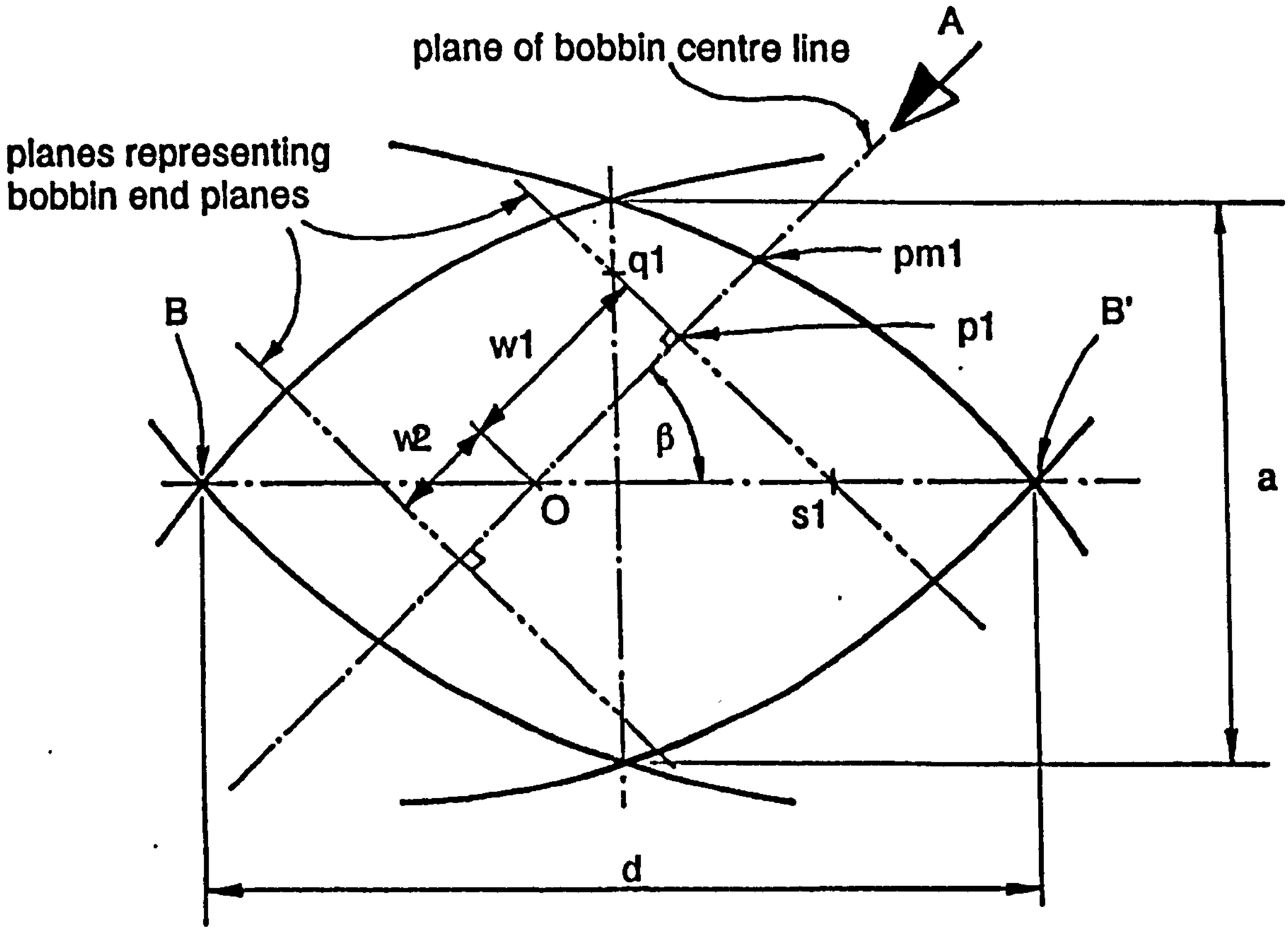

maximum inscribed circle
with centre on line p1 - lm1

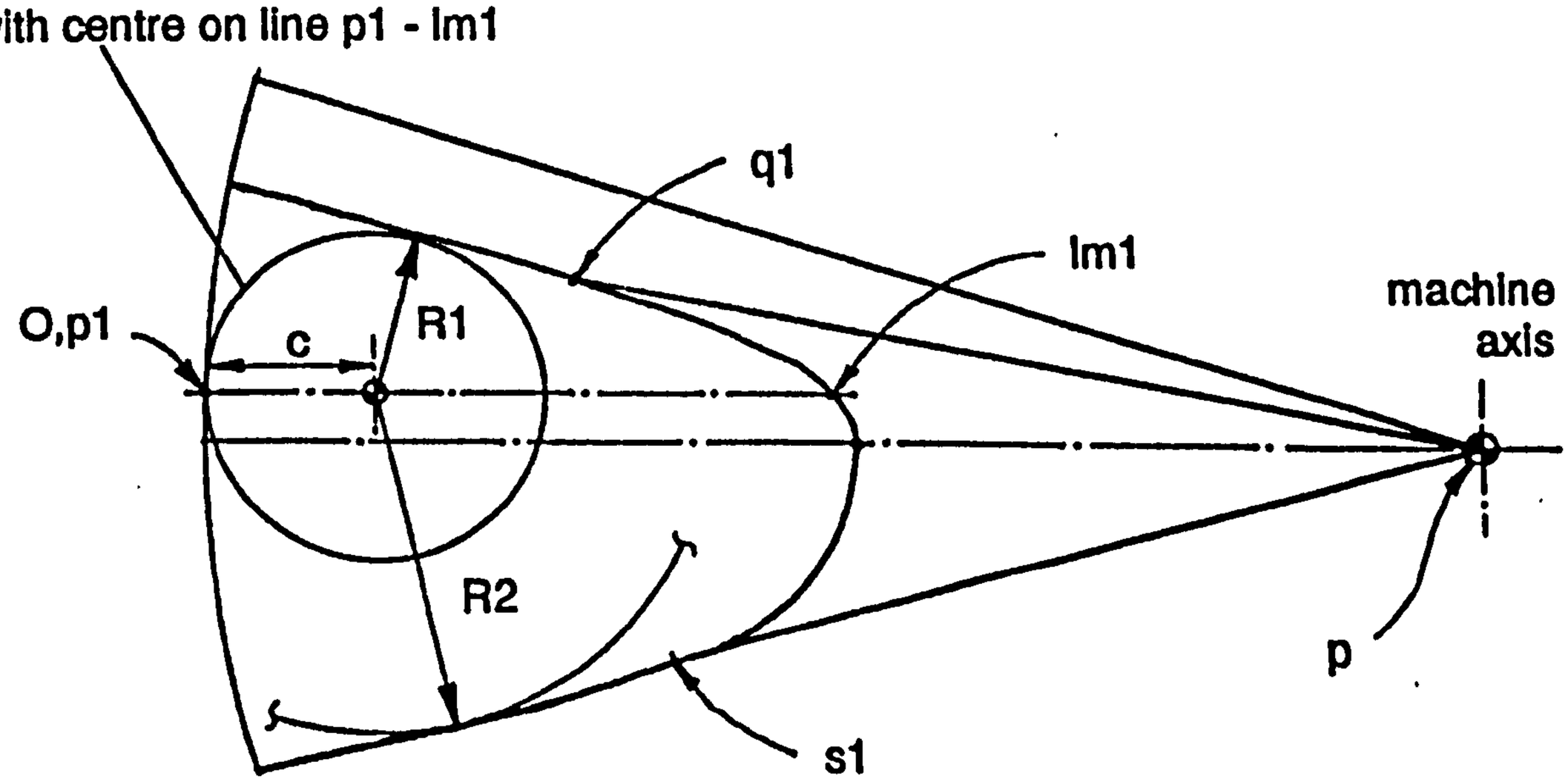

view from A of cut plane

Figure 5.2.21 Basis of bobbin type 2 orientation optimisation

The base of the conical region is again represented algebraically (Appendix 5.2.11) as four separate curves. The bobbin end face can also be represented as a straight line which is parallel to the conical regions central axis. The optimisation procedure used can be summarised as:

i) A point "O" along the horizontal axis BB' is incremented from point B to B'. For each position of "O" the following procedures are executed.

ii) The bobbin central axis tilt β is incremented from 0° to 90° (since the conical base shape is symmetric about BB'). For each value of β the following routines are executed.

iii) The "half" bobbin length w1 is incremented from 0 to length "O"-"pm1" (Fig. 5.2.21). For each value of w1 the following routines are executed.

iv) The bobbin end face plane is perpendicular to "O"-"p1" (length w1) and cuts the conical region to reveal a plane shape from which the largest bobbin diameter is found. The cut shape is determined as an array of points.

v) Each cut shape's centre line (p1-lm1) must contain the centre of the bobbin end face. The distance "c" (Fig. 5.2.21) is incremented from "p1" until c = R1 or R2, whichever is smaller. This value of c is the bobbin radius.

vi) Each value of w1 and corresponding bobbin radius (c) is stored in an array.

vii) The entire process from iii) to vi) is repeated for w2 (i.e. in the opposite direction), and an array of values of w2 and corresponding bobbin radii are again found.

viii) Each value of radius is matched with lengths of w1 and w2 and this results in a bobbin length (w1 + w2) for that radius and hence a volume.

ix) The largest volume (and corresponding bobbin radius and length) is stored for each value of β and for each position of "O" of the central bobbin axis between B and B'.

x) The maximum bobbin volume, its radius, length, angle of tilt and central axis position is then determined.

Where necessary (and possible) use is made of numerical root solving techniques (particularly the Newton-Raphson method). These techniques for optimising bobbin orientation are somewhat lengthy, yet are as accurate as any other provided the increments are small enough.

The result of this optimisation is that the ideal angle of tilt of the bobbin axis is dependent upon the ratio of a/d. As a/d approaches unity the conical region's base assumes almost square proportions (albeit distorted) and a bobbin tilt of 45° is the optimum. Indeed, at this point the volume utilisation ratio becomes marginally superior to that of bobbin orientation type 1 as shown in figure 5.2.12. However, a slight shift away from unity of the ratio a/d rapidly increases the volume utilisation ratio and the optimum orientation eventually becomes 0° or 90°.

The advantages of the type 2 bobbin orientation are:

a) The volume utilization is superior to any other, but only over a very short range of values of a/d.

b) The bobbin can be supported at each end and a spindle is therefore unnecessary.

The limitations of this bobbin orientation are:

a) Under most circumstances the value of a/d is not very near unity and the volume utilisation ratio is far from the minimum possible.

b) A bobbin brake mechanism, for wire tension control, is difficult to incorporate without detracting from the volume of the bobbin.

To achieve a wire volume of $550cm^3$ the aspect ratio of the bobbin is approximately 1.0 (Fig. 5.1.02) but the ratio a/d is only 0.59 with a volume utilisation approaching 5. The corresponding machine radius from braiding point to wand pivot is approximately 590mm.

5.3 Conclusions On Inner Bobbin Optimisation

The bobbin form chosen is the standard cylindrical bobbin. The conically wound bobbin represents difficulties (not least in acceptance by braiding machine users) in winding to a reasonable quality. However, the increase in volume for a conical bobbin is such that the ability of a bobbin orientation to take advantage of this is highly desirable. Bobbin orientation type 1 does this whilst orientation type 2 does not.

Of the two basic bobbin orientations realistically viable, (Fig. 5.2.01 and Fig. 5.2.02), orientation type 2 gives the marginally better volume utilisation, but only for a certain "shape" of base of the conical region. This fact may be utilised to good effect if no restraints are placed on the system. But the wand tip amplitude is restricted (220mm) for aesthetic reasons and the wire volume on the bobbin is specified (550cm^3) for the machines target market. However, under these restraints the type 2 bobbin orientation cannot support a 550cm^3 wire volume and have a better volume utilisation ratio than bobbin orientation type 1.

For these reasons orientation type 1 is chosen since it can support the specified wire volume bobbin within a smaller machine (wand tip) diameter and, therefore, the load on the inner carrier bearings are lower. This machine diameter is, theoretically, 960mm and the conical region's base shape has an a/d ratio of 0.72 (Fig. 5.2.12) which results in a volume utilisation ratio of 2.95 (i.e. Bobbin volume is 0.34 of the total conical region volume). The aspect ratio of this optimised bobbin is 0.5 which is close to the optimum for maximum wire volume (Fig. 5.1.02).

The assumption that the inner bobbin carrier and bearing unit will fit into the volume left by the bobbin within the conical region is absolutely vital to the optimisation routine. If this is not the case, the optimisation of bobbin orientation must be revised and recalculated.

CHAPTER SIX

INNER CARRIER TRACK BEARING SELECTION

6.0 Introduction

Each inner bobbin is supported by a carrier which also acts as a bearing against the track on which they rotate around the machine. To effect the braid at the machine centre, each of the wires from the contra-rotating outer bobbins are passed first over, then under, every second inner bobbin and carrier. The combined outer wire paths completely encompass each inner bobbin and the drive which propels the bobbin and carrier around the machine must be intermittent. The drive must be passed from one region to another, to avoid fouling an outer wire, in "bucket brigade" fashion. This inner carrier drive system is covered in chapter 8 and is usually kept separate from the carrier-to-track bearing system (although one carrier bearing system outlined is capable of combining the two functions).

There are basically three types of inner carrier track arrangements, which are:

i) Where there is no track as such and the carriers are supported and located by the drive system as shown in figure 6.0.01.

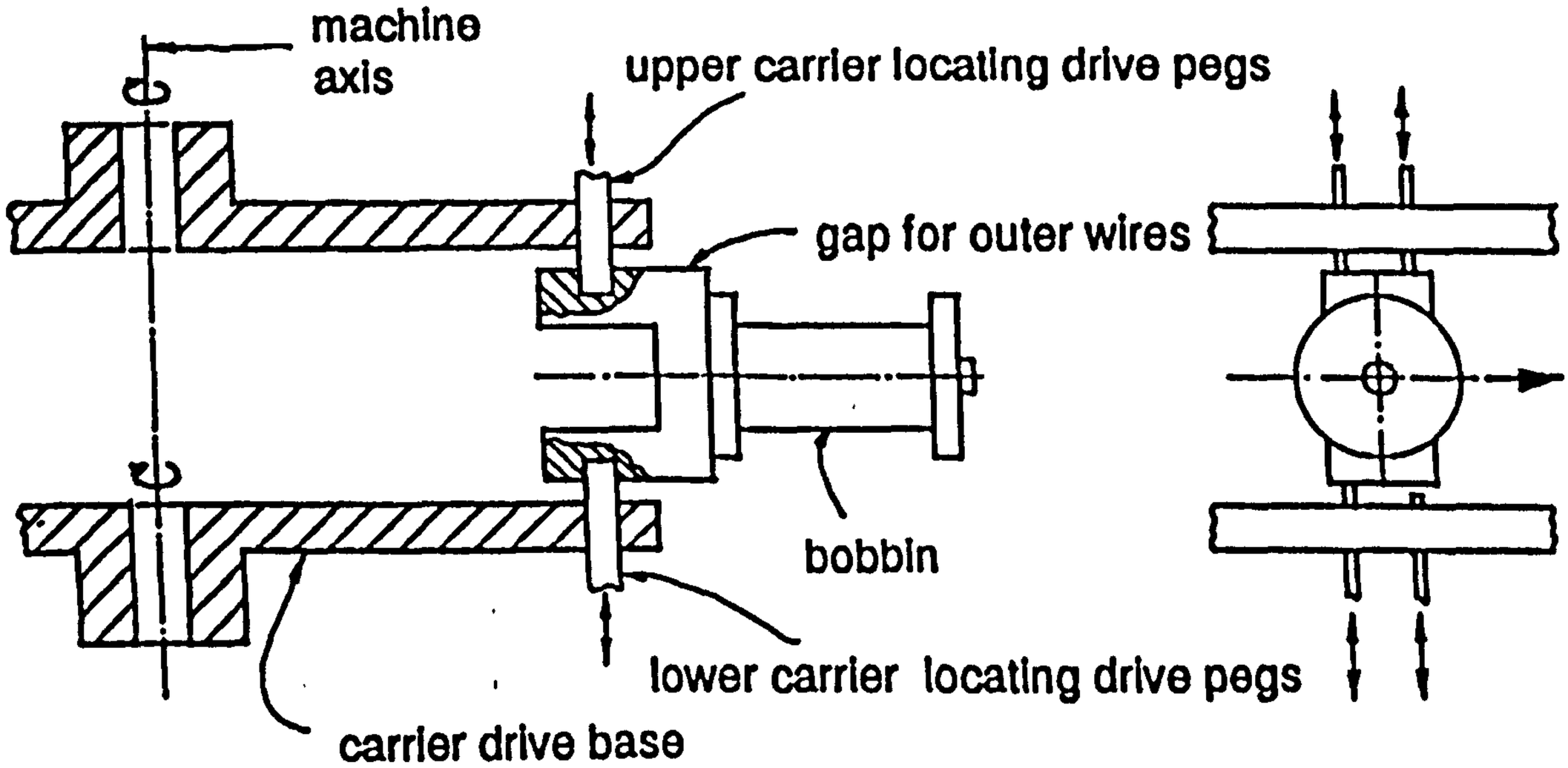

Figure 6.0.01 Inner carrier supported by the drive system

This system is practical only at very low speeds since to locate fully requires contact at four precise points. This cannot be maintained at high speed as the bearing surfaces are subject to continuous impacts (rather than sliding, or rolling etc.) and excessive wear results.

ii) Where the track is stationary, as depicted in figure 6.0.02, and has a continuous slot machined through it to allow the passage of the outer wires which all move along the same path relative to ground.

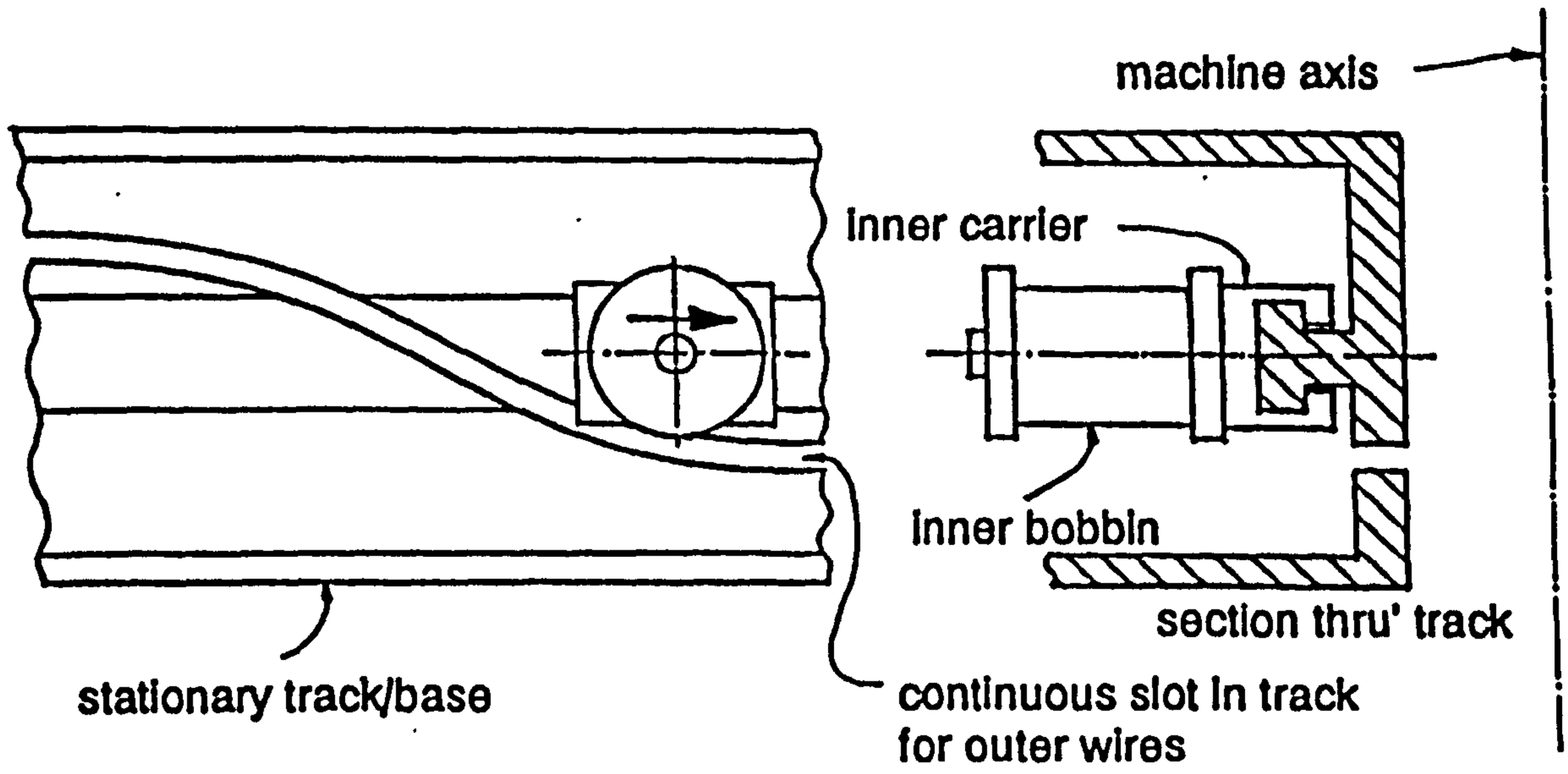

Figure 6.0.02 Stationary track system

The major advantage with this system is that the relative speed of the inner carriers is low (equivalent to the machine speed). This allows the use of bearing systems which have speed limits that would be exceeded with a contra-rotating track system.

The drawbacks with this system are that the track must be supported from both "sides" of the machined slot (ie. the track is in two halves). This is extremely difficult and costly without severely compromising the performance of other areas of the braided machine. A minor drawback is that to change braid pattern (from over 2, under 2) the track and wand drive must all be changed.

iii) Where the track rotates with the outer bobbins and their respective wand mechanisms, and the wire path becomes a simple slot machined in the track at approximately 90° to the direction of travel of the inner bobbins and carriers. This system is represented in figure 6.0.03.

This track system is the simplest and least costly, but the relative speed of the inner carrier is twice machine speed. However, if the bearing system can tolerate the high speed, this track system is preferred to all others on cost grounds alone.

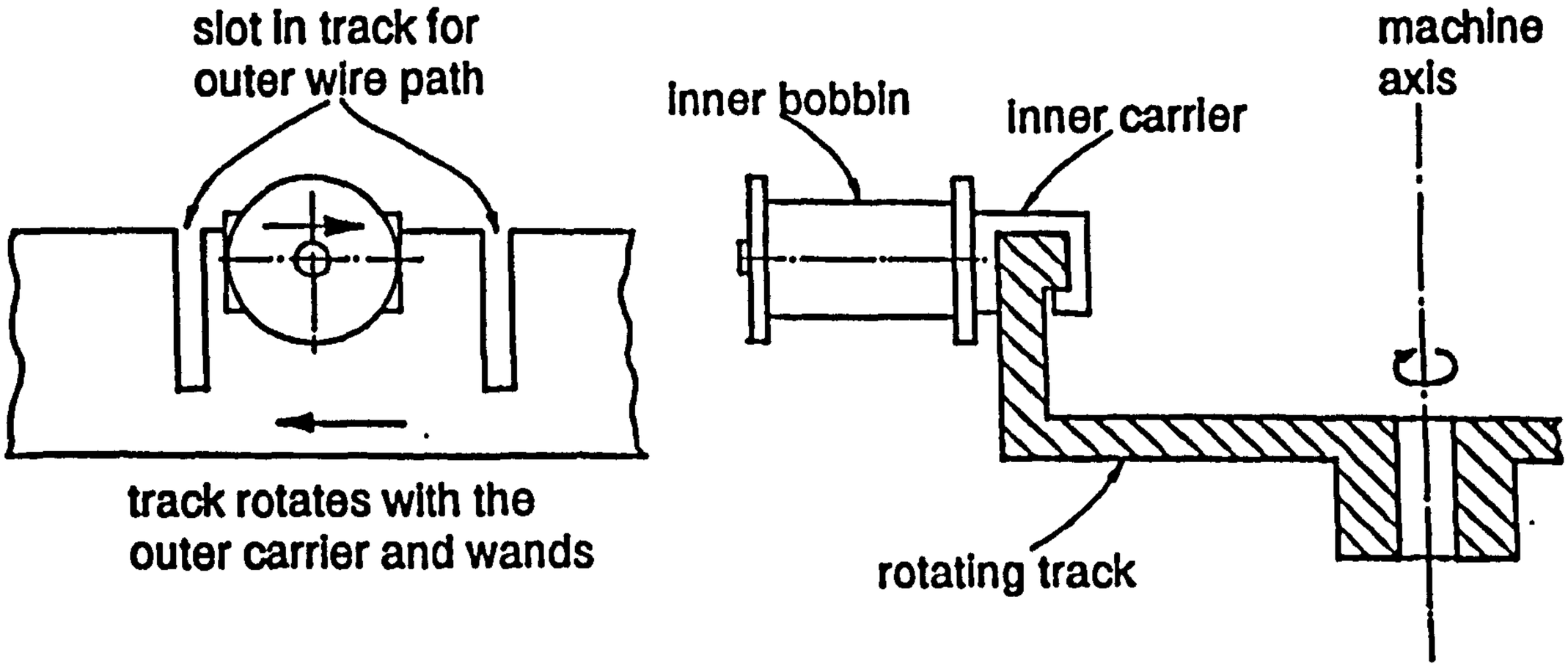

Figure 6.0.03 Moving track system

The forces existing between the track and carrier change with machine speed and bobbin mass. As the speed increases the load becomes predominantly due to centrifugal force and not merely the weight of the carrier and bobbin. On a horizontal machine the acceleration of the carrier changes by ±g (gravity) for every revolution. On a vertical machine (most common), the weight of the carrier is perpendicular to the centrifugal force and so the ideal angle of tilt of the bobbin, and therefore the braiding angle, should be 85°, [$\arctan(rw^2/g)$, where r is the carrier centre of mass radius, and w is its angular velocity]. However, this angle is close to a 90° braiding angle (assumed for the wand cam design, etc.) and changing the braiding angle increases substantially the cost of the wand cam and associated components. For this reason a 90° braid angle is chosen.

The other external forces which contribute to the total carrier bearing loads are; wire tension, driving force and corresponding shock loads, and any shock loads resulting from the carrier crossing the slot in the track.

In most bearing systems the load capacity is proportional, to some degree, to the area of the bearing "surface", and the speed is limited. This indicates that a bearing featuring several bearing areas in parallel is the most effective means of increasing the overall load capacity. However, this method requires (with most bearing systems) very high tolerances between the adjacent bearing sets which is not feasible. The shape of the space into which the inner carrier must fit (conical) is such that the further from the machine centre (braiding point) the larger the sectional area available to each carrier bearing, and so the higher the potential load capacity.

However, the inner carrier system is constrained to the same conical shaped space as the bobbin. Also for effective bobbin volume utilisation the carrier should not impinge on the space required by the bobbin. This effectively positions the carrier radially inside the bobbin. The ideal inner carrier bearing system is one which does not require the conical region (formed by the outer wire paths) to be increased over that necessary for optimum bobbin orientation. However, this may not be the optimum bearing system and an increase in the conical region volume to accommodate a carrier bearing situated radially outside the bobbin may result in a higher performance system. Such a system would allow a large bearing surface area but also has a higher speed.

The inner carrier bearing system must perform certain fundamental functions:

a) The bearing must support all the loads at the speeds envisaged.

b) The bearing system must have a life of at least 15,000 hours at full speed with normal bobbin masses.

c) The carrier bearing system must not transgress the surface of the conical region formed by the superposition of the outer wire paths (and into which the inner bobbin also fits).

d) The bearing must possess adequate stiffness in roll, yaw and pitch whilst subject to all the envisaged forces, to allow correct location for the carrier drive system.

e) The bearing must not contaminate the product to any great extent, with oil or other undesirable substances.

f) The bearing must not be severely affected by the contamination of the track/bearing interface with braid material debris (ie. wire or yarn).

g) The bearing system should consume as little power as possible. This includes both frictional power loss and any power required for operation of the bearing.

In choosing an inner carrier bearing system the cost has a relatively high priority and the compromise between cost and performance will hopefully also satisfy the criteria in a) to g) above. Four different types of inner carrier bearing systems are studied and appraisals made on the critical areas described above in a) to g).

The four systems studied are:

i) Aerostatic bearing systems.
ii) Magnetic and electromagnetic bearing systems.
iii) Plain bearings systems.
iv) Roller bearing systems.

6.1 Appraisals of Inner Carrier Bearing Systems

6.1.1 Aerostatic Bearing Systems

A theoretical and experimental study of aerostatic bearings is detailed in Appendix 6.1.1. The study showed that the correlation of theory and experimental results gave a reasonably accurate model of an aerostatic bearing system.

The minimum running clearance chosen for such a model is 0.025mm (0.001") which is a compromise between the prohibitive cost of manufacturing a system using very small clearances and the decreased efficiency of a system utilising larger clearances. The estimated air mass flow rate for such a system, using an 11 kg inner carrier and bobbin running at 150 rpm, is 0.084 kg/s (118 cfm) which requires a 15 kW (20 Hp) compressor. The high cost of manufacturing a precision air bearing track together with this large power requirement, and the inability to tolerate braiding product debris, render aerostatic bearing an impractical solution for supporting the inner carriers. In addition, the stability of an aerostatic bearing running at speed is marginal (ref appendix 6.1.1) and resonance of the system due to impulse loadings is probable at some point as the bobbin mass is consumed.

6.1.2 Magnetic and Electromagnetic Bearing Systems

A study is made into the feasibility of using four different types of magnetic and electromagnetic bearing systems, which are: (ref appendix 6.1.2 for detailed appraisal)

i) Permanent magnets in repulsion.
ii) Eddy current repulsion using mains frequency excitation.
iii) Levitation using superconducting magnets.
iv) Attraction using controlled D.C. electromagnets.

All these "bearing types" are non-contact systems (ie. there is always an air gap between bearing surfaces). At least one of the powered systems are capable of combining the carrier drive in addition to the bearing function. However, the speeds envisaged are such that a relatively complex drive system would be necessary, adding further cost to an already expensive system.

The most promising system is the permanent magnet system, however all suffer from major drawbacks which are:

i) The size of magnets required adversely effects the bobbin optimisation within the conical region.

ii) The non controlled magnets have low stiffness which severely reduces the load capacity if opposing bearing faces are used for location.

iii) The non controlled magnetic bearing systems are underdamped due to air being the damping medium.

iv) All but permanent magnet systems require appreciable power (in the order of 1 kw per carrier) to operate, and this generally necessitates water cooled track magnet cores.

For these reasons a magnetic or electromagnetic inner carrier bearing system is deemed unsuitable.

6.1.3 Plain Bearing Systems

There are three basic types of plain bearings considered:

i) Non-lubricated (dry) bearings using a self lubricating bearing material.

ii) Boundary layer, oil lubricated bearings.

iii) Hydrodynamic, oil lubricated bearings.

The loads which the carrier bearing must support may be separated into the major centrifugal force component which acts radially from the machine centre and the carrier weight which acts vertically (assuming a vertical machine, which is most common).

The major problem when selecting a plain bearing is the surface speed. A stationary track, ideally situated radially inside the bobbin, results in the lowest surface speed of approximately 6 m/s at 150 rpm machine speed. However, this type of track is too costly to produce accurately and a track which rotates with the outer bobbins and carriers is preferred. The surface speed of this system is 12 m/s at 150 rpm machine speed.

The pressure due to the centripetal acceleration on an 11 kg bobbin and carrier at this point is approximately 180 KPa for a single bearing surface. The performance of both self lubricating bearings and boundary lubricated bearings is dictated by the value of PV, where P is the pressure, and V is the surface speed of the bearing. The factor PV is used to determine both bearing life and relubrication periods (if required), but each combination of bearing materials has a limiting value of PV. The individual values of pressure (P) and velocity (V) also have limits.

Dry bearings running with self lubricating materials are generally low speed, low pressure systems and will not run continuously at 12 m/s (or 6 m/s).

Hydrodynamic bearings are not suitable as the volume of oil flow required is such that product contamination becomes inevitable.

Boundary layer lubricated bearings have a higher speed potential and P.V. value than dry bearings, with bronzes and irons having the highest PV values of 1750 KPa m/s. However both have maximum rated sliding velocities of 4 m/s and 7.5 m/s respectively. The PV value for a bearing used on an inner carrier is approximately 2260 KPa m/s with a velocity of 12 m/s. For this reason a boundary layer lubricated bearing is not acceptable for supporting the main centrifugal load on an inner carrier. It is, however, capable of supporting the relatively light loads associated with the carrier and bobbin weight provided the bearing surfaces are regularly re-lubricated.

6.1.4 Roller Bearing Systems

The three types of rolling element bearing systems considered are:

i) Recirculating ball "linear" bearing systems.

ii) Roller bearings which form the track (the carriers incorporate plain track sections).

iii) Roller bearings mounted on the carriers running on a plain or contoured track (which features slots for the outer wire paths).

A curved recirculating ball linear bearing system whilst having the required load capacity does not allow speeds greater than 5 m/s and is unsuitable for this reason.

A system of roller bearings forming a track ((ii) above), as shown in figure 6.1.40, is broadly similar to the inverse where the rollers are mounted on the carrier ((iii) above). However, it has the disadvantages of having to machine all the roller centres accurately to each other rather than only those on one carrier, and of having a larger effective gap between the track sectors (mounted on the carriers), since adjacent carriers cannot be positioned as close to one another as can a single slot in a track moving with the outer wires (ie. the system with rollers mounted on the carriers).

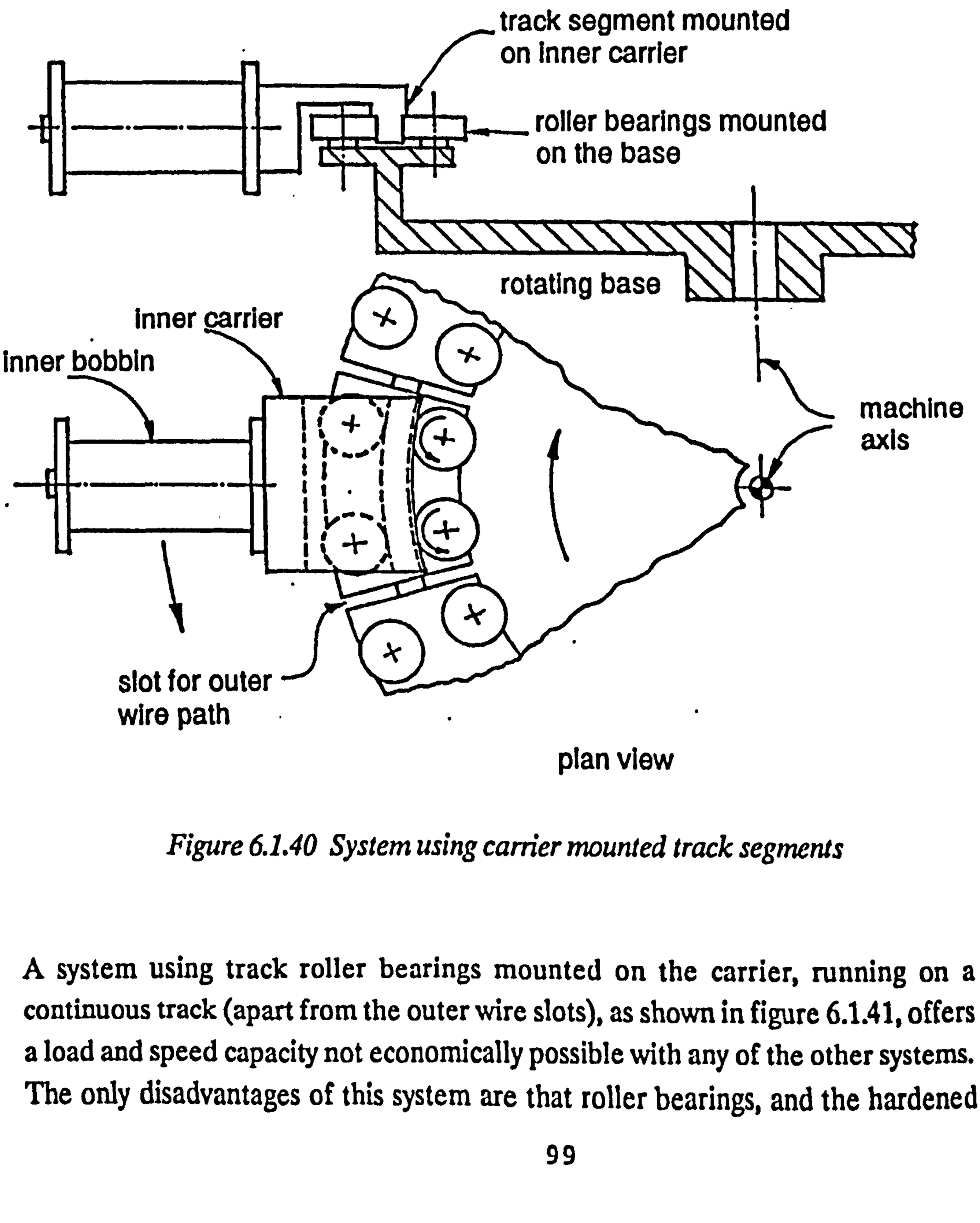

Figure 6.1.40 System using carrier mounted track segments

A system using track roller bearings mounted on the carrier, running on a continuous track (apart from the outer wire slots), as shown in figure 6.1.41, offers a load and speed capacity not economically possible with any of the other systems. The only disadvantages of this system are that roller bearings, and the hardened

and ground track they require, is bulky and expensive relative to a boundary lubricated plain bearing.

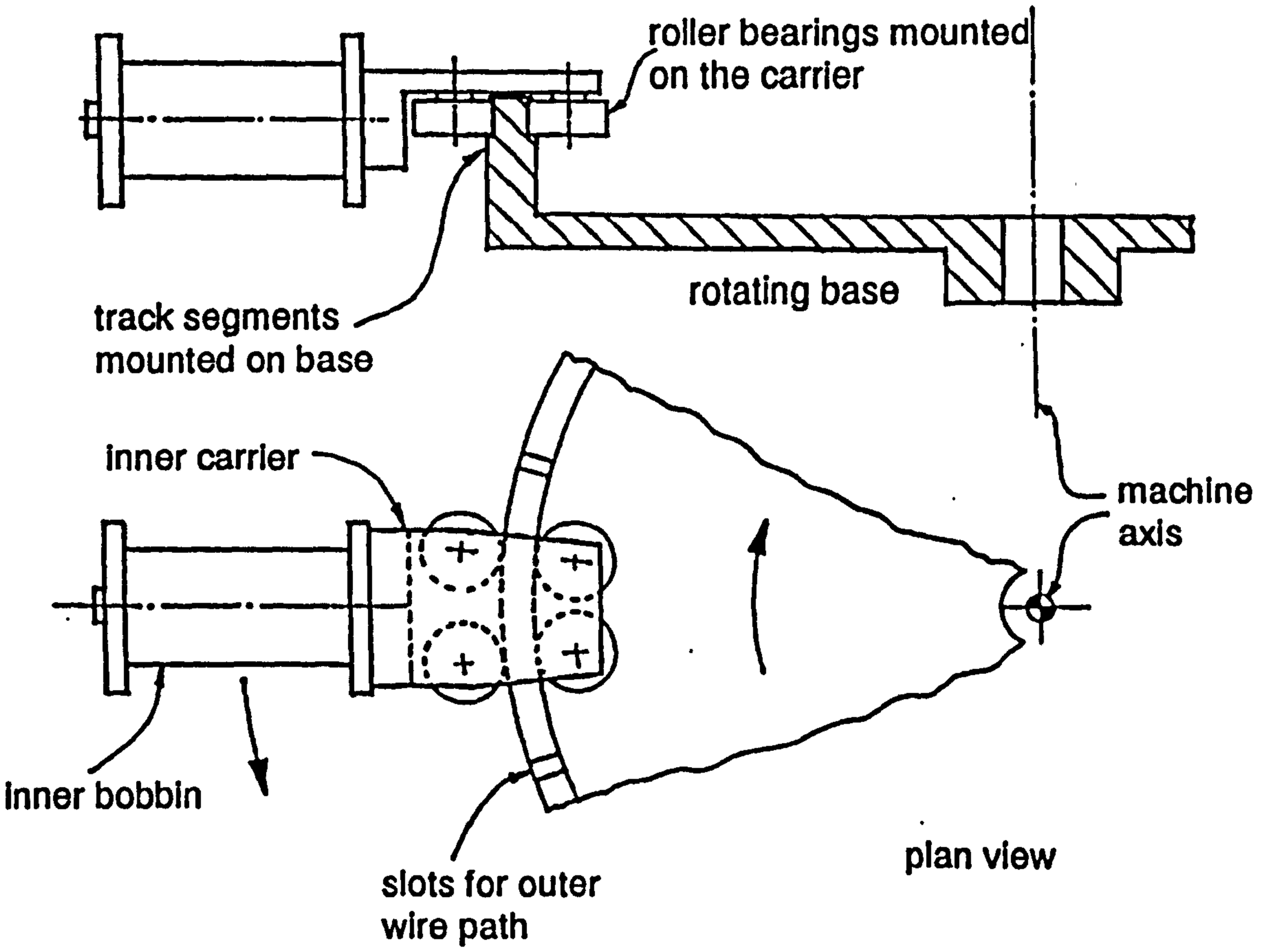

Figure 6.1.41 System using carrier mounted rollers

A high capacity, high speed bearing system is only required for the major centrifugal load between carrier and track. The weight of the carrier and bobbin, together with any additional location bearing surfaces may be supported by a series of plain boundary lubricated bearings, provided the loads are low (ref section 6.1.3).

6.2 Conclusions to Inner Carrier Track Bearing Selection

Of the various bearing systems studied only the roller bearing systems are suitable for use on the inner carriers of a rotary braider.

Plain, boundary lubricated, bearings are limited particularly in maximum speed but in principle are suitable for light loads at high speeds (ie. locating the carrier but not for supporting the main load). The machine concept may be changed to alleviate this problem in two ways.

First, the use of a stationary track halves the relative speed, but this leads to a complex and costly machine design.

Secondly, the inner bobbins may be stationary and both the product core and outer bobbins rotate. This eliminates the major centrifugal force on the carrier bearings and allows a larger diameter machine with a lower outer wire/wand amplitude. However, this is impractical on all but the smallest machines (less than 24 carrier) as the product wind on/wind off drums are generally too large.

For a 24 carrier machine the simplest method is a track which rotates with the outer bobbins and wand mechanisms. Only a roller bearing system is suitable in this situation as it offers high load and high speed capacity.

The roller bearing system is studied in greater depth in order to determine its longevity and performance limits.

CHAPTER SEVEN

TRACK ROLLER BEARING SYSTEM DESIGN

7.0 Introduction

The main issues that need considering in designing a roller bearing system for inner carrier support are the exact nature of loads on each bearing and the optimum configuration of the rollers within the carrier.

a) Roller Bearing Loads

The main continuous load on the rollers is due to the centrifugal force of the carrier and bobbin as it revolves around the machine. However, as the carrier crosses the slots in the track (necessary for the outer wire paths) the bearings experience a loss and sudden resumption of load. In the worst case the roller will hit the corner of the next track sector after the slot and this will induce a shock load on the bearing which must be quantified.

The longevity of track roller bearings is well documented and is determined to a degree, by the contact stresses in the roller. These stresses may be determined theoretically for any shape of contact surface between track and roller. Applying these contacting surface stress factors to the actual peak shock loads, found experimentally, results in an equivalent load which may be used in the standard bearing life theory.

b) Roller Bearing Configurations

The trajectory of the rollers as they fall into the slots in the track is affected by the number of rollers and their configuration and this ultimately determines the shock load on each bearing. Experiments performed on test rigs measure inner carrier movement and roller trajectories, and show the practicalities (and feasibility) of using multi roller bearing configurations. This is used with the theory for bearing life to predict the optimum configuration of the rollers which must fit into the space left in the conically shaped region by the optimised bobbin.

7.1 Theoretical Analysis of Roller Bearing Systems

7.1.1 Contact Stress

A track roller bearing will usually fail due to the hardened outer race, or "tyre", breaking up as a result of Hertzian contact stresses induced as it rolls. The longevity of a bearing is determined using this stress, in that the standard life equation is valid only when the roller is running on a flat surface. In this way the bearing load is directly related to the maximum Hertzian contact stress (which occurs slightly below the contact surface).

If the roller contacts the corner of the track sector, after crossing the gap, the stress will increase dramatically, and even a 1 mm radius at the track sector edge results in an increase in contact stress of 135 times that of a flat surface.

If the track surface is not flat a contact stress factor may be found relative to that for a flat surface. This may then be used to yield an equivalent load which would give rise to the same peak stress were the track surface flat. This contact stress factor rises sharply for a convex track surface as the radius of curvature decreases but becomes less than 1 (lower contact stress than a flat track) when the track is concave. This is the situation which is predominant as the carrier roller ran radially inside the track.

The criteria for the track sector edges is, therefore, to ensure the rollers always run on a surface with as low a contact stress factor as possible. Ideally this is a concave or a flat surface.

This applies mainly to the leading edge on which each roller impacts after crossing the slots in the track. Indeed, the ideal situation above is impossible to achieve for a single roller on the trailing edge of each track sector, but is possible if two or more rollers are used per carrier.

7.1.2 Roller Trajectory and Carrier Movement

The manner in which each roller falls into the gap in the track is largely dependent on the number of rollers on the carrier. Systems using one or two rollers per carrier are relatively simple to model (ref Appendix 7.1.2), but as the number of rollers increase a dynamic model is required which must include the stiffness and damping of each of the rollers. These parameters cannot be accurately calculated and must be found experimentally. In addition, the load on each roller cannot in practice be identical and this leads to the theoretical model being of little more than academic use.

The nature of standard track roller bearing design and load/speed rating indicates that for a given space (left by the bobbin in the conical region defined by the outer wire paths) the more numerous and smaller the bearings, the higher the overall carrier load capacity. This configuration of bearings allow a lower variation in loading and carrier "ride height", as the rollers cross the slots in the track. The disadvantage with this system is that if one of the many rollers runs with a higher loading, its longevity is substantially reduced. The machining of roller centres in the carrier also becomes critical but systems which compensate for this, such as pairs of rollers in bogies, or independently suspended roller systems, are too costly.

A simple method to reduce the change in load on a roller is to slant the slot and use a cylindrical roller (barrelled rollers are standard). The slot slant prevents the roller ever losing contact with the track, as shown in figure 7.1.20, and hence the fall of the roller into the slot and subsequent impact upon the next track sector leading edge is removed. The slant is provided by skewing the wand so that its pivot no longer lies along the path representing the wand tip amplitude mid point. However, this reduces the volume of the conical shape produced by the outer wire paths but does allow an 85° braid angle (ref chapter 6) at relatively low cost. The other disadvantage is that the rollers must now not only be centred correctly but must be absolutely parallel to prevent the rollers running on the corners. The contact stress factor for a roller running over a slanted slot edge is also higher than that of a straight slot and may be as high as 470 for a square slot edge. However, this system is tested experimentally along with the straight slot with profiled edges.

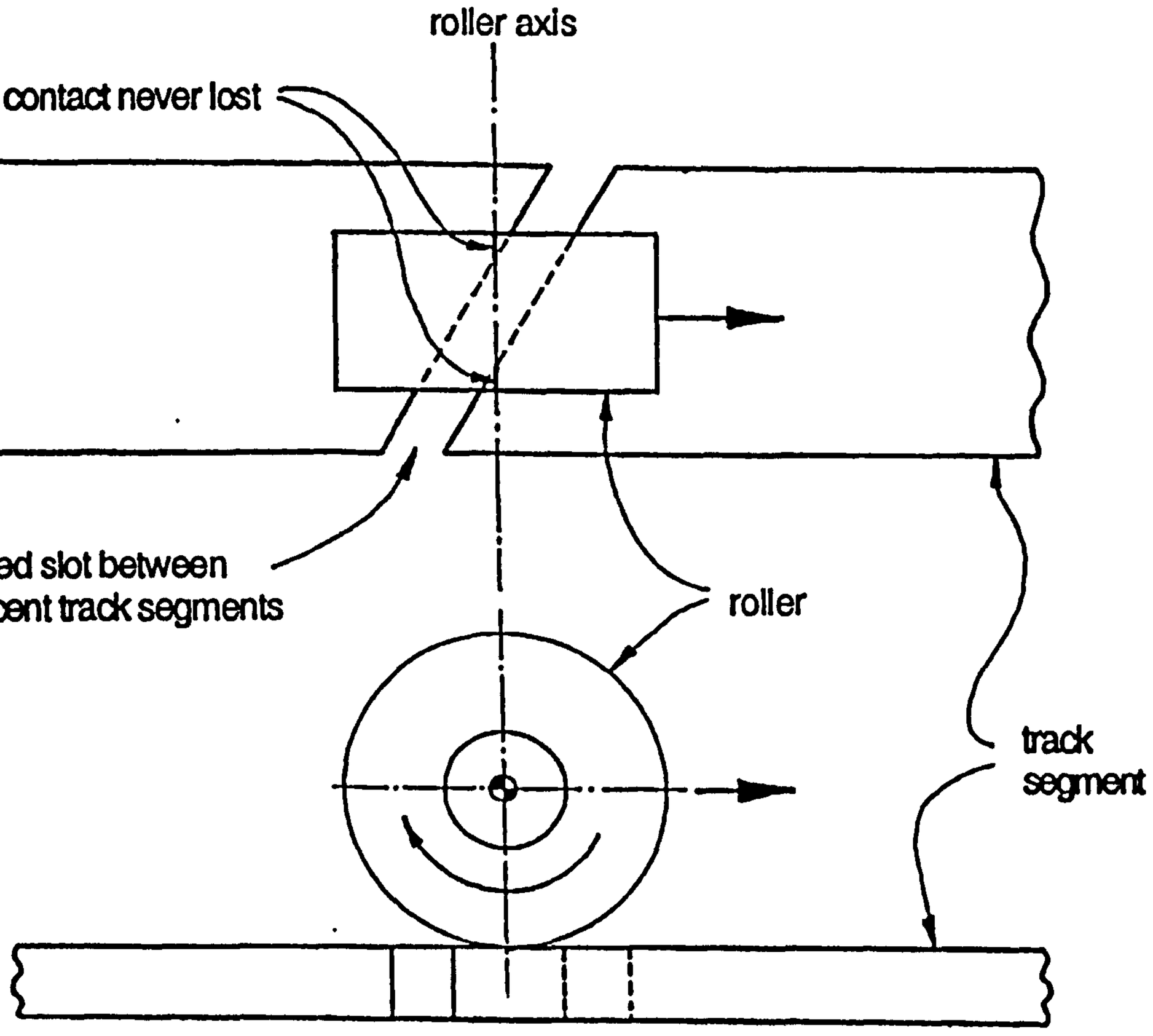

Figure 7.1.20 Slanted slot and roller system

7.2 Experimental Analysis of Roller Bearing Systems

The purpose of the experimental analysis is to:

i) Measure the load history of the track rollers as they run over the slots in the track.

ii) Measure the displacement of the carrier relative to the track as it crosses the slot.

These tests are performed for various roller numbers and configurations, and for a number of different profiled slot edges. The noise and temperature are also monitored.

7.2.1 Experimental Test Rig

The test rig, as shown in figure 7.2.10 (over leaf), consists of a rotating disc with slots machined in its surface to represent the inner carrier track of the rotary braider.

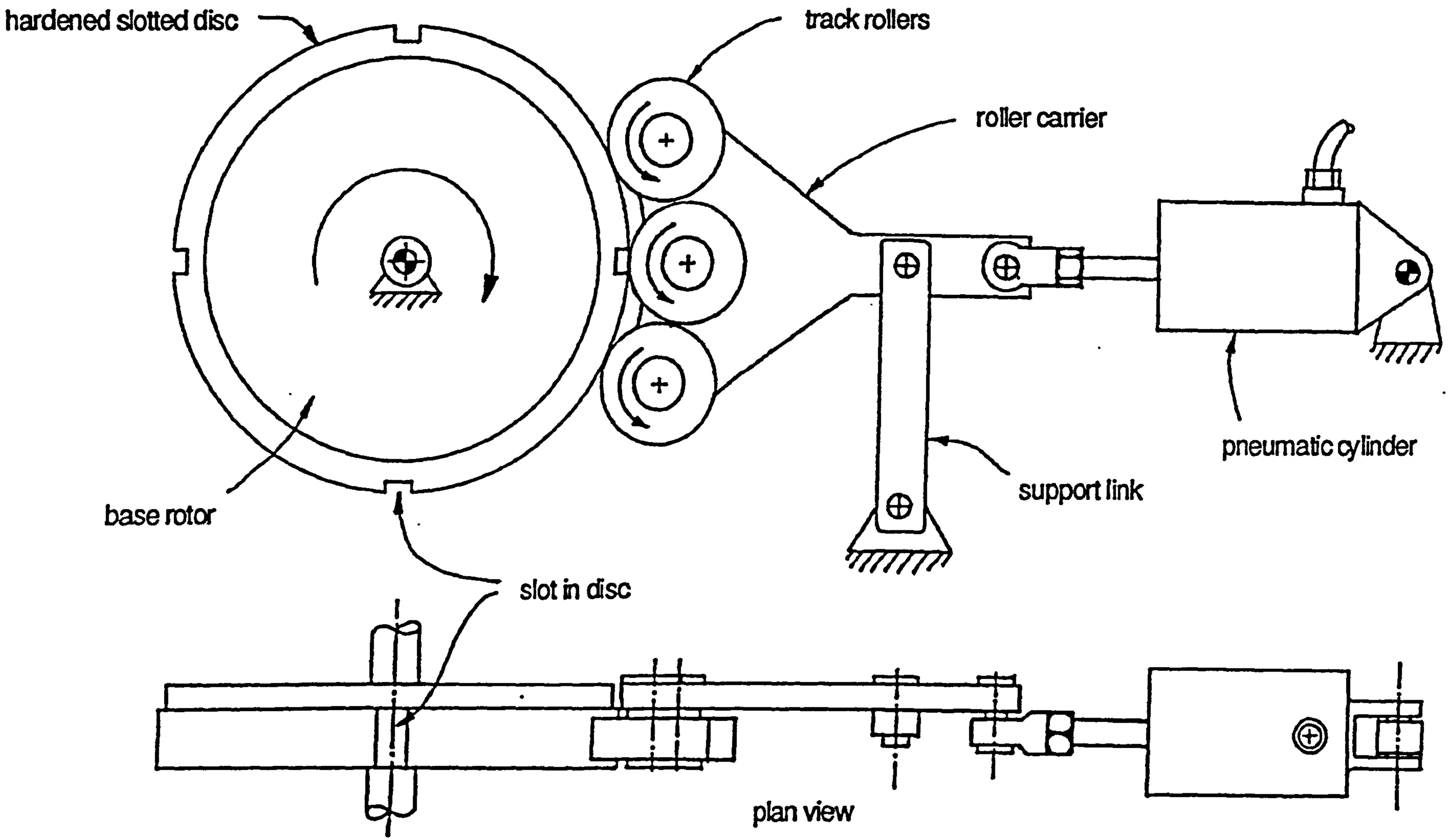

Figure 7.2.10 Schematic of track roller test rig

The slots in the discs are 5 mm wide initially with square edges. Two discs are tested, as shown in figure 7.2.11, one with slots perpendicular to the peripheral motion and the other with slots 60° to the peripheral motion.

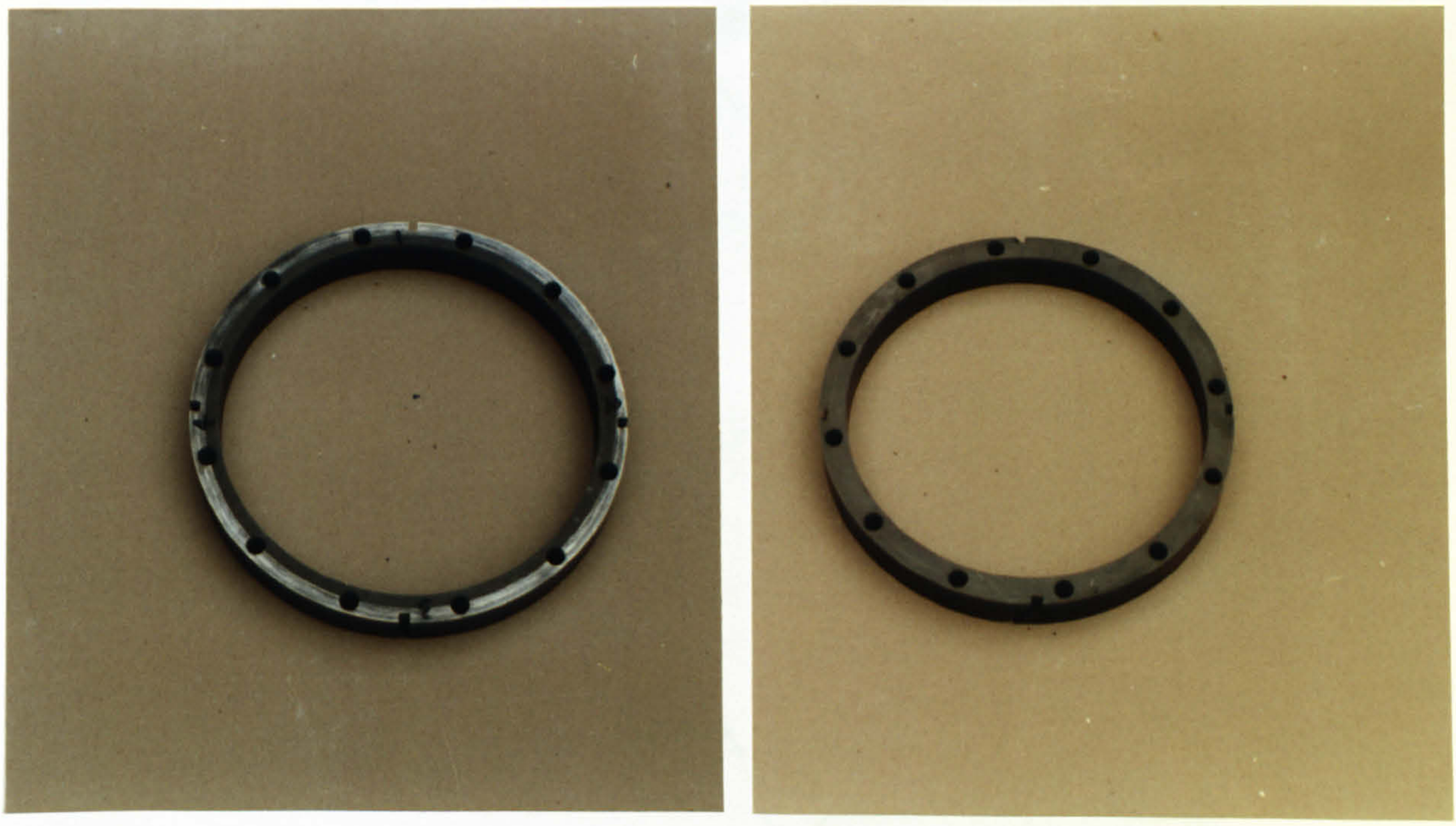

Figure 7.2.11 Straight and slanted slot discs used in tests

The rollers are mounted on a stationary carrier plate which is loaded against the disc by a pneumatic cylinder. The carrier mass and movement of inertia about the roller/track contact points are similar to that of an empty bobbin and carrier. The disc surface is ground, nitrided and hardened to 950 HV.

The load on the rollers is measured using strain gauges secured to flats on specially adapted roller shafts, as shown in figure 7.2.12. The shaft acts as a cantilever beam to transmit the roller load to the carrier body. These roller load indicators are calibrated and prove relatively linear in nature, although they are not suitable for very low loads (ie. at less than half the nominal carrier load they become inaccurate).

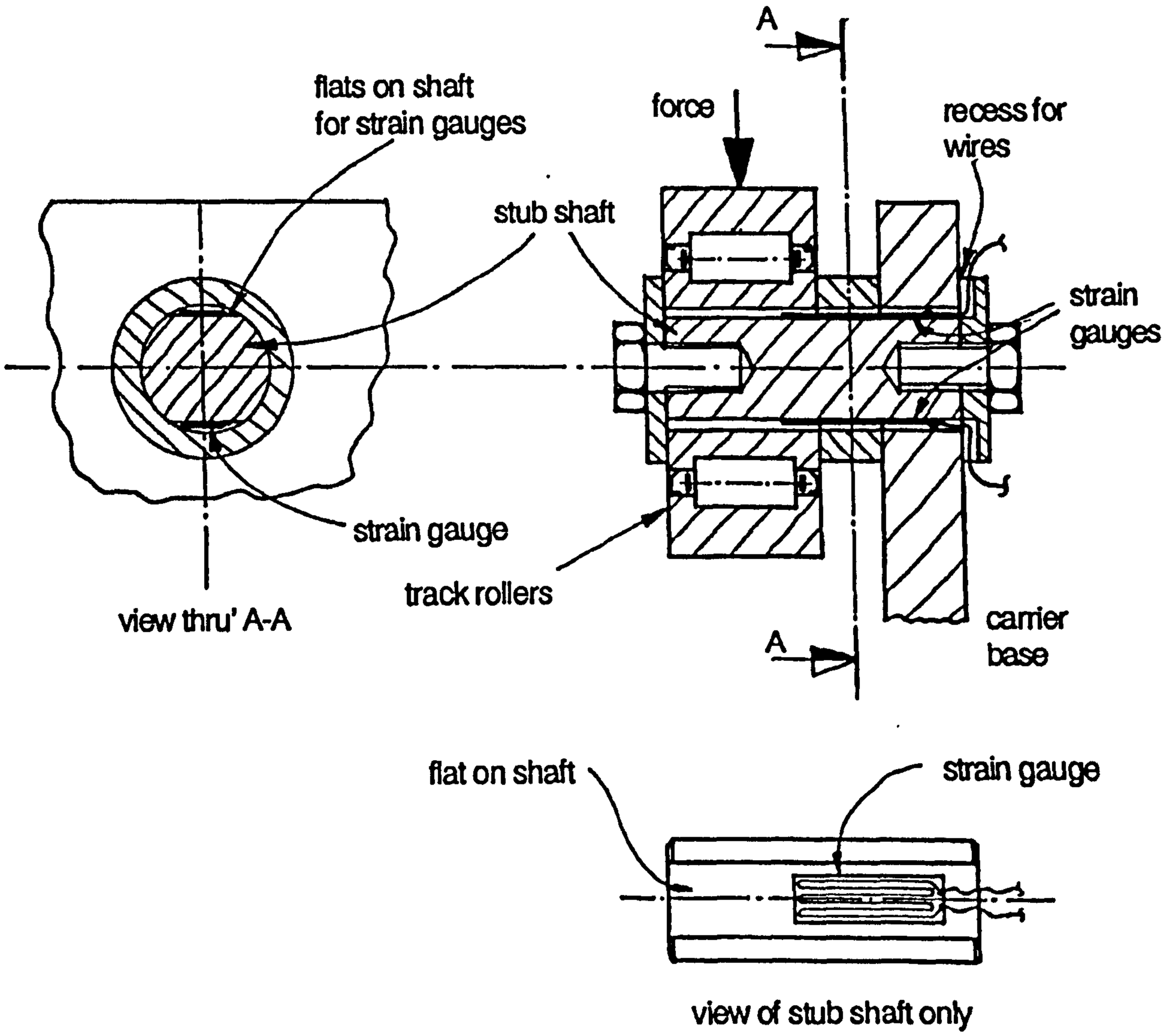

Figure 7.2.12 Track roller load measurement system

The point of contact across the rollers width must also be known to allow for correction of the load, as calibration assumes a central contact point. Barrelled rollers almost always run with central contact points, but cylindrical rollers, whilst crossing the slanted slot in the track, have a contact point which moves from one side of the roller to the other. In addition, cylindrical track roller bearings often run on their edges due to incorrect alignment. The contact point is determined by applying ink to the disc surface and the running contact point is indicated by the ink transfer to the rollers.

The displacement of the carrier is measured using proximity sensors mounted at each end of the carrier which register against the track surface. These sensors also indicate the location of the slots as the disc rotates.

7.2.2 Experimental Results - Straight Track Slot

The load and carrier displacement histories are measured for three different slot edge profiles which are:

i) A simple square edge, which is used as the datum for all the tests. Because the disc contains four slots all profiles are tested and compared simultaneously (ie. only one slot is contoured with any particular profile, and at least one slot remains square).

ii) A tapered slot profile N1, shown in figure 7.2.20 which complies with the theoretical trajectory for a two roller system. The roller is intended to land on a near flat surface 0.013mm below the mean track surface. This is based on a theoretical drop trajectory of 0.0032mm plus approximately 0.01mm of bearing radial clearance.

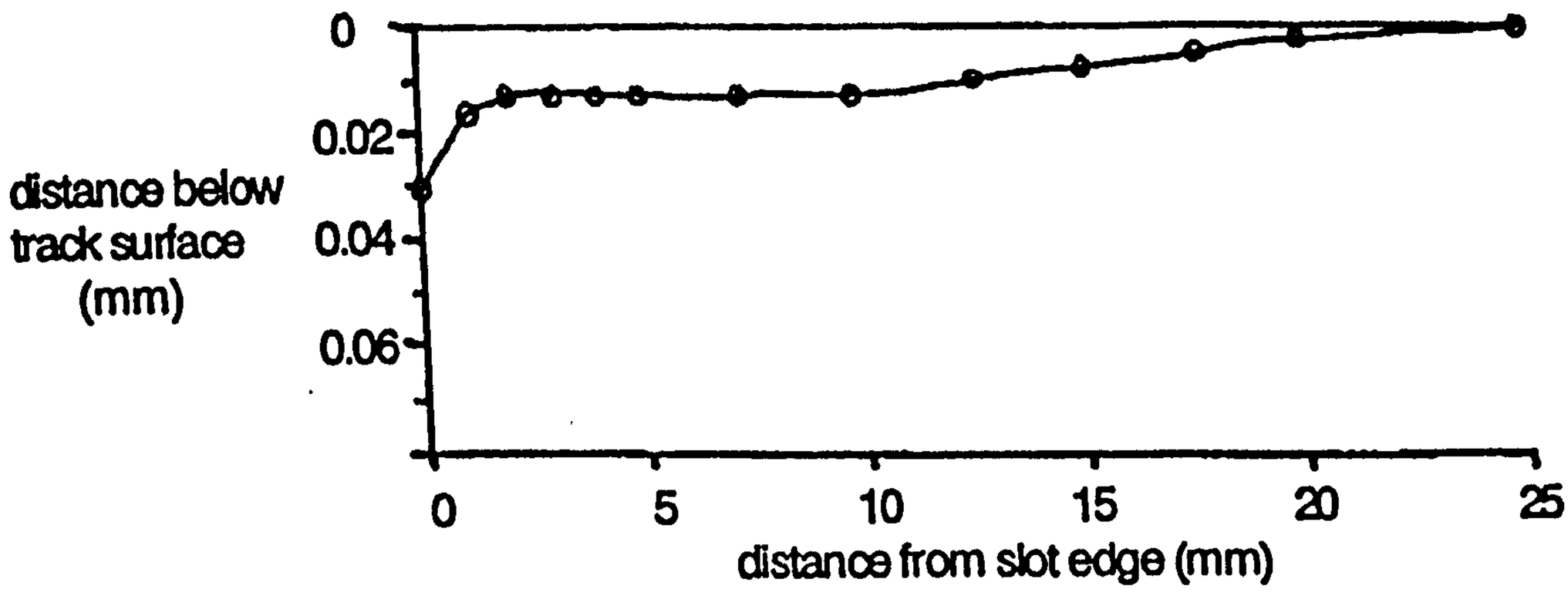

Figure 7.2.20 Straight slot profile N1

iii) A tapered slot profile N2 which was developed as testing continued and allows the rollers of a twin roller system to impact on a flat surface at least 0.5 mm from the leading edge. Figure 7.2.21 shows the final form machined into the track sector leading edge.

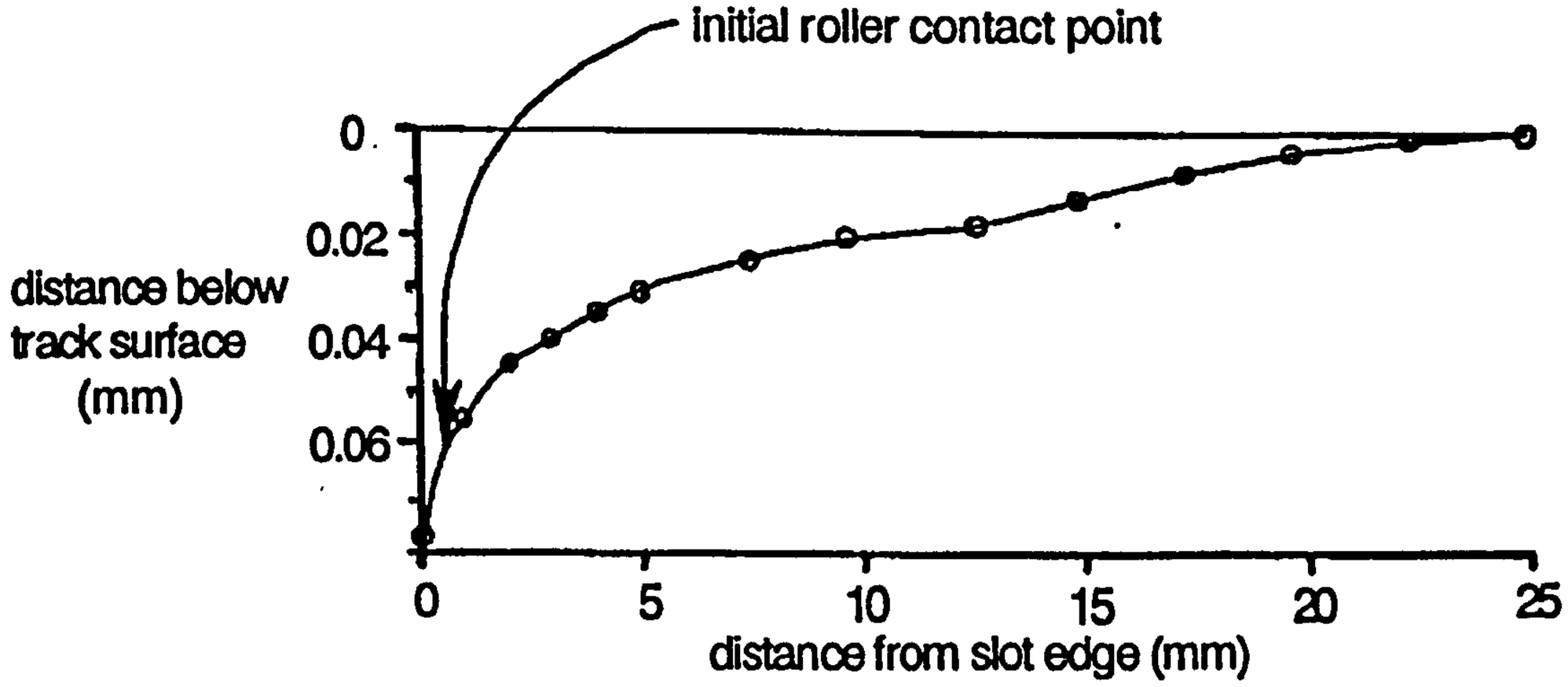

Figure 7.2.21 Straight slot profile N2

Due to the very small taper dimensions required on the profiled track slot edges, the actual profile is not as regular as desired and the degree of the taper is generally higher than intended. The results are summarised in figure 7.2.32.

Twin Roller System

The two 62 mm diameter barrelled track rollers tested represent the maximum possible which fit within the envisaged conical region available to bobbin and carrier.

i) Figure 7.2.22 and figure 7.2.23 show typical roller load history and carrier motion respectively for a square edge slot.

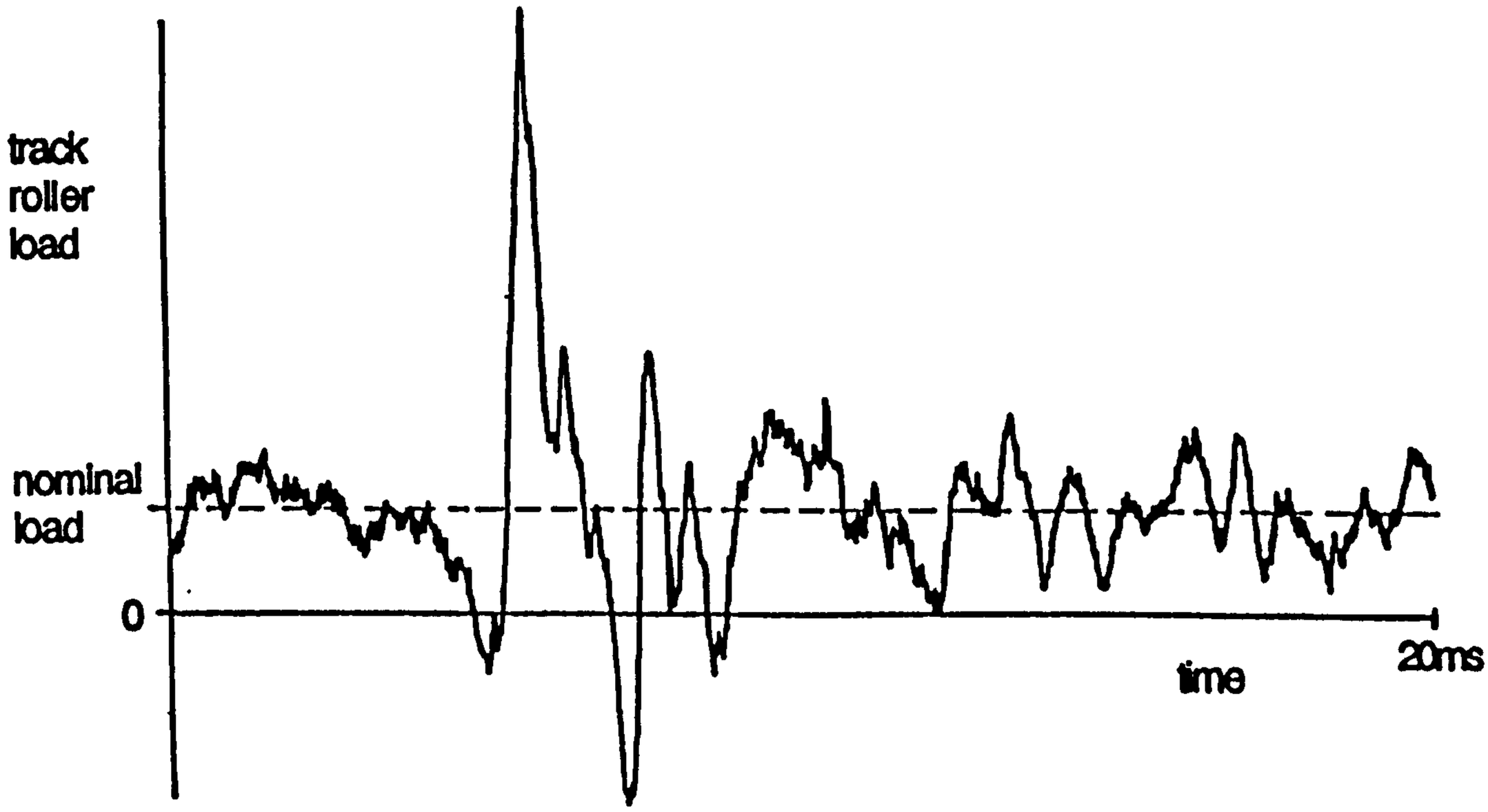

Figure 7.2.22 Load history for a twin roller system over a square slot

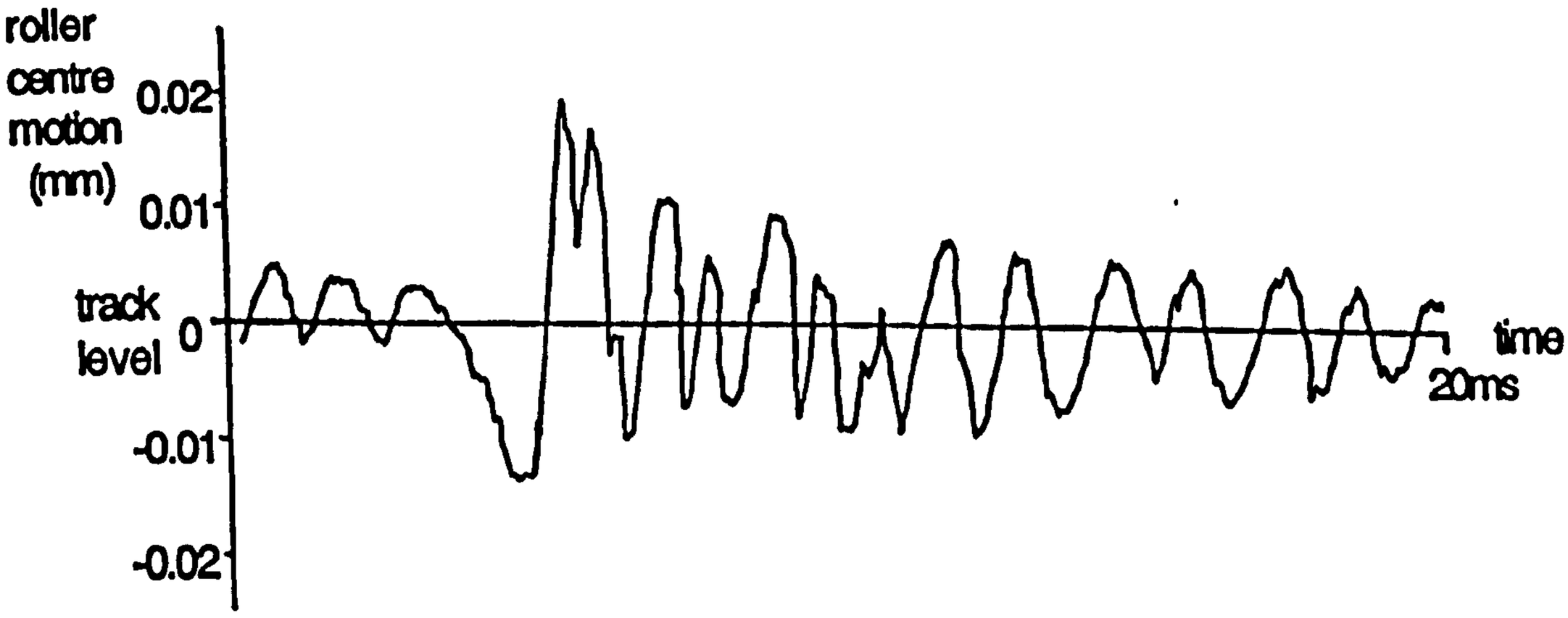

Figure 7.2.23 Carrier motion of a twin roller system over a square slot

The shock load when the rollers, particularly those leading, impact the slot edge is very high and represents an average load factor of 6.5, with a maximum of 8.5. The load history and carrier motion indicates that the roller bounces upon impact and this is confirmed by the roller contact areas found using marker blue on the rollers (fig 7.2.24).

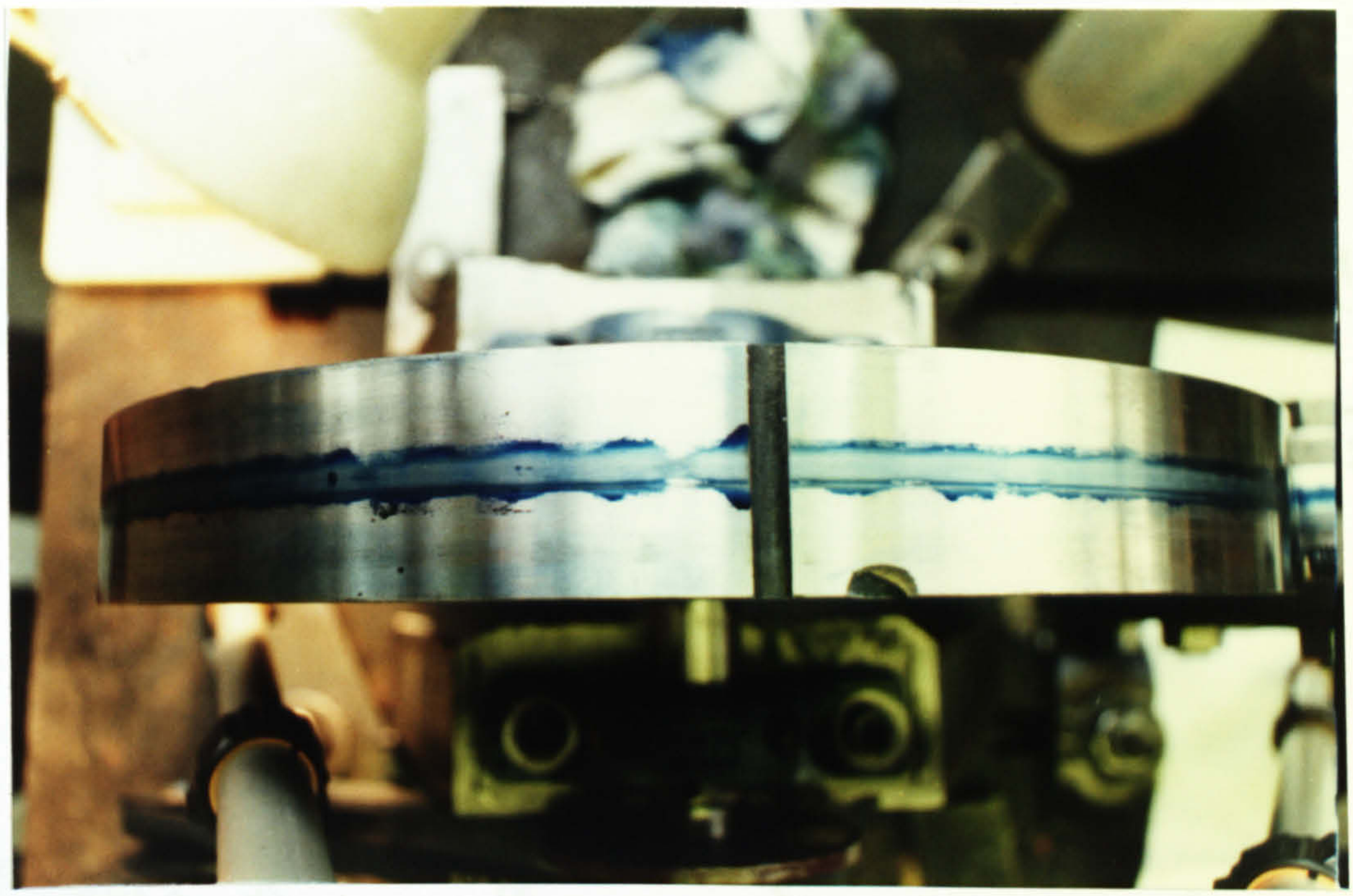

Figure 7.2.24 Twin roller system contact patch over a square slot

The leading roller runs with a higher load than the trailing roller due to the frictional torque in the bearings. However, the shock loads on each reveal a similar load factor, and the carrier has stabilised (ie. the leading roller has stopped bouncing) before the trailing roller crosses the slot. The average maximum drop into the slot is 0.016 mm and the maximum bounce of the leading roller is approximately 0.02 mm. The theory suggests a drop of 0.0032 mm, with a possible static maximum of 0.145 mm. The fact that this drop does not correlate with practical results is almost certainly due to not accounting for the stiffness and damping within each track roller in the theory. However, the measured roller drop and bounce is in fact that of the roller spindle centre, and the roller outer race (or tyre) drops further due to clearances within the bearing.

ii) The load history and carrier motion when running over slot profile N1 is shown in figures 7.2.25, 7.2.26 and 7.2.27. This slot profile represents that required in theory to allow the rollers to land on a flat surface.

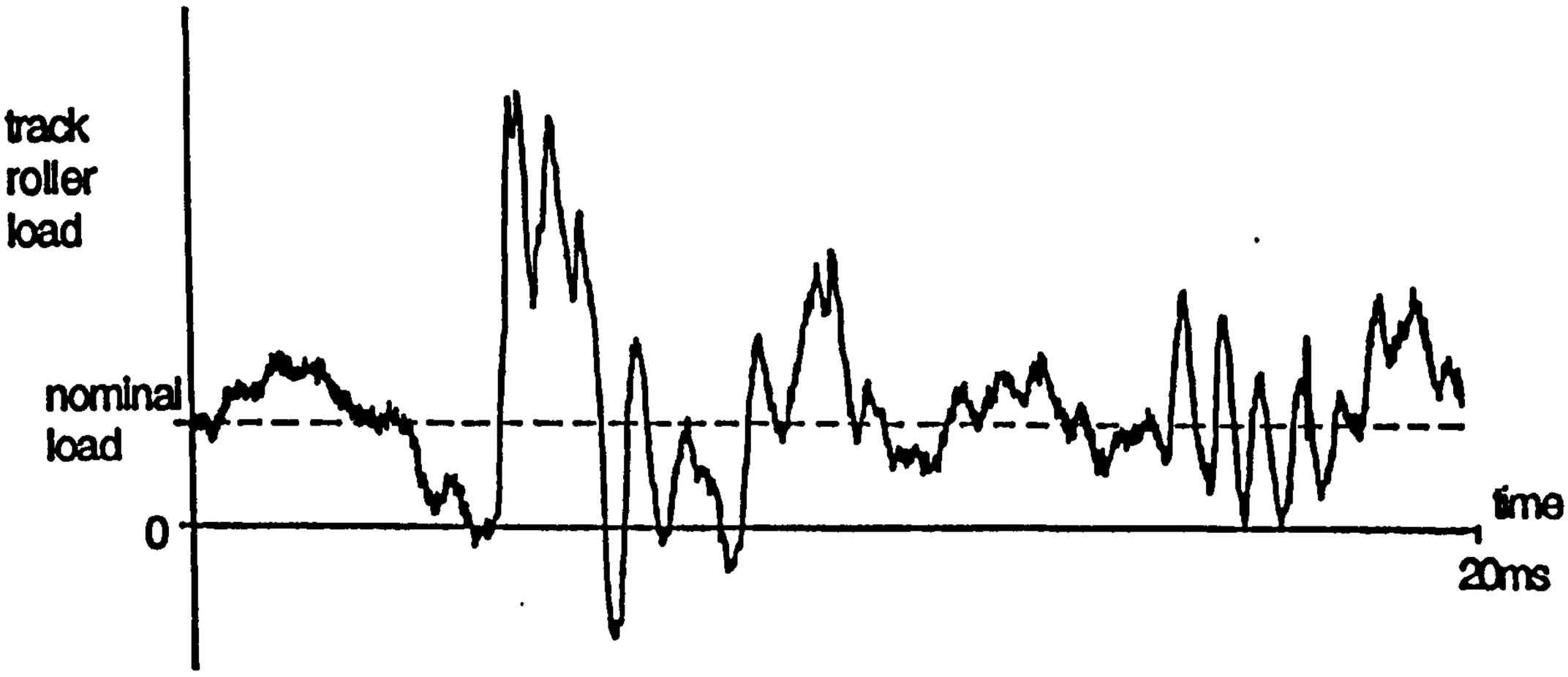

Figure 7.2.25 Load history for a twin roller system over slot profile N1

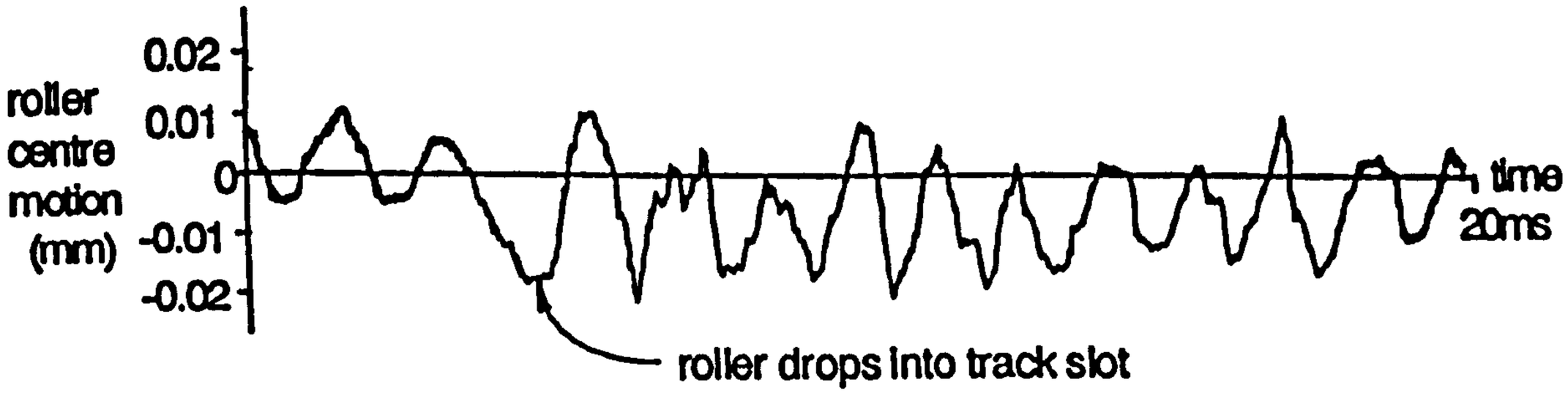

Figure 7.2.26 Carrier motion of a twin roller system over slot N1

The average load factor is reduced to 4.0 (with a maximum of 4.7) and the drop into the slot is approximately equal to that for a square edged slot. The roller bounce is substantially reduced to less than 0.01 mm, but the roller/track contact area shows that at least one (or both) of the rollers does not leave contact with the track. In addition, the rollers still impact on the slot edge "corner" which suggests that the discrepancy between theory and practice is increased when the actual roller surface is considered. The slot profile must therefore be increased to achieve a flat landing area for the roller surfaces.

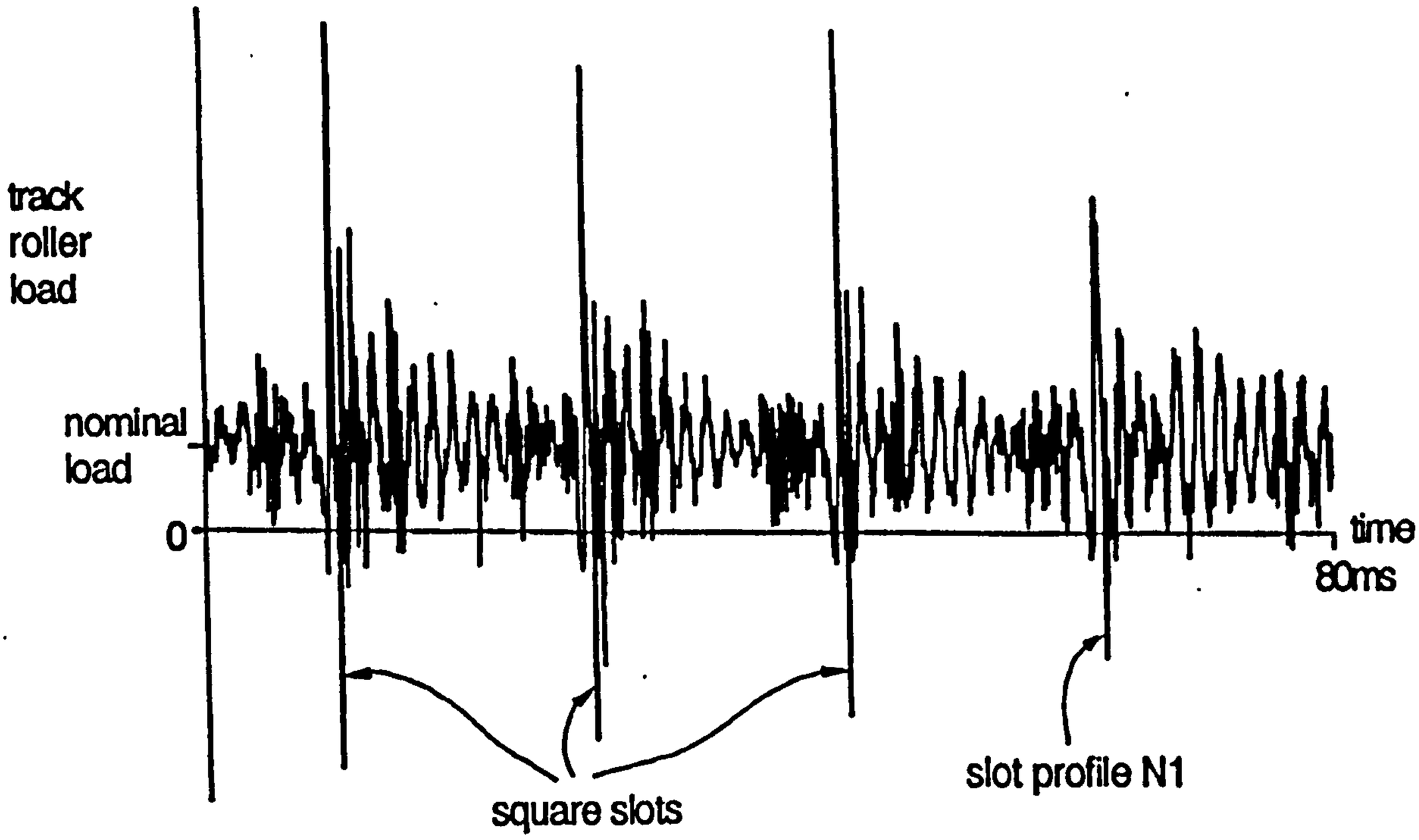

Figure 7.2.27 Load on a twin roller system over square and N1 slots

iii) The load history when running over slot profile N2 is shown in figure 7.2.28.

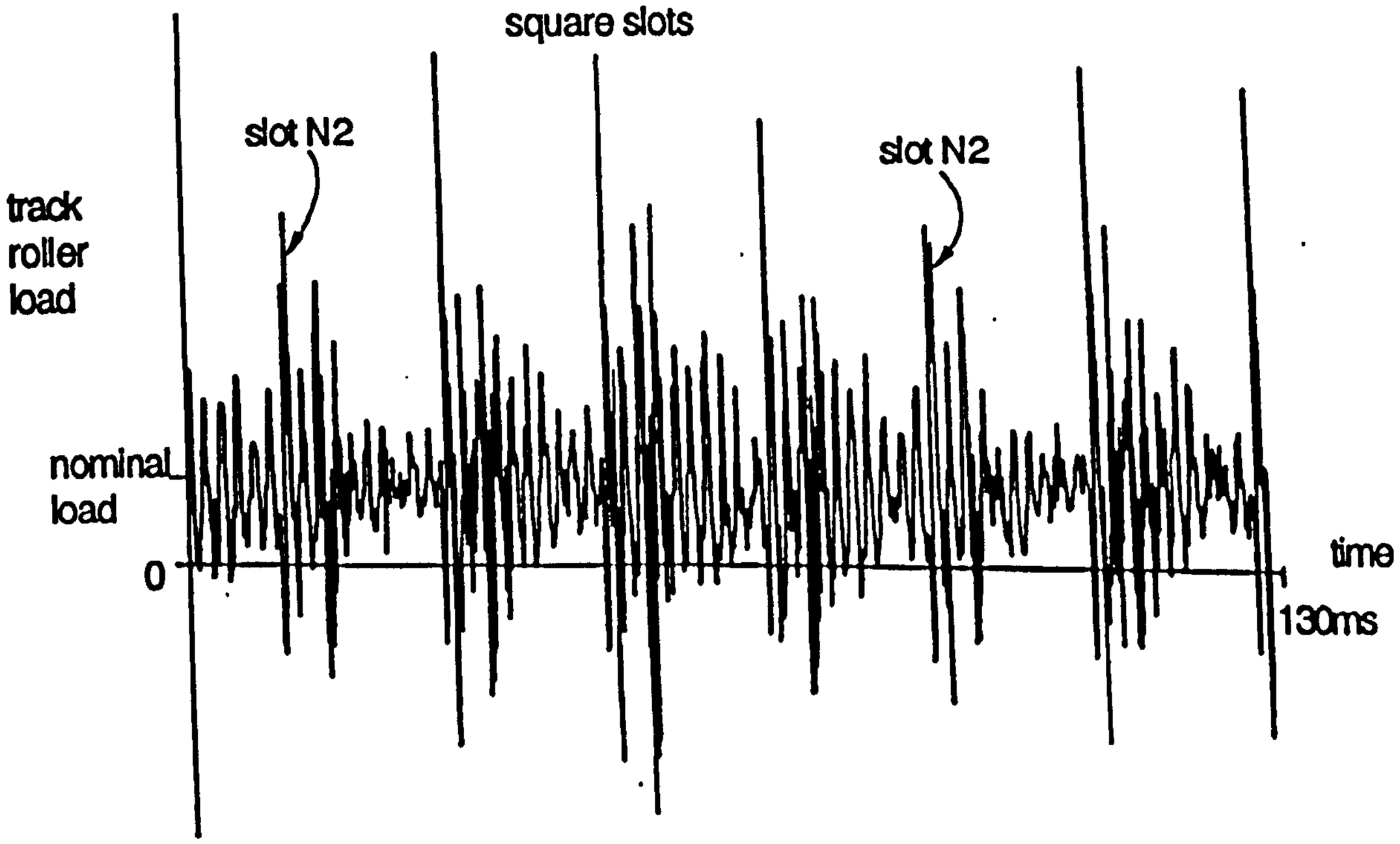

Figure 7.2.28 Load on a twin roller system over square and N2 slots

The average load factor is again reduced to 3.5 (with a maximum of 3.8) and the drop into the slot (0.015 mm) is again equal to that for a square edged slot. The roller spindle centre bounce is less than 0.01 mm but no bouncing appears on the roller/track contact area, as shown in figure 7.2.29. The rollers also land 0.6 mm from the slot edge which is an approximately flat region of the profile N2. Yet this region represents over 0.060 mm drop at the roller surface which indicates a radial clearance in the bearing of 0.045 mm which is taken up when loaded. This radial clearance, which is damped by the roller lubricant, becomes the dominant feature of the roller surface drop and the final track profile reflects this.

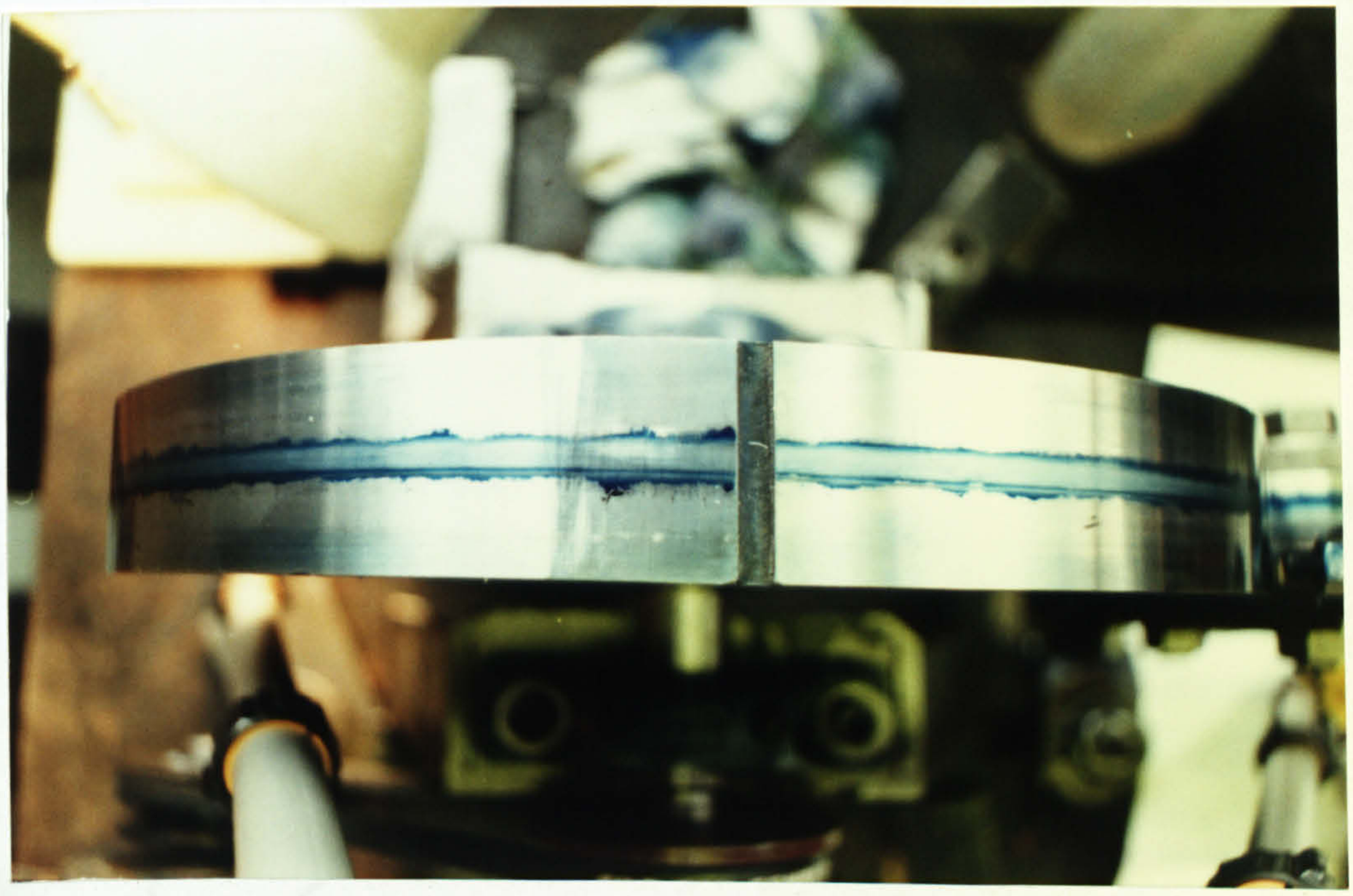

Figure 7.2.29 Twin roller contact patch over slot profile N2

The slot profile N2 is the optimum since any increase in profile depth results in the rollers impacting the track surface at higher speed. To achieve these load factors and for correct operation of a twin roller system the machine (carrier) must be running at or near its full speed.

A summary of the results is shown in figure 7.2.32.

Multi Roller Systems

Multi roller systems cover three, four and five roller systems and use 40mm diameter barrelled rollers.

The major advantage with multi roller systems is that a roller crossing the slot does not fall as far into the slot as a roller of a twin roller system would do since the carrier is supported by at least two other rollers.

The major problem with this system is aligning the roller centres to ensure the load is supported evenly between rollers. The test rig incorporates two fixed rollers and one (or two) rollers on an eccentric collar to allow for adjustment. Three roller systems prove relatively easy to adjust but four roller systems become extremely difficult and throughout the tests equal load distribution between rollers was never achieved (although all four rollers would turn they did not support the same load). The five roller system proved so difficult to adjust for even loads that this system was not fully tested.

i) Typical load histories for three and four roller systems when running over the square edged slot are included in figures 7.2.30 and 7.2.31 respectively.

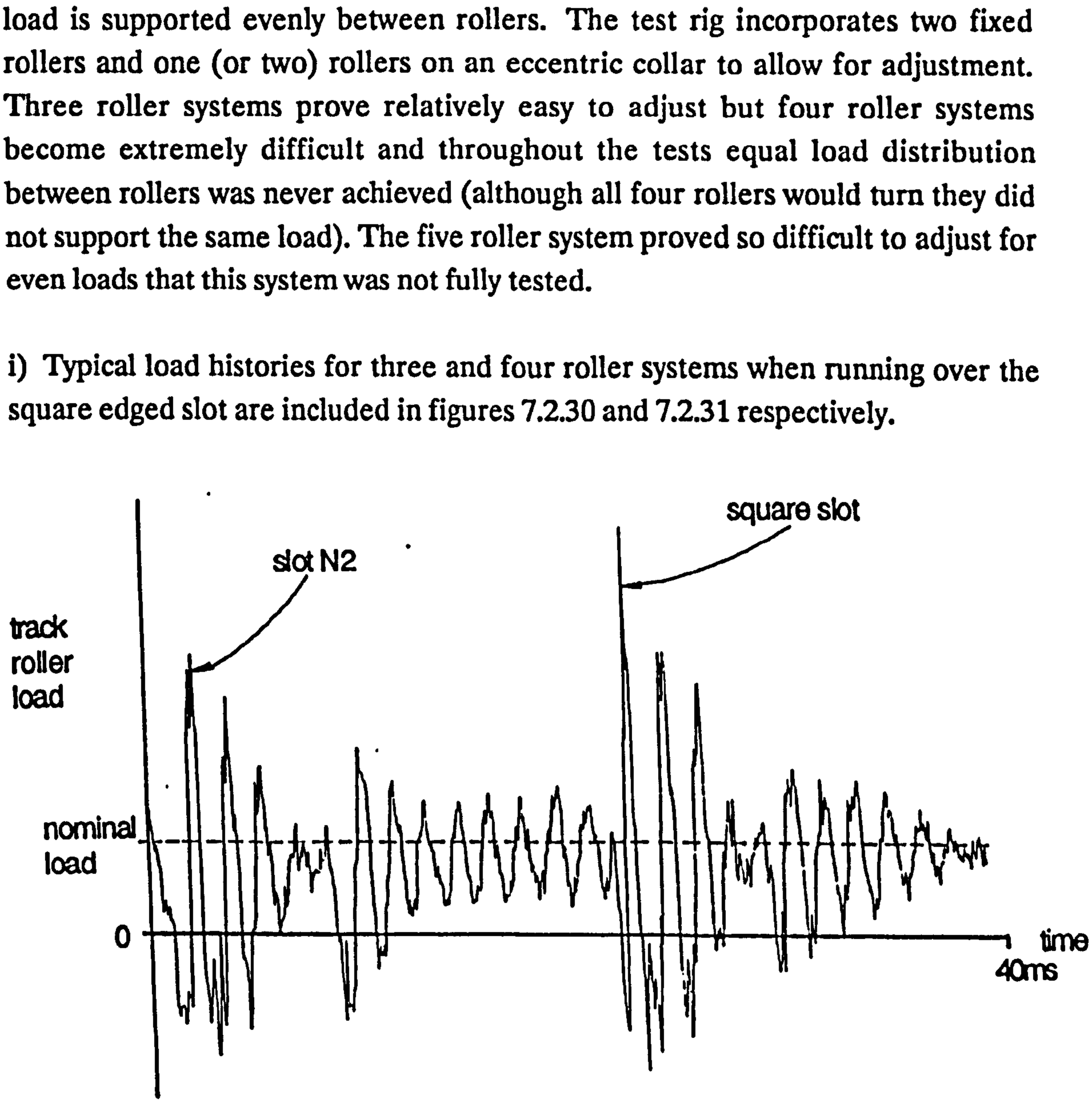

Figure 7.2.30 Load on a three roller system over square and N2 slots

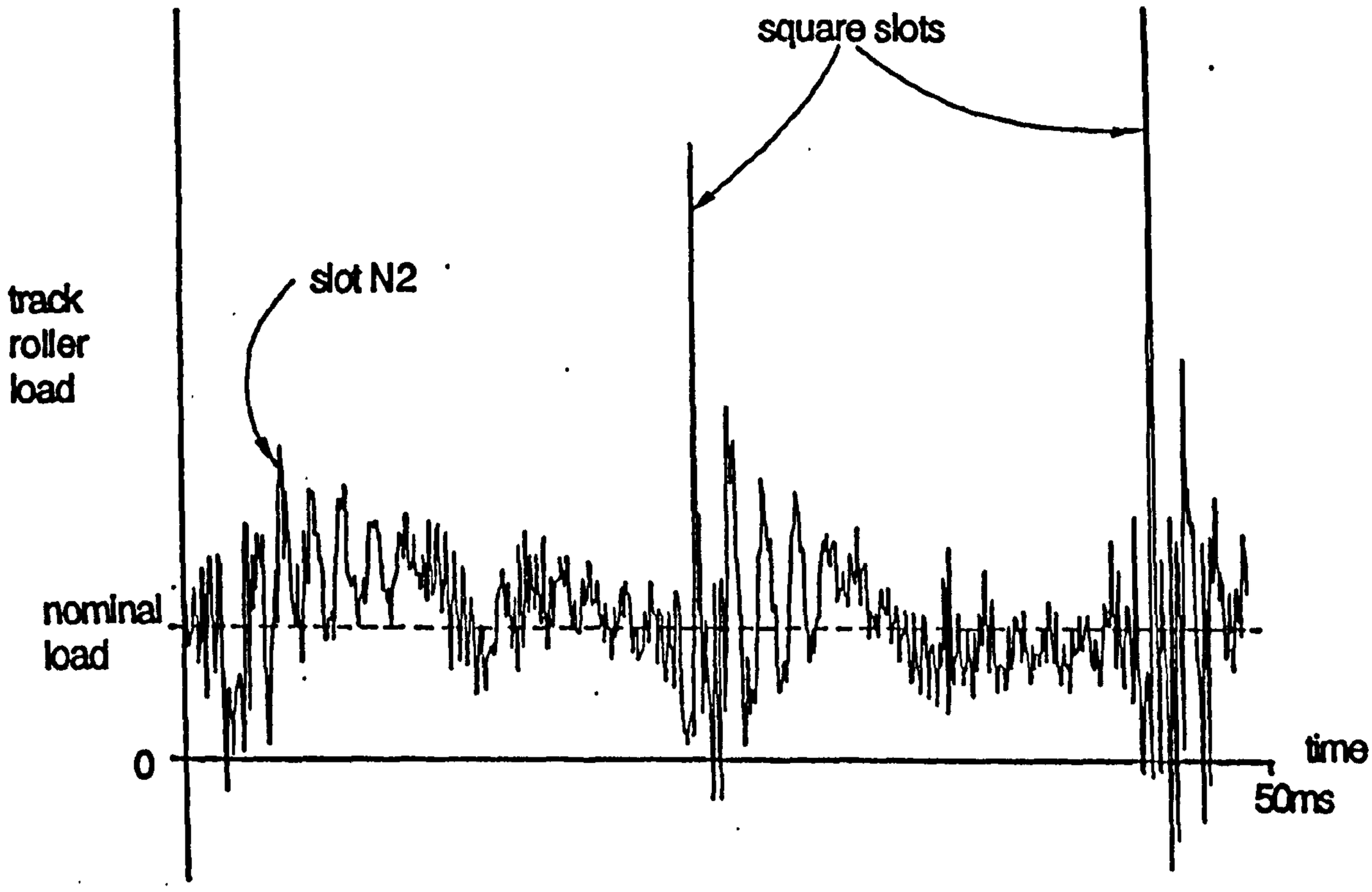

Figure 7.2.31 Load on a four roller system over square and N2 slots

The average load factors for both three and four roller systems is 6.5 (ie. practically identical to the twin roller system). The drop and bounce of each roller is difficult to quantify but carrier motion suggests the maximum drop occurs for the leading roller and is approximately 0.010 mm whilst the minimum drop is for the middle roller or rollers and is less than 0.005mm. The maximum bounce is 0.020mm and generally occurs at the two most heavily loaded rollers.

ii) The load histories for multi roller systems running over slot profile N1 result in load factors of 4.0 for a three roller system, and 3.7 for a four roller system. The carrier motion is similar to that for the square edged slot but bounce is reduced to below 0.007mm. The track/roller contact area suggested no bounce was occurring.

iii) Typical load histories for three and four roller systems when running over profiled slot N2 are included in figures 7.2.30 and 7.2.31 respectively. The load factor for the three roller system is reduced to 3.2 and the roller (carrier) bounce is negligible. The load factor for the four roller system is reduced to 2.5 and the rollers drop less than 0.01mm, whilst the roller (carrier) bounce is negligible. The rollers impact at a point approximately 0.9mm from the edge of the profiled slot which represents a drop of 0.055mm at the roller surface. This equates to a radial bearing clearance of approximately 0.045mm which, again, appears as the dominant factor in bearing drop and slot profile design.

The lower load factors recorded for the four roller system (over the two roller system) together with the lower carrier drop, indicate that this system is performing partially as intended (ie. the carrier is always supported by at least two rollers whilst one crosses the slot).

A summary of the results is shown in fig 7.2.32.

	Square edge slot			Slot profile N1			Slot profile N2		
	Load factor	Max. drop (mm)	Max. bounce (mm)	Load factor	Max. drop (mm)	Max. bounce (mm)	Load factor	Max. drop (mm)	Max. bounce (mm)
Two Roller System (62 mm dia.)	6.5	0.016	0.020	4.0	0.016	0.010	3.5	0.015	0.007
Three Roller System (40 mm dia.)	6.5	0.010	0.020	4.0	0.010	0.007	3.2	0.010	0.007
Four Roller System (40 mm dia.)	6.5	0.010	0.020	3.7	0.010	0.005	2.5	0.010	0.003

Figure 7.2.32 Summary of Experimental Results with a Straight Slot

7.2.3 Experimental results - Slanted Track Slot

The slanted slot is 5mm wide and angled at 30° to the disc axis. The slot edge profiles tested are the square edged slot and a profiled slot S2, shown in figure 7.2.33. The profile is based on that used on the straight slot profile N2.

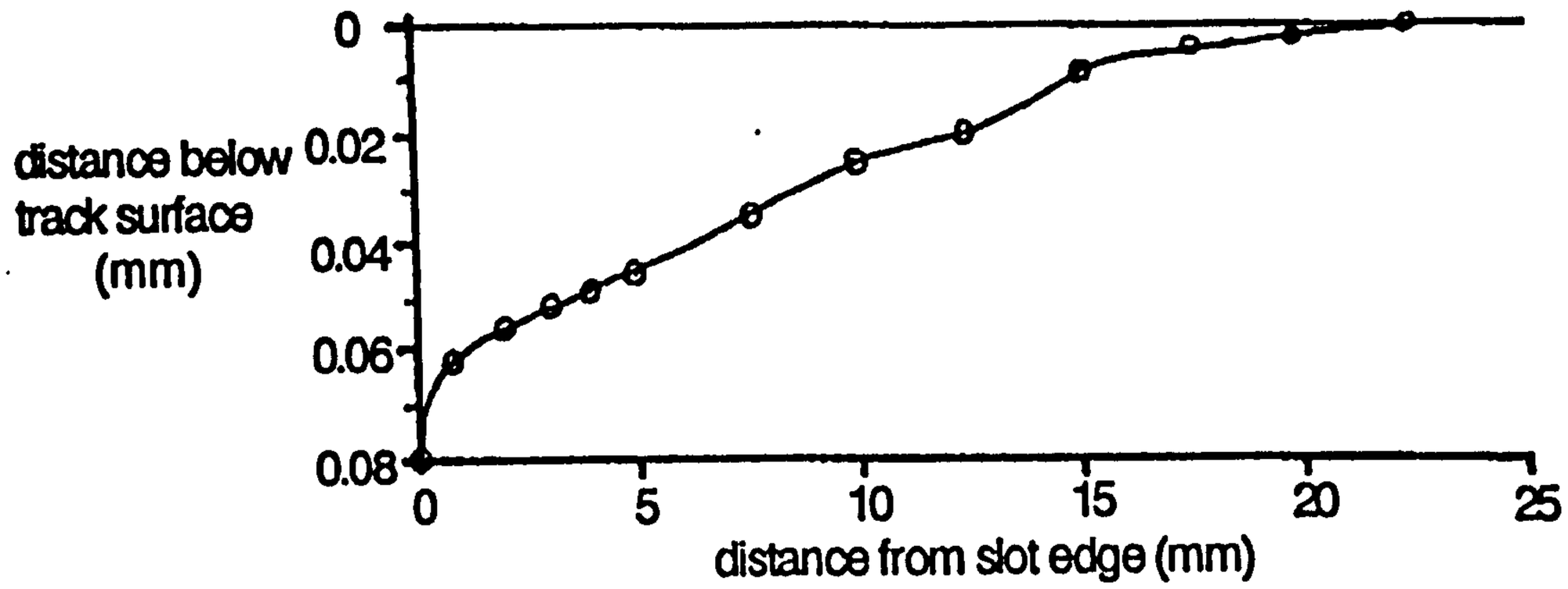

Figure 7.2.33 Slanted slot profile S2

The concept behind the slanted slot demands the use of cylindrical rollers (ie. not barrelled or crowned). Tests showed that setting up two cylindrical rollers to run with an even load distribution across the roller width was extremely difficult and that achieving this with three or four rollers was virtually impossible. This results in the rollers running on the edges which leads to premature failure. However the contact area of barrelled rollers is wide enough to allow some benefit to be gained by using a slanted slot system. Tests are performed on two, three, and four barrelled roller systems running over square and profiled (S2) slot edges.

The load history and carrier motion is recorded and the resulting load factors and roller centre "drops" and "bounces" are summarised in figure 7.2.34.

	Square edge slot			Slot profile S2		
	Load factor	Max. drop (mm)	Max. bounce (mm)	Load factor	Max. drop (mm)	Max. bounce (mm)
Two Roller System (62 mm dia.)	4.4	0.020	0.040	4.1	0.020	0.040
Three Roller System (40 mm dia.)	4.2	0.012	0.030	2.9	0.011	0.007
Four Roller System (40 mm dia.)	4.0	0.010	0.040	2.0	0.010	0.007

Figure 7.2.34 Summary of experimental results with a slanted slot

The results show that when using a profiled slanted track slot, a two roller system is inferior to the two roller straight slot system but that the multi roller systems are significantly better than the straight slot systems. The profile S2 allows both the three and four roller systems to impact on a flat section of the profile whilst the twin roller system requires a deeper profile to achieve this. However, the fact that the rollers loose contact at all defeats the object of the slanted slot.

7.2.4 Roller Temperatures and Noise Levels

The roller temperatures generally stabilised at between 75° C and 85° C provided the correct grade and quantity of grease was present in each bearing. The leading roller generally runs hotter by 5 - 10° C than the others due to the higher loads it must support. This difference in loading can be reduced by offsetting the centre of mass of the carrier from the "centre" of the roller system thereby negating the effects of the frictional torque in the bearings.

The noise levels are the highest recorded at a distance of 1m from the rollers of a single carrier:

Straight Slot system noise levels:

Twin roller system, square edge slot = 94dB(A)
Twin roller system, slot profile N2 = 93dB(A)
Four roller system, square edge slot = 93dB(A)
Four roller system, slot profile N2 = 92dB(A)

Slanted Slot system noise levels:

The profiled slot edge had little effect on the noise levels recorded. However the noise level of this system is susceptible to changes in roller loading, whether the rollers run on their edges and the degree of load sharing between rollers.

Twin roller system = 89 - 93dB(A)
Three and Four roller systems = 87 - 91dB(A)

The changes in noise level (for the straight slot) between profiled and square slot edges is remarkable in that only one of the four slots in the disc was profiled. This suggests that the square edges wore down after prolonged periods of running, or that a resonance in the disc was interrupted when one of the four slots was profiled.

When the track sector trailing edge is radiused (2 - 3mm) the noise is reduced further by 2 - 3dB(A) which represents a useful decrease and is also desirable to reduce contact stress concentration at the slot edge and in the roller.

The problem of noise may become critical at a later stage and this enhances the overall desirability of the slanted slot system which when running is appreciably quieter at 87 dB(A) than any straight slot system.

7.3 Conclusion to Track Roller Bearing Design.

The theory suggests that a large number of small diameter rollers offer the best performance. But in practice more than four cannot be accurately aligned to ensure equal load sharing.

Experimental tests verify that four rollers have a lower shock load factor (of 2.5) as they cross the track slot, which supports the outer wire path. However to achieve this a tapered profile must be machined into the leading edge of each track section. This should be at least 0.06mm at its greatest point (at the slot edge). The trailing edge of each track sector must also be profiled to relieve stress concentration and reduce noise. Because the rollers impact on a flat surface, after crossing the slot, the standard bearing life equation may be used to predict roller life. This suggests that a four roller bearing system will last at least 15,000 hours running at a full speed of 150rpm on a 24 carrier machine carrying 3.7kg of copper wire on each bobbin.

However the major problem with a three or four roller carrier is that the system demands tolerances of ±0.005mm on bearing centres, which is at best extremely costly, and realistically unlikely on a production machine.

The result of inaccurate roller centres effectively reduces to a two roller system utilising small rollers which leads to premature failure. A twin roller system using larger rollers, whilst bulkier and noisier, offers performance levels near multi roller systems without the high tolerances.

A slanted slot in conjunction with a multi roller system offers the lowest load factor (ie. highest bearing performance) and a reduced noise level. However this system requires changes to the wand system which are not conducive to high performance.

The final carrier bearing system is determined by the machining accuracy of the roller centres. The overall layout of the system is determined in conjunction with the inner carrier drive system and carrier design (chapter 8).

CHAPTER EIGHT

INNER CARRIER DRIVE AND LAYOUT

8.0 Introduction

The superimposed outer wire paths completely encompass each inner bobbin and carrier. The drive to the inner carriers must, therefore, be intermittent in nature with the carriers propelled around the machine by the drive being passed from one region to the next in a "bucket brigade" manner. The drive must provide exact circumferential location of the carriers as they rotate about the machine. Ideally, the portion of the drive system located on the carrier (if any) should fit within the space left in the conical region by the bobbin and carrier track bearing. The drive should not compromise either the bobbin optimisation or the carrier track bearing performance.

The layout of the components of the inner carrier within the conical region formed by the outer wire paths, determines the framework of the carrier. The carrier must support the bobbin, bobbin brake, tension control mechanism, bobbin quick release mechanism (if necessary), main roller bearings, secondary location bearings and carrier drive system.

8.1 Drive System Appraisals

Inner carrier drive systems may be categorised in two ways:

i) The drive system requires the outer wires to pass along a precise path, or alternatively the wire must be guided along a precise path.

ii) The drive system is independent of the outer wire path.

To maintain outer wire control a drive system which does not potentially affect the outer wire motion is desirable.

8.1.1. Drive Systems Requiring Precise Wire Control

a) Finger or rotating dog systems, as shown in figures 8.1.10 and 8.1.11, achieve drive by locating the carrier against a rotating base.

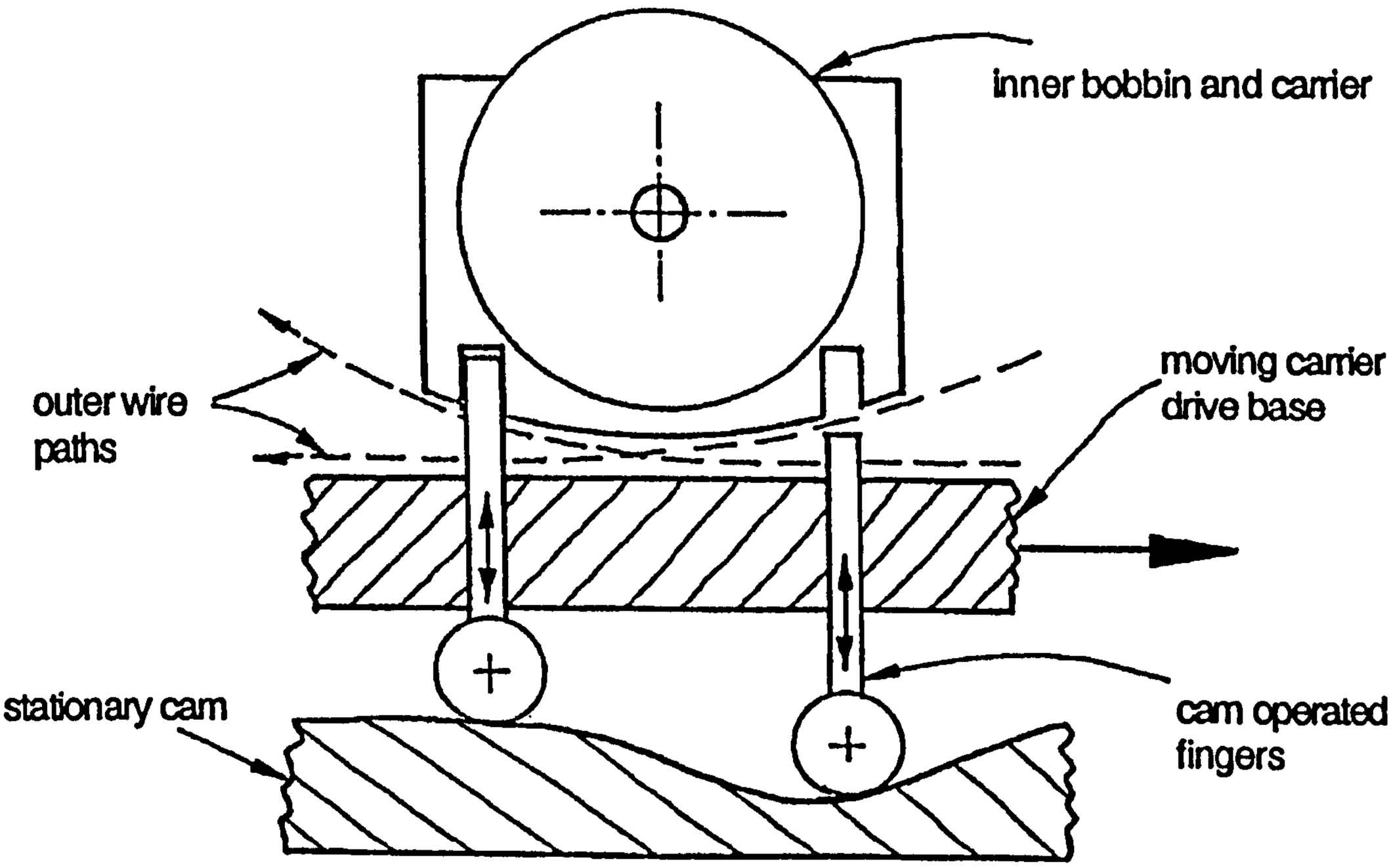

Figure 8.1.10 Finger drive system

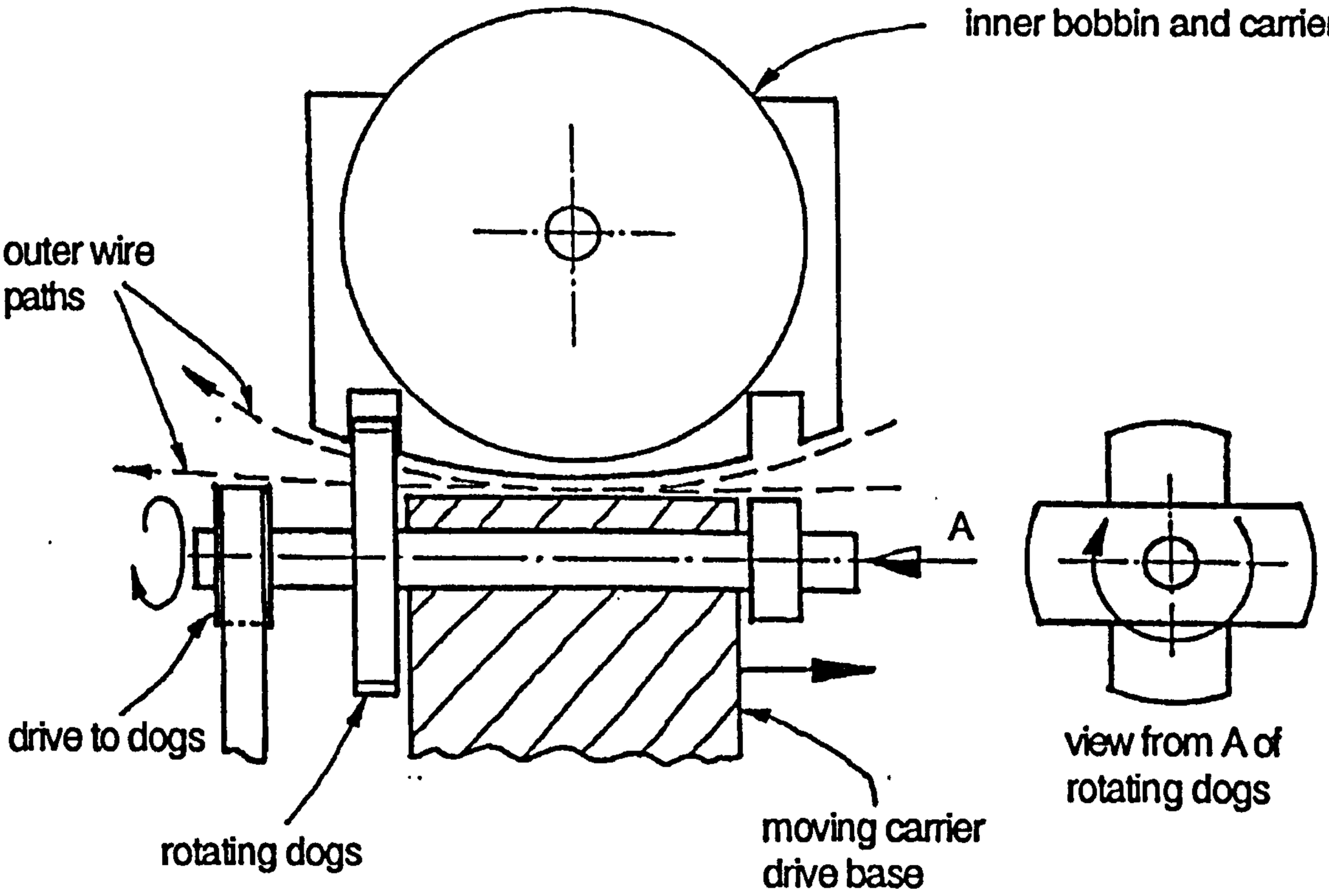

Figure 8.1.11 Rotating dog drive system

Location is provided to each carrier by two fingers (etc) which span the gap between carrier and rotating base . This gap has the form of the outer wire path at that point and the wire is able to pass through the gap by disengaging and reengaging first one finger, then the next. The smaller the gap across which the fingers (or dogs) must move, the higher the performance potential of the system as the fingers are generally linkage or cam driven. However, this criteria conflicts with the requirements for outer wire control at high speed.

b) A variation on the rotating dog system (in (a) above) is the single rotating sleeve as shown in figure 8.1.12. This system removes the need for accurately aligning the separate dogs but requires increased accuracy of outer wire location.

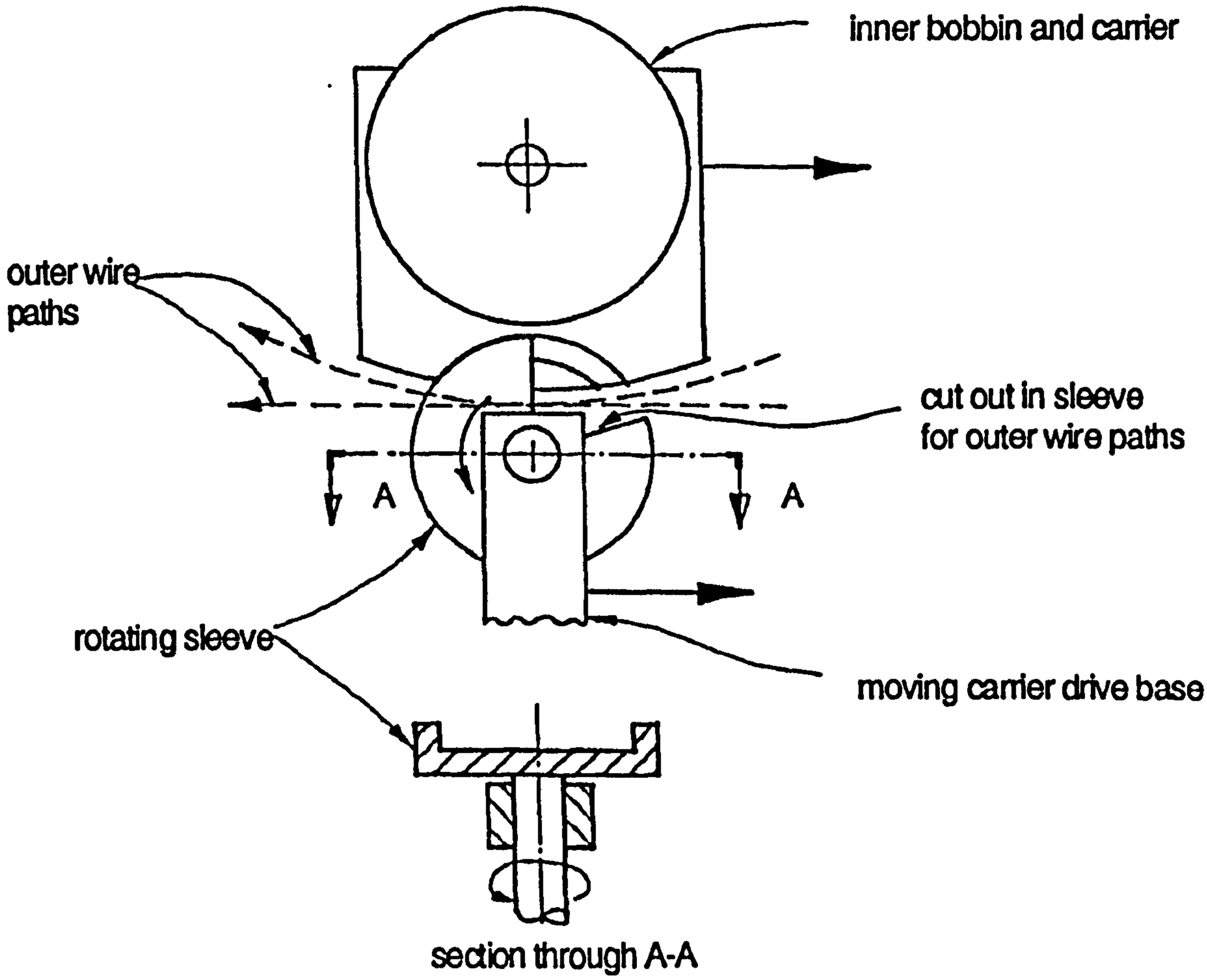

Figure 8.1.12 Rotating sleeve drive system

c) The carrier may be located to the base with permanent magnets or electro magnets as shown in figure 8.1.13. This system is attractive as no contact between base and carrier is required. However, the mass and bulk of permanent magnets necessary would compromise the carrier bearing or bobbin size, and an electromagnetic system is costly. In addition, if the carrier bearing frictional load (drag) varies greatly a controlled electro-magnet is required.

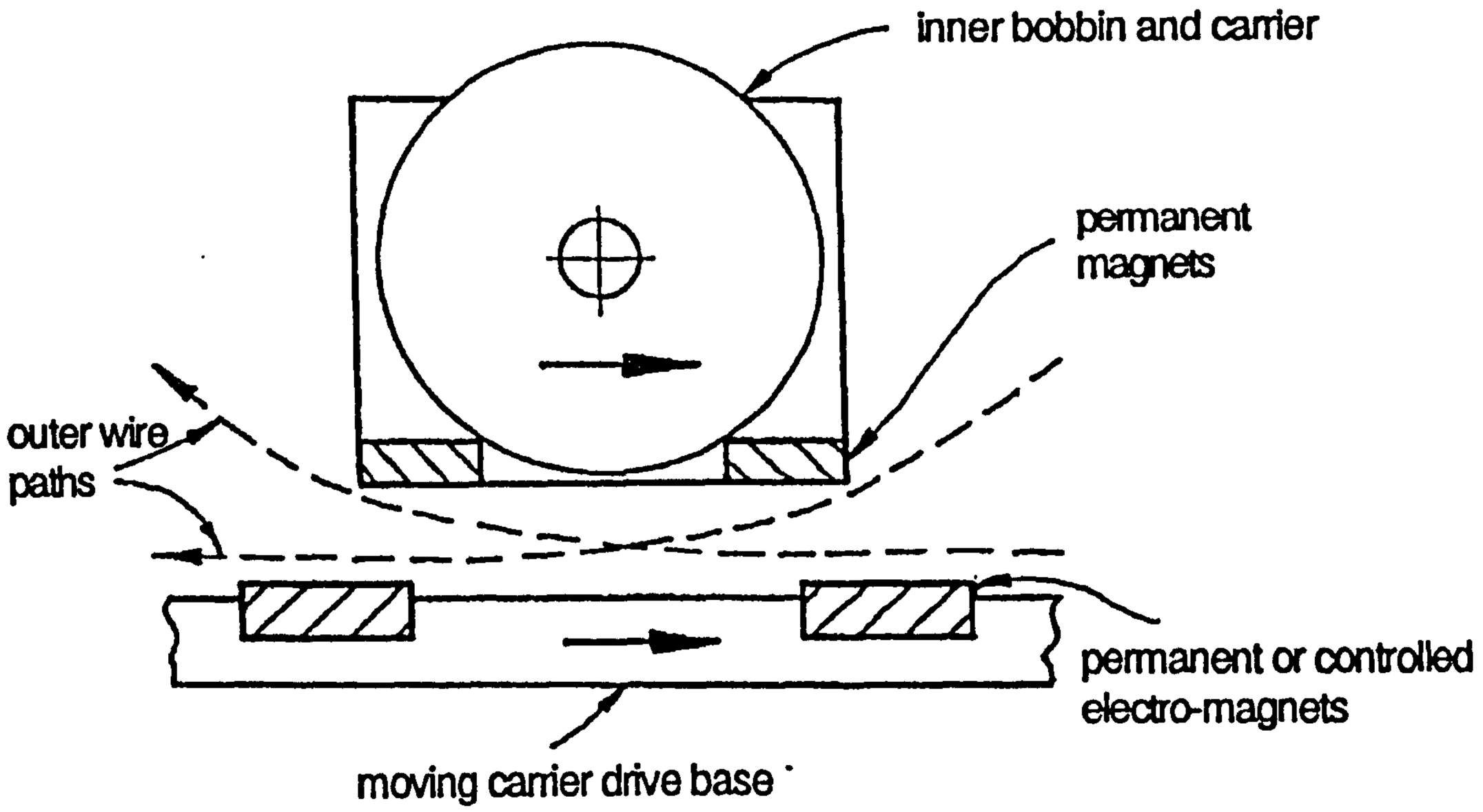

Figure 8.1.13 Magnetic drive system

All these systems have been tried by various braider manufacturers and the cam or linkage operated fingers have proved the best solution. Both Wardwell and Rockwell use this finger system for inner carrier drive.

8.1.2. Drive Systems Independent of Outer Wire Path

a) The induction motor principle may be used to propel the inner carriers around the track. The track sectors contain windings and each carrier incorporates a large aluminium reaction plate. The drawback with this system is that each carrier position must be sensed and controlled by a relatively costly control system.

b) A system of gears located around the machine which act as the planetary gears in an epicyclic arrangement may be used to drive the carriers as shown in figure 8.1.20. Each carrier contains a section of a gear which meshes with the planetary gears and which spans at least two planetary gears. In this way the planetary gears which are driven from a main sun gear, propel the carriers from one region to the next. The planetary gears are therefore mounted on the same base as the wands, and the outer wires merely pass between two gears, which do not restrict its motion.

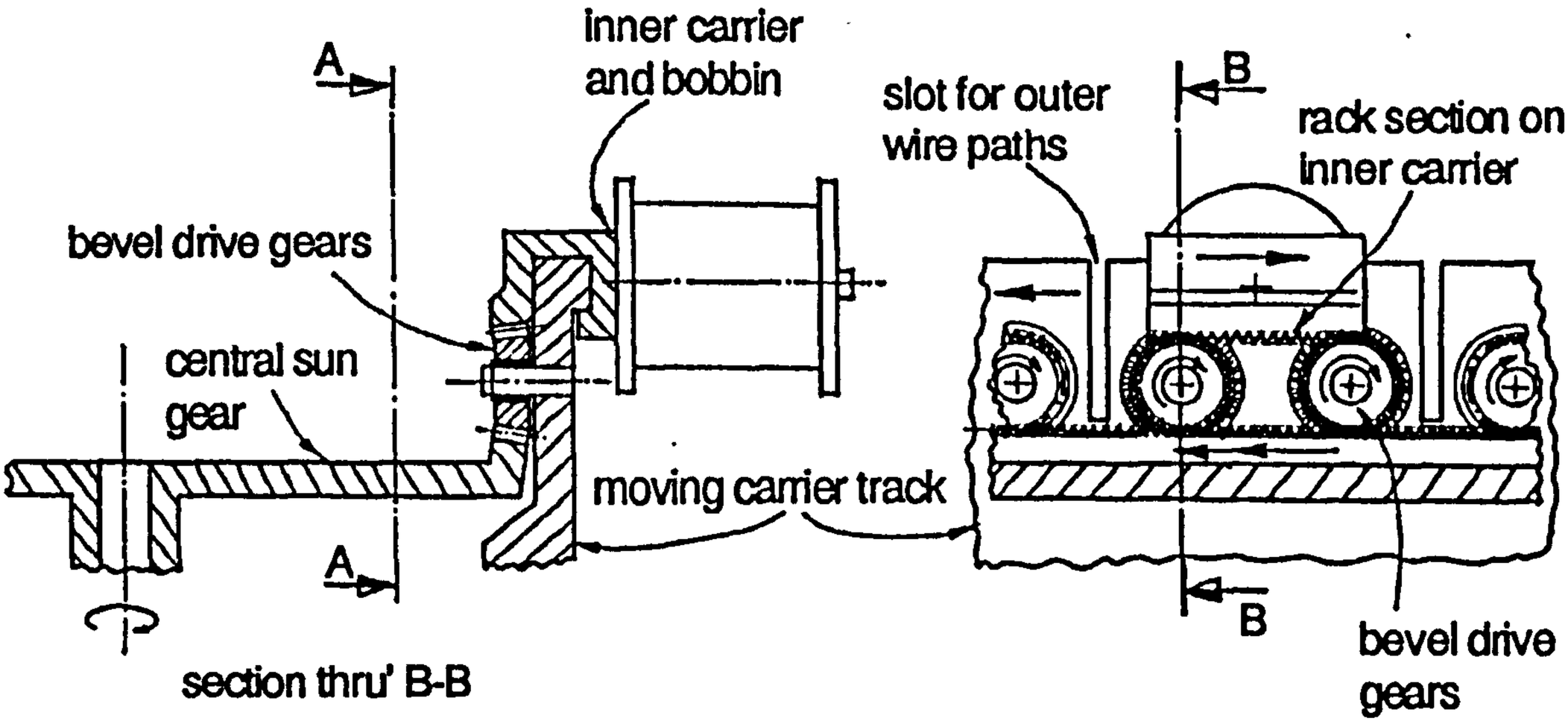

Figure 8.1.20 Bevel gear drive system

However, if a bevel gear arrangement is used the maximum motion of the outer wire is restricted by the sun drive gear. To circumvent this restriction to outer wire motion a system using spur gears may be used as shown in figure 8.1.21.

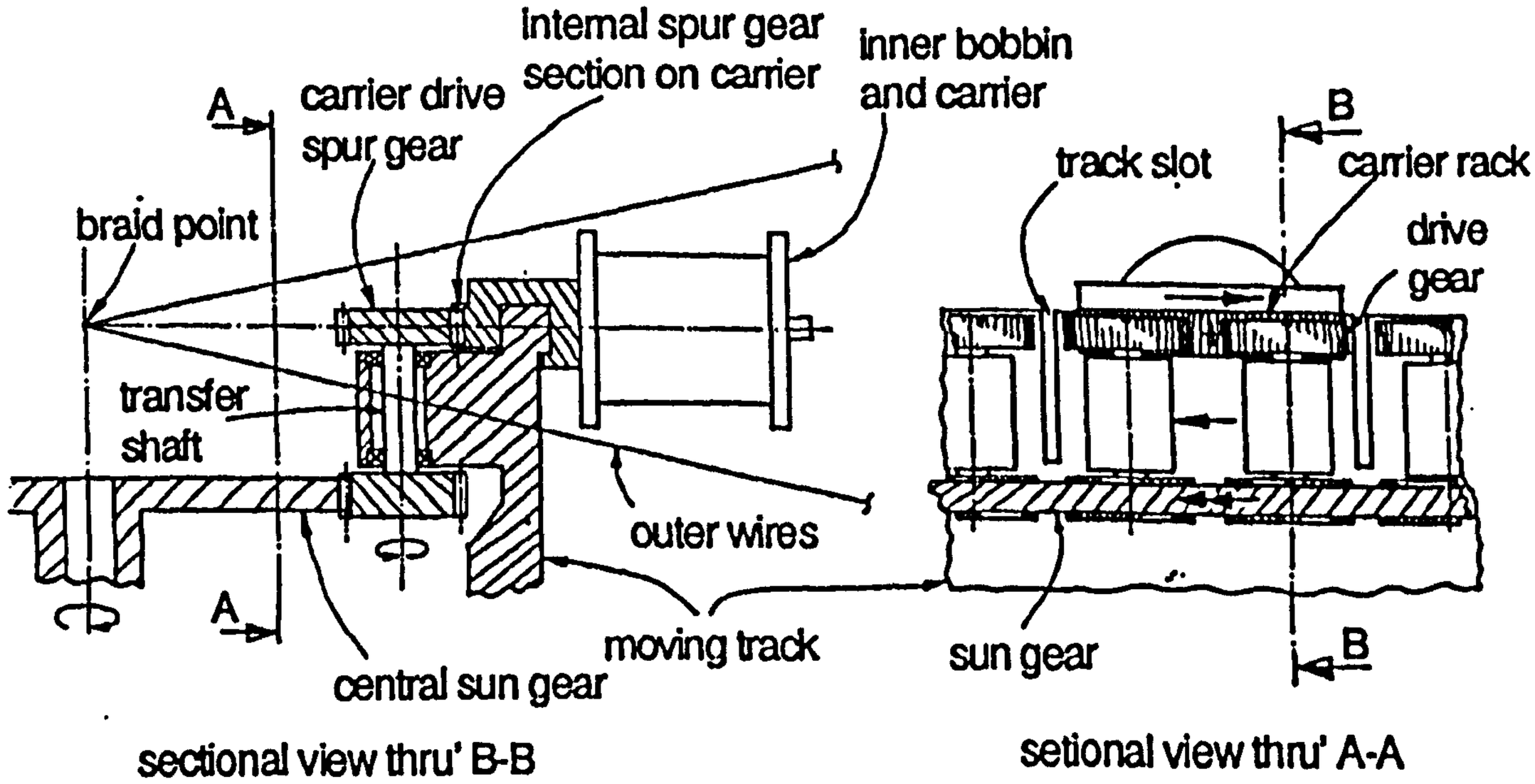

Figure 8.1.21 Spur gear drive system

This duplicates the planetary gears with one set used to drive the carriers and the other to take drive from the sun gear, which may now be situated away from the outer wire path.

A bevel gear system is successfully employed on Spirka rotary braiders, and a variation of the spur gear system is used on Karg braiders.

8.1.3. Summary of Drive Systems Appraisal

Of the systems appraised two stand out as a suitable means of driving the inner carriers. These are the cam or linkage operated finger system, and the gear system.

However, the criteria for an ideal drive system is that the motion of the outer wire should not be constrained by the carrier drive system since this compromises outer wire and wand performance. For this reason the system employing spur gears is chosen for the inner carrier drive system.

8.2. Carrier Layout

8.2.1. Gear Drive System

The only part of the inner carrier drive system which is situated on the carrier, and must, therefore, not transgress the surface of the conical region formed by the outer wire paths, is the section of gear (or gear "rack") which meshes with the planetary gears. This gear rack should be as long as possible and must be at least as long as the planetary gear pitching. For this reason the gear rack must lie along the "horizontal" centre line of the section of the conical region as shown in figure 8.2.10.

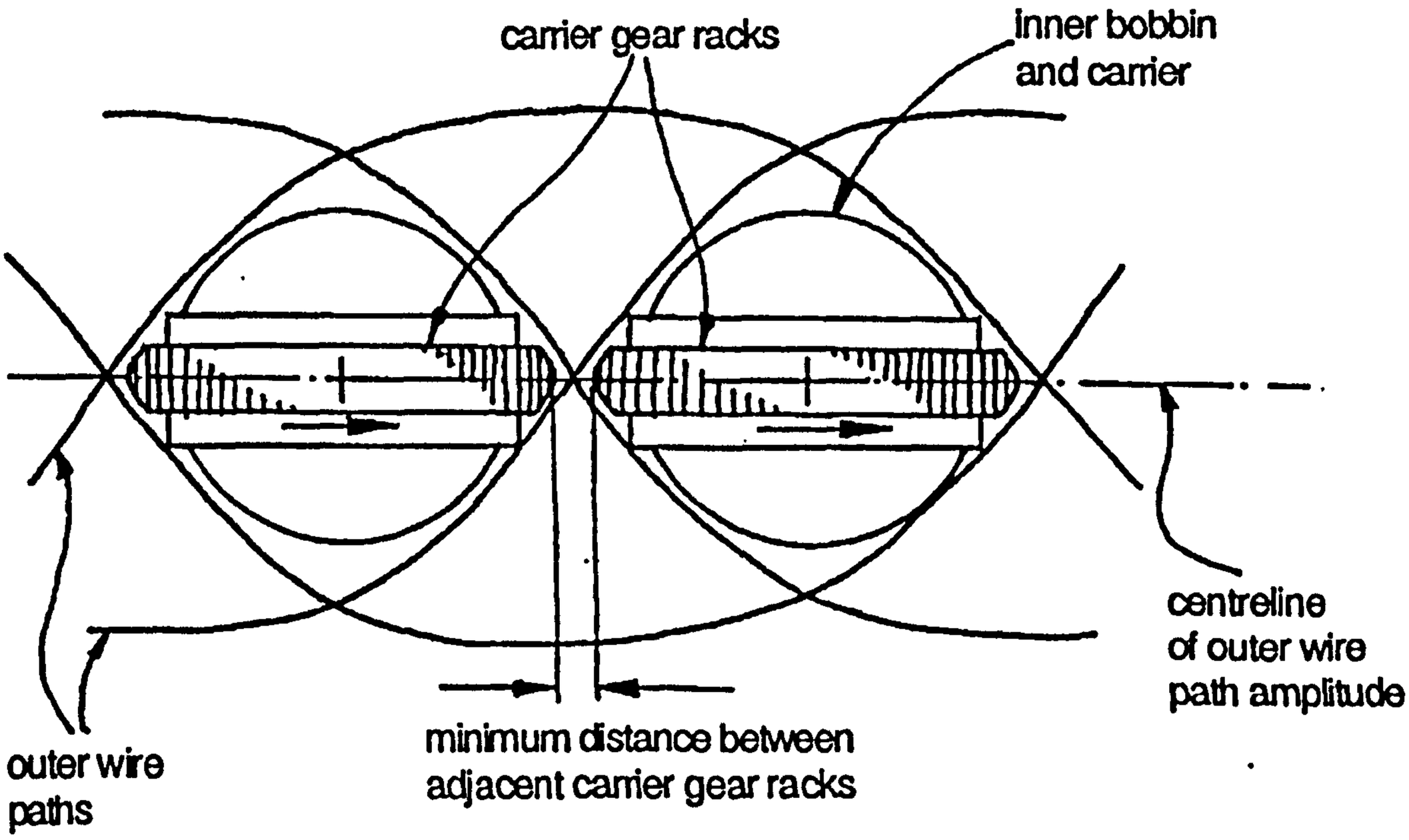

Figure 8.2.10 Ideal location of inner carrier drive gear rack

The ends of the rack are tapered to allow an effectively longer rack. The gap between adjacent carrier racks is therefore reduced, which in conjunction with a suitably coarse planetary gear (having a large tooth contact ratio) allows adjacent carrier racks to mesh with the same planetary gear simultaneously. This removes the possibility of backlash induced shock loads on the planetary gear teeth due to incorrect meshing upon drive takeup (i.e. the planetary gears never loose contact with the carrier racks). A gear module of 2.5 is sufficient to achieve this when the outer wire path is based on a triple harmonic wand motion.

A twenty four carrier braider requires at least twenty four planetary gears. This places a restraint on the practical diameter of each planetary gear, and hence restricts the ratio between carrier rack and planetary gears to a minimum of 11:1. The material used for the planetary drive gears is a type of "Nylatron" which allows a high pitch line velocity without lubrication. Although the ingress of stray wire strands causes increased wear this is offset by the low cost of replacement (typically under £6 for an injection moulded gear). The carrier rack gear sections are hardened steel and are intended to last substantially longer than the planetary gears. The tooth width should be as wide as possible but 20mm is acceptable for the envisaged power transmitted to each carrier of 0.5kW at 150 rpm machine speed.

8.2.2 Track Bearing System

The four roller bearing system chosen (by Babcock Wire Equipment) represents the most compact arrangement practical. To benefit fully from this system the four rollers should lie along the horizontal axis of the conical region section. This is also a pre-requisite for the carrier drive rack and so the two should ideally lie radially apart with the rollers at the greater radius as shown in figure 8.2.20.

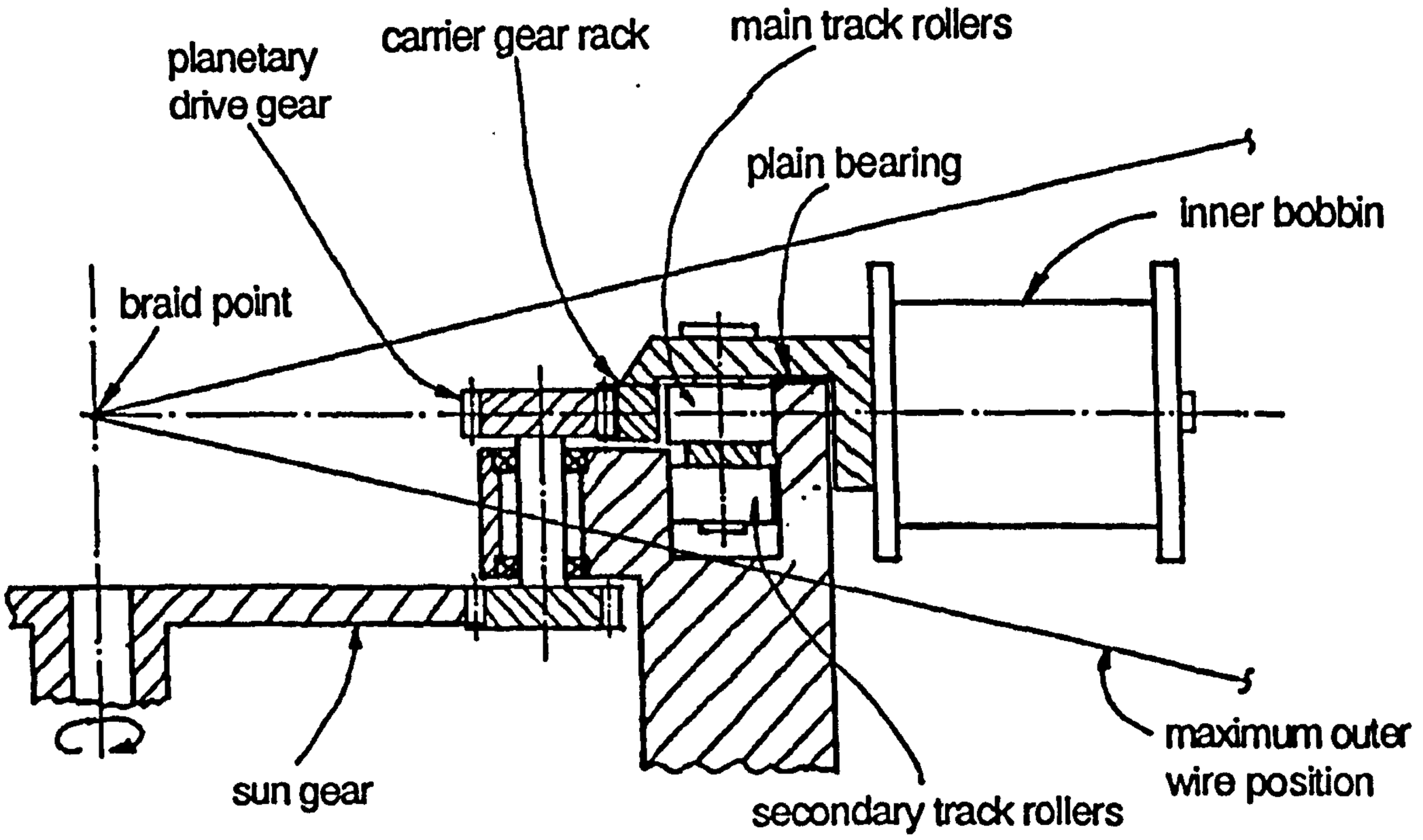

Figure 8.2.20 Ideal inner carrier layout

The bobbin, being the carriers raison d'etre, lies in the largest part of the conical region, radially outside both rollers and drive rack. The four roller system only supports the major centrifugal force and requires location in both roll and pitch. The bearing which provides pitch location must also support the carrier mass (on a vertical axis machine). A boundary layer lubricated plain bearing is suitable in this application and this runs on the top surface of the main roller bearing track (fig. 8.2.20). The roll location is provided by a pair of secondary track rollers (or a plain bearing) below the main set. These run on the outside face of the track as depicted in figure 8.2.21a, until a certain speed is reached when the net moment about the main roller contact points ('O') changes due to the increased centrifugal force. The lower secondary rollers, or plain bearing, now run on the inside edge

of the track as depicted in figure 8.2.21b and complement the main rollers.

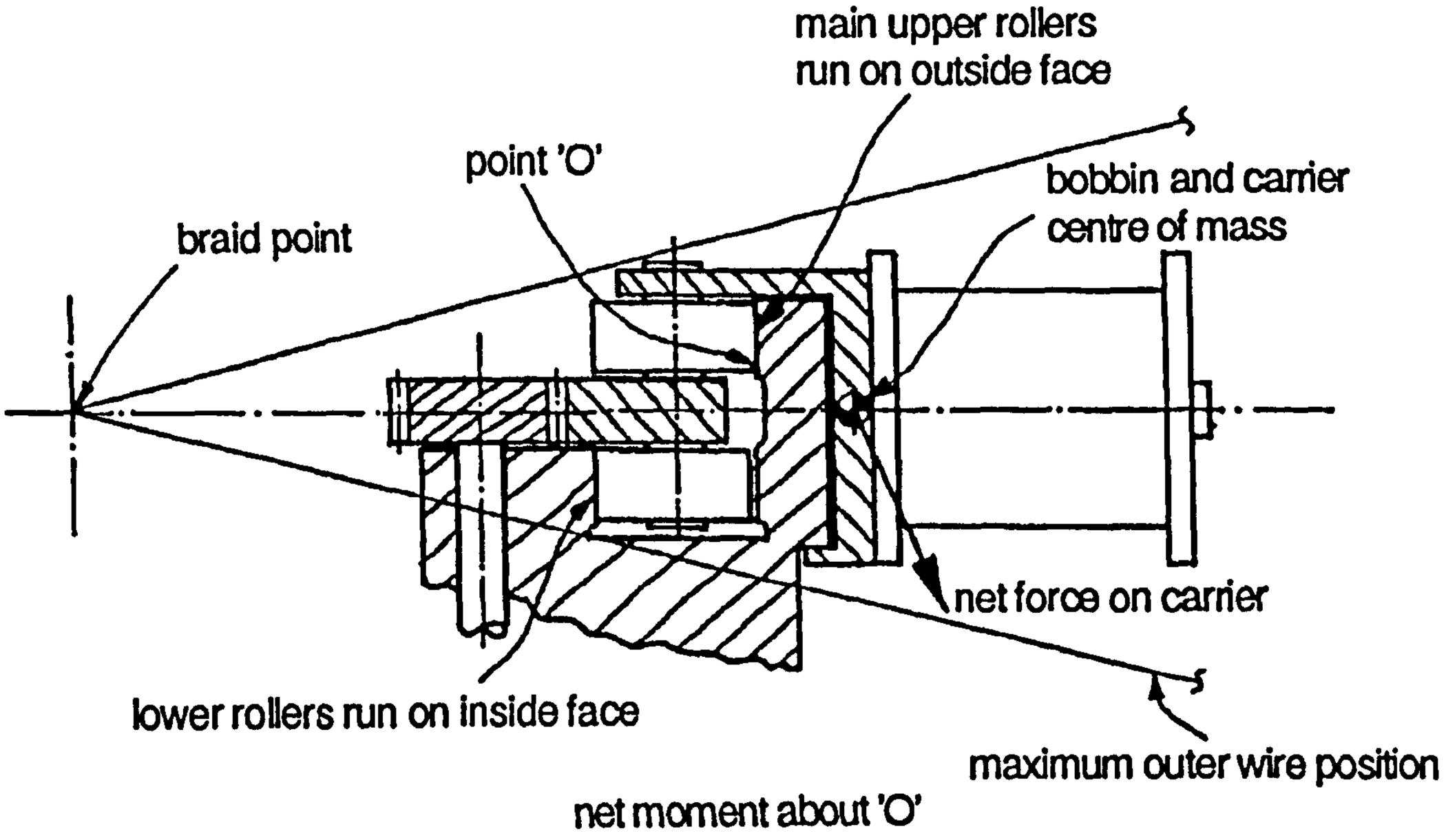

a) Carrier running at low speed

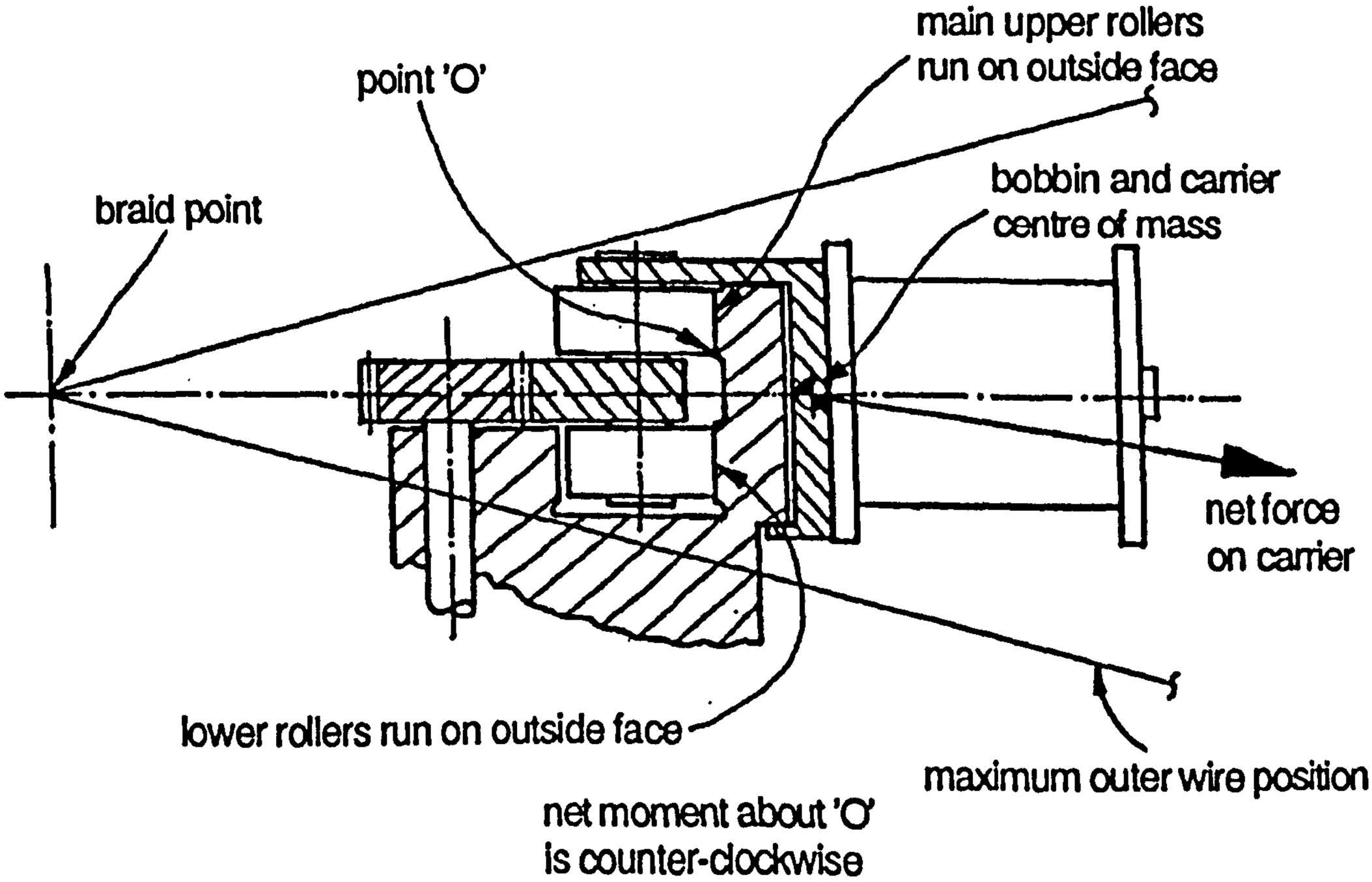

b) Carrier running at high speed

Figure 8.2.21 Modes of carrier operation

For correct operation of this scheme the centre of mass of the whole carrier must be a specific distance below the main roller contact points ('O' in figures 8.2.21). This entails moving the main rollers slightly above the section centre line and either tilting the bobbin downwards or reducing its diameter and moving it downwards to lower the overall centre of mass. This is necessary on a vertical machine since the inherent positions of the carrier bearing and bobbin result in a moment about the track which increases the load on the main rollers. Thus to achieve the longevity required of the track roller bearings at the speeds of operation specified, the optimum bobbin size and position is compromised. (i.e. The bobbin diameter is reduced and the bobbin positioned as low as possible within the conical region).

The ideal solution is to use an 85° braiding angle which naturally positions the carrier centre of mass the correct distance below the main bearing contact points. However, this braiding angle increases the cost and complexity of the machine.

8.2.3 Bobbin and Tension Controller

The bobbin must be quickly removable but the vicinity of the wand mechanisms do not allow the simple radial removal of the empty bobbins. The bobbin must be supported at its outer flange and so a central locating pin hinged at its outer point is used as shown in figure 8.2.30. The hinged pin also incorporates the bobbin brake drum radially outside the bobbin, whilst the brake shoe and wire rundown compensating device remain attached to the carrier frame as the bobbin is pivoted up for removal. Although the optimum position for the bobbin brake is radially inside the bobbin this severely complicates the quickly detachable bobbin arrangement and is not considered a worthwhile trade-off.

Since the only tension variation is from the inner wires interacting with the outer wires near the braiding ring the tension control needs only to be a simple brake with compensation for the amount of wire on the bobbin (ie. a bobbin run-down device). The nominal tension control is manually adjusted and a simple wire break etc, lever is incorporated on top of the carrier which is sensed externally.

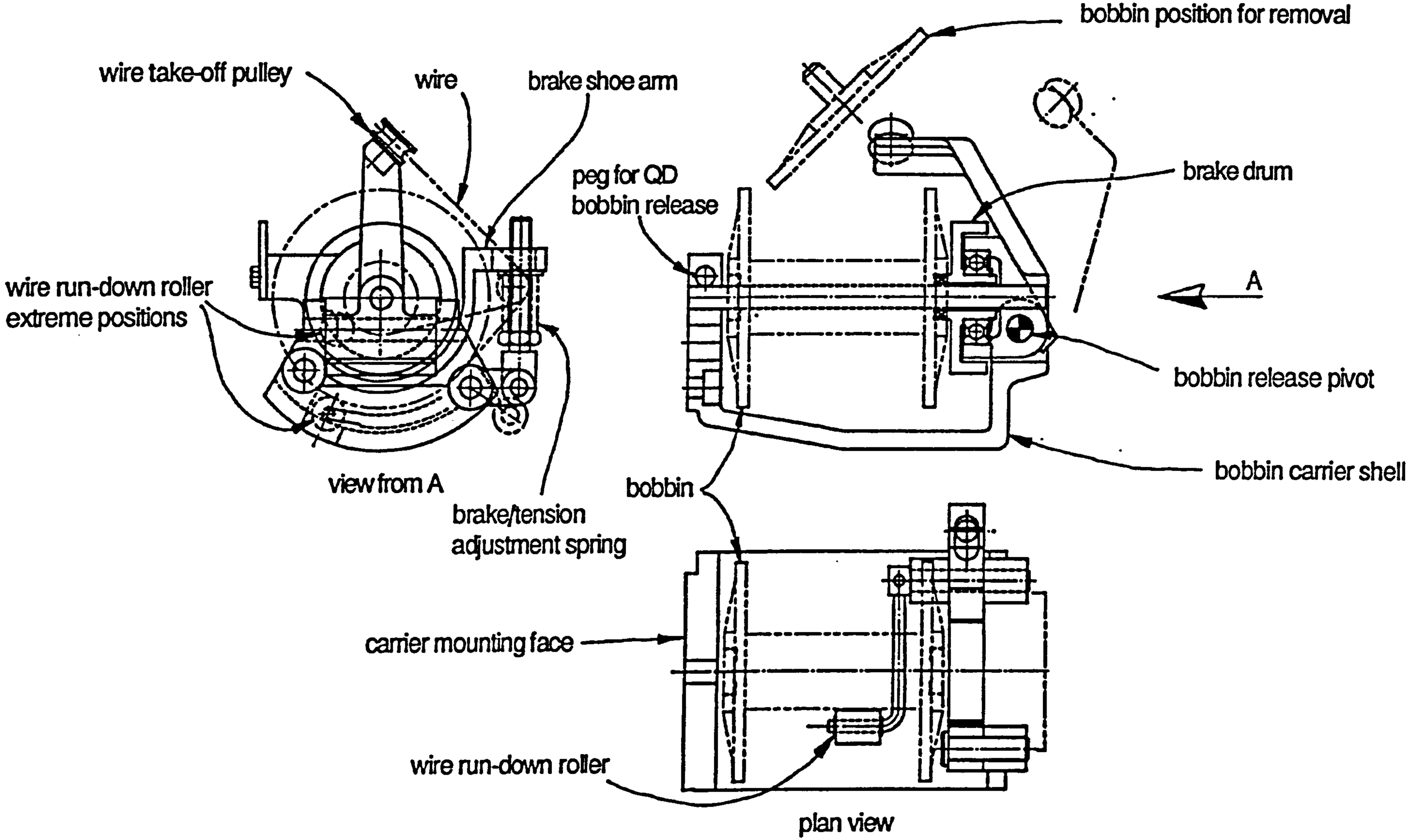

Figure 8.2.30 Inner carrier bobbin holder

8.3 Conclusions

The inner carrier drive system chosen is a gear system featuring 24 nylon based (Nylatron) spur gears which mesh with the sections of hardened steel gear "racks" on each carrier as shown in figure 8.1.21. The drive to the 24 planetary gears is from a main "sun" gear via a duplicate set of planetary gears situated below the track region. The planetary gears are located on, and rotate with, the moving track and outer wands. The minimum ratio between the 24 planetary gears and the carrier gear sections is 11:1. The carrier gear "rack" sections are positioned on the horizontal centre line of the conical region to minimise the gap between adjacent carrier "racks". A gear tooth module of 2.5 is chosen to allow a large contact ratio which enables a single gear to contact adjacent carrier gear racks simultaneously. This reduces the shock loads due to gear backlash which leads to greater gear longevity.

Experimental testing of this gear drive mechanism is not feasible without a full size machine base. However, Spirka use a similar method, using bevel gears, which runs reliably at up to 120 rpm machine speed in certain circumstances.

The bobbin carrier features a quickly detachable bobbin holder and wire tension control by means of a drum brake with compensation for the amount of wire on the bobbin.

The main bearing system is a four track roller arrangement which is positioned slightly above the conical section horizontal centre line. Carrier yaw and roll is controlled by a pair of track rollers mounted below the main rollers (ref. chapter 9, fig. 9.1.01) and pitch is controlled by a plain boundary lubricated bearing which supports the carrier weight and runs on the top surface of the main roller track. Maximum carrier bearing performance is achieved by positioning the carrier centre of mass a certain distance below the main roller contact points. The ideal way to achieve this is with an 85° braid angle, but this complicates wand cam manufacture which becomes prohibitively expensive. The alternative is to lower the bobbin and its carrier within the conical space. This entails reducing the bobbin diameter to below the maximum possible. The final bobbin position is, therefore, determined by the carrier bearing performance and the prohibitive cost of using an 85° braid angle and not solely by the optimisation routines covered in chapter 5.

CHAPTER NINE

FINAL MACHINE DESIGN

9.0 Actual Design Procedure

The actual analysis and design procedure approximately followed the proposed design procedure (Chapter 1, section 1.5.2). However, both changes to the original specification and concessions, usually to economics, altered the intended design program away from that for a dynamically optimum machine. The program of design adopted is described below.

a) The criteria for the outer wire vibration is found as a correlation of theory and experimentation. For a given outer wire and wand system a single harmonic motion is ideal. Adding odd harmonics increases the volume available to the inner bobbins and carriers, but this also increases the amplitude of wire vibration.

b) A survey of outer wire deflecting (wand) mechanisms concludes that a simple crank or cam driven rocker is ideal with a relatively large wand tip amplitude to provide a single harmonic motion (or approximately single harmonic in the case of the crank drive).

However, a restriction on wand amplitude of 220mm was imposed by the collaborating company for aesthetic reasons which were perceived as a market requirement. The motion of the wand is limited by two factors:

i) The amplitude of vibration of the wire over the span from wand tip to braid point.
ii) The longevity of the wand cam follower (or drive). This is dependent upon the wand inertia which is limited economically, and the position of the follower which is limited by pressure angle considerations.

There is, therefore, a certain outer wire span above which the harmonic content of the wand motion is limited by the wire vibration, and below which it is limited by the wand drive, or cam follower, longevity. The ideal is to achieve the former without having to resort to exotic materials to reduce the inertia of the wand.

c) The optimisation of the inner bobbin proportions and orientation within the conical region, formed by the super position of all the outer wire paths, was performed in conjunction with the wand motion selection. The aim was to find the minimum radius at which the initially specified 10kg inner bobbins may be positioned in order to reduce the inner carrier bearing loads. This also allows the shortest outer wire span and so a wand motion with a higher harmonic content may be successfully utilised. At this point the optimum motion law (bearing in mind the restricted 220mm amplitude) was found to be a triple harmonic law.

d) The inner bobbin carrier, track bearing, and drive must also fit into the conical region along with the inner bobbin. A study of track bearing systems shows that a multi roller bearing arrangement offers the highest performance. Optimising the bearing arrangement in conjunction with the optimised wand motion and bobbin orientation showed that a bearing system capable of performing at 150 rpm would not fit in the space available. The radius at which the inner bobbins are positioned was then determined in conjunction with the inner carrier bearing performance criteria. However, the optimum wand motion was still the triple harmonic motion law but the inner bobbin radius and, therefore, outer wire span had increased slightly over that for an optimised 10kg bobbin. The inner carrier gear drive system chosen could also be accommodated within the optimum bearing system since only the gear section is mounted on the carrier.

e) At this point in the project the original specification was again changed and the bobbin capacity reduced from 10kg to 3.5kg (of copper wire). The bobbin proportions were also specified as those used by Spirka (i.e. Spirka bobbins were specified for the machine). In addition, the longevity required from the carrier roller bearings was reduced from 25,000 hours to 15,000 hours.

f) These changes clearly allow an increase in performance over a 10kg bobbin machine, but the inner bobbin optimisation routines are now redundant. However, the inner carrier bearings required for a running speed of 150 rpm would still not fit into the space left in the conical region by the inner bobbin. Again, the optimum machine performance is achieved using an increased inner bobbin radial position and outer wire span than is necessary for the bobbin alone. The bobbin is positioned within the conical region to allow the most effective use of the available bearing performance and although an 85° braiding angle is uneconomic due to complications in wand cam manufacture, this is equivalently

achieved by lowering the bobbin relative to the carrier bearing.

The span of the outer wire is such that a triple harmonic motion, with a relatively high third harmonic content, is the optimum wand motion. This motion results in the maximum wire vibration tolerable whilst allowing the use of a forged aluminium alloy wand driven by a single wall cam and a return spring.

The inner carrier bearing arrangement allows the carrier drive gear segment to be positioned almost across the widest part of the conical region cross section. This allows the minimum gap between adjacent carrier gear segments.

The bobbin brake, tension control and quick release mechanisms were integrated into the arrangement but were designed from an ergonomic and economic viewpoint.

9.1 Summary of Final Machine Design

The general assembly and detail drawings of the prototype machine based on the results of this research work were produced by Babcock Wire Equipment Ltd.

Whilst the overall machine concept and most of the relevant details of the machine are as intended, a few of the more subtle details, which may well effect performance have been misinterpreted or corrupted in the transfer from machine schemes to detail drawings. This is accepted as inevitable at the end of a collaborative project and the aberrations may be easily rectified, if required, for a production machine. Various sectional general assembly drawings of the machine are shown in figures 9.1.01, 9.1.02, and 9.1.03.

9.1.1 Wand Mechanism

The wands are forged aluminium alloy rocker arms whose pivot axes pass through the braiding point. Each wand features a single roller bearing cam follower which runs on a triple harmonic motion, single sided, stationary wall cam situated around the machine periphery. Follower contact with the cam is maintained by a spring return system. The cam running surface is crowned with a radius of 80mm to prevent "corner running" between cam and follower, and hardened to 650HV. The cam is machined as a flat plate and then rolled and fitted into a sleeve before being welded up as a ring.

The forged alloy wand is initially a "C" section but changes to an "L" section from halfway along its length, as shown in figure 4.2.04 (chapter 4). The wand tip features a bonded ceramic eyelet for wire control. A second ceramic eyelet guides the wire along the wand to a pulley situated on the wand pivot axis. The wand is shown with the follower axis displaced from the wand central axis. This is incorrect for optimum cam design and leads to a 3° increase in maximum pressure angle.

9.1.2 Inner Carrier Drive

The inner carrier drive is achieved by spur gear segments mounted on the carriers driven by 24 drive pinions mounted on the track base (figs. 9.1.01 and 9.1.02).

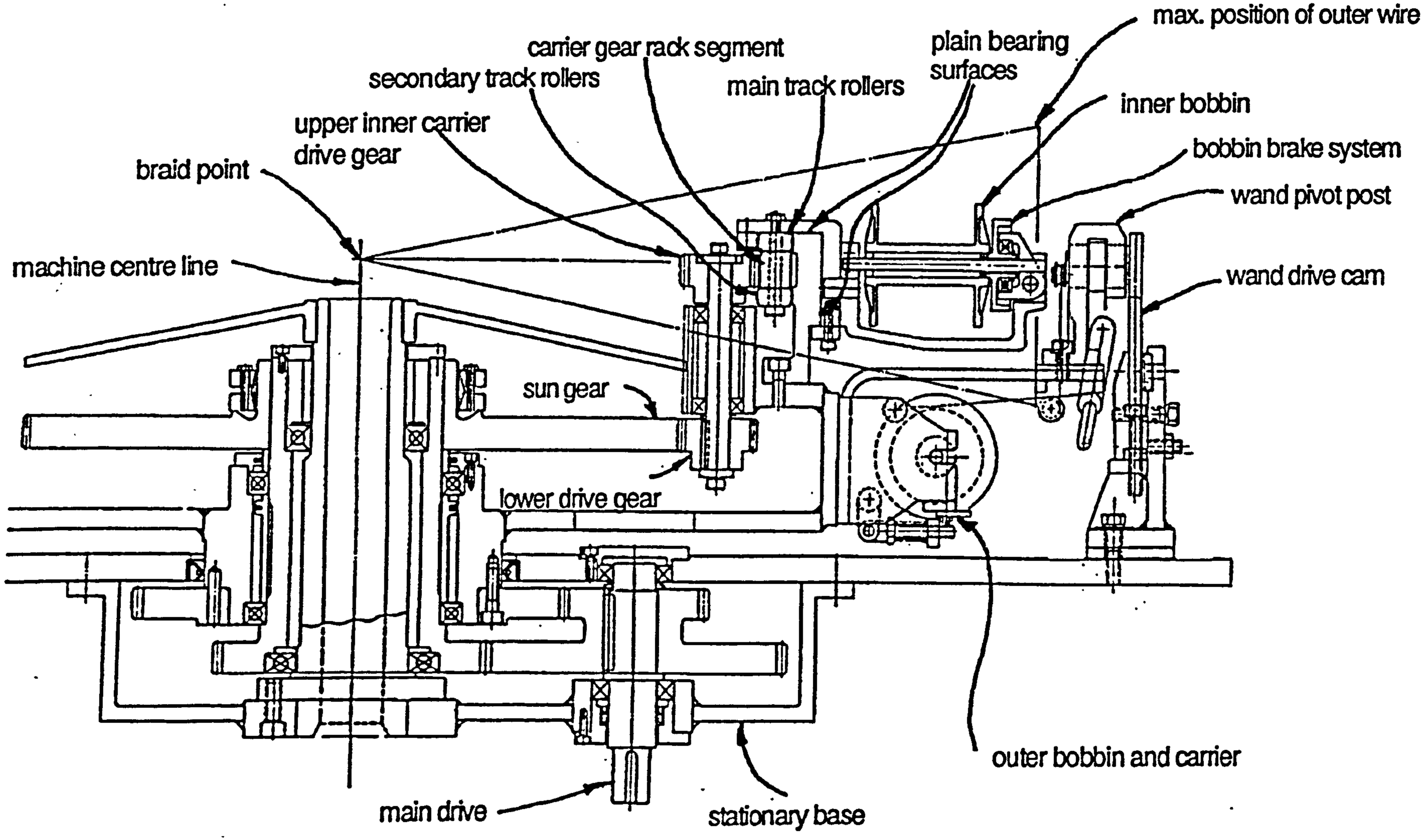

Figure 9.1.01 Sectional G/A of the final rotary braider design

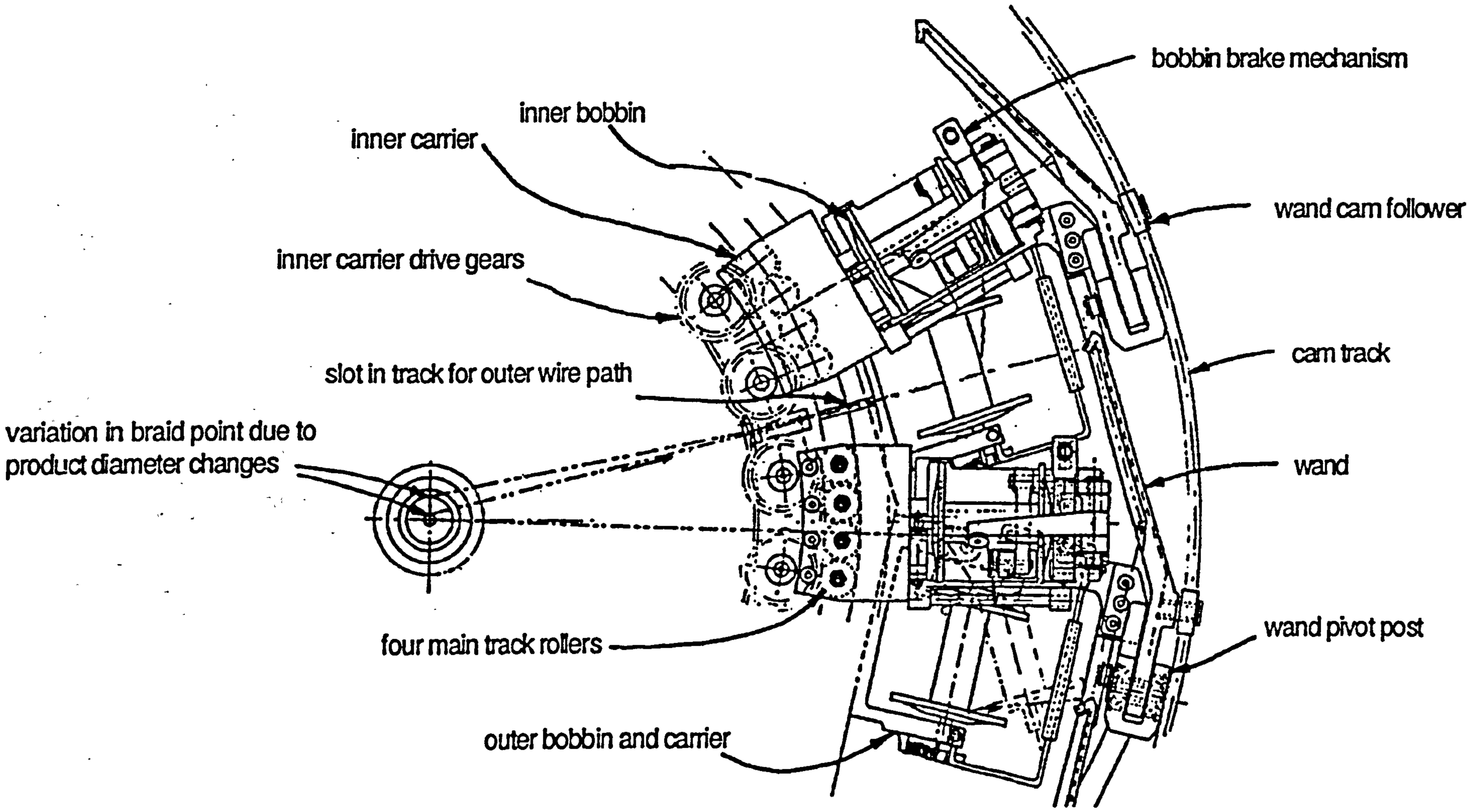

Figure 9.1.02 Scrap plan view of final rotary braider design

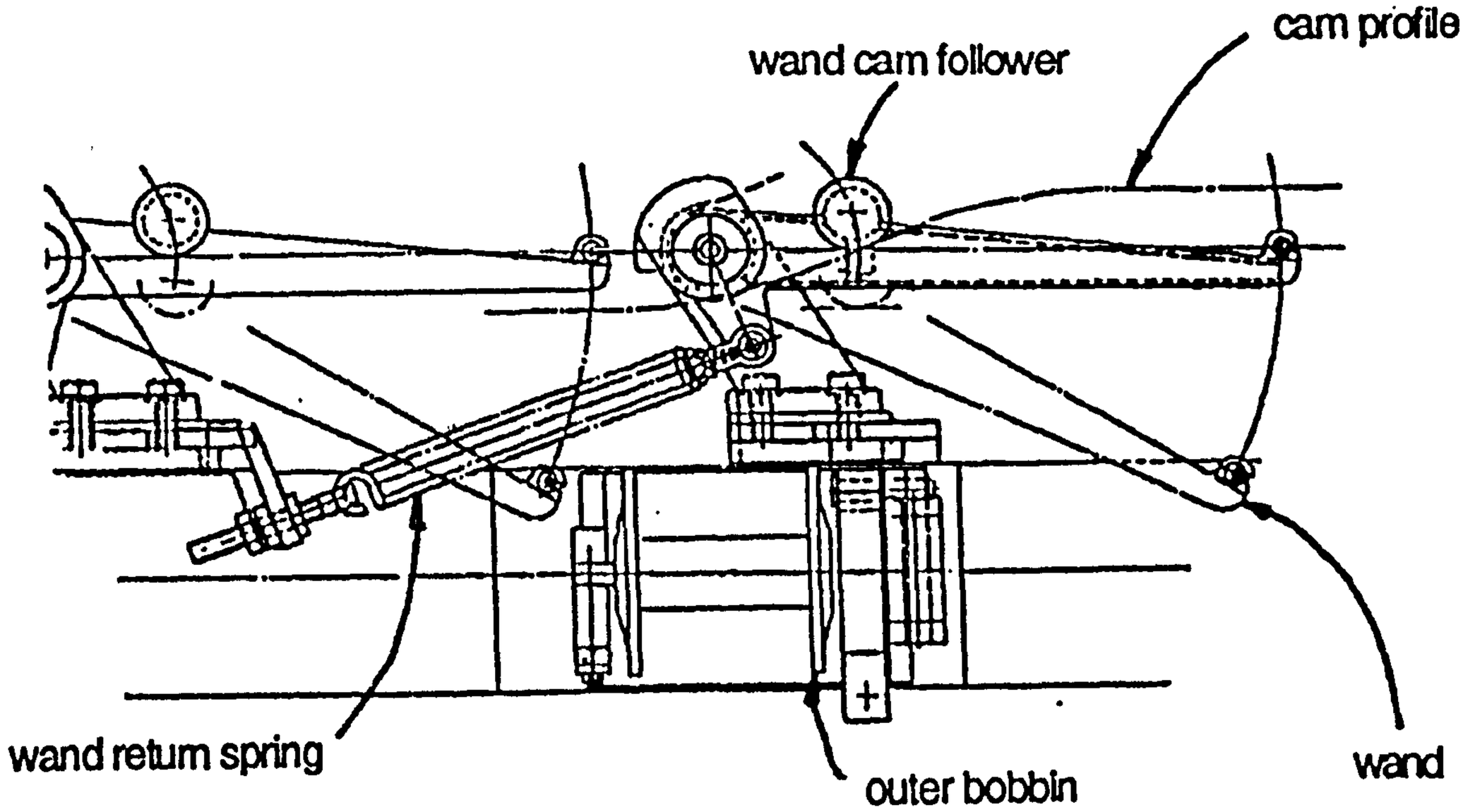

Figure 9.1.03 Scrap view of rotary braider wand arrangement

The drive to these is from a large central sun gear via a second set of spur gears mounted on the drive pinion shafts. The ratio between the carrier gear segments and the drive pinions is 11:1 which is the maximum ratio possible and prevents each drive pinion ever loosing contact with a carrier gear segment (i.e. There is a point when two carrier gear segments are in contact with one drive pinion). This is aided by the small gap between adjacent carrier gear segments made possible by mounting the segments almost on the widest part of the conical region cross section (into which the carrier, bobbin and gear segments must fit). The carrier gear segments are made from steel but the drive pinions are a nylon based material and can run with no lubrication, although a little is desirable.

9.1.3 Inner Carrier Bearings

The number of roller bearings used for the main bearing system is determined by the machining accuracy of the centres (ref. Chapter 7). The collaborating company claim to be able to achieve $\pm$0.005mm by jig boring and this allows four 30mm diameter rollers to be used. This, when operating correctly, is the highest performance system. The secondary pair of rollers are situated directly below the two centre main rollers. When running at low speed these rollers do not contact the track and the carrier is supported by the plain bearings running on the outer face of the track. At approximately 60 rpm (with a full bobbin) the carrier swings

due to centrifugal force and the secondary rollers complement the main rollers in supporting the major centrifugal force on the carrier. All the rollers are located in the gear segment which lies between the two roller sets. The weight of the carrier is supported on a self lubricating plain bearing mounted to the carrier top plate which runs on the top face of the main track. This bearing surface must have periodic lubrication. All the track roller bearings are sealed but must also be periodically lubricated with grease.

The track is built up from twelve segments, hardened to 700 HV, which are located by dowels and bolted to the main outer carrier rotor before grinding. The gaps between adjacent segments constitutes the track slots for the outer wire paths. A taper is ground on the leading edge of each segment based on the profile N2 (ref. chapter 7). This is intended to taper from 0.05mm at the slot edge, to 0 linearly over 20mm.

9.1.4 Inner Carrier Bobbin and General Layout

The inner and outer bobbins used are those from a 24 carrier Spirka. The bobbin is orientated with its axis below, but parallel to, the central axis of the conical region formed by the outer wire paths (i.e. Bobbin orientation type 1, refer chapter 5). The bobbin is situated radially outside the carrier track bearing and drive system. The bobbin brake system is situated radially outside the bobbin which is necessary to allow a simple quickly detachable bobbin device. This allows the bobbin complete with spindle and brake drum to swing upwards for bobbin removal whilst the brake pad and bobbin run-down compensator remain fixed in the carrier body (figure 8.2.30). The wire tension is adjusted manually and increases the spring preload on the brake shoe. The amount of wire on the bobbin is compensated for by a roller arm which runs on the bobbin flank and effectively reduces the brake pad spring preload as the wire on the bobbin is consumed. The brake assembly is supported by a thin casting bolted to the carrier top plate assembly.

The outer bobbins are situated below the inner carriers on the main wand pivot rotor and are virtually identical to the inner bobbin tension control arrangement.

CHAPTER TEN

CONCLUSIONS

10.0 General Conclusions

Every current rotary braiding machine on the market fails to fully utilise the inherent dynamic advantages of the rotary braiding concept. This is because, in general, these machines have been designed with only one area of the process optimised. The remainder of the machine merely complements this.

The aim of the research work was to design a machine which optimises all the performance critical processes involved in the rotary braiding concept in unison, thereby ensuring a machine with a superior level of performance.

The rotary braiding machine market chosen by Babcock Wire Equipment Ltd. for a new machine is the 24 carrier medium load capacity braider used primarily for cable armouring and screening. This is the market dominated by Spirka with a 24 carrier braider which runs at 85 rpm with a 3.5kg bobbin.

The original specifications for the new machine were:

i) To cost approximately £27,000 or less.
ii) A longevity of 25,000 hours for all component parts.
iii) An initial target speed of 150 rpm.
iv) An initial target bobbin size of 10kg.
v) A reasonable power consumption (a Spirka requires 5kW).
vi) A maximum noise level of 85 dB(A) when inside a sound proof enclosure.

Changes to these original specifications were continuously made to move the performance capabilities away from the "super maypole" hose braiders (which Babcock Wire Equipment were also developing) and nearer the specification of the Spirka. The changes which had a major effect on machine performance (and ultimately design) were:

i) Spirka bobbins (or exact replicas) were specified, with a capacity of 3.5kg.
ii) The wand tip amplitude was restricted to 220mm (for aesthetic reasons).
iii) The inner carrier bearing longevity was reduced to 15000 hours.

The research work completed here has optimised the critical areas of the rotary braiding process through theoretical analysis and experimental tests. The optimisation begins with the fundamental behaviour of the outer wires and uses this criteria to determine an appropriate wand mechanism. The optimisation of inner bobbin orientation within the conical region formed by the superposition of the outer wire paths allows the most effective utilisation of any chosen wand/wire motion. Inner carrier bearing systems are appraised and the roller bearing supported carrier, which is considered most suitable, is investigated in detail. Finally the position of the carrier bearing is optimised to complement the optimised inner bobbin.

The overall result is a machine concept and final design which are optimised for maximum dynamic performance and which has a theoretical performance some 76% above that of the current market leading machine.

Each of the machine elements and processes tested operated satisfactorily and based on these results it is considered highly likely that the prototype machine, built to the final machine design, will perform at, or above, the level cited in the specifications.

The power requirements of the machine as a whole are estimated as approximately 19kW which is acceptable considering the increase in speed (of 76%) over that of a Spirka.

The cost of a production machine based on the prototype is estimated to be £30,000. The noise level has yet to be determined as is the reliability of the complete machine.

A prototype machine based on the final machine design described in chapter 9 is, at the time of writing, undergoing final assembly at Babcock Wire Equipment Ltd., Bolton. Figure 10.0.0 shows the prototype machine in almost complete form.

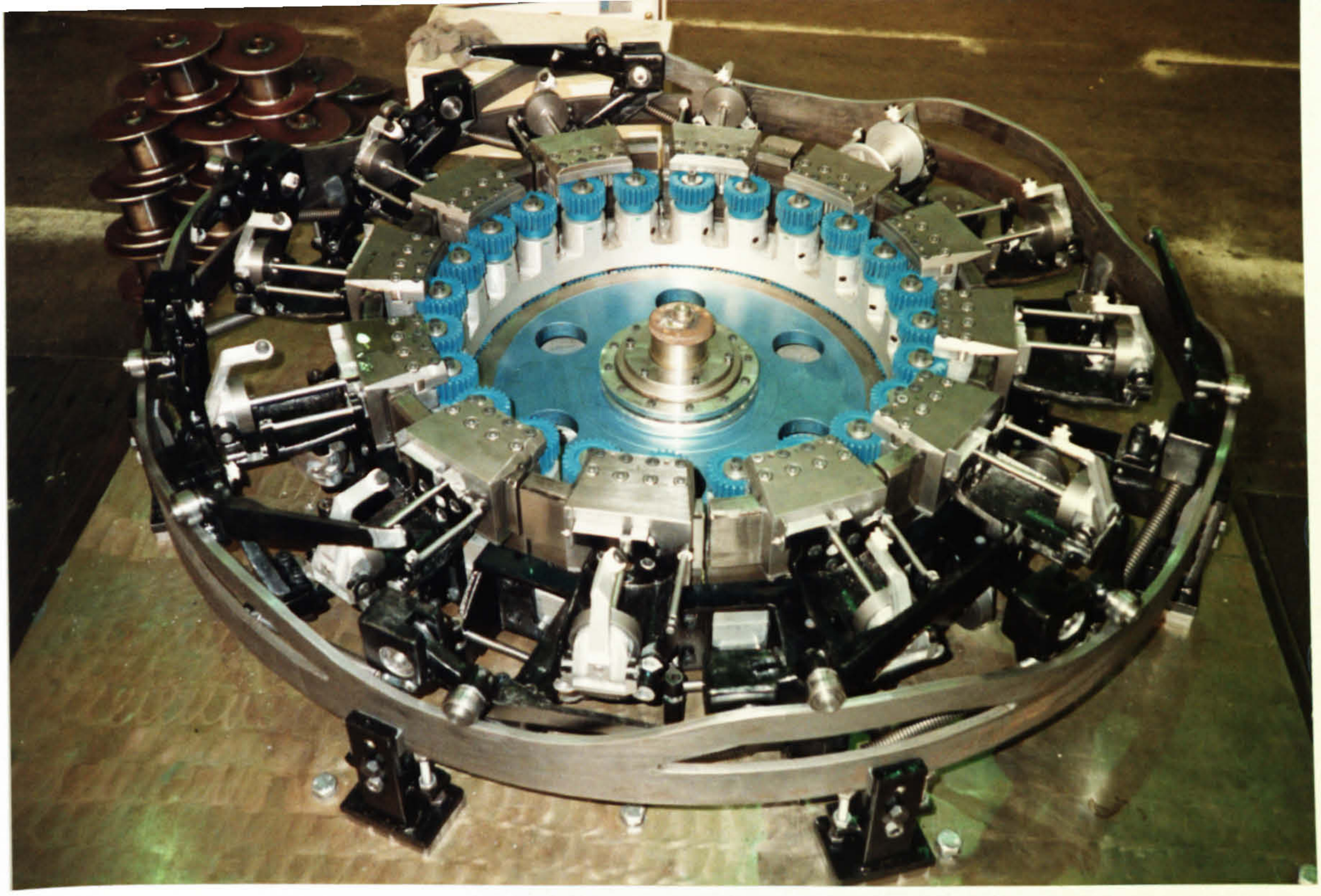

Figure 10.0.0 Prototype rotary braider in final assembly

10.1 Towards a Next Generation Rotary Braider

It is clear that the final machine design presented in chapter 9, whilst representing the optimum machine within the detailed specification, is not by any means the highest performance machine possible within the general specification for bobbin size and reliability. However, all design involves compromise and certainly economic restraint is necessary to achieve a marketable machine. But an over restrictive specification, however well intentioned, can only lead to a machine with unduly compromised performance (re.- the restriction on wand tip amplitude and the use of Spirka bobbins, both of which were ill conceived and unfounded). Further more, it is relatively easy for a competitor to pinpoint the short comings in such a design, to their advantage.

It has become obvious throughout the studies that the area of the present design (chapter 9) which limits performance is the inner carrier track bearing and not, fundamentally, the outer wire control.

Indeed the bobbin capacity finally specified (3.5kg) suggests an increase in performance may be gained by positioning the bearing radially outside the bobbin. However, the bobbin proportions must differ from the Spirka bobbin for this to be the case.

The logical remedy is to allow stationary inner carriers and rotate the product (and wind on and wind off drums). The inner carrier bearing load is thus reduced by a factor of approximately ten. The machine speed is then limited by the outer wire motion (which, with a single harmonic law allows far higher speeds than at present), together with the carrier bearing (and drive) speed capacity. This format of machine, whilst somewhat costly and bulky for large machines (but not entirely impractical), is ideal for smaller machines in allowing the full benefits of the rotary braiding concept to be realised.

Other less radical methods of increasing inner carrier bearing performance are:

a) To utilise the braiding angle which allows the optimum bearing performance (in the case of the final design in chapter 9 this angle is 85°). This will usually incur a cost penalty.

b) To use a stationary track which halves the bearing speed, effectively doubling longevity. This system incurs a prohibitive cost penalty at present, but improvements in plain bearing technology may allow an economic design of this type.

The other area fundamental to possible increases in rotary braider performance is the outer wire/wand motion. The ideal form is a single harmonic motion and not a multi harmonic system.

Finally, the concepts of rotary braiding appear to be ideal for application to a larger hose braider to compete directly with the super maypoles. The design presented in chapter 9 needs relatively little fundamental change in order to accept large (10kg) bobbins and allow an increased wire tension (which is good for outer wire control). The cost of such a machine would not in theory be much more than the machine design presented here. Although it would not possess high levels of performance relative to the design presented in chapter 9, would still comprehensively out perform all current super maypole braiders.

BIBLIOGRAPHY

(1) **Evans, W.E.,** *Hose technology*, 2nd ed., 1979, (Applied Science Publishers Ltd., England).

(2) **Douglass, W.A.,** *Braiding and braiding machinery,* 1964, (Butterworths, London).

(3) **Quensel, P., Vetterli, W., Billington, R., Buhler, R.,** *Review 1974,* 1974, (Ciba Geigy Ltd., Basle, Switzerland).

(4) **Tregurtha, J.,** *Braiding machine* , US patent no. 447262, 1891.

(5) **Pain, H.J.,** *The physics of vibrations and waves,* 3rd Ed., 1983, (J Wiley & Sons, Bristol, UK). Ref. chapter 4.

(6) **Baldock, G.R , Bridgeman, T.,** *The mathematical theory of wave motion,* 1981,(Ellis Harwood Ltd, Chichester). Ref. chapters 1.6, 1.10, 2.

(7) **Timoshenko, S., Young, D.H., Weaver, Jnr.W.,** *Vibration problems in engineering,* 4th ed., 1974, (Wiley, New York). Ref. sections 1.12, 5.3, 5.4.

(8) **Main, I.G.,** *Vibrations and waves in physics,* 2nd ed., 1984, (Cambridge University Press, Cambridge). Ref. chapters 9, 12.1.

(9) **Meirovitch, L.,** *Elements of vibration analysis,* 2nd ed., 1986, (McGraw Hill, Singapore). Ref. sections 5.1 to 5.10.

(10) **Kreyszig, E.,** *Advanced engineering mathematics,* 4th ed., 1979, (Wiley, New York, USA). Ref. chapters 11, 19.2, 19.6.

(11) **Oldham, K., Walker, M.J.,** *A procedure for force balancing planar linkages using counter weights,,* 1981, (Dept. of mechanical engineering, University of Newcastle Upon Tyne).

(12) **Lowen, G.G., Tepper, F.R., Berkof, R.S.,** *The quantitative influence of complete force balancing on the forces and moments of certain families of four-bar linkages,* Mechanism and Machine Theory, Vol. 9, 1974, (Pergamon Press, Oxford, England).

(13) **Schwartz, M.,** *Composites material handbook,* 1984, (McGraw Hill, Singapore).

(14) **Anderson, J.C., Leaver, K.D., Rawlings, R.D., Alexander, J.M.,** *Materials science,* 3rd ed., 1985, (Van Nostrand Reinhold UK). Ref. chapters 9, 11, 16.

(15) **Piggott, M.R.,** *Load bearing fibre composites,* 1980, (Pergamon International Press, Oxford, England). Ref. chapters 2,4,9,12.

(16) **Hearn, E.J.,** *Mechanics of materials,* Vols. 1 and 2, 1981, (Pergamon Press, Oxford, England). Ref. chapters 1, 5, 7, 8, 13, 16, 20, 21, 23, 25, 26.

(17) **Koenigsberger, F.,** *Design principles of metal cutting machine tools,* 1964, (Pergamon press, Oxford, England). Ref. chapter 5.

(18) **Shigley, J.E.,** *Mechanical engineering design,* 3rd ed., 1977, (McGraw Hill, Singapore).

(19) **Calladine, C.R.,** *Engineering plasticity,* 1969, (Pergamon press, Oxford, England).

(20) **Grassam, N.S., Powell, J.W.,** *Gas lubricated bearings,* 1964, (Butterworths, London).

(21) **Powell, J.W.,** *Design of aerostatic bearings,* 1970, (The Machinery Publishing Co. Ltd., London). Ref. chapters 1, 2, 4, 8, 9, 10.

(22) *Pneumatic Handbook,* 4th ed., 1980, (Trade and Technical Press Ltd., London).

(23) **Jayawant, B.V.,** *Electromagnetic levitation and suspension techniques,* 1981, (Edward Arnold, London).

(24) **Jones, B.E., Wilson, B.,** Linear induction motors controlling carriages moving round a circular track, *IEE Proc.,* Part D, Nov. 1980, Vol. 127, No. 6, (University of Manchester).

REFERENCES

(1) **Timoshenko, S., Young, D.H., Weaver, Jnr.W.,** *Vibration problems in engineering,* 4th ed., 1974, (Wiley, New York). Ref. section 5.4.

(2) **Jayawant, B.V.,** *Electromagnetic levitation and suspension techniques,* 1981, (Edward Arnold, London). Ref. page 2.

APPENDIX 2.2.1

Effect of Air Resistance on Wire Shape

One end of the wire is stationary, the other has an absolute velocity V. The wire deflection, y, is measured in the same direction as the velocity, V.

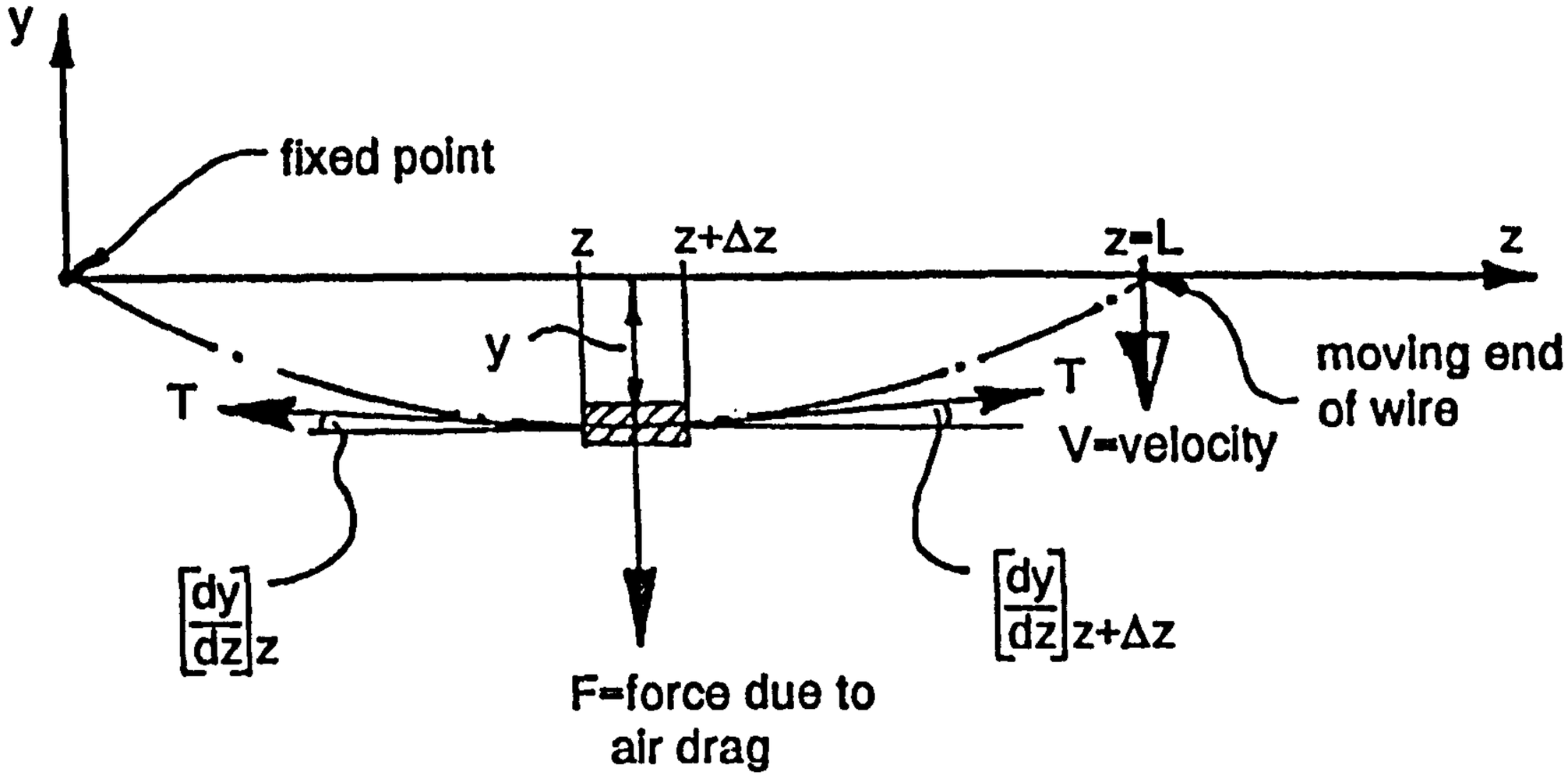

Figure A2.2.10 Wire model for air resistance theory

The forces on any segment of wire are the tension and the drag force due to air resistance. Summing these forces in the y direction.

$$T\left(\frac{\delta y}{\delta z}\right)_z - T\left(\frac{\delta y}{\delta z}\right)_{z+\Delta z} = F.\Delta z$$

$$\therefore\ T\left(\frac{\delta^2 y}{\delta z^2}\right)\Delta z = F.\Delta z$$

But the force due to drag $F = Cd.d.ro.V(z)^2$ (N/m)

where Cd = total drag coefficient of the wire (~1.0)
ro = air density
d = wire diameter
V(z) = V.z/L

$$\left(\frac{\delta^2 y}{\delta z^2}\right) = Cd.d.ro.V^2.z^2/(T.L^2)$$

$$\left(\frac{\delta y}{\delta z}\right) = [Cd.d.ro.V^2/(T.L^2)].z^3/3 + C1$$

$$\therefore\ y = [Cd.d.ro.V^2/(T.L^2)].z^4/12 + C1.z + C2$$

But $y = 0$ when $z = 0$ $\therefore\ C2 = 0$

Also $y = 0$ when $z = L$ $\therefore\ C1 = -Cd.d.ro.V^2.L/(12.T)$

$$\therefore\ y = Cd.d.ro.V^2.[z^4/L^2 - L.z]/(12.T)$$

Now y is a maximum when $(\delta y/\delta z) = 0$

$$\therefore\ z_{(ymax)} = 0.63\ L$$

The total absolute velocity of the wire end (wand tip) has two components. The velocity of the wands around the machine axis is typically 9 m/s (150rpm) and the component perpendicular to this due to the wand oscillation is typically 16 m/s for a triple harmonic wand motion.

Combining these two results in a velocity of 18.2 m/s.

Other typical values are :

$T = 5\ N$
$L = 0.6\ m$
$Cd = 1.0$
$d = 0.3\ mm$
$ro = 1.5\ kg/m^3$

The maximum wire deflection due to air resistance is: $y_{max} = 0.78$ mm.

This is considered negligible for a 0.3 mm diameter wire.

APPENDIX 2.2.2

Relative Effect of Wire Stiffness

We will attempt to show the relative effect of wire stiffness on the theories for wire behaviour.
The assumption is made that the stiffness has a negligible effect if when the wire is treated as a beam its radius of curvature, adopted due to its self weight, is at least an order of magnitude less than the radius of curvature of the wire span when treated as an elastic string under tension (5N minimum).

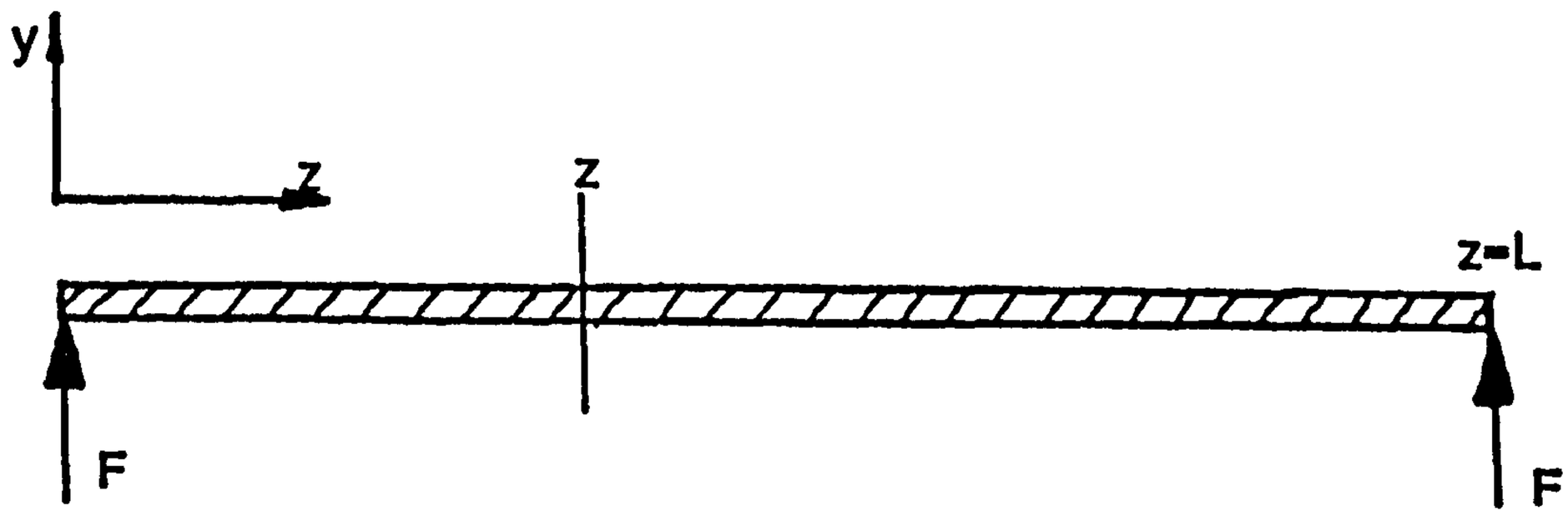

Figure A2.2.20 Wire modelled as a beam

Moment at section z,

$$M(z) = (L - z).(F - (L - z).\mu.g/2) = \mu.g.(L.z - z^2)/2$$

where: μ = specific mass of wire
d = wire dia.
L = wire span

Beam radius of curvature (R),

$R = (I.E/M)$ which is a minimum when $z = L/2$

$I = \pi.d^4/64$
E = Youngs modulus (210 GPa)

If $\mu = 0.00056$ kg/m
d = 0.3 mm
L = 0.6 m

Then $\underline{R = 0.34\ m}$

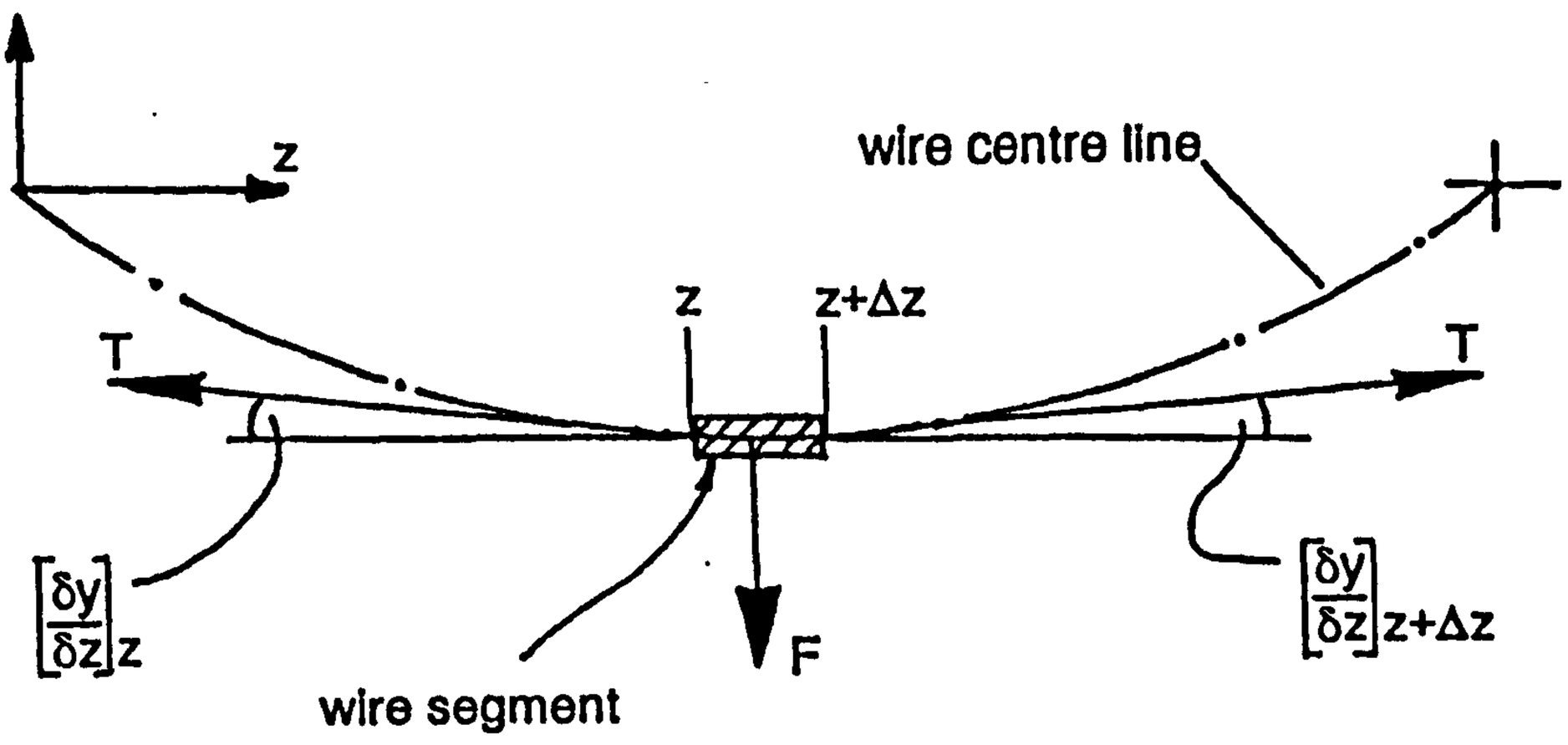

Figure A2.2.21 Wire modelled as an elastic string

Weight of segment of wire $F = \mu.\Delta z.g$
Summing forces in the y direction,

$$T\left(\frac{\delta^2 y}{\delta z^2}\right)\Delta z = \mu.\Delta z.g \qquad \text{(for small deflections)}$$

$$\therefore \left(\frac{\delta^2 y}{\delta z^2}\right) = \mu.g/T$$

$$\therefore \quad 1/R = \mu.g/T \qquad \text{and for a tension of 5N:}$$

$$\underline{R = 910\ m}$$

The radius of curvature of the wire as a beam is substantially less than the same wire treated as an elastic string under tension. The assumption is made that the stiffness of the wire has a negligible effect on the deflection shape of the wire motion.

APPENDIX 2.2.3

Theory for Wire Behaviour in the ψ - z Plane

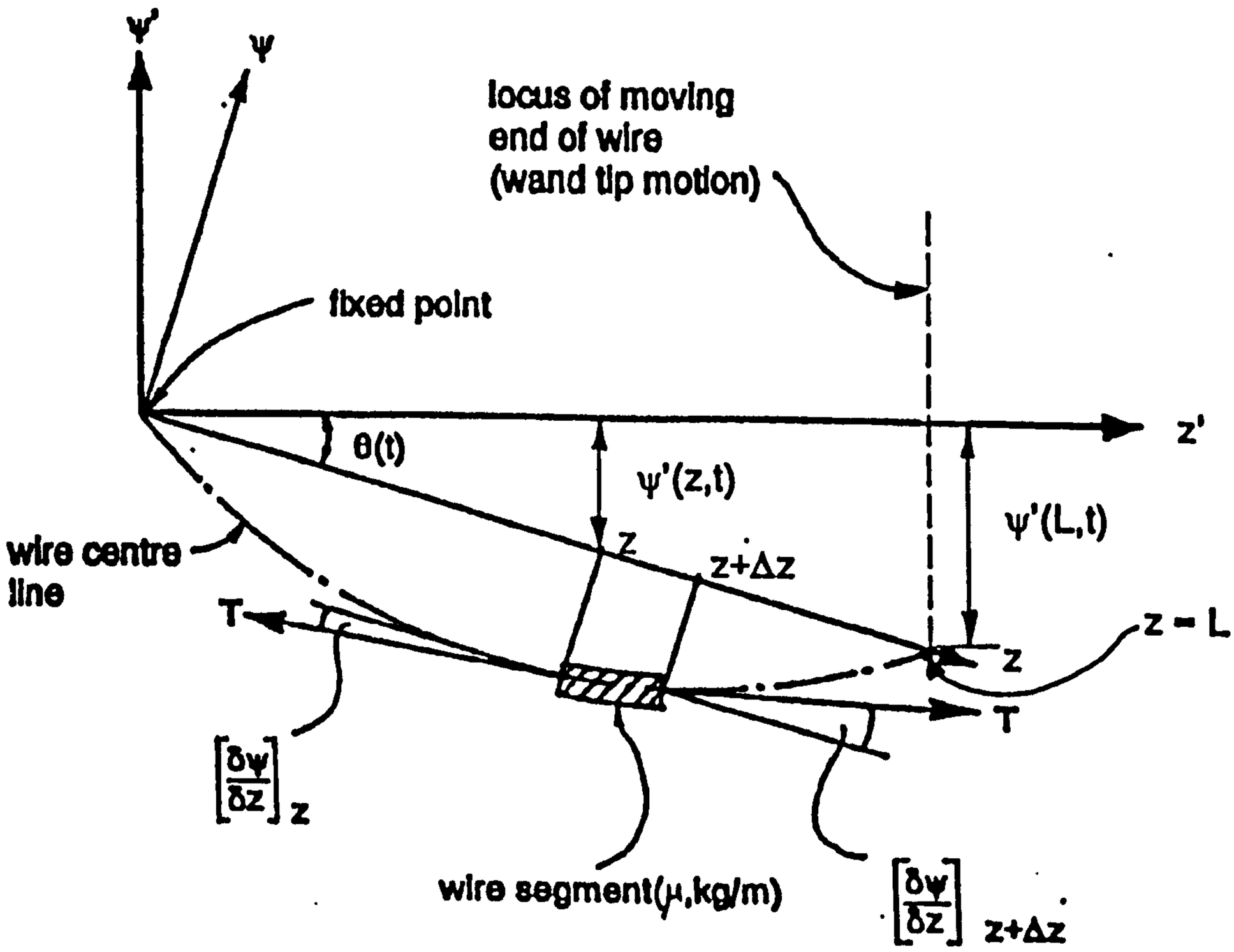

Figure 2.2.10 Segment of moving wire in the ψ - z plane

The wire is continuously moving towards the fixed point with velocity V.
Resolving tension forces and accelerations in the ψ direction.

$$-T\left(\frac{\delta\psi}{\delta z}\right)_z + T\left(\frac{\delta\psi}{\delta z}\right)_{z+\Delta z} = \mu.\Delta z\left[\frac{\delta^2\psi}{\delta t^2} + \cos\theta.\left(\frac{\delta^2\psi'}{\delta t^2} + \frac{2.V}{z}.\frac{\delta\psi'}{\delta t}\right)\right]$$

where $\theta = \arctan(\psi'(L,t)/L1)$ and $L1 = (L^2 - R^2)^{0.5}$

Thus;

$$T\left(\frac{\delta^2\psi}{\delta z^2}\right)\Delta z = \mu\Delta z\left[\frac{\delta^2\psi}{\delta t^2} + \cos\theta\left(\frac{\delta^2\psi'}{\delta t^2} + \frac{2.V}{z}\frac{\delta\psi'}{\delta t}\right)\right]$$

$$\frac{T}{\mu}\left(\frac{\delta^2\psi}{\delta z^2}\right) - \left(\frac{\delta^2\psi}{\delta t^2}\right) = \cos\theta.\left(\frac{\delta^2\psi'}{\delta t^2} + \frac{2.V}{z}\frac{\delta\psi'}{\delta t}\right) \quad (1)$$

Now $\psi'(z,t)$ is the input motion derived from the wand motion $\theta_1(t)$ by:

$$\psi' = (R.z/L).\sin\theta_1 \quad (2)$$

$$\left(\frac{\delta\psi'}{\delta t}\right) = (R.z/L).\dot{\theta}_1.\cos\theta_1 \quad (2a)$$

$$\left(\frac{\delta^2\psi'}{\delta t^2}\right) = (R.z/L).(-\dot{\theta}_1^2.\sin\theta_1 + \ddot{\theta}_1.\cos\theta_1) \quad (2b)$$

where typically for a triple harmonic wand motion,

$$\theta_1(t) = A1.\sin(\omega t) + A2.\sin(3.\omega t) \quad (3)$$

$$\dot{\theta}_1(t) = A1.\omega.\cos(\omega t) + 3.A2.\omega.\cos(3.\omega t) \quad (3a)$$

$$\ddot{\theta}_1(t) = -A1.\omega^2.\sin(\omega t) - 9.A2.\omega^2.\sin(3.\omega t) \quad (3b)$$

The right hand side of equation (1) is the forcing function, denoted now as $\ddot{g}(z,t)$, and the left is the familiar "wave equation".

Rewriting equation (1) in normalised coordinates gives:

$$\ddot{\Phi}i + pi^2.\Phi i = -\int_0^L \ddot{g}(z,t).Xi.dz \quad (4)$$

Where Xi is the normal modal shape of the i^{th} mode of the wire vibration. Typically we can assume that;

$$Xi = (2/L)^{0.5}.\sin(pi.z/s)$$

where $s = (T/\mu)^{0.5}$ and $pi = i.\pi.s/L \quad (i = 1, 2, 3, ...)$

Using Duhamels integral method to calculate the response of the i^{th} mode in equation (4) gives,

$$\Phi i = -1/pi \int_0^L Xi \int_0^t \ddot{g}(z,t').\sin(pi.(t - t'))\, dt'\, dz \qquad (5)$$

Superimposing all the normal mode responses gives,

$$\psi = -\sum_{i=1}^{\infty} Xi/pi \int_0^L Xi \int_0^t \ddot{g}(z,t').\sin(pi.(t-t'))\, dt'\, dz \qquad (6)$$

Combining equations (2) and (3) gives :

$$\psi' = R.z/L.(A1.\sin(\omega t) + A2.\sin(3\omega t)) \qquad (7)$$

and so on for $\left(\frac{\delta \psi'}{\delta t}\right)$ and $\left(\frac{\delta^2 \psi'}{\delta t^2}\right)$

In solving equation (6) we must first integrate for t'

$$\text{Now } \ddot{g}(x,t') = \cos(\Theta(t'))\left(\frac{\delta^2 \psi'}{\delta t'^2} + \frac{2.V}{z}.\frac{\delta \psi'}{\delta t'}\right) \qquad (8)$$

But the relative complexity of integrating this term in full necessitates the use of a numerical integration technique.

Equation (6) may now be expressed as,

$$\psi = -\sum_{i=1}^{\infty} Xi/pi \int_0^L Xi.(z.I1 + I2)\, dz \qquad (9)$$

where $$z.I1 = \int_0^t \frac{\delta^2 \psi'}{\delta t'^2}.\cos(\Theta(t')).\sin(pi.(t-t'))\, dt' \qquad (10)$$

and $$I2 = \int_0^t \frac{2.V}{z}.\frac{\delta \psi'}{\delta t'}.\cos(\Theta(t')).\sin(pi.(t-t'))\, dt' \qquad (11)$$

Integrals I1 and I2, both with respect to normalised time (t'), are achieved by numerical methods. A simple trapezoidal rule is employed although for higher harmonic forcing functions a more accurate method may be desirable.
This approach allows the potentially complex wand motion to be integrated rapidly (relative to analytic integration) whilst leaving the integrals generic to the wave equation to be solved with higher precision analytically.

The total response (ψ'_t) of the wire with respect to the wand pivot axis is then:

$$\psi'_t(z,t) = \psi'(z,t) + \psi(z,t).\cos(\theta(t)) \qquad (12)$$

As the modal shapes are summed in equation (9) there is a point above which no significant change in wire deflection occurs. This point was found to be when
i = 5.
All the plots represent summed modal shapes up to 5.

Typical values for a single wire used in the plots of wire behaviour/form (and the experimental tests) are:

μ = 0.00056 kg.m
T = 5 N
ω = 94 rad/s
R = 0.265 m
L = 0.62 m

Figure 2.2.11 in chapter 2 shows the wire behaviour $\psi(z,t)$ (relative to a straight wire) for single, triple, and quintic harmonic wand motions.

APPENDIX 2.2.4

Theory for Wire Behaviour in the ϕ - z Plane

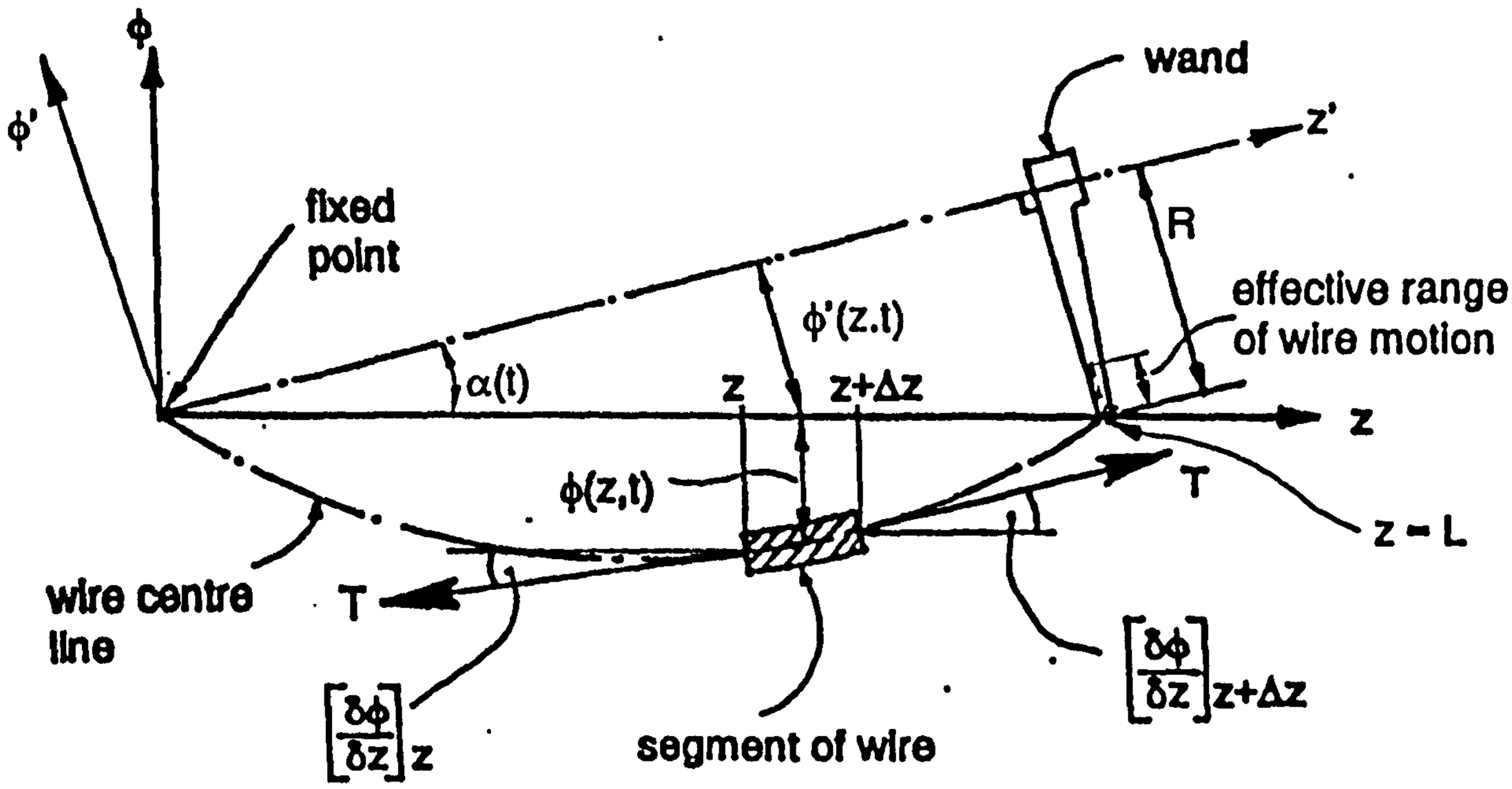

(view from arrow B in figure 2.1.02)

Figure 2.2.20 Segment of moving wire in the ϕ - z plane

The wire is continuously moving toward the fixed point with velocity V.
Resolving tension forces and accelerations in the ϕ direction.

$$-T\left(\frac{\delta\phi}{\delta z}\right)_z + T\left(\frac{\delta\phi}{\delta z}\right)_{z+\Delta z} = \mu.\Delta z\left(\frac{\delta^2\phi}{\delta t^2} + \cos\alpha.\ \frac{\delta^2\phi'}{\delta t^2}\right)$$

where $\alpha = \arctan(\phi'(L,t)/L1)$ and $L1 = (L^2 - R^2)^{0.5}$

The coriolis term present in the theory for the ψ - z plane is now negligible due to the limited range of motion and low angular velocity the wire experiences in this plane.

Thus;

$$T\left(\frac{\delta^2\phi}{\delta z^2}\right)\Delta z = \mu\Delta z\left(\frac{\delta^2\phi}{\delta t^2} + \cos\alpha\ \frac{\delta^2\phi'}{\delta t^2}\right)$$

$$\frac{T}{\mu}\left(\frac{\delta^2\phi}{\delta z^2}\right) - \left(\frac{\delta^2\phi}{\delta t^2}\right) = \cos\alpha.\left(\frac{\delta^2\phi'}{\delta t^2}\right) \qquad (13)$$

Now $\phi'(z,t)$ is the input motion derived from the wand motion $\theta_1(t)$ by:

$$\phi' = (R.z/L).\cos\theta_1 \qquad (14)$$

$$\left(\frac{\delta\phi'}{\delta t}\right) = -(R.z/L).\dot{\theta}_1.\sin\theta_1 \qquad (14a)$$

$$\left(\frac{\delta^2\phi'}{\delta t^2}\right) = -(R.z/L).(-\dot{\theta}_1^{\,2}.\cos\theta_1 + \ddot{\theta}_1.\sin\theta_1) \qquad (14b)$$

where typically for a triple harmonic wand motion (as in appendix 2.2.3),

$$\theta_1(t) = A1.\sin(\omega t) + A2.\sin(3.\omega t) \qquad (3)$$

$$\dot{\theta}_1(t) = A1.\omega.\cos(\omega t) + 3.A2.\omega.\cos(3.\omega t) \qquad (3a)$$

$$\ddot{\theta}_1(t) = -A1.\omega^2.\sin(\omega t) - 9.A2.\omega^2.\sin(3.\omega t) \qquad (3b)$$

The right hand side of equation (13) is the forcing function for the ϕ - z plane, and the left is the familiar "wave equation". The solution to equation (13) is found by the same method used for equation (1) in appendix 2.2.3. Although the forcing function is now simpler than that in the ψ - z plane, the numerical integration method is again employed.

The general solution in the ϕ - z plane is now;

$$\phi = -\sum_{i=1}^{\infty} Xi/pi \int_0^L Xi.z.I3\ dz \qquad (15)$$

where $$z.I3 = \int_0^t \frac{\delta^2\phi'}{\delta t'^2}.\cos(\alpha(t')).\sin(pi.(t-t'))\ dt' \qquad (16)$$

The variables Xi and pi , which are generic to the wave equation, are unchanged from those in appendix 2.2.3.

The total response (ϕ'_t) of the wire with respect to the wand pivot axis is now:

$$\phi'_t(z,t) = \phi'(z,t) + \phi(z,t).\cos(\alpha(t)) \qquad (17)$$

Again, as the modal shapes are summed in equation (15) there is a point above which no significant change in wire deflection occurs. This point was again found to be when i = 5.

Typical material parameters for a single wire used in the theory of wire behaviour/form (and the experimental tests) are:

μ = 0.00056 kg.m
T = 5 N
ω = 94 rad/s
R = 0.265 m
L = 0.62 m
A1 = 0.48 rad
A2 = 0.053 rad (for triple harmonic wand motion)

The form of the wire in the ϕ - z plane is virtually identical to that shown in the ψ - z plane (figure 2.2.11) but with lower amplitudes.

The peak deflection in the ϕ - z plane is 4.5 mm , for a typical triple harmonic motion, and this occurs at the limit of wand travel.

However, the deflection at the mid point of wand travel, when $\theta_1 = 0$, is 2.5 mm. This is the deflection of the wire as it enters the critical inner carrier track slot region.

APPENDIX 5.1.01

Increase in Wire Capacity using Conical Bobbins

An optimised bobbin will have a length of one a third of the length of the conical region defined by the outer wire paths (ref. appendix 5.2.12).

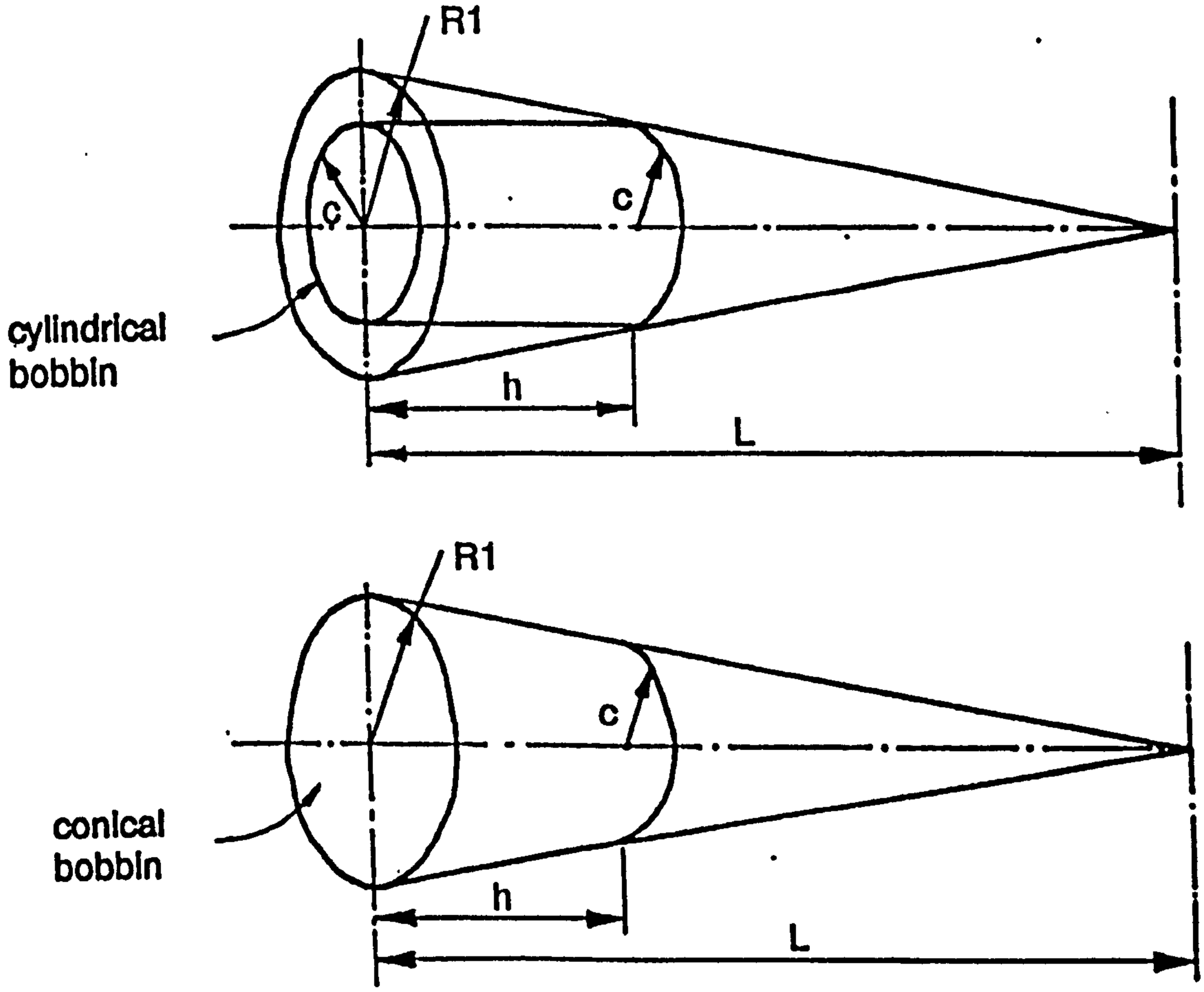

Figure A5.1.01 Cylindrical and conical bobbin dimensions

The increase in bobbin volume including the spool and spindle may be determined.

Assume $h = L/3$

volume of cylindrical bobbin $Vc = \pi.c^2.L/3$

from appendix 5.2.12 $c = 2/3.R1$

therefore $Vc = 4/27.\pi.R1^2.L$

The volume of a conical bobbin of the same length, Vn, is:

$Vn = 1/3.\pi.R1^2.L - 1/3.\pi.c^2.2/3.L$ where $c = 2/3.R1$

$\therefore Vn = 1/3.\pi.R1^2.L.(1-8/27)$

The ratio of volumes of the two bobbins is:

$Vn/Vc = 1.58$

Now assuming the bobbin core radius is typically 1/3.c and that the flanges lie outside the bobbin volume, the actual increase in wire capacity is found.

Volume of wire on cylindrical bobbin, Vcw:

$Vcw = 4/27.\pi.R1^2 L - L/3.c^2.\pi/9$

$\therefore Vcw = 10/81.\pi.R1^2.L$

Volume of wire on conical bobbin, Vnw:

$Vnw = 19/81.\pi.R1^2.L - L/3.R1^2.\pi.4/81$

$\therefore Vnw = 53/243.\pi.R1^2.L$

Volume ratio is :- $Vnw/Vcw = 1.77$

A conical bobbin provides a 77% increase in wire capacity.

APPENDIX 5.1.02

Bobbin Aspect Ratio

Ratio of wire volume to total bobbin (wire plus spool) volume as the aspect ratio of the bobbin changes.

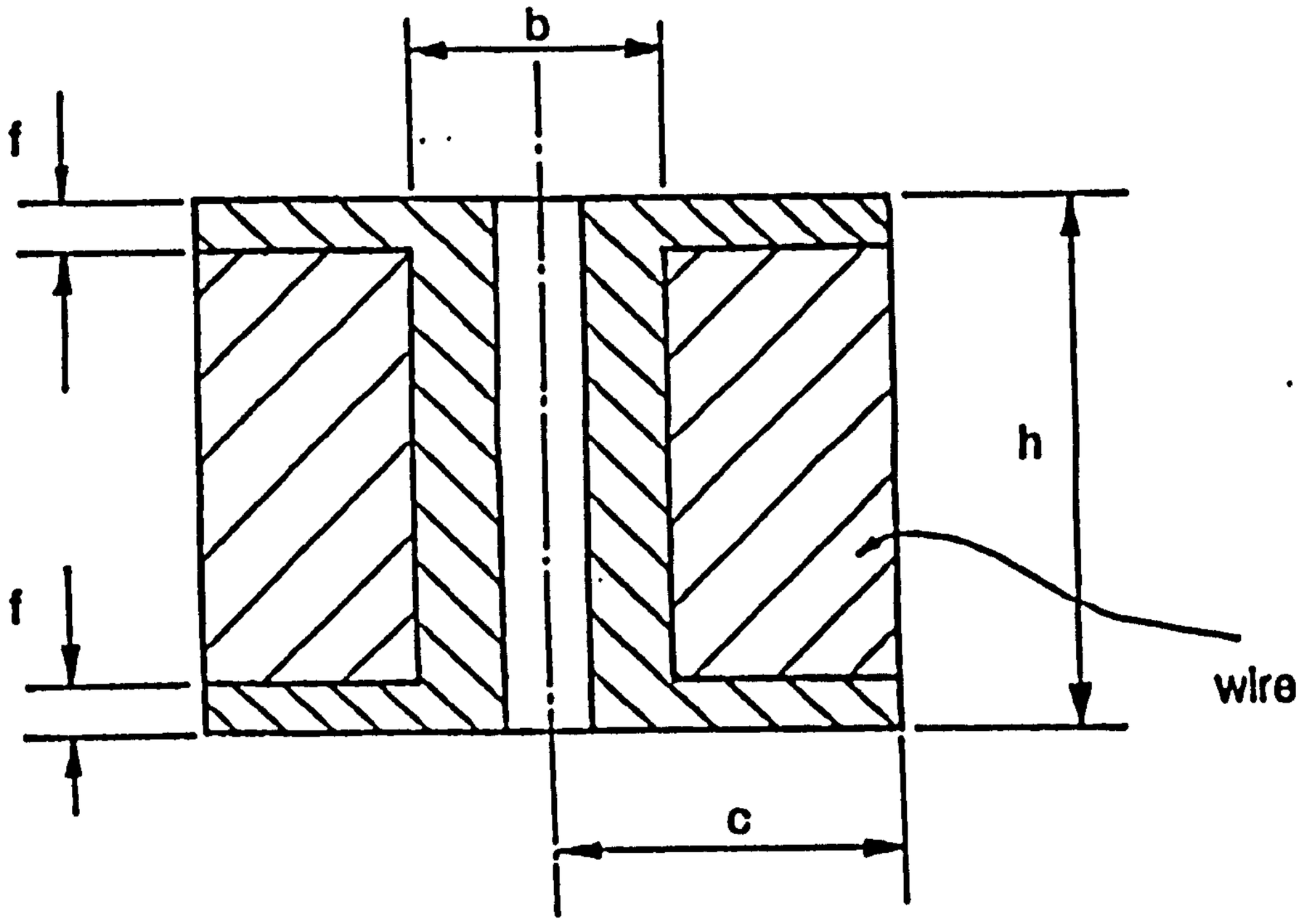

Figure A5.1.02 Bobbin dimensions

Vw = wire volume
Vt = total bobbin volume
Aspect ratio = 2.c/h
Bobbin volume ratio = Vw/Vt

$Vt = \pi.c^2.h$

$Vw = Vt - 2.f.\pi.c^2 - (h - 2.f)\pi.b^2/4$

$$Vw = \pi.(c^2 - b^2/4).(h - 2.f)$$

Now f and b are approximately constant due to manufacturing constraints and other practicalities.

Typical values are:

b = 33mm.
f = 9mm.

Thus, for a wire volume of 550000 mm^3 the bobbin volume may be plotted against the bobbin aspect ratio. This is shown in figure 5.1.02, chapter 5.

APPENDIX 5.2.11

Wand Tip Path Relative to Inner Bobbin

The model used for the wand is that shown in figure A5.2.11 , below, together with a triple harmonic motion law.

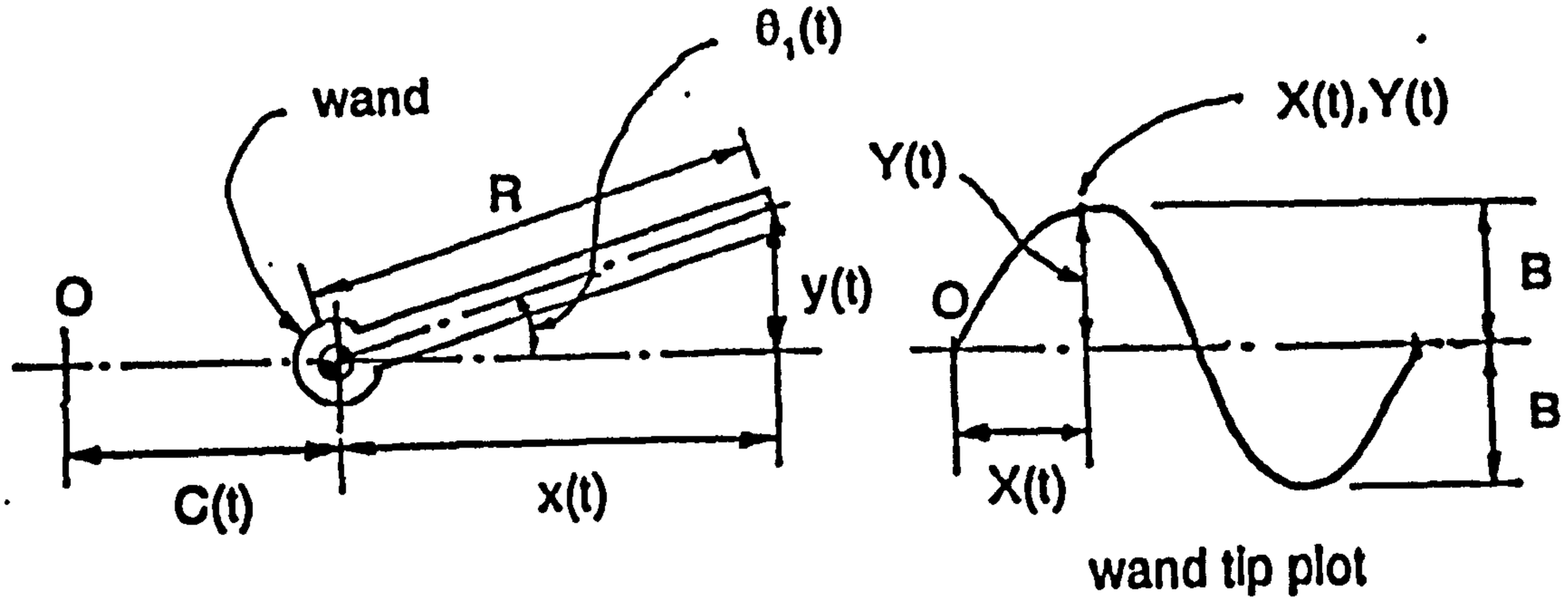

Figure A5.2.11 Wand tip coordinate system

$\theta_1(t) = A1.\sin(\omega.t) + A2.\sin(3.\omega.t)$

where A1 and A2 are constants such

that $\theta_{1\,max} = B$ and $A2 = 0.11.A1$

A numerical technique is used to find A1 and A2 for a prescribed value of B of 0.444 rads, which is equivalent to a wand tip amplitude of 110mm.

$$y(t) = R.\sin(\theta_1(t))$$

$$x(t) = R.\cos(\theta_1(t))$$

$C(t) = L\omega.t/3$ (relative to the inner bobbins)

$$\therefore \underline{Y(t) = y(t) = R.\sin(\theta_1(t))}$$

$$X(t) = C(t) - R + x(t) = L\omega.t/3 - R + R.\cos(\theta_1(t))$$

$$\therefore \underline{X(t) = L\omega.t/3 - R.(1 - \cos(\theta_1(t))}$$

APPENDIX 5.2.12

Maximum Cylinder Volume Which Fits in a Cone

To find the dimensions of the largest volume cylinder which will fit within a cone.

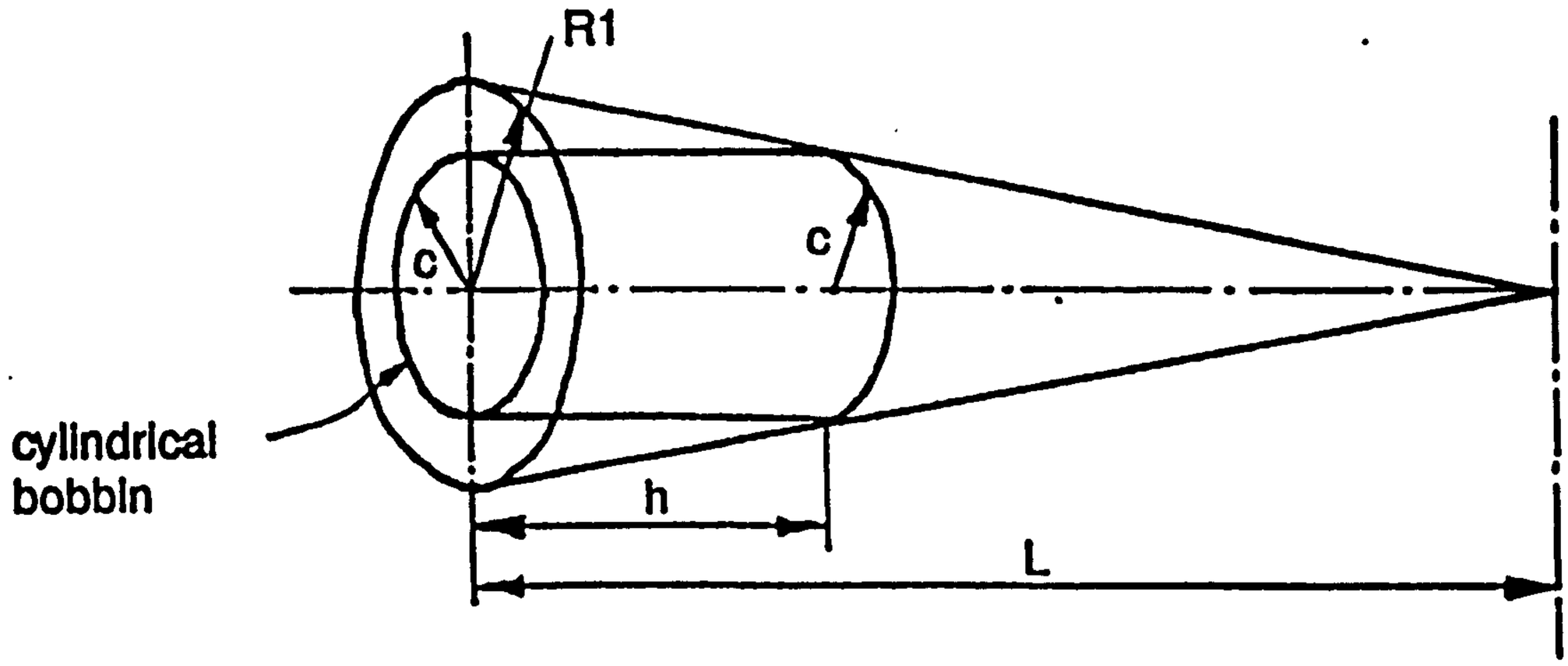

Figure A5.2.12 Bobbin and cone dimensions

$$h = L.(1 - c/R1)$$

Volume of cylinder, $Vc = \pi.c^2.h$

$$Vc = \pi.c^2.L.(1 - c/R1)$$

Maximum volume occurs when $dVc/dc = 0$

$$dVc/dc = 2.L.\pi.c - 3.L.\pi.c^2/R1 = 0$$

$$\therefore \quad \underline{c = R1.2/3 \quad \text{and} \quad h = L/3}$$

$$\therefore \quad \frac{\text{volume of cylinder}}{\text{volume of cone}} = 0.444$$

APPENDIX 6.1.1

Air Bearing System Appraisal

Air bearings may be broadly categorised into two types, aerodynamic and aerostatic. As the name implies aerodynamic bearings rely on the relative motion of the two bearing surfaces to form a converging wedge of gas which provides the support pressure. Aerostatic bearings rely on the pressure of the supplied air, introduced into a reservoir under the track and exhausted through holes in the track surface, to levitate the bearing load (i.e. the carrier).

No lubricant is needed since there is no contact between the carrier and track. The slots in the track surface are of little consequence as the carrier is resupported as it crosses the gap, although they do induce instability in moving carrier motion.

Only aerostatic bearings are suitable as an inner carrier support system for a rotary braiding machine.

(a) Design Parameters

Bearing Clearance

For a specific type of gas, supply pressure and air jet size, the pressure factor (Kg), which is proportional to the load capacity of the bearing, can be plotted against the clearance (Fig. A6.1.10). The point of maximum bearing stiffness is the position of the maximum gradient on the curve and corresponds, ideally, to the greatest load condition experienced. As the load becomes less (the carrier spool empties as the wire is drawn off it to form the braid) the operating point will move down the curve and the clearance will increase.

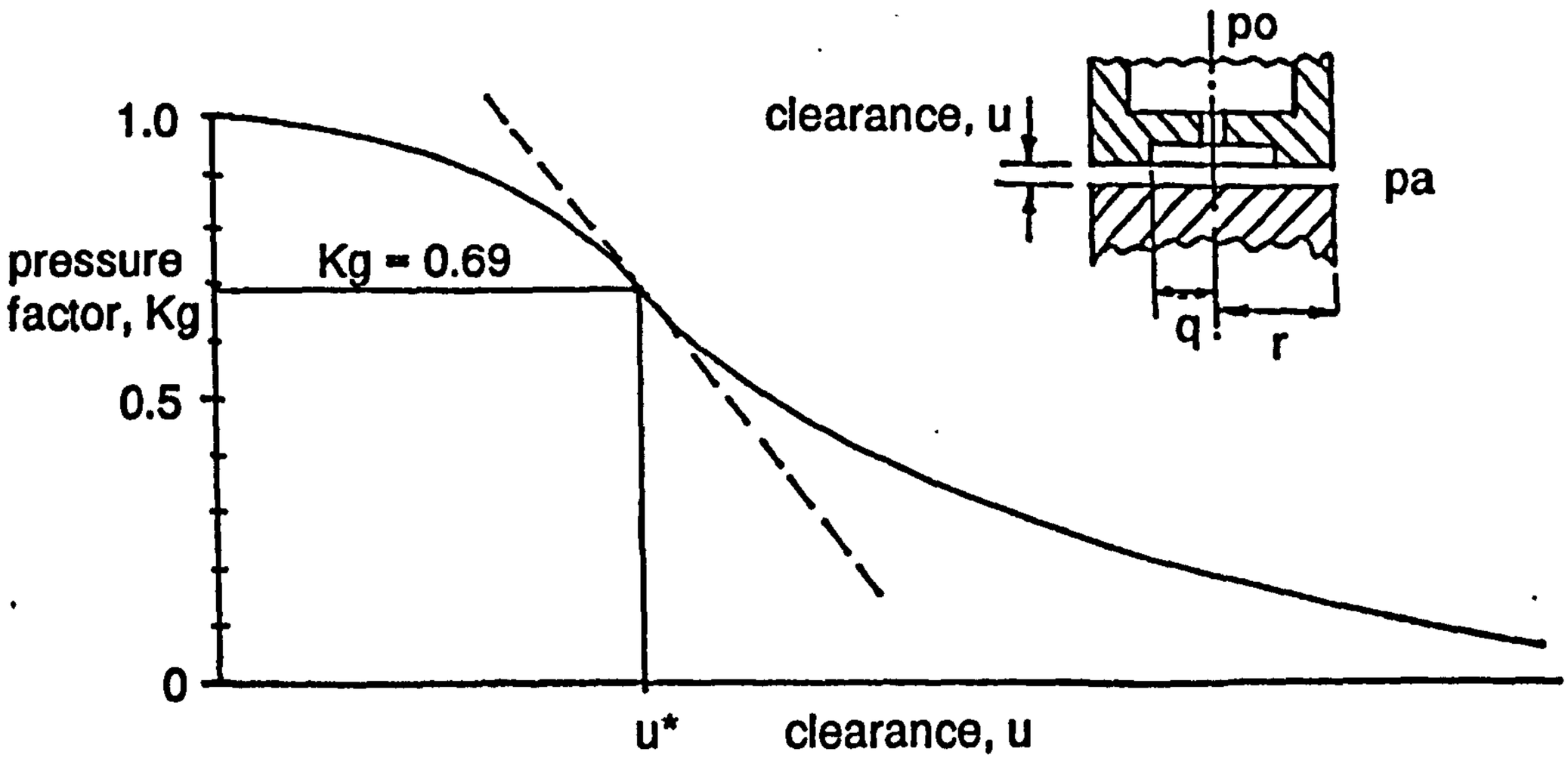

Figure A6.1.10 Pressure factor vs. bearing clearance

Tolerances

Aerostatic thrust bearings, although capable of running with less surface uniformity than aerodynamic bearings, typically require clearances of between 0.01mm (0.0004") and 0.125mm (0.005"). The tolerance of uniformity of the bearing surfaces, however, need to be a tenth of these figures. This required tolerance greatly increases the cost of manufacturing a track (usually of about 0.7m diameter) to the dimensions necessary for correct running as an aerostatic bearing face.

Track Design

The carrier track would, ideally, be constructed such that the main centrifugal load is supported on one main bearing face. The carrier would be supported fully by two other secondary bearing faces (Fig. A6.1.11). Another method, to avoid such accurate machining of three track surfaces, is to support the carrier on two faces perpendicular to each other and locate the carrier fully with a roller. When the machine is run the centrifugal force is sufficient to seat the air bearings and the roller leaves the track (Fig. A6.1.12).

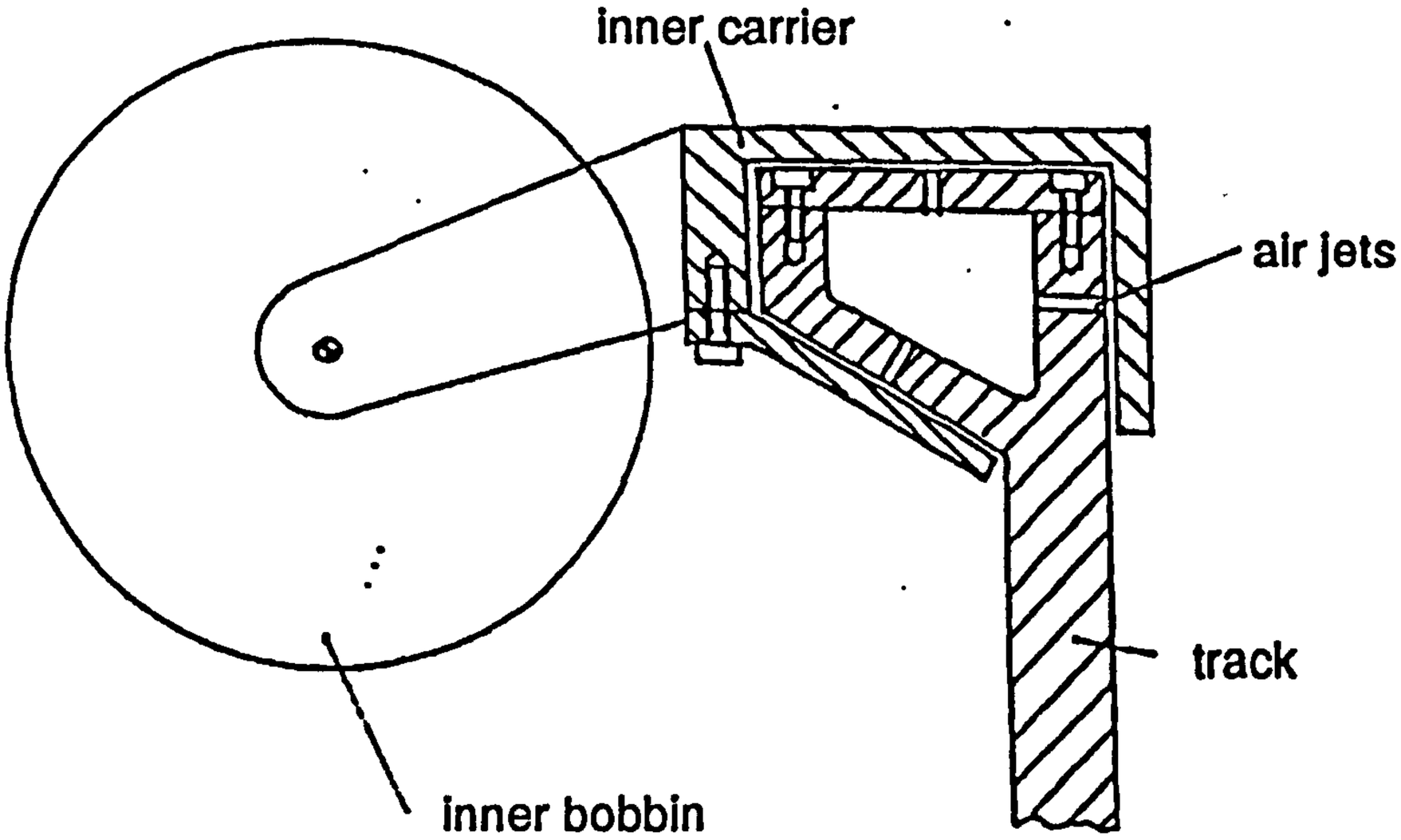

Figure A6.1.11 Carrier supported by air bearing only

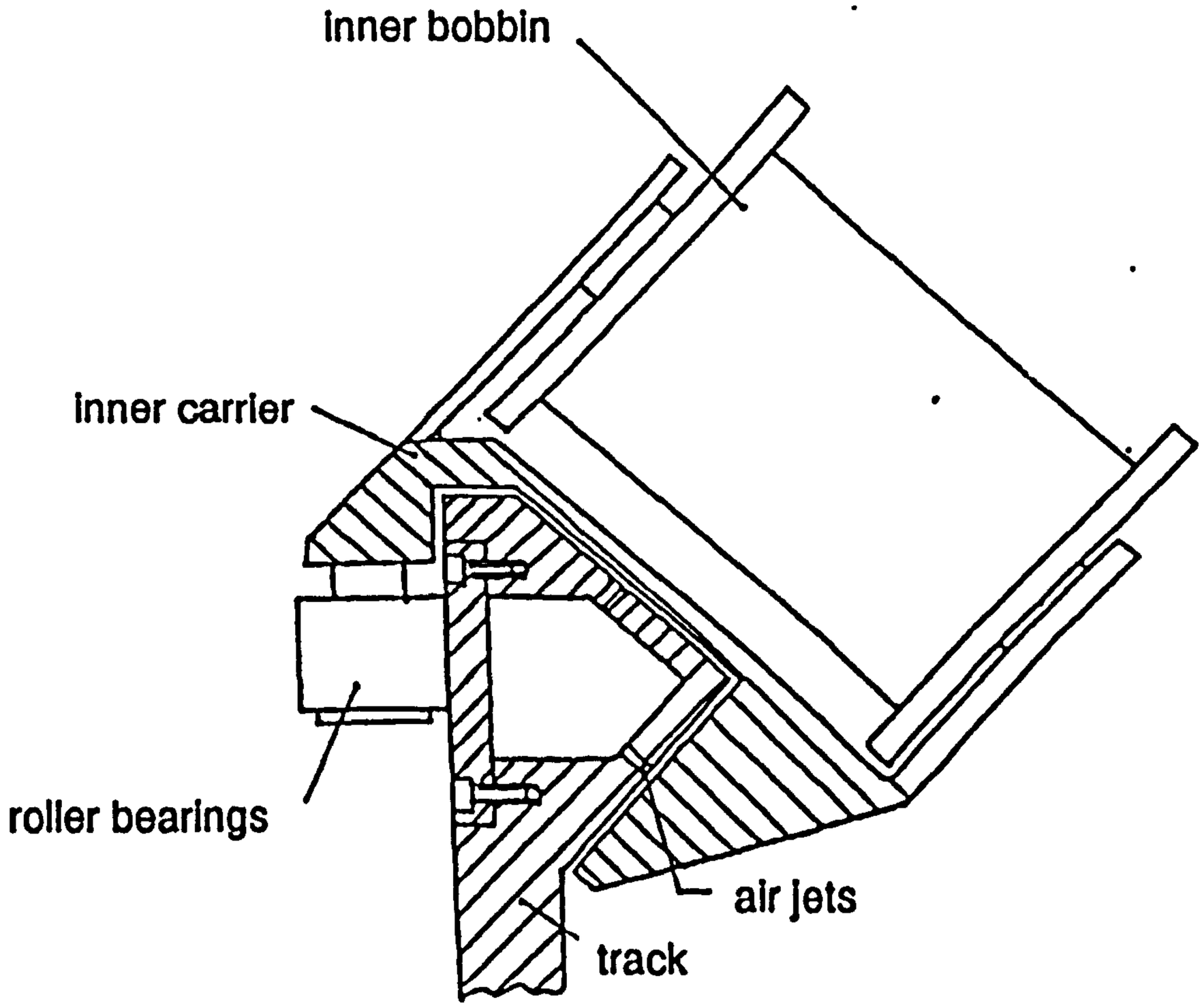

Figure A6.1.12 Carrier supported by air bearings and rollers

Air Jet Selection

Several types of air jet configurations are used. The two main types are plain jets and recessed jets which have a shallow pocket of a larger diameter than the jet (Fig. A6.1.13). To support a given load plain jets require larger jets and consume more air than recessed jets. Plain jets are only used when a recessed jet hole size is too small to manufacture economically. For minimum power consumption the recessed jet ratio of r/q has been found to be 2.

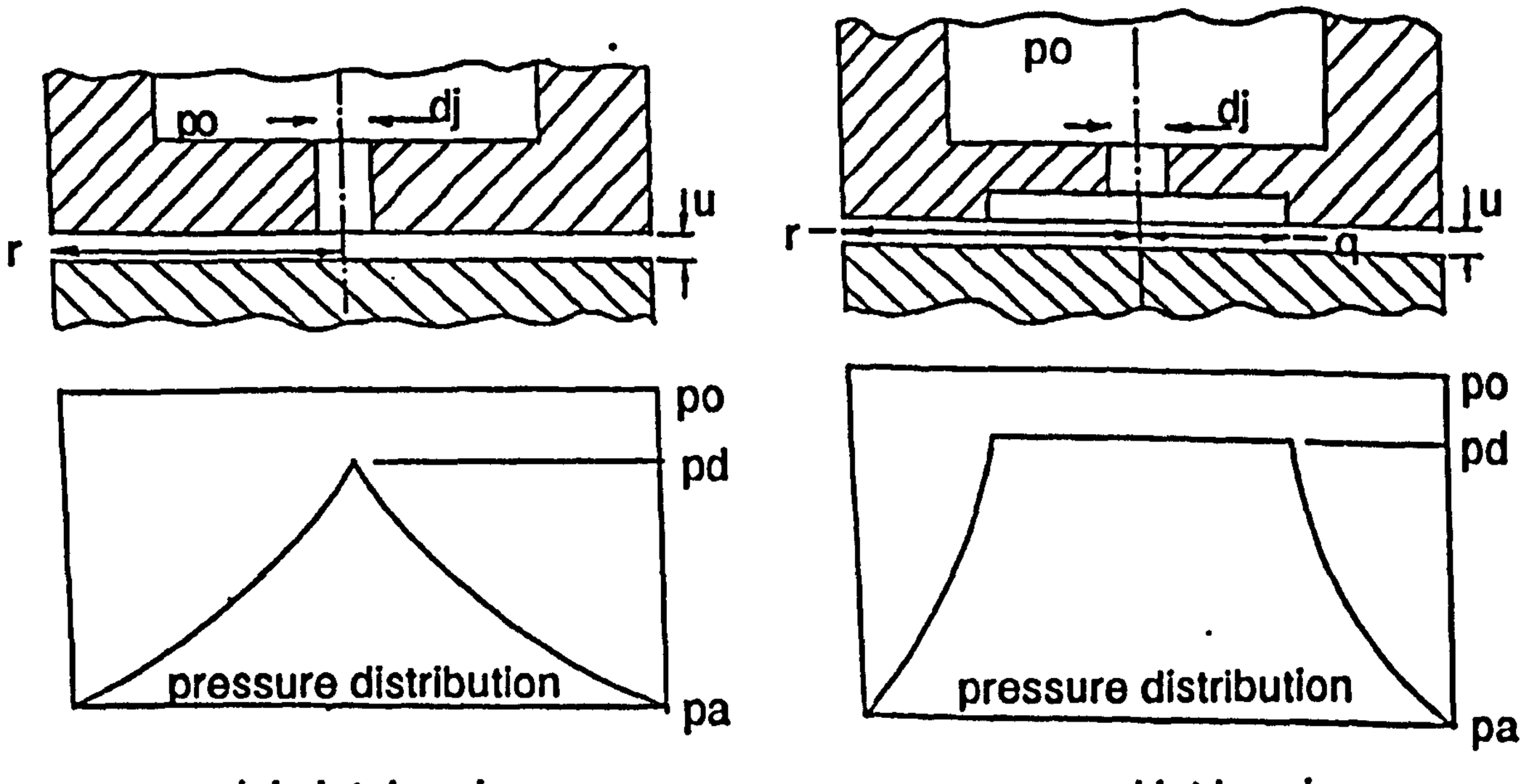

plain jet bearing recessed jet bearing

Figure A6.1.13 Air jet types

Air Mass Flow Rate

The mass flow rate of air through an aerostatic thrust bearing is proportional to the cube of the clearance. The air must be supplied by a compressor unless a very small mass flow rate is required, and the power required together with the associated noise must be set at a practical limit.

(b) Design Theory

The load capacity of a, single jet, circular air bearing is given by:

$$W = Kg(po - pa)\pi(r^2 - q^2)/(2.\log(r/q)) \quad (1)$$

where W = load capacity
po = supply pressure
pa = atmos. pressure
pd = discharge pressure
G = slot factor
Rg = gas constant (287 J/kgK)
Tg = gas temperature
Cd = discharge coefficient
mu = air dynamic viscosity

and Kg is the pressure factor, and defined as:

$$Kg = (pd-pa)/(po-pa) \quad (2)$$

If the compressibility is neglected then

$$Kg = 2/[1 + (1+4/G^2)^{0.5}] \quad (3)$$

where G, the "slot factor", is given by:

$$G = \frac{(pa/po).24.mu.(2.Rg.Tg)^{0.5}.Cd.dj^2.\log(r/q)}{(1-pa/po)^{0.5}.(1+pa/po) \quad pa.8.u^3} \quad (4)$$

Now maximum bearing stiffness is achieved when Kg = 0.69 which corresponds to G = 1.25 and thus the bearing dimensions may be found for a specific maximum load from equation (1).

By substituting the values of the bearing design parameters into equation (4) a value for the running clearance, u can be found. Conversely the minimum clearance may be specified and the bearing parameters may be found to achieve this. The mass flow rate of air (Ma) is found, for a given bearing system, from equation (5).

$$Ma = \pi.u^3.(pd^2\text{-}pa^2)/[12.mu.Rg.Tg.\log(r/q) \qquad (5)$$

The value for pd is found from equation (2) for Kg = 0.69.

The compressor power required to supply a given flow rate is found from standard tables.

(c) Experimental Test Rig

The test rig (fig. A6.1.14) used to verify the theory is a circular track of 500mm diameter and 30mm width and consists of eight separate sectors which support 8 separate shuttles, or carriers. The top face of each segment has 4 air bleed holes (i.e. 4 bearing pads) and the 2 holes (jets) nearest the track sector gaps are of larger diameter (0.35mm) than the 2 centre holes (0.2mm dia.).

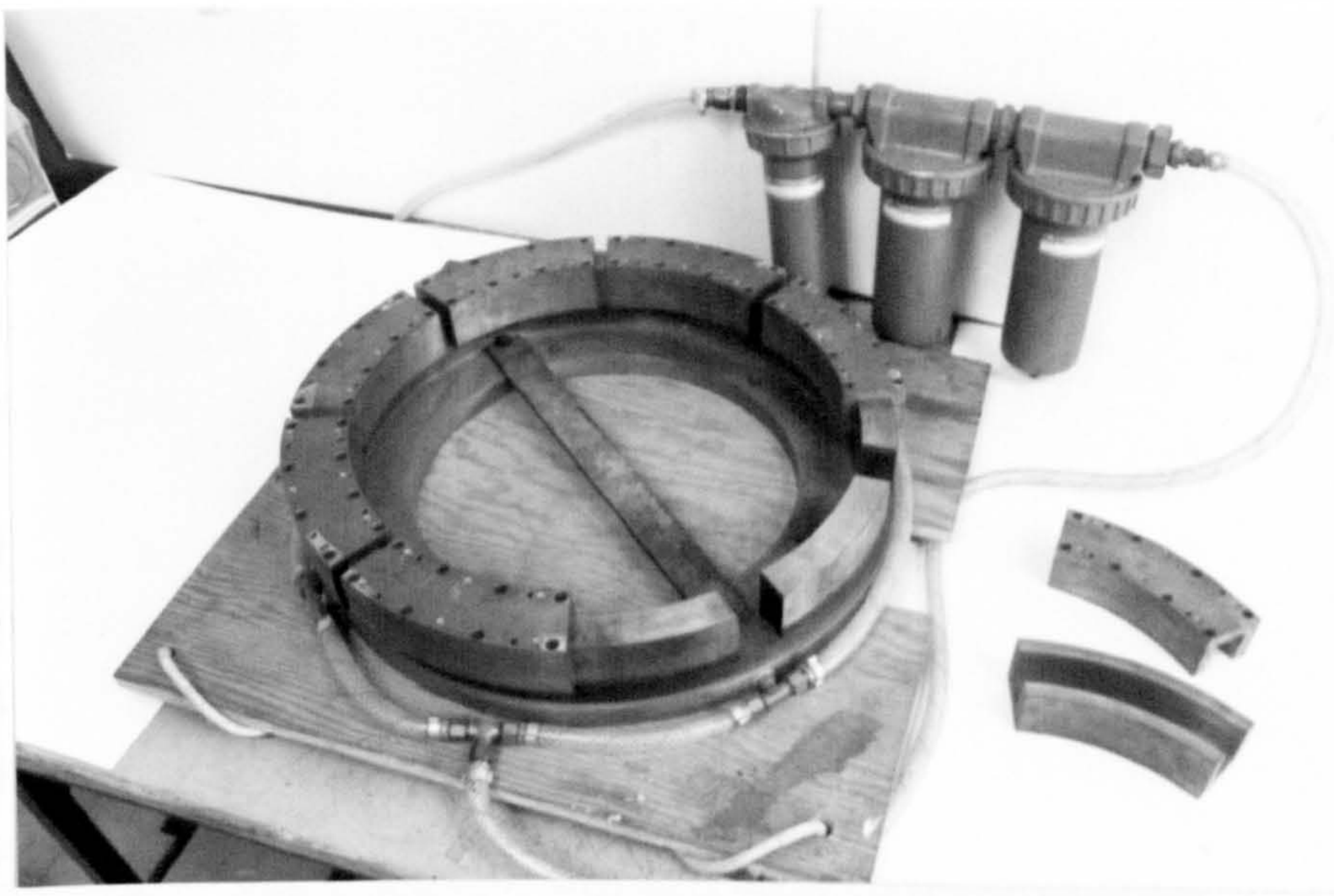

Figure A6.1.14 Air bearing test rig

Each side of each track sector has 12 jets (two rows of six jets) of the same diameter (0.2mm). Every air jet has a recess of 0.9mm diameter and 0.25mm depth.

The track sectors and carriers are constructed from a bronze based material to prevent damage should the surfaces make contact whilst moving and the rig is

designed to operate with a supply air pressure of 80 psi.

The air bearing test rig is used to correlate the theory with practical results for an aerostatic bearing and also to determine the stability of a carrier when in motion and when crossing the gaps between the track sectors.

The change in clearance between a carrier and the track is measured using a proximity transducer. This allows the static and dynamic behaviour of the carrier to be found. The different modes of vibration of the carrier on the track are determined using a spectrum analyzer which indicates the major frequencies present in the carrier when subject to an impulse. The different modes are found to predict when the carrier becomes unstable since the load is continually changing due to the gaps between track sectors.

Static Tests

The static tests involved loading both single and multiple air bearing pads to determine the effect of multiple air jets acting on a continuous surface. The load capacity of two separate air pads is obviously less than two adjacent air jets acting on a single surface of equivalent area. This is due to the pressure at the edge of the bearing pad not falling to zero where it "meets" the adjacent pad, and this consequently alters the pressure profile of the entire bearing.

The increase in load capacity of a single surface, multijet air bearing over a system employing a number of separate air pads is expressed as a scaling factor (xs) for inclusion in the theory. This factor (xs) is found to be 1.5 for a two jet system, and 3 for a four jet system (i.e. Two adjacent jets behave as three separate pads and four adjacent jets behave as twelve separate air pads) and rises to a maximum of four using eight jets (two rows of four jets). Thus a modified theory is used to formulate a model of the test rig air bearing by including xs as a simple multiplier in equation (1).

$$W = xs.Kg(po - pa)\pi(r^2-q^2)/(2.\log(r/q)) \qquad (1a)$$

Taking xs as 3 the predicted running clearance for the carrier, supporting merely its own weight is 0.0616mm.

The test rig results using the proximity transducer show the actual clearance to be 0.0656mm.

The difference in results represents an under prediction of theoretical bearing clearance of 6% and this corresponds to an error in load capacity of 2.5%, both of which are adequately accurate for the purposes of modelling an actual air bearing supported inner carrier system.

Dynamic Tests

The dynamic tests involve recording the undulation in carrier to track clearance as the moving carrier crosses the slots in the track (where the carrier is not supported). The sudden lack of support (albeit short) as a carrier begins to cross a slot, and equally sudden resumption of suspension by the first air bearing pad on the next track sector, initiates and oscillation in the carrier motion. This is recorded using a proximity transducer mounted on one end of the moving carrier (Fig. A6.1.15).

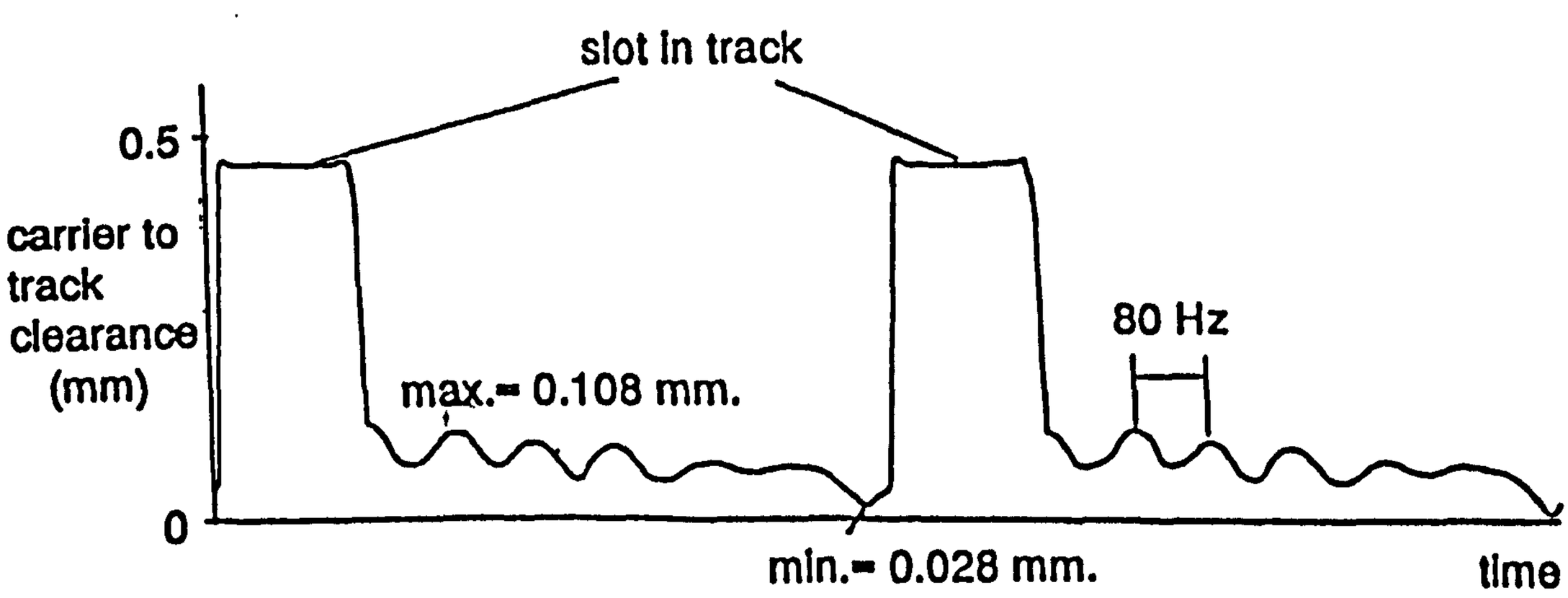

Figure A6.1.15 Test carrier running clearance

This oscillation has a total amplitude of 0.0875mm and the carrier reaches a maximum distance of 0.1075mm and a minimum distance of 0.028mm from the track surface.

The different modes of oscillation of the carrier are determined using a spectrum

analyzer. Signals from accelerometers mounted on the carrier and on the head of a striker, used to subject the carrier to an impulse, are processed by the analyzer to reveal the various frequencies present as the carrier oscillates on its air bearing (Fig. A6.1.16).

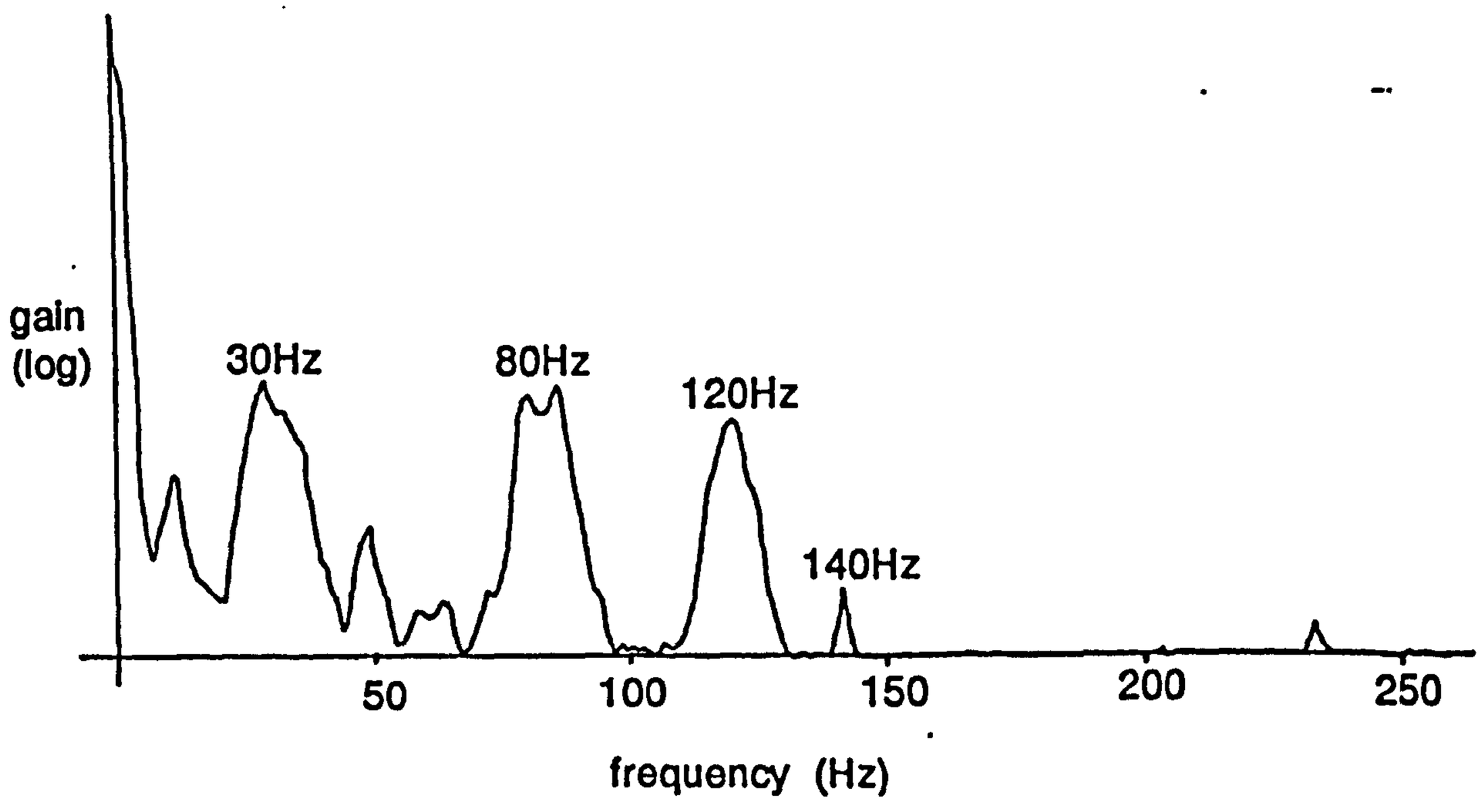

Figure A6.1.16 Spectrum analyser plot of a vibrating air bearing carrier

From this the various modes of oscillation are estimated.

The carriers pass over the track slots at a rate of between 60 times/second (150 r.p.m. machine speed) and 80 times per second (200 r.p.m.) depending on the final machine speed. Thus, with an air bearing system similar to that of the test rig, the carriers will resonate as the machine approaches 200 r.p.m. (i.e. the carrier "rocks" at approximately 80Hz) and carrier to track contact is probable.

(c) Theoretical Model of a Full Size Carrier System

Assuming a standard air supply pressure (po) of 5.5 bar (80 psi) and a minimum running clearance (u) of 0.05mm (0.002") (at which point the air bearing should be at its maximum stiffness and G = 1.25) the jet diameter (dj) may be found from equation (4).

If r/q = 2

Cd = 1.0

Then dj = 2.64 mm.

The load (Fc) on a carrier is given by:

$$Fc = Mc.rc.om^2$$

where Mc = carrier mass (10 kg)
rc = carrier C of G radius (500 mm)
om = carrier angular velocity (15 rad/s)

Now assuming each carrier is supported by at least three circular air bearing pads at any time (i.e. each track sector has four jets), the load which each air bearing pad must support (W) is given as:

$$W = Fc/3 = Mc.rc.om^2/3$$

Substituting into equation (1a) allows the bearing pad radius (r) to be found (for r/q = 2)

$$Mc.rc.om^2/3 = xs.Kg.(po-pa).3.\pi.r^2/[8.\log(r/q)]$$

$$\therefore \quad r = [8.Mc.rc.om^2.\log(r/q)/(9.\pi.xs.Kg.(po-pa))]^{0.5}$$

$\therefore$ r = 13.9 mm when xs = 3
Kg = 0.69
(po-pa) = 5.5 bar

The track radius (rt) may be expressed in terms of pad radius (r), (since 48 pads are employed) and slot width (Lg) (which is assumed to be 5mm).

$$rt = (12.Lg + 96.r)/(2.\pi) = 0.222\ m$$

The value of the mass flow rate, Ma, of air required from the compressor is found from equation (5):

$$Ma = \pi.u^3.(pd^2 - pa^2)/(12.mu.Rg.Tg.\log(r/q))$$

Since Ma is dependent on the variables u, pd and pa, the proximity of adjacent pads, and consequent rise of pa along part of the periphery of each bearing pad, reduces the mass flow rate in a similar manner to which it increased the load capacity. Thus xs, the load capacity scaling factor is taken as an approximate scaling factor and is introduced into equation (5).

$$Ma = \pi.u^3.(pd^2 - pa^2)/(12.xs.mu.Rg.Tg.\log(r/q)) \qquad (5a)$$

This is the value of air mass flow rate for a single pad, which must be multiplied by 48 to give the total flow rate for the major load bearing face. However, the carrier must be located by at least two other bearing surfaces and so a further factor, of approximately two, is included to account for this. The total mass flow rate Mt is thus:

$$Mt = 96.Ma$$

For the typical air bearing carrier system described, the total mass flow rate Mt is 0.224Kg/s which corresponds to a volume flow rate of $0.15 m^3/s$ (317 cfm).

The power of a compressor required to deliver this flow rate is found from standard tables to be approximately 40.3 Kw, (54 HP).

(d) Conclusions of Air Bearing Study

The correlation of both theory and practical results enables a reasonably accurate model of an air bearing suspended inner carrier system to be formulated.

The minimum running clearance chosen for such a model is 0.05mm (0.002") which is a compromise between the prohibitive costs of manufacturing a system using very small clearances and the decreased efficiency of an air bearing utilising larger clearances.

The estimated air mass flow rate for such a system is 0.224Kg/s (317 cfm) which requires a 40.3KW (54 HP) compressor.

Indeed, even using a clearance of 0.025mm (0.001") requires a mass flow rate of 0.084 Kg/s (118 cfm) which still requires a compressor power of 15 kW (20 Hp). The high cost of manufacturing a precision air bearing track together with this large additional power requirement render aerostatic bearings an impractical solution for supporting the inner carriers on a rotary braiding machine.

In addition, the noise generated by a compressor and by the air bearing itself also reduces the desirability and feasibility of such a system.

The relative inviscidity of air compared to other bearing mediums accounts for the test rig carriers (and air bearings in general) being underdamped with the possibility of several modes of vibration aggravated by the carrier continually crossing the track slots. Although this instability does not compromise the exact positional control of the carriers (due to the small magnitudes of oscillation) it does lead to a resonance situation as carrier rotational speed increases (200 r.p.m. in the case of the test rig carriers). A full size machine modelled on the test rig, may resonate at or below its envisaged maximum speed with a mode shape best described as rocking about its central axis. The leading and trailing edges of such a resonating carrier will alternately contact the track resulting in damage and eventual system failure due to loss of surface uniformity. Also, as the material on the inner carrier bobbin is consumed the mass decreases. However, the carrier bearing stiffness experiences a much lower reduction since it is located and supported on three faces, thus the resonant frequencies of each carrier change continuously and the likelihood of a carrier resonating at some time is high.

APPENDIX 6.1.2

Electromagnetic Carrier Suspension Appraisal

Magnetic and electromagnetic suspensions may be broadly categorized into four groups most applicable to a rotary braiding machine track and carrier bearing system.

(i) Permanent magnets in repulsion
(ii) Eddy current repulsion using mains frequency excitation
(iii) Levitation using superconducting magnets
(iv) Attraction using controlled D.C. electromagnets.

The basic requirements of a rotary braider carrier bearing system practically rule out the use of superconducting magnets due to the need to cool the bearing magnets to close to -273 ° C (absolute zero) which is both expensive and complex on a rotating machine.

In addition, systems which require the carriers to be supplied with electrical power are inappropriate due to the intermittent nature of the drive to the inner carriers. Indeed, any system requiring external power or complex control using feedback from track or carrier sensors must considerably out perform other, non powered, bearing systems to justify the additional running and construction costs entailed.

A fundamental theorem, proved mathematically by Earnshaw (ref. Jayawant, reference (2)) states that it is impossible for a pole placed in a static field of force to have a position of stable equilibrium when an inverse square law operates. Thus, stable suspension is impossible using an uncontrolled system of permanent magnets, or fixed current electromagnets.

The carriers on a rotary braider track are located precisely in the circumferential direction by the drive system and levitation is needed only to counteract the centrifugal and mass forces of the rotating carriers and so stable suspension may be achieved.

(i) Permanent Magnets in Repulsion

Relatively new advances in rare earth magnets have led to ceramic materials which offer resistance to demagnetisation of 20 to 50 times that previously available from "alnico" magnets, and magnetic repulsion forces of 5 to 12 times greater. One of the best permanent magnet materials available is Colbalt Samarium which has a magnetic repulsion force of up to 12 times that of alnico.

The advantages with permanent ceramic magnets as inner carrier bearings are:

(a) No energy is required to achieve levitation

(b) No maintenance is required

(c) As the magnets are made of non-conducting ceramics there are no eddy currents and resultant drag forces

(d) There is no noise or contamination of the rest of the machine by the bearing medium.

The disadvantages with this type of bearing system are:

(e) The carrier must be supported on at least three separate bearing faces

(f) The bearing stiffness, especially in roll, is poor and the system is very underdamped

(g) The bearing load capacity changes as the carrier magnet crosses the track slots and is resupported by the magnet on the next track sector

(h) The size and mass of the magnets required results in a bulky carrier and a large bearing surface area.

(i) The cost of ceramic magnets is high.

Although the analytic estimation of repulsion forces between two magnets is complex and difficult to achieve accurately, an approximate value for the size of magnets required in a rotary braider may be found from previous experimental work. A Colbalt-Samarium magnet of 5 kg mass is capable of supporting approximately 2000N force over a bearing area of 314 cm^2 (200mm diameter circle) with an air gap of 5mm. This shows that the size of magnets required would adversely affect the bobbin volume optimisation since the bearing must be positioned radially outside the bobbin.

The major drawback when using permanent magnets is that the carrier must be supported on three separate faces since the drive mechanism requires precise

carrier location at all times. The carrier must therefore utilise two opposing magnetic bearings (which greatly reduce the load capacity of the system in any one direction), or employ a second bearing type (such as rollers) to locate the carrier whilst not at full load and speed conditions. The use of two different bearing technologies is not justified in view of the fact that permanent magnet bearings show no overall advantages over other bearing systems.

(ii) Eddy Current Repulsion using Mains Frequency

Suspension of a carrier by eddy current repulsion uses the concepts employed in a single sided linear induction motor (LIM), modified to allow near constant repulsion throughout the speed range. The most compact, and appropriate, form is a geometry known as a transverse flux machine (or transverse flux LIM). The energised electromagnetic primary core represents the track of the rotary braider with the secondary core, which represents the carriers, consisting of a conducting plate (aluminium) of suitable thickness.

Whilst the envisaged centrifugal forces can easily be accommodated, the power and area of the bearings are excessive. The reactive input to the machine (VAR) may be expressed in terms of the normal repulsive force required.

VAR = 2Fn.Ag.Sr where Fn = normal repulsive force
Ag = air gap between primary and secondary cores
Sr = 2.π.Sf where Sf is the supply frequency.

For Fn = 2000N
Ag = 1.00mm
Sr = 314 Rad/s (50Hz)

The reactive input, VAR = 1.256 kW

This value, for one carrier only, is too high since 12 such bearing units are required. In addition, to achieve such repulsive forces the primary core must be directly water cooled if the bearing is to fit into the region available at the end of an inner bobbin.

Thus, this form of bearing system is inappropriate as a rotary braider carrier support arrangement.

(iii) Levitation using Superconducting Magnets

Although this system is capable of supporting the carrier load, the electromagnets used must be cooled to near absolute zero. This is clearly impractical on a small rotating machine, and therefore this system of inner carrier support is eliminated.

(iv) Attraction using Controlled D.C. Electromagnets

Suspension using controlled D.C. electromagnets requires the electromagnets, amplifiers and sensors to be mounted on the moving carrier, since track mounted sensors would witness discontinuities as successive inner carriers are detected. The current required, for an acceptable bearing area, to achieve the lift force necessary is excessive and requires the magnet cores to be water cooled. The major problem of power pick up by the inner carriers is also unresolved due to the intermittent nature of the drive to the carriers.
A carrier bearing system using levitation by controlled D.C. electromagnets is eliminated since the extra initial, and running, costs and increased complication, result in no advantage in overall performance over other less costly bearing systems.

Conclusions for Electromagnetic Suspension Study

A review of the various methods of magnetic and electromagnetic suspensions suitable for use on a rotary braiding machine has indicated that such an inner carrier support system is inappropriate, at present, and offers no advantage in performance over other types of bearings.

The major drawbacks with electromagnetic suspension systems are:-
(a) The size of magnets required for a permanent magnet system adversely affect the bobbin optimisation.
(b) A permanent magnet system requires two opposing bearing faces to operate which severely decreases the load capacity.
(c) Magnetic and electromagnetic suspension bearings generally have low a stiffness and are underdamped
(d) All but permanent magnet systems require appreciable power (in the order of 1kW per carrier) to operate and this leads to the necessity of water cooling the cores.

APPENDIX 7.1.2

Trajectory of a Twin Roller Carrier over a Track Slot

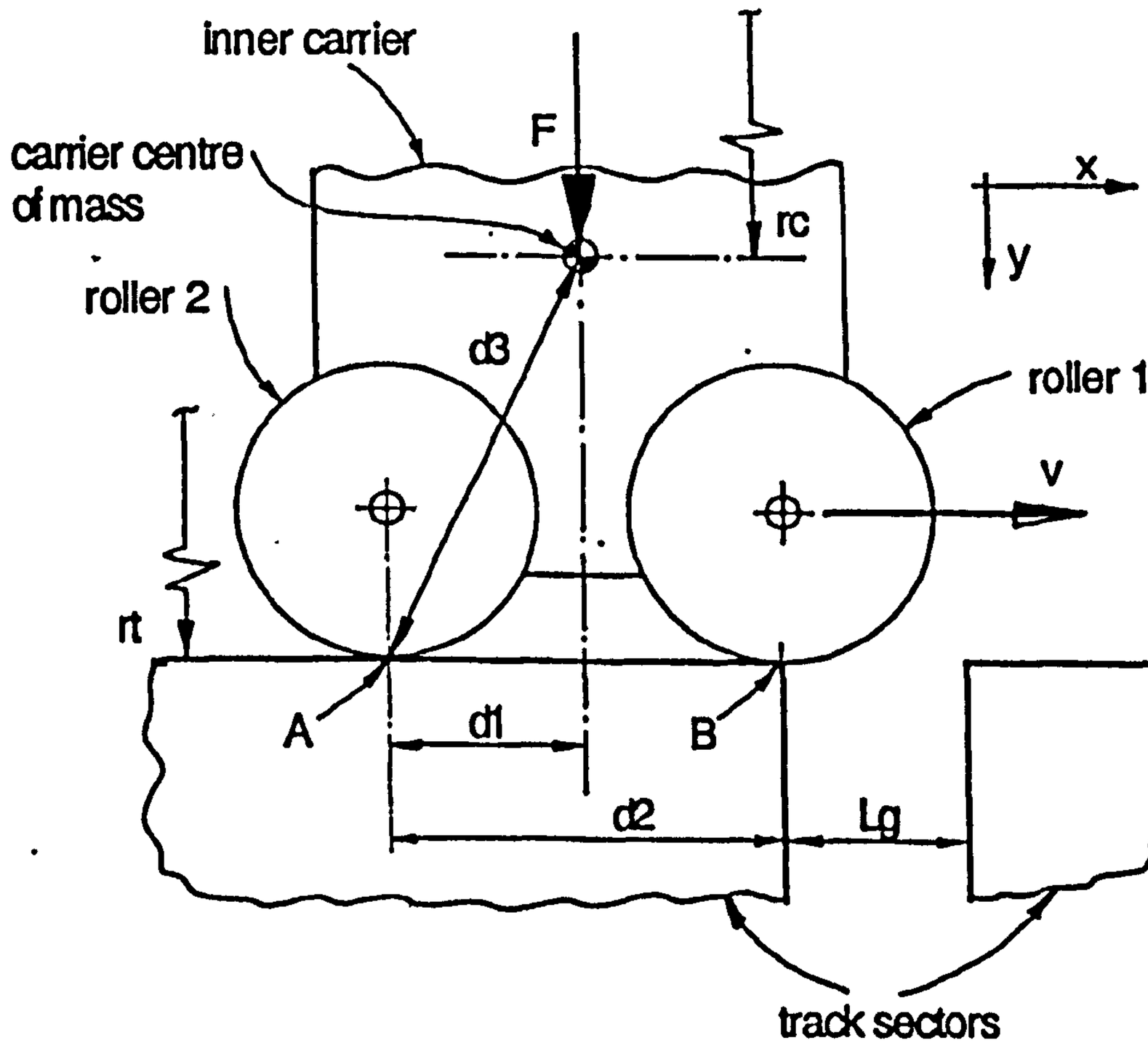

Figure A7.1.2 Simple twin roller carrier trajectory model

Io = inertia of carrier about C of G.
Mc = carrier mass
rt = track radius
rc = carrier C of G radius
v = relative velocity between carrier and track
F = external force on carrier (due to secondary rollers supporting couple from overhung load at low speed)
om = angular velocity of carrier around machine
Ta = torque about A causing roller 1 to fall into the gap

Relative velocity $v = 2.rt.om = dx/dt$

$\therefore \quad x = 2.rt.om.t \qquad$ and $\qquad t = x/(2.rt.om)$

Torque about A;

$Ta = Ia.y''/d2$ where Ia = moment of inertia about A

y'' = acceleration of roller 1 into slot

y' = velocity of roller 1 into slot

$Ia = Io + Mc.d3^2$

Centrifugal force on carrier = $Mc.rc.om^2$

Total force on carrier = $Mc.rc.om^2 + F$

$(Mc.rc.om^2 + F).d1 = Ia.y''/d2$

$y'' = d1.d2.(Mc.rc.om^2 + F)/Ia$

$y' = d1.d2.(Mc.rc.om^2 + F).t/Ia + C3$

If when $t = 0$, $y' = 0$ (at the edge of the slot as shown)then $C3 = 0$

$y = d1.d2.(Mc.rc.om^2 + F).t^2/(2.Ia) + C4$

If when $t = 0, y = 0$ then $C4 = 0$

therefore $y = d1.d2.x^2.(Mc.rc.om^2 + F)/(8.rt^2.om^2.Ia)$

Now substituting typical values:

$x = Lg = 6$ mm	$rc = 410$ mm
$d1 = 32$ mm	$rt = 362$ mm
$d2 = 64$ mm	$om = 15$ rad/s
$Ia = 0.09$ kgm^2	$Mc = 10$ kg
$F = 0$ (at high speed)	

Therefore $y = 0.0032$ mm.

This is the theoretical depth of the next track sector leading edge which ensures the roller does not impact the corner. (Refer to chapter 7 for experimental correlation).